Improvement in Inspection Methods for Aeroengine Components using Computer Linked Electro Optical Techniques.

by

BERNARD SPENCER HOCKLEY

A Doctoral Thesis

Submitted in partial fulfilment of the requirements for the award of

Doctor of Philosophy of the Loughborough University of Technology

October, 1973.

Supervisor: Professor J. N. BUTTERS, Ph.D.

Department of Mechanical Engineering

SUMMARY

An improved technique for inspecting aero engine turbine blades was developed. The technique increased the area of the blade that was examined and presented the difference information in an easily assimilated form without increasing the overall inspection time above that of present methods. To achieve this an optical contouring technique was used to measure the blade shape and this was linked to a computer to enable the dimensional information to be processed quickly.

Two holographic methods of surface contouring, two wavelength and two refractive indices, and a moiré fringe shadow technique were studied on the basis of forming part of a routine inspection system. The moiré fringe method was found to be the most suitable technique and a modified version of moiré contouring was developed for use in conjunction with image scanning and computer processing.

Methods of comparing the shape of a component with that of a master were studied. To obtain sufficient accuracy the optically measured shapes were compared rather than the direct contour fringe patterns. This technique relied upon the use of a computer to process the data.

A method of generating the shape of the component from the contour fringe information was formulated together with a method of comparing the shape of the component with a master. The results of the comparison were presented in the form of the overall differences in two orthagonal directions and an angular rotation plus details of any abnormal localized differences superimposed on the overall values. The contour fringe information was read in to the computer at a rate of 1000 words per second with the aid of a slow scan television interface.

The work described in this thesis was carried out by the author at the Advanced Research Laboratory, Rolls-Royce (1971) Limited, Derby, during the period October 1969 to September 1973. The slow scan television and digital tape recorder interface was designed and built by the Electronic Services Section of the Advanced Research Laboratory in co-operation with the author.

Table of Contents

List of Tables.

List of Figures

Fig. No. | Page

List of Appendices.

List of Symbols.

A	amplitude of optical wavefront.
b	distance of the shadow from the moiré grid.
C	constant.
D	diameter of the lens aperture.
d	lateral distance between the point source and the point of observation in the moiré system.
d_s	diameter of the point source.
dz	depth of field.
E	energy.
F,f	focal length.
h_1	height of source above moiré grid.
h_2	height of point of observation above moiré grid.
I	optical intensity.
J	zero order bessel function.
K	constant.
k	wave number.
ℓ	distance along moiré grid.
M	optical magnification.
N	fringe number.
P	pressure
p	period of moiré grid.
R	radial distance of a point on the image from the hologram.
s	speckle brightness.
T	transmission function.
U	distance of the object from the lens.
V	distance of the image from the lens.
$W_n(s)$	probability of speckle brightness s.
(x,y,z)	co-ordinates.
z(x,y)	depth of component.

α	angle of illumination of moiré grid.
β	angle of observation of moiré system.
γ	gradient of the linear region of the Hurter Driffield curve.
Δx	spread of moiré grid shadow.
Δz	contour depth interval.
θ_{rec}	angle of reconstruction beam.
θ_{ref}	angle of reference beam.
θ_1	angle of illuminating beam.
θ_2	angle of observation.
λ	wavelength of light.
ρ	gas density.
σ^2	variance of speckle brightness.
ϕ	phase of optical wavefront.
ψ	angular increment of spline fit.

INTRODUCTION.

The dimensional inspection of components together with the measurement of such characteristics as vibration and strain with the aid of optical techniques has greatly increased in the last decade. This is principally a result of the use of television systems and the development of the laser.

Holography made possible the measurement of complex deflections produced by static loads and the visualization of vibration mode and amplitude contour patterns for real engineering components. The potential advantages of holography for this type of deflection visualization over measuring techniques in current use prompted a study of the engineering applications of holography with particular reference to aeroengine components. Holographic methods of vibration analysis were studied by Hockley [1, 2] and a self-contained unit for applying holographic vibration analysis developed. Improvements to the basic holographic technique for vibration analysis in this context have been made including a phase modulation system to extend the amplitude range of holography from 25 microns to 500 microns, Hockley [3, 4].

The use of holography as a method of non-destructively testing honeycomb structures in aeroengines has been studied, Hockley [5].

The ability of a holographic system to record truly three-dimensional information about the surface of a component gives rise to the possibility of comparing two similar components to obtain the dimensional differences between them. The ability to obtain accurate comparisons between complex components is important in the aeroengine industry particularly since small differences can produce significant changes in engine performance and when the components are being operated very close to the limits of the materials. Work on holographic inspection by Archbold [6] demonstrated that holography could be used to measure dimensional differences on small accurately made components, provided that the differences were of the order of 1 micron. To achieve this the component had to be located to an accuracy of 0.2 microns in the six degrees of freedom.

Although the resolution of this system was considerably greater than that required in the manufacture of components such as turbine blades, the fundamental ability to measure these types of differences was extremely important. Consequently a system capable of comparing components with a measuring accuracy of approximately 25 microns (1×10^{-3} inches) as suggested by Hockley [1] would form a significant contribution in both the manufacture and testing of aeroengine components. This is particularly relevant to turbine blades because they have a complex shape and require detailed and accurate inspection over the aerofoil surface.

The cost of manufacture of each component is high because of their complexity and the relatively small quantities of each type that are made. Subsequently component wastage is expensive. Improved inspection methods that are accurate and can be used in corrective procedures to reduce the rejection rate are always of interest to the industry.

In addition to production inspection there is an important requirement for a system capable of measuring the complex distortions of turbine blade aerofoils that have been produced by tests of the blades under engine running conditions.

A possible method of desensitizing holography would be the use of optical contouring, Hildebrand and Haines [7], to generate surface contour fringes of equal depth with respect to a given reference plane. Such a system was thought feasible on turbine blades if contours of the order of 250 microns depth (1×10^{-2} inches) were formed on the blade and the dimensional differences measured to an accuracy of one tenth of the contour depth interval.

Because of the complexity of the tolerance limits and the need to develop an automatic system some form of computation would be required to manipulate the difference information. A computer system introduces the prospect of comparisons being made using computed design data rather than a physical master. This is a significant feature because the majority of turbine blades are designed by computer techniques.

The need for a fast and accurate method of dimensional inspection or analysis of components together with the potential of holography as a method of inspection prompted the research described in this thesis.

The work presented describes the investigation into the feasibility of the use of optical contouring techniques as a means of comparing two similar components. Two holographic contouring techniques were studied, two wavelength contouring, Hildebrand and Haines [7] and a two refractive index method, Shiotake et al. [8] together with a moiré shadow contouring technique, Meadows et al. [9]. The three methods were compared with respect to their use on a routine basis in an industrial environment. The moiré technique was found to be the most suitable. A simplified version was developed for use in conjunction with an image scanning system.

A method of comparing the contour fringe patterns of two similar components with the aid of a computer was formulated to provide concise and easily assimilated information on the dimensional differences.

In Chapter I the present techniques used for dimensional inspection are described and the fundamental approach used to develop optical contouring as a means of improving the inspection techniques is discussed.

In Chapter II the methods of generating optical contours are discussed together with an evaluation of their relative merits and the choice of the most appropriate system for adoption for this work.

In Chapter III the possible methods of comparing one component with a master are considered. The methods of interrogating the contour pattern to obtain dimensional information within the computer and means of manipulating the dimensional information of the component to be inspected with respect to the master component shape are described in Chapter IV, the objective being to develop a method of describing the overall differences between the two components plus any abnormal localized differences that occur.

The experimental television system used to form the interface between the optical contours and computer is described in Chapter V together with some experimental results. The conclusions and recommendation with respect to this research are presented in Chapter VI.

Chapter I.

Dimensional Measurement Techniques.

1.1 INTRODUCTION.

In this chapter the two principal methods of inspection of turbine blade aerofoils, profile following and point gauging are described, together with an analysis of the future requirements of aeroengine turbine blade inspection.

1.2 PRESENT INSPECTION TECHNIQUES.

1.2.1 Units of Measurement.

Throughout this thesis both the M.K.S. and the pound-force, inch, second system of units will be used. Although it is more appropriate to discuss optical parameters in the M.K.S. system the dimensions of the aeroengine components are still defined in inches within the Company. Hence, when referring to turbine blades and the appropriate optical contour depth used to measure their dimensions, the inch unit will be used.

1.2.2 Profile Following. (Calliperscope)

This technique consists of a self-contained machine into which the turbine blade is clamped and a pair of spring loaded pincer-like probes are drawn across the blade aerofoil in a chordwise direction. One probe is in contact with the convex surface and the other the concave surface. These probes are mechanically connected to a similar pair of slave probes that follow the movement of the probes on the blade. The outline of the slave probes are projected with a large degree of magnification (x100) on to a screen on which the blade outline and tolerance envelope is drawn. The position of the probes relative to the tolerance envelope are noted by the operator as the probes are drawn across the blade to form the inspection process. The blades are inspected across three positions on the aerofoil, centre of the aerofoil and towards the root and tip.

The calliperscope is simple in design and is easy to use. It is operated by non-specialist female personel. The blade type under inspection can be conveniently changed by modifying the clamping arrangement and renewing the master profile drawings on the viewing screen. It can be used to inspect more difficult shaped aerofoil sections than the point gauging system because only two probes are in contact with the blade at any one time as opposed to eighteen for the point contact gauge. In the point gauging system there are difficulties in getting the probes physically close enough together on the small radius curves of the concave surface of some turbine blades. However, the calliperscope is somewhat slower than point gauging.

The calliperscope does have a number of disadvantages. Only three sections of the aerofoil are examined. The sections are only measured with respect to the overall tolerance envelope. No measurements or observations are made to indicate whether the blade is overall thicker than the nominal shape, either twisted or bent within the envelope, or has a surface undulation or roughness effect. The whole of the decision-making process relies on the human operator, who is subjected to outside distractions and fatigue, resulting in lack of concentration and possible errors of judgement.

To improve the inspection technique the objective of this research was to increase the area of the blade that was inspected by covering up to 20 sections and to reduce or eliminate the decision-making responsibilities carried by the operator by the use of a computer to analyse the difference information. The overall differences can be quantised by the computer into twist and bending effects plus localised differences. Using this information it is anticipated that it will be possible to reduce the rejection rate. For example, a blade may have the correct aerofoil section but it may be bent so that it gives an out of tolerance condition on the calliperscope. This may, however, be an acceptable condition aerodynamically and the computer can be programmed to pass this condition. The computer output can either be a go/no-go indication or present the difference information in an easily assimilated form.

1.2.3 Point Gauging.

The system provides a series of point measurements of the dimensions on the whole of the blade including the fir tree root and shroud. This usually involves 18 point measurements on the aerofoil. A mechanical lever type probe is used to measure the blade and a transducer is used to measure the position of the probe lever so as to calculate the actual position of the probe head. The principal technique used to form the measuring transducer was air gauging which has now been superceded by a differential transformer transducer system. The differential transformer is more compatible with electronic instrumentation.

For air gauging the needle of a small needle valve is attached to the arm of the mechanical probe and air is fed through the valve and the effective back pressure caused by the valve measured by a manometer. This back pressure is a measure of the position of the valve needle, hence probe position. There are a number of variations to this system.

The differential transformer type transducer gives a voltage output proportional to the position of the mechanical probe of the transducer. The probe forms the core of the transformer which slides within the centre of the two windings, hence altering the coupling efficiency between the primary and secondary windings. A particular r.m.s. voltage is applied to the primary from an oscillator and the output voltage from the secondary gives the position of the transducer probe. The use of the transformer type transducer increased the flexibility of the measuring system and a number of probes can be scanned in turn and an overall go/no-go system used. Also where there are particular errors outside the tolerance band the error on any probe can be measured individually to allow more discretion to be used by the operator as to whether this component has to be rejected or not.

The point gauging system is automated to a high degree and is operated by unskilled personel. It is, however, limited to 18 point measurements per blade and when the type of blade being inspected is changed the whole of the mechanical probe assembly must be changed, at a cost of approximately £1,000.

1.2.4 Disadvantages.

Both of these systems take measurements only at specific points or along lines on the blade, leaving a large proportion of the surface unexamined. Hence, the blade could be out of tolerance over a significant proportion of its surface and still comply to the inspection requirements, which could affect its performance. More scans and points can be used, but this will greatly increase the complexity and time involved in the inspection process and consequently the cost. The point gauging system is also difficult to use on turbine blade aerofoils because the curvature of the aerofoil section is high and it is extremely difficult to set the probes in the correct measuring position at the correct angle. Consequently, in the majority of cases the calliperscope is used.

As with all mechanical probes, wear on the points of the measuring probes caused by routine use is a problem requiring frequent adjustment or replacement and a small change in the actual measurement during use.

1.3 FUTURE REQUIREMENTS.

1.3.1 Use of Computers.

Manufacturing tolerances on turbine blades are being reduced because the aerodynamic performance of the blades becomes more critical as the engine efficiency increases. As an example of the changing trend in manufacturing tolerances, the overall tolerance envelope for the majority of turbine blades has been reduced from 0.010" to 0.007". Ripples or undulations in the surface finish across the direction of the airflow are important and limits are imposed on the amplitude and frequency of this phenomenon. These factors affect the boundary layer conditions, which are becoming increasingly important as surface film cooling is being used to achieve higher gas working temperatures. Consequently, more information is required about the shapes and manufacturing tolerances of the blades being produced. This requires more point measurements, making the mechanical techniques impractical. Hence, other forms of measuring transducers must be used that are either optical or purely electronic. To cope with the increased information in a reasonable time some form of computerized analysis is required or the time penalty per blade using present techniques will be too great.

The point gauging system takes approximately 15 seconds to measure one blade giving 18 points of measurement but the number of points cannot be greatly increased above this value. The calliperscope requires approximately 45 seconds per blade for three sections. If this is increased to 10 sections this will take approximately 4 minutes allowing some time for the operator to perform some general analysis of the data. The time involved plus the burden placed on the operator to handle a large amount of visual data will make this system impractical when compared to an estimated 40 seconds per blade for an electric-optical computer linked system that includes automatic data manipulation.

The use of computers in dimensional inspection is being applied and studied within the manufacturing industries both for basic inspection and control and monitoring of machine tool performance as reviewed by Carlisle and Bugden [10]. Examples of these include tube thickness gauging, lathe control, rod diameter measurements, and precision profile measurements. The use of computers to store and manipulate dimensional data has been demonstrated by Watkins [11] and Aveyard [12]. In the system described by Watkins [11] five measurements were taken on a small mass-produced component and processed by the computer to give a go/no-go situation. The computer was also used to store and analyse the general trends of the errors to improve manufacture procedure. Aveyard [12] described a basic computer linked system which was used on turbine blades. This used a mechanical probe/transducer system to measure 30 points on the aerofoil of the turbine blade, 15 on the concave surface and 15 on the convex, and the errors compared to the master component calibration was given in a paper printout form. The systems described above still only measure a small number of points and compare this to specific information without processing the differences to determine the overall difference, such as twisting or bending. For the quantity of information provided these techniques are expensive, £10,000 for 30 points,and still require the mechanical probe retooling and setting if the component is changed, cost £1,000.

The Ferranti-Cordax 3000 inspection machine [13] represents a further development in so far as it is commercially available and takes 112 point measurements. This still uses a mechanical transducer to take the measurements and only provides point by point differences from the norm. It is principally used on large objects such as shadow masks for colour cathode-ray tubes and the overall inspection cycle takes 15 minutes.

The present computer linked inspection machines have a number of limitations with their application in industry. They are expensive, slow, and only perform a small amount of data manipulation. Thus they are not adequate for turbine blade inspection. Blade inspection requires a technique which is capable of examining the blade aerofoils at a rate greater than 1 per minute. The surface must be examined in detail with at least 50 measuring points per scan for at least 10 scans with an overall measuring accuracy of 0.001".

Small computers have a data input rate of approximately 1000 words per second, which means that in the present inspection machines the computer is being under-utilized since the data input rate is much lower at approximately 10 words per second. This is limited by the rate at which the mechanical measuring probe can be manipulated.

To increase the data input rate into the computer it is proposed to use an optical contouring system with a slow scan television interface between the optical system and the computer. This would be capable of a data input rate of 1000 words per second into the computer. With the increased quantity of data and data input rate the computer would be used more effectively and it would be possible to inspect the blade in less than 1 minute and present the dimensional differences in an easily assimilated form. In such a device the component could be changed without retooling the measuring system and the computer used to serve several measuring units.

A fundamental difference and advantage of any optical/computer system of inspection over the present methods is the possibility of comparing a component to computer generated design information rather than a physical master. Turbine blades are now designed by computer and this data is used to make drawings from which a master blade is made. The manufacture of these blades is difficult as they have complex profiles and are to a large extent hand-made to an accuracy of $\pm$ .002". A relatively large number of them have to be made as the blade designs are frequently changed in the development of an aeroengine. Consequently the direct inspection from computer data would eliminate the need for a master blade to set up the inspection machines.

1.3.2 Dimensional Analysis of Development Components.

As well as the need for optical inspection techniques in the inspection of turbine blades during manufacture there is a requirement in the dimensional measurement of blades that are under development tests. As the result of the need to continually develop the aeroengine to improve the overall efficiency, research into improving turbine systems has to be made. Subsequently turbine blades are being subjected to higher temperature conditions and higher overall stresses to increase engine thrust and efficiency. During this work there is a need to measure the distortions and resultant damage produced by these temperature and stress effects. At present the only method of obtaining this information is by the standard metrology techniques using micrometer gauges. This is laborious, slow and costly if the measurement is required over a large number of points. Because of these difficulties this type of measurement is seldom used, so that in a number of examples very little actual distortion information is used within this research. Consequently there is a requirement for a form of comparison of a component before and after it has been subjected to high thermal and mechanical stress conditions to measure the resultant distortion. The distortions are of the order of between 25 and 500 microns (0.001 to 0.02") and the detailed surface finish of the component changes during the test.

Direct holographic interferometry is not feasible in this case because the overall distortions of 25 to 500 microns are too large and result in higher spatial frequency fringes than can be resolved by the observing optics.

This specific requirement and other similar measuring problems increase the need for a method for obtaining a detailed measurement of the three-dimensional shape of a component.

1.3.3 Economic Considerations.

The basic cost of an electro-optical contouring system with a form of computerized data handling would be more expensive than present systems but would be more efficient. In the long term the overall cost of a computer linked system would be the same or less than the present calliperscope. The computer would be used on a time sharing basis to run several optical units. Each unit is expected to be faster than the equivalent calliperscope or point gauging unit. To change the type of blade to be examined would require reprogramming the computer to provide the new shape for comparison, whereas with a system such as the point gauging the whole of the mechanical probe unit has to be substantially modified or renewed at the cost of the order of £1,000. In addition, the cost of small computers is decreasing as the state of the technology advances and so makes their use more attractive.

For the examination of components subjected to thermal stressing, the actual ability to measure distortions for comparison with the theoretical predictions represents a substantial saving in time and an increase in practical knowledge of the behaviour of the component.

Chapter II.

Methods of Contour Generation.

2.1 INTRODUCTION.

In this chapter the results of the investigation into the holographic and moiré fringe methods of generating surface contours are described. Two holographic methods of surface contouring were studied, two wavelength and two refractive index. The former was first developed by Hildebrand and Haines [7] and the latter by Shiotake [8]. The main emphasis was placed on the examination of the feasibility of the use of these techniques as part of a routine inspection system. To enable the dimensional data to be automatically processed the contour information should be in a form where it could be accurately fed into a computer by the use of an electro-optical interface.

Holographic contouring was found not to be ideally suited for this purpose and a moiré shadow contouring technique as described by Meadows [9] was examined. A modified version of moiré contouring was developed for use in conjunction with image scanning and computer processing.

2.2 SPECIFICATION OF REQUIREMENTS FOR OPTICAL BLADE INSPECTION.

The requirements of the dimensional analysis system for turbine blades imposed a number of limitations and requirements upon the method of generating depth contours.

a) The size of the turbine blades to be inspected vary from an aerofoil length of 2 inches up to 7 inches with a depth variation across the blade width of between 0.2 and 1.0 inches.

b) The contour depth interval should be comparatively large, greater than or equal to 0.010", so as to keep the number of contours across the object to a reasonable number.

c) Required measuring accuracy is ± .001" indicating that the component shape or differences must be measured to an accuracy of

1/10 contour fringe interval or greater.

d) The contour technique must provide the information as quickly as possible with a minimum of adjustment or photographic processing.

e) The contoured images must be of sufficient intensity to enable a television camera to be used as an optical to electronic information interface.

f) The contour fringe intensity should have a sufficiently low noise level to enable the computer linked measuring system to comply with condition (c).

g) The comparison information must be clearly presented in a form easily assimilated by the operator, either directly as a simple optical fringe form, on a television monitor to minimize eye strain, or as a form of printout, either paper or C.R.T., denoting the general differences, bending, twisting plus details of localized differences.

h) The overall system should be simple and capable of operation on a routine basis by non-specialist personnel.

2.3 PRINCIPLES OF HOLOGRAPHY.

The detailed analysis of the formation of holograms, the coherence requirements of the illuminating source and the factors affecting the quality and resolution of the hologram have been previously documented by the author in the thesis [1] and will not be discussed in this presentation.

When a hologram plate is accurately repositioned back into the original system used to form the hologram and illuminated with the original coherent reference beam, the wavefront diffracted by the hologram is identical to the wavefront scattered from the object's surface. Since the two waves are indistinguishable they may be interchanged and hence it is possible to compare the reconstructed wavefront with the scattered wavefront originating from the object at some later time. Any difference between the object resulting, for example, from an applied stress and its original reconstruction is shown as interference fringes similar to those produced by standard interferometry. This is the principle upon which holographic interferometry is based, Haines and Hildebrand [14].

In a similar manner two holograms may be recorded on the same photographic plate representing the object at different instances in time and the resultant reconstruction will show any displacement of the object that has occurred between the two exposures in terms of fringes. This is referred to as double exposure holography.

2.4 TWO WAVELENGTH HOLOGRAPHIC CONTOURING.

Holographic interferometry may also be used to generate depth contours at much larger intervals than is possible by ~~the~~ previous methods. There are three techniques, double source, double wavelength and double refractive index. The double source technique, as shown in fig. 1, was basically a fringe projection technique. It was not able to accommodate a convoluted surface, as shown in fig. 1b, and consequently was unsuitable for turbine blade analysis. The other two were found to be suitable for turbine blade inspection and were considered in detail. The two wavelength contouring technique is based upon the interference between two images of the same object formed holographically by using two different wavelengths of laser light. The contour depth is a function of the two wavelengths used according to the relationship

$$\frac{\lambda_1 \cdot \lambda_2}{2\,|\lambda_1 - \lambda_2|} \qquad \ldots\ldots \quad (1)$$

and is thus precisely defined from a knowledge of λ_1 and λ_2. The system is limited to a laser that will operate at different wavelengths and with sufficient coherence for holography, e.g. the argon ion, or krypton lasers and some of the latest dye lasers that are optically pumped by an argon ion laser. With the continual development of dye lasers it is expected that it will be possible to generate contours of around 250 micron depth interval.

2.4.1 Contour Fringe Formation.

The two wavelength contouring technique was first discussed by Hildebrand and Haines [7] and further developed by Zelenka and Varner [15]. The optical telescope system used to generate the contour fringes is shown in fig. 2. An image of the object with unit magnification is relayed to the hologram plate, H, by a telescope. (L_1 and L_2) The object is illuminated by a plane wave propagated in the same direction as the axis of the telescope by means of the beamsplitter B.S.1. Zelenka considered the effects of two wavelengths of light upon the magnification and position of the reconstructed image in space. A holographic image of an object taken at wavelength λ_1 and then reconstructed at wavelength λ_2 will change its position in space along the axis of the telescope and also change its lateral magnification. If the object is also illuminated at wavelength λ_2 there will be a difference in position of the holographically reconstructed image and the telescope image. The difference is shown as interference fringes.

For a small portion of the hologram formed at wavelength λ_1 using a plane reference wave and then reconstructed by a plane reference wave at wavelength λ_2 the radial distance from a point on the hologram to a point on the recorded image R_1 is imaged at a distance R_1' when reconstructed. The relation between these radii is a function of the two wavelengths given by

$$R_1' = (\lambda_1/\lambda_2)\, R_1 \qquad \ldots\ldots \quad (2)$$

Because the telescope is used to form an image of the object on the hologram plate the radial distances are kept to a minimum.

The hologram plate acts as a complex diffraction grating in two dimensions to reconstruct the image when illuminated with the reference beam and so obeys the normal diffraction grating equations. Thus if the hologram is recorded in one wavelength and illuminated at a different wavelength with the reference beam still at the same angle, the image is slightly displaced by the change in the angle of the wavefront diffracted by the hologram. This effect changes both the lateral magnification and position of the image. To overcome this phenomenon and keep the two images exactly superimposed the reference beam angle must comply with the equation.

$$\sin \theta_{rec} = (\lambda_2/\lambda_1) \sin \theta_{ref} \qquad \ldots\ldots (3)$$

where θ_{ref} and θ_{rec} are the angles of the reference and reconstruction beams respectively as shown in fig. 3a.

To obtain the contour fringes the apparent displacement or difference along the optical axis of the telescope must be less than its depth of field. The depth of field for a single lens, fig. 3b, is given by Born and Wolf [16].

$$dz = 4\lambda \left(\frac{V}{D} \right)^2 \qquad \ldots\ldots (4)$$

λ = wavelength of light used.

V = distance of image from the lens.

D = diameter of the lens aperture used.

Thus for the telescope the depth of field on the object is given by

$$dz = 4.\lambda. \left(\frac{F}{D} \right)^2 \qquad \ldots\ldots (5)$$

F = focal length of objective lens, which equals that of the eye piece for unit magnification.

Using this criterion Zelenka showed that provided that a small aperture was used (F.No. ≥ 40) contours of planes perpendicular to the optical axis were formed with a depth interval.

$$\Delta z = \frac{\lambda_1 \cdot \lambda_2}{2|\lambda_1 - \lambda_2|} \qquad \ldots\ldots (6)$$

2.4.2 Limitations.

The use of the unit magnification telescope to relay the image of the object on to the hologram formed a fundamental limitation on the system in so far as the depth of field would be small. The resolution of a telescope with unit magnification is defined in terms of the minimum separation between two point sources in the object plane that can be resolved by the telescope and is given by Born and Wolf [16].

$$\text{Minimum resolvable separation} = 1.22\lambda\,(F/D) \qquad \ldots\ldots (7)$$

The telescope resolution is also defined in terms of the reciprocal of the minimum resolvable separation and denoted as the resolution limit. This is quoted in terms of cycles/mm.

$$\text{Resolution limit} = \frac{0.82}{\lambda}\left(\frac{D}{F}\right) \qquad \ldots\ldots (8)$$

A phenomenon common to coherent optical systems and known as a speckle pattern affects the subjective appearance of any object illuminated with coherent light. This gives the object an appearance of being covered by a series of speckles rather than the uniform appearance of an object illuminated with incoherent light. The speckle effect occurs because interference takes place between a large number of randomly phased disturbances generated by the light being scattered off the optically rough surface of the object, as discussed by Burch [17, 18].

The size of these speckles is defined as equal to that of the minimum resolvable separation of the optical system that is used to observe the speckles.

$$\text{Speckle size} = 1.22\lambda\,(F/D) \qquad \ldots\ldots \quad (9)$$

The variation of the apparent local intensity distribution across the image that was produced by the speckles was examined by Burch [18]. This is described in terms of the probability of the relative brightness of the speckle being between the values s and s + ds, W(s)ds. The variation is also an indication of the degree of contrast or granularity of the speckle pattern and is given by

$$\text{Variance} = \sigma^2 = \int_0 s^2\, W(s)\, ds - 1 \qquad \ldots\ldots \quad (10)$$

Burch [17] discussed the speckle brightness probability function for a finite number of n equal disturbances which was represented in terms of infinite integrals of zero-order Bessel functions.

$$W_n(s) = n/2 \int_0^\infty z\, J_o(z\,\sqrt{x.n}\,)\,.\,[J_o(z)]^n\, dz \qquad \ldots\ldots \quad (11)$$

This function varies with the number n disturbances. When the aperture D of the observing optics is reduced the number of disturbances n that can be distinguished is also reduced. Burch [17] showed that at the resolution limit of the optics where n = 2 the probability function is principally at zero or twice the average brightness of the image. Hence from equation 11 good contrast speckles are formed whose size is determined by equation 9.

The depth of focus of the telescope required to observe the majority of turbine blades varied from 5 mm to 25 mm. The corresponding aperture settings on the telescope were F.50 and F.115. These produced minimum resolvable separations of 0.03 mm and 0.06 mm. Under these F. Number conditions the speckle diameters of 0.03 to 0.06 mm produced an obtrusive speckle pattern on the contoured image and degraded the overall quality of the image.

The object size was limited to less than that of the effective diameter of the objective lenses used in the telescope. The amount of light from the object transmitted through the telescope to the hologram was limited by the small aperture, which increased the exposure time of the hologram.

The requirement that the reference beam angle should be rotated through an angle when moving from the recording to reconstruction mode, to keep the two images exactly superimposed, involved an adjustment to the reference beam which must be made by the operator. The angle of rotation was of the order of 3 mrad for a reference beam angle of 23° using wavelengths of 476.5 nm and 472.7 nm. Varner [19] used a diffraction grating set perpendicular to the optical axes of the telescope and so in a plane parallel to that of the hologram. This was illuminated by the collimated reference beam at normal incidence and the overall position of the grating arranged so that the light from one of the diffraction orders was projected on to the centre of the hologram.

2.4.3 Experimental Results.

A two wavelength laser with the correct wavelength separation to produce 250 micron (0.01") contours was not available. The tests were carried out using a Coherent Radiation Ltd 2W argon laser with power outputs of 150 mW each at wavelengths 501.7 nm and 496.5 nm to give 15 micron ($\div .5 \times 10^{-3}$") contour depth interval and 250 mW at 476.5 nm and 30 mW at 472.7 nm for 30 micron contours.

A telecentric optical system was used as shown in fig. 2 with an adjustable mirror used to change the reference beam incident angle on the hologram for the two wavelengths. A coin was used as an initial test object and this represented an irregular and complex shaped surface with a depth variation of approximately 0.01" so as to produce a reasonable number of contour fringes. A turbine or compressor blade was not initially used at these contour intervals, as the 0.30" change of shape represented 300 to 600 fringes which were beyond the resolution capabilities of the optical system.

Initially live fringe holographic interferometry was used to observe the contour fringes. This involved taking a hologram with one wavelength, developing the hologram, relocating it in the original position and then illuminating the interferometer with the second wavelength. The telescope and holographic images were observed as the reference beam angle was changed. This produced little success as only very low contrast fringes were obtained. This was primarily caused by the inherently low diffraction efficiency of the hologram (5%). Consequently the reconstructed image was extremely weak even though the reference beam intensity was increased to compensate. Photography of the resultant contour images was just possible.

Some spurious fringes were formed in the holographic interferometer by emulsion shrinkage on developing and drying the hologram. Additional fringes were produced by misalignment when relocating the hologram even though a kinematic design of plate holder was used, as described by Hockley [1]. To overcome this an in situ processing liquid gate hologram plate holder similar to the type described by Biedermann [20] was made and used, which improved the overall quality of the contour fringes.

The required accurate adjustment of the reference beam between recording the hologram at wavelength λ_1 and reconstructing the processed hologram at λ_2 greatly detracted from the usefulness of the system as a routine method. To overcome this a diffraction system in the reference beam was used as discussed in section 2.4.2. The experimental system used is shown in fig. 2. The grating was lined at 30,000 c/inch with a first order diffraction angle at 36° 12' at 501.7 nm with a change of angle by 26' to 35° 54' at 496.5 nm. To obtain good quality contour fringes using the single exposure holographic interferometer extreme care was required to set up the diffraction grating at the correct attitude to within a fraction of a minute of arc. This was achieved by using a rigorous setting up procedure.

The double exposure method of generating the contours was also used in which the hologram was exposed in two stages illuminated at different wavelengths and reconstructed with one of them. The contour fringes were frozen on to the reconstructed image. This method eliminated the image intensity mismatch and the tests proved that it was possible to obtain repeatable and reasonably good fringes although the same rigorous setting up procedure was needed. Contours at both 30 and 15 microns were obtained. Fig. 4a shows a photograph of the contoured image of the coin, contoured at 30 micron intervals. The coin was tilted slightly with respect to the optical axis of the contouring system as shown by the horizontal fringes. Fig. 4b shows a contoured reconstruction of a test object with four angular slopes at 1°, 2°, 3° and 5°. These slopes were clearly defined by the contours.

Part of a small compressor blade was contoured but the fringes were only formed over a small portion of its chord due to the curvature producing a large number of 30 micron contours, and the observable depth over which the contours occurred was approximately 1.2 mm.

The overall system was generally inefficient in the use of the available light,due to the use of the beamsplitter in the telescope for normal incident illumination and the F.No. 50 optics needed for blades, but this was a factor in both holographic systems. It was not possible to use the beam transmitted through the beamsplitter as the reference beam, due to the effects of the fringes produced by internal reflections within the mirror even though an anti-reflection coating was used on the second surface.

Hence summarizing, the system advantages were:-

a) Any shaped object could be considered.

b) Contour depth intervals were accurately repeatable.

c) Simple to operate although complex to set up.

Disadvantages:-

a) Contour depth not variable; 30 microns was the maximum depth obtainable using an argon ion laser, although tunable dye lasers are now becoming available.

b) The object size must be less than the usable diameter of the telescope objective lens.

2.5 TWO REFRACTIVE INDEX CONTOURING.

Two wavelength contouring was found to be feasible but the need for a two wavelength laser would increase the cost above that of standard holographic systems. The two refractive index method of contouring, however, could be operated using normal single wavelength lasers, thus reducing the overall cost of the system.

This method principally involves the double exposure method of taking holograms as discussed in section 2.3 and the contour fringes are formed by the interference between two images formed in different refractive index media. The object is placed in an enclosed tank with a window through which it can be observed. A standard holographic system as shown in fig. 5a can be used to observe the object. The first exposure of the double exposed hologram is formed with the object immersed in a medium of refractive index n_1. The tank is then replenished with a second medium of refractive index n_2 for the second exposure of the hologram. The refractive index media can either be a gas or a liquid. The effect of the different refractive index media within the immersion tank is to change the effective wavelength of the light. The wavelength of light λ_1 in any medium with refractive index n_1 is related to its absolute wavelength in vacuo, λ, by the function

$$\lambda_1 = \lambda/n_1 \qquad \ldots\ldots \quad (12)$$

Similarly $$\lambda_2 = \lambda/n_2 \qquad \ldots\ldots \quad (13)$$

The two images reconstructed by the processed hologram have consequently been formed at different wavelengths and the images interfere to produce depth contours as described by equation 1 in section 2.4, where the wavelength difference is defined by the refractive index change.

The accuracy and repeatability of the contour depth interval is dependent upon the accuracy with which the refractive index is changed. The basic setting up procedure is less complex than that of the two wavelength technique.

2.5.1 Two Refractive Index Contour Fringe Formation.

This contouring technique was first introduced by Shiotake [8] and later discussed by Zelenka and Varner [21]. The contour hologram is recorded as described in section 2.5. On reconstruction of the hologram the two images produced in the tank, using different refractive indices, will be in different positions relative to the tank's glass window, and will interfere to produce difference contours as in the two wavelength contouring process. The optical path length differences between the resultant images are only affected by the two refractive indices within the tank n_1 and n_2. When the holographic reconstruction is imaged onto the plane of a viewing system the complex amplitudes of the two images will be of the form

$$A_{Im} = A_1 \exp [i\phi_1] + A_2 \exp [i\phi_2] \quad \ldots\ldots (14)$$

where A_1 and A_2 are the amplitudes directly related to the brightness of the two images. These are usually made equal by exposure control. The phase terms are dependent upon the optical path length in each optical medium. For an immersion tank system as shown in fig. 5b the phase terms ϕ_1 and ϕ_2 for a point (x,y) on the object a distance z(x,y) from the inner surface of the window.

$$\phi_1 = k_1\, z(x,y)\, (\cos\theta_{11} + \cos\theta_{12}) \quad \ldots\ldots (15)$$

$$\phi_2 = k_2\, z(x,y)\, (\cos\theta_{21} + \cos\theta_{22}) \quad \ldots\ldots (16)$$

k_1 and k_2 = the wavenumbers in the refractive index media n_1, n_2.
θ_{11}, θ_{21}, θ_{12} and θ_{22} are as defined in fig. 5b.

The incident and observing angles are related by Snells Law.

$$\frac{\sin\theta_{11}}{n_1} = \frac{\sin\theta_{21}}{n_2} \quad \ldots\ldots (17)$$

and

$$\frac{\sin\theta_{12}}{n_1} = \frac{\sin\theta_{22}}{n_2} \quad \ldots\ldots (18)$$

The resultant intensity of the image is

$$I = (A_{Im})^2 = 2A^2\, [1 + \cos(\phi_1 - \phi_2)] \quad \ldots\ldots (19)$$

In practice the angles of illumination and observation are made to be equal or close to zero hence equation 19 becomes

$$I = 2A^2 \left[1 + \cos\left(2(k_1 - k_2)\ z(x,y)\right)\right]$$

Substituting for the wavenumber k_1 and k_2

$$I = 2A^2 \left[1 + \cos\left(\frac{4\pi}{\lambda}(n_1 - n_2)\ \ z(x,y)\right)\right]$$

This function represents plane contours parallel to the inner surface of the window with an interval

$$\Delta z = \frac{\lambda}{2|n_1 - n_2|} \qquad \ldots\ldots \quad (20)$$

If this is considered in terms of effective wavelength with the two refractive media

$$\lambda_1 = \lambda / n_1$$

and $$\lambda_2 = \lambda / n_2$$

Then equation 20 becomes

$$\Delta z = \frac{\lambda_1 \cdot \lambda_2}{2|\lambda_1 - \lambda_2|} \qquad \ldots\ldots \quad (21)$$

which is identical to that of the two wavelength contouring system.

To obtain plane contours the incident and observing angles are kept equal to zero and to achieve this a concentric telescope holographic system is used. In this case the hologram is placed in the Fourier transform plane of lens L_1, where the telescope aperture is located.

At the Fourier plane the optical information is distributed in the form of a spatial frequency spectrum with zero frequency on the optical axis of the telescope and the spatial frequency increasing radially from the axis. Under these conditions the maximum quantity of useful information is transmitted through the optical system on to the hologram for a given aperture diameter. This leaves the image plane free for normal observation and photography.

2.5.2 Refractive Index Media.

The media used to change the refractive index can be a gas or a liquid. Since the technique is for use on turbine blades on a routine system a liquid which will wet the blades and get contaminated by dirt from the blade is not suitable. Hence a gas with a high refractive index must be used. Freon 12 or Arcton 12 (Dichlorodifluoromethane CCl_2F_2) has suitable properties and is reasonably inexpensive. The refractive index at 20° C. and a pressure of 760 millimetres of mercury is 1.001055 at the mercury green line 546.2 nm., Horvath [22]. This is related to the density of the gas by the Gladstone-Dale equation, Partington [23].

$$(n - 1) = \rho.k. \qquad \ldots\ldots \quad (22)$$

n = the refractive index

ρ = gas density

k = a constant.

For the change of refractive index with gas pressure the ideal gas equation gives the change of density with pressure at constant temperature as

$$\frac{\rho_2}{\rho_1} = \frac{P_2}{P_1} \qquad \ldots\ldots \quad (23)$$

ρ_1, ρ_2 = the densities at pressures P_1 and P_2.

In a practical system care must be taken to keep the general surroundings at a constant temperature and ensure that the temperature within the pressure chamber remains constant when being pressurized to avoid any change in the pressures caused by temperature variation. This will impose some environmental control on the overall system and impose a maximum rate at which the chamber can be pressurized.

The change in refractive index with respect to increase in pressure is given by the equation

$$n_2 - n_1 = \left(n_1 - 1\right)\left(\frac{P_2}{P_1} - 1\right) \qquad \text{..... (24)}$$

Therefore the effective contour depth is

$$\Delta z = \frac{\lambda}{2}\left[\left(n_1 - 1\right)\left(\frac{P_2}{P_1} - 1\right)\right]^{-1} \qquad \text{..... (25)}$$

Hence for an increase in pressure from one to two atmospheres the contour depth at 514.5 nm is 0.24 mm (0.0094"). So the pressure increase from atmospheric pressure needed to produce 0.25 mm contour is just less than one atmosphere.

Fig. 6 shows a graph of the pressure increase required to produce various contour depth intervals.

Similarly the refractive index change from vacuum to Freon 12 at one atmosphere produces a contour depth interval of 0.24 mm.

2.5.3 System Limitations.

As a telecentric hologram recording system was used to obtain plane contours the limitation on the available depth of field, resolution and object size as discussed for the two wavelength technique, section 2.4.2, were applicable to this system. However, the image size limitation could be relaxed if a single observing lens system was used and the angle of observation increased from near zero provided that a correction for the change in contour depth interval was applied as the angle was increased.

2.5.4 Experimental Study.

The telecentric hologram system was used as shown in fig. 2 and discussed by Zelenka and Varner [21]. The blade was placed in an enclosed chamber with a 9 inch internal diameter and a 10" diameter x 0.75" thick armour plate glass window. A strong chamber was used to allow air to be pressurized up to four atmospheres to produce a refractive index change of 1.013×10^{-3} for 0.01" depth interval contours. Freon 12 (CCl_2F_2) was the gas used rather than air as this had a significantly higher refractive index change with pressure. Two principal methods of using the freon to change the refractive index were used. Firstly the chamber was evacuated and the refractive index difference between vacuo and the Freon at just above atmospheric pressure was used to produce the 0.01" contours. Secondly without the need for a vacuum pump the chamber was flushed with freon for a short period to expel the air and the refractive index difference between atmospheric pressure and at a pressure of 15 psig used to give 0.01" contours. This was the simpler and faster of the two methods for a routine system and was used for most of this work. Fig. 6 shows a graph of the required pressure difference above atmospheric required to produce various depth contours.

The telescope lenses used in this system were the same as used for the double wavelength system to obtain a direct comparison between the techniques. The chamber was angled slightly with respect to the optical axis of the telescope to avoid the specular reflection from the chamber window. This did not affect the contours as they were referenced with respect to the chamber window but did slightly decrease the effective depth of field of the telescope due to the skew of blade. Both the holographic interferometer and double exposure techniques were used with excellent results with various depth contours, an example of which is shown in fig. 7.

An aperture setting of F. No. 40 and above was required to produce contour fringes over most of the turbine blade. At these apertures the limited resolution and laser speckle effect gave the contour fringes a definite granular appearance. The contours were observable but the accuracy with which the exact location of the maximum and minimum of the fringes was greatly reduced. Fig. 8a shows the appearance of 0.010" contour fringes of the concave surface of a turbine blade (1:1 magnification) with an aperture of F.No. 40. The fringes were visible only over part of the surface and towards the trailing edge the spatial frequency of the fringes were getting towards the limit of the optics due to the speckle effect. Decreasing the aperture to F.No. 80, fig. 8b, showed the increasing prominence of the speckle effect and that the fringes towards the trailing edge could not be resolved. A microdensitometer scan across the negative of fig. 7., along the blade chord, fig. 9, illustrated the effects of the speckle noise. It was extremely difficult to locate the positions of the maximum and minimum intensity points of the fringes. The spurious peaks and troughs produced by the speckles would make automatic reading of such information difficult.

The high spatial frequency of the contours towards the trailing edges of the blade in fig. 8 and the limiting effect of the optics showed that contour depths of greater than 0.01" depth must be used to enable the whole surface to be analysed. Hence to retain a $\pm$ 0.001" dimensional measuring accuracy the contour positions must be known more accurately.

It was found difficult to obtain good contrast contours on the normal finish of a turbine blade because of the specular reflection effect of the surface.

The overall system was simple to operate but the need to change pressures between exposures and the time taken to load and remove the blade from the chamber would be extremely inconvenient for a routine system.

Advantages.

a) Simple optical system.

b) Any contour depth could be achieved.

Disadvantages.

a) Required a chamber to enclose the object.

b) Access to the component was limited.

c) Size of component was limited by the diameter of the telescope objective.

d) Contour depth repeatability depended on the accuracy of the gas pressure adjustment.

2.6 MOIRE FRINGE CONTOURS.

The holographic contouring techniques produced good contoured images of turbine blades but for any electro-optical measuring system had a distinct disadvantage created by the speckle pattern moiré superimposed on the contour fringe intensity function as illustrated in fig. 9. This made the accurate location of the contour fringe peaks and troughs by an intensity measuring device difficult and the measurement between these values to better than a 20% accuracy impossible. This raised serious doubts as to the suitability of holographic contouring for the envisaged inspection system as an electro-optical measuring device must be used to link the optical system to a computer to cope with the increased number of measuring points being used, as discussed in chapter I.

To overcome this problem and to simplify the overall concept of the contour generation system the alternative moiré fringe contouring technique was examined. This method of contour generation had been known for a number of years, Theocaris [24] and was re-introduced in the literature in 1970 as a measuring technique with the evolution of contour holography and its applications by Meadows [9], Takosaki [25] and Allen [26]. The first application of moiré techniques to any form of component inspection was by Burch, in 1968 [27] who used a combined holographic and moiré system to form contour fringes on a master component and compared the production component with the contoured holographic image of the master. This was a complex system and suffered greatly from the problems of the low diffraction efficiencies of holograms and was not developed into a practical system.

Moiré contouring had a number of basic advantages over holography in so far as it was a real time system, and did not require a photographic process before the contour information was available. Nor was a laser required, as a white light source would be used. However, the minimum contour depth interval obtained would be limited by diffraction effects.

2.6.1 Moiré Contour Fringe Formation.

The theoretical analysis of moiré fringe systems for strain measurement has been well documented by Theocaris [24] and others. The formation of moiré contour fringes has been recently described by Meadows [9]. However, the basic formation of moiré fringe contours are discussed here in detail in order to introduce the concept of the fringe projection/image scan method of generating shape information.

The moiré contouring technique operates by comparing two grid patterns. A particular moiré technique is used where a shadow of a moiré grid is projected on to the surface of the object, fig. 10a, and its image is observed through the same moiré grid. In fig. 10a the grid is illuminated by a collimated beam of incoherent light, making an angle α with the normal to the grid. The shadow of this is viewed through the grid at an angle β with the normal to the grid. The light from the source is modulated by the grid to produce the shadow lines on the object.

Let the grid have a sine wave modulation function so that the light transmitted through the grid is modulated by the function.

$$T(x) = \tfrac{1}{2}(1 + \sin 2\pi x/p) \qquad \ldots\ldots \quad (26)$$

x = the position of any point across the grid

p = the period of the grid.

For a point (x,y,z) on the object, fig. 10a, the light illuminating it is from the point $(x - z \tan \alpha, y, o)$ on the grid. Assuming that the object's surface is near to a pure Lambertian diffuse surface where the light scattered from all parts of the surface is scattered by equal amounts in all directions, i.e. the amount of the source I scattered in any direction is a constant K, the light scattered from the surface is

$$I_o(x,y,z) = \frac{I.K.}{2}\left[1 + \sin[(2\pi/p)(x - z \tan \alpha)]\right] \qquad \ldots\ldots \quad (27)$$

This function is demodulated by the action of viewing the function through the original grid.

In this case the intensity function passes back through the grid at the point $(x + z \tan \beta, y, o)$ fig. 10a, and hence is modified by the function

$$T(x_1 + z \tan \alpha, y, o) = \left[1 + \sin[(2\pi/p)(x + z \tan \beta)]\right] \qquad \ldots \quad (28)$$

The resultant intensity reaching the observer is

$$I_I(x\ y\ z) = \frac{IK}{2}\Big[1 + \sin\left(\frac{2\pi}{p}\right)\left(x - z \tan \alpha\right) + \sin\left(\frac{2\pi}{p}\right)\left(x + z \tan \alpha\right)$$

$$- \tfrac{1}{2}\cos\left(\frac{2\pi}{p}\right)\left(2x + z(\tan \beta - \tan \alpha)\right)$$

$$+ \tfrac{1}{2}\cos\left(\frac{2\pi z}{p}\right)\left(\tan \alpha + \tan \beta\right) \qquad \ldots\ldots \quad (29)$$

From this equation the only term that is solely dependent upon the depth z is the last term.

$$\frac{IK}{4} \cos\left(\frac{2\pi z}{p}\right)\left(\tan\alpha + \tan\beta\right)$$

This produces the depth contours with a contour depth interval

$$\Delta z = \frac{p}{(\tan\alpha + \tan\beta)} \qquad \ldots\ldots (30)$$

These contours represent planes of equal depth parallel to the surface of the moiré grid. In the majority of practical cases the direction of observation will be perpendicular to the moiré grid, i.e. $\beta = 0$. Hence the contour depth interval is given by

$$\Delta z = \frac{p}{\tan\alpha} \qquad \ldots\ldots (31)$$

The other terms in equation 29 are dependent upon x and produce noise at approximately the same spatial frequency as the moiré grid.

In a practical system the illuminating source and point of observation are a finite distance from the grid so that the angles α and β vary across the object. In this case consider a point of illumination a distance h_1 above the grid and a point of observation a distance h_2 above the grid that are separated by a distance d, as shown in fig. 10b. The apparent frequency of the shadow of the moiré grid cast on to the object is dependent both on the distance z of the point from the grid and the height of the illuminating source above the grid. By similar triangles the apparent grid frequency p' becomes

$$p' = \frac{(h_1 + z)}{h_1} p \qquad \ldots\ldots (32)$$

This modifies the intensity modulation function at the object's surface to

$$I \propto \tfrac{1}{2}\left(1 + \sin\left(2\pi h_1 x/(h_1 + z)p\right)\right) \qquad \ldots\ldots (33)$$

Meadows [9] showed that in this case if the point of illumination and observation are at the same distance from the grid h contours are produced whose depth interval is dependent upon the depth being measured.

$$z_2 - z_1 = \frac{N_2\, ph}{d - pN_2} - \frac{N_1\, ph}{d - pN_1} \qquad \ldots\ldots (34)$$

where N_1 and N_2 are the fringe number.

If the distance h was much greater than z_1 this simplifies down to

$$z_2 - z_1 = \frac{Nph}{d} \qquad \ldots\ldots (35)$$

where N is the number of fringes between the two points.

In practice it is less difficult to make square wave moiré grids than sine wave grids. For the square wave transmission grid the intensity modulation function can be described in the form of a Fourier series.

$$T(x) = \frac{1}{2}\left[1 + \frac{4}{\pi} \sum_{\substack{n=1 \\ n\ \mathrm{odd}}}^{\infty} \frac{1}{n} \sin\frac{2\pi nx}{p}\right] \qquad \ldots\ldots (36)$$

In this case if $h \gg z$ contour depth interval is still

$$\Delta z = Nph/d \qquad \ldots\ldots (37)$$

and the intensity function of the contour fringes is of the form, Meadows [9].

$$I(\text{contours}) = C\left[1 + \frac{2}{\pi^2} \sum_{\substack{n=1 \\ n\ \mathrm{odd}}}^{\infty} \frac{1}{n^2} \cos\frac{2\pi}{p}\left(\frac{ndz}{h + z}\right)\right] \qquad \ldots\ldots (38)$$

This is a triangular intensity function as described by Rektorys [28].

2.6.2 Limiting Parameters.

A practical system for generating moiré contours using a square wave grid is shown in fig. 11. The overall size of the object is limited to the size of the grid. The quality of the resultant contours are also dependent upon the quality and accuracy of the grid lines so as to retain the higher order terms of equation 36. For the inspection technique and contour depth of 0.01", grids of spatial frequencies of the order of 100 cycles/inch are required. The limits on the performance of system to produce good quality contours depend upon depth of focus of imaging optics, diffraction effects and penumbra.

2.6.2.1 Depth of Focus.

As with the holographic methods of generating contours the depth of focus of the imaging optics was the principal limitation on the system. In this case both the moiré shadow fringes on the surface of the object and moiré grid must be within the depth of focus of the optical system. Beyond these limits the definition of both sets of grids diminish, which would reduce the contrast in the modulation of the function forming contour fringes. As in section 2.3.2 the depth of field is defined as

$$dz = 4\lambda \, (V/D)^2$$

Consequently, the component had to be placed as close to the grid as possible to obtain the maximum benefit of the depth of field of the system. This in fact was a disadvantage but not a significant one for turbine blades, which could be placed close to the grid.

2.6.2.2 Diffraction Effects.

The spread function produced by diffraction at the edge of the interface between maximum and minimum transmission of the lines of the square wave can be described by Fresnel diffraction. To a first approximation the position of the first maximum of intensity beyond the geometrical edge of the interface is given by Longhurst [29].

$$x = \left(b\,(r + b)\; 2\lambda/r\right)^{\frac{1}{2}} \qquad \ldots\ldots \quad (39)$$

r = the distance of source from the grid.

b = the distance from the grid of the surface on which the shadow is formed.

Examining this function for the laboratory contouring system, where the grid was illuminated at 45° with a point source .71 m. from the grid and the shadow of the grid falling on the object placed 12 mm behind the grid, the spread in the position of this maximum with illumination wavelength variation from .4 to .7 microns was approximately 1×10^{-3} inches. This also approximately represented the distance by which the light intensity spread into the geometrical shadow of the grid line. For a moiré grid of 100 cycles/inch this represented a spread function operating over 20% of the half period and so produced a marked blur on the shadow fringes. For grids of higher spatial frequencies the diffraction effects became even more significant and prohibit the use of contour depths of less than 0.01" on turbine blades.

2.6.2.3 Penumbra Effect.

The penumbra effect is defined as the extent of the blurring or spread Δx of the geometrical shadow of an edge of a line on a moiré grid at a distance b behind it when the grid is illuminated by a source of a finite diameter d_s situated a distance r in front of the grid. The region over which this function extends into the shadow from the geometrical edge is given by simple geometry as

$$\text{Extent of spread } \Delta x = \frac{b\, d_s}{r} \qquad \ldots\ldots \quad (40)$$

The effect of the penumbra effect was to decrease the size of the dark shadow of the grid and reduce the clarity of the grid line edges and this reduced the overall definition of the contour fringes.

For a small diameter source such as a high pressure mercury arc with a diameter of 1.0 mm the penumbra effect would be small but for a source such as a quartz halogen bulb with an overall filament diameter of 6 mm this effect would become significant. For the laboratory moiré contouring system where $r = .71\text{m}$ $b = .012\sqrt{2}\,\text{m}$ from incident angle of 45° $\Delta x = 0.02$ mm for the arc source and 0.12 mm for the quartz halogen source. The penumbra effect was negligible for the arc source with the 100 cycles/inch grid but for a quartz halogen source the shadow was considerably blurred which resulted in low contrast contour fringes.

2.6.3 Moiré Contouring Experimental Results.

The experimental evaluation of moiré contouring was carried out using a 100 W high pressure mercury arc light source, with a source diameter of approximately 1.0 mm. Moiré contour fringes were produced by the optical system shown in fig. 11 using turbine blades as test objects. Their aerofoil lengths varying from 40 mm to 80 mm. The quality of the moiré contours was heavily dependent upon the quality of the moiré grids. The initial results using an inferior quality master moiré grid gave very poor contrast fringes. A new 10" x 14" 50 cycles/inch master grid was obtained and secondary grids taken from the master using Agfa Gevaert 10E56 high resolution (3000 c/mm) holographic plates with a high photographic gamma. These were made with spatial frequencies from 50 c/inch to 150 c/inch.

Using the grids the quality of the moiré contours greatly increased. An example is shown in fig. 12. The contour depth interval is 0.02" using a 50 cycles/inch moiré grid with a 45° incident angle. The contoured shape of the blade was clearly visible and the grid lines were set parallel to the blade chord to:- a) minimize the variation of the blade's surface to the incident illumination to obtain uniform scattering intensity of the light across the blade, b) eliminate the grid noise when scanning along the blade chord as discussed in section 2.7, and c) to prevent aliasing between the contour fringes and the grid lines towards the trailing edge of the blade when the contour fringes approach the same spatial frequency as the grid lines.

Although the depth contours in fig. 12 were well defined over most of the blade the image of the moiré grid lines impaired the clarity of the contour fringes towards the trailing edge where the spatial frequency of the fringes was relatively high and made detailed analysis difficult. To overcome this effect Takosaki [25] suggested moving the moiré grid in its own plane at right angles to the grid lines during the formation of the photographic image. This was later discussed by Allen [26] in greater detail. This had the effect of averaging out the grid line fringes as the grid was moved, whereas the contour fringes remained stationary and unaffected, thus increasing the overall clarity of the contour fringes. For the square wave grid the movement was linear.

The effects of moving the grid in its own plane to average out the grid fringes showed a marked improvement in the quality of the contour fringes. In this case the grid was set parallel to the chord of the blade and a camera aperture of F.32 was used. Fig. 13a shows the contours at 0.02" depth interval plus grid lines and in fig. 13b the grid was moved linearly in its own plane by approximately 0.25" during the 2 sec. exposure time. The improvement in the clarity of the fringes was quite discernable.

A rig was made to enable the contour depth intervals to be set accurately. The Hg arc, moiré grid and camera were tied rigidly together by the rig with the axis of observation of the camera set perpendicular to the moiré grid to form the contour planes perpendicular to the axis of observation. The moiré grid to camera axis was set with the aid of a laser and then permanently clamped. The Hg arc was set on an optical bench rail at right angles to the camera axis. The arc slid along the rail to enable the illuminating angle to be accurately set by triangulation. A lens was used to relay a real image of the arc to any point along the arc to grid line so that the point source and camera aperture were in the same plane parallel to the grid.

2.7 FRINGE PROJECTION/IMAGE SCAN CONTOURING.

For the inspection system envisaged in this research the optical information had to be converted into an electronic signal by some form of interface. In the case of this work a slow scan television system was used. In such a system the television line scan would be as described in section 2.6.1 and would traverse the intensity function described by equation 29 across the moiré grid lines as well as the contour fringes. Hence the output signal would include the spurious grid fringes as well as the required contours. The intensity function described by equation 29 applied to a turbine blade is illustrated by a microdensitometer trace across the negative of a moiré contoured blade shown in fig. 14a. The intensity modulation produced by the grid lines made a detailed analysis of the contour fringes extremely difficult.

The investigation into methods of eliminating this grid noise when the contoured image was scanned led to the development of the fringe projection/image scanning method of generating shape information. The theoretical analysis of this technique is described on the basis of a mechanism for eliminating the grid line noise on an image scan system.

The fringe projection/image scanning system is a development of moiré shadow contouring which eliminates both the grid line noise and the need to have a moiré grid physically close to the object. An image of the moiré grid is projected directly on to the object as shown in fig. 15. The grid lines formed on the surface of the object are distorted by the shape of the object. The image of the object with the superimposed moiré grid lines is scanned in a direction parallel to the lines of the projected grid by a small aperture. This generates a light intensity distribution equivalent to that obtained by scanning the normal moiré shadow system in a direction parallel to the grid lines. The aperture size used to scan the resultant image is equivalent to half the period of the projected grid at the object plane of the viewing optics. In effect the scanning aperture replaces the analyser grid of the moiré shadow contouring system.

2.7.1 Elimination of grid lines on a scanning system.

As shown in fig. 14a the intensity modulation produced by the grid lines when the contour pattern was scanned makes detailed measurement of the contour fringes difficult. This could be reduced by moving the grid in its own plane at right angles to the grid lines while exposing the photographic image as suggested by Takosaki [25] and Allen [26] and discussed in section 2.6.6. The resultant microdensitometer trace across a contoured negative taken with the grid moving, fig. 14b, showed that the contour fringes were then well defined and the effects of the grid lines were greatly reduced.

This form of averaging would be possible with photography but not practical for a television system which would scan the resultant image at a high speed and would have a short exposure time (< .02 secs). To blur the grid fringes under these conditions the grid must be moved or vibrated by an amplitude greater than the period of the grid at a frequency of 50 Hz or greater, depending upon the integration time of photo cathode.

To overcome this problem, consider the effect of scanning the moiré contour system in the direction parallel to the grid lines with a finite sized detector.

The total energy incident on the detector surface in the image plane of the optical system is proportional to the intensity of the image times the effective area of the object being observed.

Hence,

$$\text{Total Energy} \propto I_{\text{object}} \times \text{Area} \qquad \ldots\ldots \quad (41)$$

Consider now the effect of examining the light scattered from the surface of the object by a finite sized slit extending, or being traversed, in the y direction.

For a point (x,y,z) on the object a distance z(x,y) from the modulating square wave grid the intensity scattered from this point is given by equation 30 and the symbols are as for fig. 10a.

$$I_o = \frac{C}{2}\left[1 + \frac{4}{\pi} \sum_{\substack{n=1 \\ n \text{ odd}}}^{\infty} \frac{1}{n} \sin \frac{2\pi n}{p} \left(x - z(x,y) \tan \alpha\right)\right]$$

The energy emitted from this point is dependent upon the area over which it is integrated in the (x,y) plane.

$$\text{i.e.} \qquad \text{Energy} = \iint I_o \, d\,x.d\,y \qquad \ldots\ldots \quad (42)$$

$$= \frac{C}{2} \int_{y_1}^{y_2} \int_{x_1}^{x_2} \left[1 + \frac{1}{\pi} \sum_{\substack{n=1 \\ n \text{ odd}}}^{\infty} \frac{1}{n} \sin \frac{2\pi n}{p} \left(x - z(x,y) \tan \alpha \right) \right] d\, y . d\, x$$

$$E = \frac{C}{2} \left[y \left[x - \frac{2p}{\pi^2} \sum_{\substack{n=1 \\ n \text{ odd}}}^{\infty} \frac{1}{n^2} \cos \frac{2\pi n}{p} \left(x - z(x,y) \tan \alpha \right) \right]_{x_1}^{x_2} \right]_{y_1}^{y_2} \qquad \ldots\ldots \quad (43)$$

This is a triangular wave form similar to that of equation 38 and illustrated in fig. 16a and does not contain any of the spurious fringe terms associated with equation 29. To obtain the maximum signal and contrast of the fringes the sum of the series must be a maximum and as near to the value of the left hand term as possible when integrated between the limits x_1 and x_2.

This occurs when phase difference of the series is π between the limits x_1 and x_2. That is over a slit equal to half the period of the grid. Hence integrating over the limits $x_1 = x - p/4$, $x_2 = x + p/4$.

$$E_{p/2} = \frac{C}{2} \Delta\, y \left[\frac{p}{2} + \frac{4p}{\pi^2} \sum_{\substack{n=1 \\ n \text{ odd}}}^{\infty} \frac{1}{n^2} \sin \frac{2\pi n}{p} \left(x - z(x,y) \tan \alpha \right) \right] \qquad \ldots\ldots \quad (44)$$

For a slit size less than p/2 the contour fringe function becomes more rounded towards a combination between a triangular and square wave. For a slit width above p/2 the contrast reduces to zero at p, i.e.

$$E_p = \frac{C\, \Delta\, y}{2}\, p \qquad \ldots\ldots \quad (45)$$

As the width is varied above p some contrast returns to some extent with a secondary maximum at $3p/2$ then decreases to zero at 2p and so on, as shown in fig. 16b.

If the area of examination is now scanned in the y direction, x being constant, the intensity function is purely dependent upon the value of $z(x,y)$ so as to generate the depth contour fringes without any of the spurious grid line fringes.

For the standard moiré shadow contouring system, fig. 11, the moiré grid is still superimposed on the contoured image as shown in fig. 12, and so an integrating slit length greater than $p/2$ can be used as the integration region is 0 to $p/2$, p to $3p/2$ . . . . $(n - 1)p$ to $(2n - 1)\ p/2$ as shown in fig. 16c, rather than over the full period of the grid. This increases the total energy observed without decreasing the fringe contrast. The limit upon the extent of the slit length is dependent on the rate at which z changes with respect to x.

This shows that it is possible to eliminate the noise produced by the moiré grid by scanning the contoured image in the direction parallel to the moiré grid lines.

2.7.2 Fringe Projection/Image Scan Method of Contouring.

The above section described a method of eliminating the grid line noise from the moiré shadow contouring system. However, the implications of equation 44 are even greater than just forming a method of noise reduction in so far as it is not necessary to view the moiré shadow cast onto the object through the original grid. The scanning aperture in effect acts as the moiré analyser to generate the depth contour information. Hence if the slit width used on any scanning device is less than or equal to $p/2$, as for example with a television system, the grid in front of the object can be removed and the basic moiré grid projected on to the surface of the object.

The modified contouring system is shown in fig. 15a where the grid is projected by the lens system and the object observed in the normal way. The structure of the moiré fringes projected on to a turbine blade is shown in fig. 17. The curved nature of the fringes gives a clear indication of the shape but detailed analysis of this fringe pattern would be difficult by purely visual means. Consequently this technique is only applicable to a scanning system.

2.7.3 Advantages of Fringe Projection/Image Scanning.

The fringe projection/scanning technique reduces many of the practical limitations on the moiré contouring technique. The principal advantage is the reduction in the depth of field requirement which in the standard moiré contouring system requires that the shadow fringes on the object together with the grid in front of the object must be within the depth of field of the observing optical system. The modified requirement is that the moiré grid projected on to the object's surface must be in focus by both the fringe projection system and observing system over the whole of the depth of the object's surface. This now relies solely on the depth of the object as with any photographic system rather than object depth plus object to grid distance.

The diffraction and penumbra effects of the shadow fringes are reduced because the grid is imaged directly on to the object and the required depth of field is less than that for the moiré shadow technique. The quality of the projected fringes relies heavily on the quality of projector lens, principally the ability of the lens to overcome chromatic aberration and to produce a flat focal plane.

The system eliminates the requirement to have a moiré grid physically close to the object and so it is possible to measure the shape of surfaces in restricted places where it would not be possible to put a moiré grid in front of the surface. This extends the use of the technique in the aeroengine field to parts of engine casings and similar components. The size of object that can be analysed is also increased as the magnification of the projection system is variable over a wide range. Providing the projected fringes are of a suitable spatial frequency and the object can be imaged on to the television system and the element scanned is less than p/2 on the object depth contours will be obtained. It should be possible to examine components several feet in diameter with a suitable increase in the contour depth interval.

2.7.4 Visual Observation of Contour Fringes with Fringe Projection.

As discussed in section 2.7.2, it is not possible with the basic fringe projection system to obtain an accurate visual impression of the shape of the object as only the projected fringes are visible, fig. 17. However, in some cases not necessarily connected with computer linked dimensional measurements it may be desirable to observe the contour fringes visually.

This is achieved by placing a straight line moiré grid in the image plane with the lines parallel to the projected grid and of the same spatial frequency as the effective projected grid frequency on the image. The visual effect is the same as in the standard moiré contouring technique. This is moving towards the more classical moiré fringe techniques, Theocaris [24] but to obtain depth information rather than strain information. Fringe projection has recently been used to measure deflection and vibration amplitude by Der-Hovanesian [30] and Brooks [31]. The system shown in fig. 15 can be modified to produce visual contours by putting a demodulation grid in the image plane instead of the T.V. system and using a relay lens to view the resultant contours. Such a modification with a projected moiré grid would overcome the depth of field of the standard moiré contouring system, fig. 11. However, the use of this would be limited in so far as the demodulation grid would have to be changed every time the projection grid was changed or the magnification of either the projection or observing systems was changed.

2.7.5 Experimental Results.

The quality of the fringes projected on to the turbine blade determined the ultimate quality of the depth contours obtained when scanning across the blade. To utilize the depth of field advantage of this system to its full extent the focal plane of the projected fringes must be parallel to the object as shown in fig. 15a. To achieve this the actual grid used in the projection system must be angled with respect to its image as shown in fig. 15b. This would result in a variation in the image magnification across the moiré grid and so to obtain a projected image with uniform fringe spacing across it the spatial frequency of the master grid must vary to compensate. Hence a special grid must be used.

Consider the diagram shown in fig. 15b where U is the distance of the master grid from the projection lens, V is the image to lens distance, M_o is the image magnification on the axis of the optical system and ℓ is the distance along the image plane from the axis.

The image magnification (M) at any point ℓ along the image plane is given by the equation

$$M = M_o - \frac{\ell \sin\theta}{f} \qquad \ldots\ldots \quad (46)$$

where f is the focal length of lens used.

The resultant magnification at the master grid is 1/M and for any point ℓ' along the grid is given by

$$\frac{1}{M} = \frac{1}{M_o}\left(1 + \frac{\ell' \cos\beta \tan\theta}{f}\right) \qquad \ldots\ldots \quad (47)$$

The angle θ and β are as shown in fig. 19.

To achieve the correct angular position of master grid to produce the angled image plane the master grid angle must conform to the equation

$$\tan \beta = \tan \theta \left(\frac{V}{M_o f} - 1 \right) \quad \ldots\ldots \quad (48)$$

Thus if the magnification is 1:1 $\tan \beta = \tan \theta$.

The required master grid was conveniently made using Agfa Gevaert 10E56 photographic plates by photographing a linear grid, positioned in the image plane of the projected fringes, with the fringe projection optics. The photographic plate was angled to comply with equation 48. The lens used for the projection system was of good optical quality to minimize the aberrations produced by the effects of the angled object and image.

The resultant projection fringes were of good quality, fig. 17, over the whole of the aerofoil section of the turbine blade. The advantages of being able to focus the projected fringes directly on to the blade are shown by the ability to obtain clear fringes across the whole of the convex surface of the blade which has a depth of approximately 1.0" towards the blade tip.

The contour fringes obtained by scanning the blade image with a suitable aperture is shown in fig. 18. The fringes were comparatively noise-free, particularly in the region of the shape direction inversion, and the intensity function was triangular. These results compared favourably with the fringes obtained by the standard moiré contouring technique.

2.8 COMPARISON OF CONTOURING TECHNIQUES.

The comparison between the methods of contour generation described in this chapter was made with the view towards the application of optical contouring as a routine means of production inspection and dimensional distortion analysis. Consequently the system must be accurate, reliable, require little attention while in operation and be fast. The overall inspection system must be capable of producing the difference information in a visual form such as on a television monitor or be used in conjunction with an on line computer. Hence the quality information generated by scanning the image must be good.

The holographic techniques suffered from the need of a photographic process before the contour information was available but they could not be prematurely condemned on these grounds. It would be possible to eliminate the need for a photographic process in these systems by the use of alternative storage media such as Lithium Niobate crystals, Chen [32], or thermoplastic materials, Lin [33] and Bellamcy [34]. These techniques enable holograms to be recorded and processed within a few seconds. An alternative process would be to reduce the spatial frequency of the information so that the 'hologram' could be imaged on to a good quality television camera and recorded on a standard video tape or disc recorder. This technique has been developed by Leendertz and Butters [35, 36] in the U.K. and Macovski [37] in the U.S.A.. All these systems would be attractive alternatives to photographic processing and should be available as usable techniques in the near future. Work carried out by the author on the use of the Laser Speckle Pattern/T.V. System described by Butters [38] used for vibration analyses indicated that the technique had a definite potential. The use of video storage was not studied, as no suitable equipment was available.

From the investigation carried out on the double wavelength technique the contouring results were reasonable using the double exposure technique. (The comparison of the systems with respect to measuring accuracy, equipment required and ease of operation on a routine basis is summarised in Table I.) Although difficult to set up, it would be simple to operate on a routine basis and the handling of the component would be straightforward using a kinematic relocation mounting for the blade with a 0.001" accuracy. It was restricted in the available contour depths but for a routine application variable contour depth intervals would not be needed, so that a dye laser with the required wavelength separation would be used. The object size was limited to the diameter of the telescope objective lens. The double refractive index technique gave excellent results; the contour depth was variable over a wide range but the repeatability depended upon the accuracy of setting the gas pressure differential. It had the same size and depth of field limitation as the double wavelength technique. For routine application the major disadvantages were the need for a pressure chamber, the use of a gas which would be expensive if a large number of components were tested and the time involved loading the component into and out of the chamber and adjusting pressure between exposures. These disadvantages precluded the double refractive index method as a routine system.

In comparing holographic and moiré fringe contouring the moiré had a number of advantages. The information content was the same, although they had different intensity distribution functions, but the moiré system was more flexible in the range of components to which it could be applied. It would be considerably cheaper, not requiring a laser, simple to operate and produced a contoured image instantly without requiring any photographic processing. The moiré system was limited to contour intensity of 0.010" and above by diffraction effects but, because of the shape and depth of the blades, contour intervals of above 0.01" would be required.

The principal factor in the comparison of the techniques was the fringe intensity distribution when the image was scanned, as any automatic inspection system would have an optical to electronic interface in the form of a television system. The effects of the speckle pattern structure on the holographic image produced a considerable quantity of noise on any scan signal, fig. 9. This made the true location of the centres of the fringes difficult. This was particularly true of the small apertures that had to be used to provide sufficient depth of field. The scan across a moiré contoured blade along the direction of the grid lines produced a fringe intensity with very little spurious noise, fig. 18, which was more appropriate for automation analysis.

The holographic and laser speckle pattern techniques would be more applicable to shapes that did not have such large depths in relation to the required inspection accuracy. The required measuring accuracy would be of the order of $\pm$ .25 times the contour interval and an overall visual impression of the difference between the two objects would be required rather than a computer linked analysis.

For the reasons stated above the moiré contouring was selected as the most suitable system for the application to aeroengine component dimensional inspection and was used for the remainder of this research.

Chapter III.

Methods of Obtaining Comparative Information.

3.1 INTRODUCTION.

In this chapter the possible methods of comparing the shapes of two turbine blades are examined. There were three principal methods, direct optical subtraction of the two contour patterns, subtraction of the two contour patterns by electronic (computer) methods and subtraction of the shapes produced by the contours using a computer. These methods were compared with respect to the accuracy with which the differences were measured and their suitability for use on a routine basis.

The overall difference between an uncompleted blade and its master was normally less than + 0.02" and the tolerance envelope on a completed blade is + 0.007". Hence the comparison system must be capable of accurately discerning small differences between the blades. This would be particularly relevant when discussing the direct optical subtraction technique. The difference information must be fed into a computer via an electro-optical interface to enable the difference information to be processed quickly and presented to the inspector in a clear form.

The comparison of the blade shapes rather than the direct subtraction of the contour fringe patterns was found to be the most accurate and the most compatible with computer processing.

3.2 DIRECT OPTICAL CONTOUR SUBTRACTION.

This method is the most simple and direct method of generating the difference between two sets of contours and the technique is fundamentally the same as the well-known moiré measuring devices. The contoured image of the master object is formed in a standard moiré contouring system, fig. 11. The image is photographed on a high resolution photographic plate, processed, and the resultant negative relocated into the same position at which it was taken. This forms the master grid of the moiré subtraction system as shown in fig. 11. The resultant image transmitted through this master grid is observed by a second camera, with lens L_2, to form the resultant moiré subtraction. This lends itself to two possible systems. Firstly the moiré difference fringe pattern is displayed directly on to a television monitor screen. The differences are then read directly off the screen or the position of the component is adjusted to eliminate or minimize the moiré fringes and the required movement gives the overall shape differences. The latter method becomes difficult when the full six degrees of freedom of movement are utilized. In the second technique the computer is used to obtain the dimensional differences from the resultant moiré pattern and apply suitable fit calculations to calculate the overall differences. On a practical basis the second technique was preferred where the computer would be used to calculate the dimensional differences.

For turbine blades the contours of equal depth lie in the direction parallel to the blade axis as can be seen in fig. 12 and the inspection requirements are that sections parallel to the chord and so normal to the blade axis are taken and measured. This is a result of the techniques used in the design of the blades. Hence the analysis is taken in scans along the chord of the blade and so across the majority of contours on the blade. The difference in depth of the two blades in the Z direction of the co-ordinate system produced by blade twist, bending, etc. is shown as a difference in spatial frequency of the contours across the blades as the section is scanned rather than a skew effect of the contours with the spatial frequency remaining the same, as in normal moiré strain measurements. This makes the visualization of the dimensional differences more difficult than conventional moiré techniques where the grid frequencies are kept constant. The formation of the difference fringes formed by direct optical subtraction is discussed in greater detail in the next section.

3.2.1 Difference Fringe Generation.

For the contoured blade shown in fig. 12 the contour fringe intensity distribution for the moiré shadow contours, neglecting the grid fringes which can be eliminated as shown in section 2.7.1, is given by the triangular intensity function equation 38.

$$I_M(x,y) = C_M \left[1 + \frac{2}{\pi^2} \sum_{\substack{n=1 \\ n \text{ odd}}}^{\infty} \frac{1}{n^2} \cos \frac{2\pi n}{p} \left(\frac{d\ z(x,y)}{h + z(x,y)} \right) \right]$$

This is used to expose a high resolution photographic plate to form the master grating.

The transmission of the negative T is related to the optical density of the photographic plate D by

$$\log \frac{1}{T} = D \qquad \ldots\ldots \quad (49)$$

The optical density of the emulsion of the negative is given by the Hurter-Driffield (H & D) curve of optical density versus log (Exposure)

$$D = \log \left(\frac{1}{T} \right) = \gamma (\log E - \log K) \qquad \ldots\ldots \quad (50)$$

γ (photographic gamma) = the gradient of the linear region of (H & D) curve.

E = the energy used to expose the film.

log K = the projected intercept of the linear region of the curve in to the log (Exposure) axis.

$$E = (\text{Incident intensity}) \times \text{time} \propto \text{Intensity}$$

$$\therefore\ T = K^{\gamma} E^{-\gamma} \propto E^{-\gamma} \propto I^{-\gamma} \qquad \ldots\ldots \quad (51)$$

Hence the transmission of the master negative is proportional to the intensity of the master contour pattern to the power $-\gamma$. Gamma is a function of the film used and the developing process.

Hence for a point (x_1,y_1) on the image representing the point (x,y) on the object the transmission is given by

$$T_M(x_1,y_1) = C_M\left[1 + \frac{2}{\pi^2}\sum_{\substack{n=1 \\ n \text{ odd}}}^{\infty} \frac{1}{n^2} \cos\frac{2\pi n}{p}\left(\frac{d\ z(x,y)}{h + z(x,y)}\right)\right]^{-\gamma} \qquad \ldots\ldots (52)$$

The contour pattern of the production component is modified by the master negative by the above transmission function and forms an image in the plane shown in fig. 11.

Let $z_1(x,y)$ = the depth of the master object

$z_2(x,y)$ = the depth of the production object

$z_1(x,y) - z_2(x,y)$ = the dimensional difference between the two objects.

The production contour pattern on the image plane of the master negative has the intensity of the form

$$I_P(x_1y_1) = C_P\left[1 + \frac{2}{\pi^2}\sum_{\substack{m=1 \\ m \text{ odd}}}^{\infty} \frac{1}{m^2} \cos\frac{2\pi m}{p}\left(\frac{d\ z_2(x,y)}{h + z_2(x,y)}\right)\right]$$

Therefore the transmitted intensity through the master negative is

$$I_{Image}(x_1y_1) = I_P(x_1y_1) \times \left(I_M(x_1y_1)\right)^{-\gamma} \qquad \ldots\ldots (53)$$

$$= K \left[1 + \frac{2}{\pi^2} \sum_{\substack{m=1 \\ m \text{ odd}}}^{\infty} \frac{1}{m^2} \cos \frac{2\pi m}{p} \left(\frac{d\ z_2(x,y)}{h + z_2(x,y)} \right) \right] x$$

$$\left[1 + \frac{2}{\pi^2} \sum_{\substack{n=1 \\ n \text{ odd}}}^{\infty} \frac{1}{n^2} \cos \frac{2\pi n}{p} \left(\frac{d\ z_1(x,y)}{h + z_1(x,y)} \right) \right]^{-\gamma} \quad \ldots\ldots \quad (54)$$

K is a constant. Letting the photographic $\gamma = 1$ (a low contrast negative) to simplify the equation and expanding the transmission function by a Taylor series and neglecting terms squared and above the equation becomes of the form

$$I_{Image}(x_1 y_1) = K \left[1 + \frac{2}{\pi^2} \sum_{\substack{m=1 \\ m \text{ odd}}}^{\infty} \frac{1}{m^2} \cos \frac{2\pi m}{p} \left(\frac{d\ z_2(x,y)}{h + z_2(x,y)} \right) \right] x$$

$$\left[1 - \frac{2}{\pi^2} \sum_{\substack{n=1 \\ n \text{ odd}}}^{\infty} \frac{1}{n^2} \cos \frac{2\pi n}{p} \left(\frac{d\ z_1(x,y)}{h + z_1(x,y)} \right) \right]$$

$$\ldots\ldots \quad (55)$$

The argument of the cosine functions can be further simplified by expanding $\left(h + z(x,y)\right)^{-1}$ as a Taylor series.

$$\left(h + z(x,y)\right)^{-1} = \frac{1}{h}\left[1 - \frac{z(x,y)}{h} + \frac{z(x,y)^2}{h^2} \right] \quad \ldots\ldots \quad (56)$$

Putting this into the cosine argument it becomes

$$\frac{2\pi\, n\, d}{p\ h} \left(z(x,y) - \frac{z(x,y)^2}{h} + \frac{z(x,y)^3}{h^2} \text{-------} \right.$$

$$\div \frac{2\,\pi\,n\,d\,z(x,y)}{p\ \ h} \qquad \ldots\ldots (57)$$

Therefore multiplying out equation 55 then becomes

$$I_{Image}\,(x_1,y_1) = K\Bigg[1 + \frac{2}{\pi^2}\sum_{\substack{m=1\\ m\ odd}}^{\infty} \frac{1}{m^2}\cos\frac{2\,\pi\,m\,d}{p\,h}\,z_2(x,y)$$

$$-\frac{2}{\pi^2}\sum_{\substack{n=1\\ n\ odd}}^{\infty} \frac{1}{n^2}\cos\frac{2\pi\,n.d}{p\,h}\,z_1(x,y)$$

$$-\frac{4}{\pi^4}\sum_{\substack{n=1\\ n\ odd}}^{\infty}\sum_{\substack{m=1\\ m\ odd}}^{\infty} \frac{1}{n^2}\cos\frac{2\,\pi\,n.d}{p\,h}\,z_1(x,y)\,\frac{1}{m^2}\,.$$

$$\cos\frac{2\,\pi\,m\,d}{p\,h}\,z_2(x,y)$$

$$\ldots\ldots (58)$$

Expanding the last term of the equation

$$I_{Image}\,(x,y) = K\Bigg[1 + \frac{2}{\pi^2}\sum_{\substack{m=1\\ m\ odd}}^{\infty} \frac{1}{m^2}\cos\frac{2\,\pi\,m\,d}{p\,h}\,z_2(x,y)$$

$$-\frac{2}{\pi^2}\sum_{\substack{n=1\\ n\ odd}}^{\infty} \frac{1}{n^2}\cos\frac{2\,\pi\,n\,d}{p\,h}\,z_1(x,y)$$

$$- \frac{2}{\pi^4} \sum_{\substack{n=1 \\ n \text{ odd}}}^{\infty} \sum_{\substack{m=1 \\ m \text{ odd}}}^{\infty} \frac{1}{n^2} \frac{1}{m^2} \cos \frac{2\ \pi\ d}{p\ h} \Big(nz_1(x,y) + mz_2(x,y) \Big)$$

$$- \frac{2}{\pi^4} \sum_{\substack{n=1 \\ n \text{ odd}}}^{\infty} \sum_{\substack{m=1 \\ m \text{ odd} \\ n \neq m}}^{\infty} \frac{1}{n^2} \frac{1}{m^2} \cos \frac{2\ \pi\ d}{p\ h} \Big(nz_1(x,y) - mz_2(x,y) \Big)$$

$$- \frac{2}{\pi^4} \sum_{\substack{n=1 \\ n \text{ odd}}}^{\infty} \frac{1}{n^4} \cos \frac{2\pi d}{ph}\ n \Big(z_1(x,y) - z_2(x,y) \Big) \Bigg]$$

..... (59)

From this equation the term solely dependent upon $z_1 - z_2$ is the last expression in the equation. Hence the resultant intensity distribution that gives the direct difference information is of the form

$$f(z_1 - z_2) = 1 - \frac{2}{\pi^4} \sum_{\substack{n=1 \\ n \text{ odd}}}^{\infty} \frac{1}{n^4} \cos \frac{2\ \pi\ d\ n}{p\ h} \Big(z_1(x,y) - z_2(x,y) \Big)$$

..... (60)

The two basic contour patterns of the two shapes also modulate the intensity distribution as can be seen from the second and third terms of the equation to form a carrier grid frequency which is amplitude modulated to form the difference contours. This consequently makes interpretation of the difference pattern more difficult.

The direct measurement of the difference in depth (z) is possible using direct optical subtraction. The overall visual impression of the difference can thus be obtained from the moiré pattern as with the

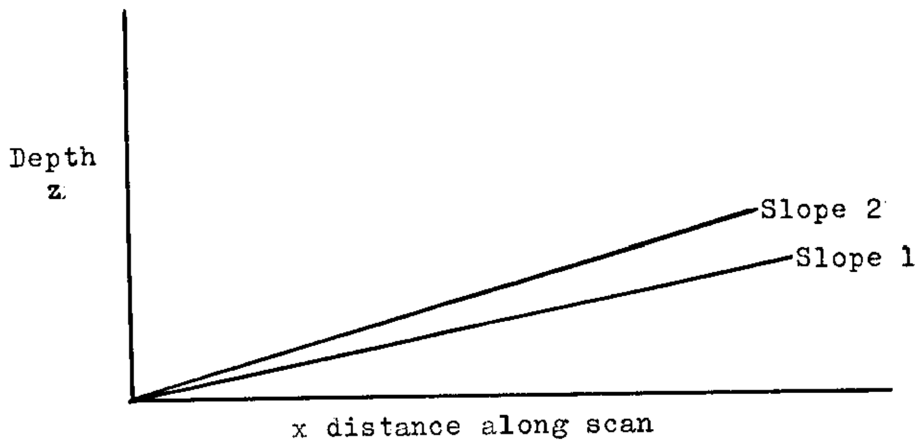

Computer Simulated Shapes for Moire Differencing standard moiré technique.

3.2.2 Computer Simulated Optical Subtraction.

To obtain an insight into the intensity distribution of equation 59 and to examine the accuracy with which the difference information $z_1 - z_2$ could be measured from the resultant fringe pattern a computer model of the subtraction of two contour patterns was formed. A Conversational Programming computer system (C.P.S.) was used with a teleprinter terminal linked direct into an IBM 360 computer system.

In the program a cosine contour intensity distribution $(1 + \cos \frac{2 \pi z}{Delta})$ was used rather than the triangular wave function series to reduce the computation. Two contour patterns were generated of a linear shape, with 0.010" contours (Delta = .01) but each with a different angle. As x, see sketch opposite, increased the difference in depth increased. One contour formed the master negative through which the second, production, pattern was transmitted using equation 53 and an effective photographic gamma = 1. The resultant intensity distribution of the fringes for increasing x, the distance along the object, is shown in fig. 19. At x = 0 the depths z_1 and z_2 were equal. The difference moiré fringe was seen as the amplitude modulation of the carrier fringe pattern formed by the shape contours given by the 2nd and 3rd terms of equation 59. The difference contours were formed by joining the peaks of the shape fringes.

The moiré differences were calculated by fitting a cosine function to the modulation using the contour peaks as reference points. From fig. 19 it could be seen that the difference fringe was well defined and the moiré fringe formed a symmetrical modulation as the difference increased in a linear form. Using this computer method it was possible to form the moiré difference fringe intensity distribution and it was possible to calculate the dimensional difference for any given value of x. The difference value calculated from the moiré fringes was within

± .001" of the actual value of the difference which was within the predicted accuracy of the system.

The linear shapes represented the ideal case but was not, however, representative of the case of a turbine blade which had a curved shape where the frequency of the shape contour fringes was continually changing. To simulate the curved surface a solid sphere was used as the master object and an ellipsoid as the production object. The axis of observation (the z axis) was the same as the major axis of the ellipsoid and a diameter of the sphere. The length of the minor axis of the ellipsoid (the x axis of the co-ordinate system) was 1.8" compared to 2.0" of the major axis and diameter of the sphere. The ellipsoid was symmetrical about the x axis. Computer scans of the moiré subtraction image were taken along the x axis at y = 0 and other values of y to form three dimensional information. Part of the computed moiré pattern as scanned along the x axis (y = 0) is shown in fig. 20a. In this case dimensional difference increased in a non-linear form as x increased, fig. 20b, and the resultant moiré difference pattern was less well defined, particularly in the minimum intensity region. Calculations to find the dimensional differences from the fringe pattern were possible but the accuracy decreased around the minimum intensity region from ± .001 to ± .0015".

As the rate of difference increased as x increased, fig. 20b, the number of contours or carrier fringes that defined the moiré difference decreased, making accurate measurement of the difference more difficult. As x increased further a state was reached where the difference fringes approached the frequency of one of the contour patterns and aliasing occurred. These calculations showed that it was possible to measure to the dimensional difference to an accuracy of between ± .001 and ± .0015 for any part of an object by analysing the intensity distribution of the resultant moiré fringes. This method did, however, rely upon having sufficient carrier fringes to define the shape of the difference fringe. At least three carrier fringes were required to define the shape of the difference fringe. This restricted the rate of change of the dimensional difference $(z_1 - z_2)$ to less than one third of the maximum slope of one of the contoured surfaces. Also there must be a dimensional difference over the component greater than one contour depth to enable the contour difference fringe to be fully defined. The measurement accuracy of this technique depended directly upon the accuracy of the intensity values of the peaks. Consequently the accuracy would be impaired by any noise on the fringe intensity distribution such as non-uniform surface scattering, or illumination and noise caused by surface marks on the object.

3.2.3 Experimental Verification.

The experimental work carried out on these effects showed that the accurate analysis was difficult and could only be carried out under particularly favourable conditions. Fig. 21a shows subtraction of two contour patterns of a flat metal bar that has been deflected. The bar was loaded at one corner to produce a twisting as well as a bending effect so that deflection could be seen more easily.

The deflection was most clearly indicated by the lines of minimum contour fringe visibility, i.e. the two superimposed contours were in phase, representing a zero or n times $\Delta/2$ deflection. Δ is the contour depth interval. It was difficult to accurately locate the regions where the deflection was $(n + \frac{1}{2})\Delta/2$, the contours out of phase, and subsequently practically impossible to estimate by eye a deflection between these two positions.

As shown by equation 59 and the computer results measurements of less than half a contour depth relied on actual intensity measurements.

The eye is not capable of judging relative intensities of the form generated by equation 59 to any degree of accuracy. It is good at estimating distances (width etc.) and changes in colour but has a logarithmic response to intensity and operates on a local reference system. Hence it is not possible to accurately estimate the intensity variation of the contour fringe peaks shown in fig. 21a, to measure the deflection between the moiré in-phase and out of phase condition.

From the intensity information of such a system, fig. 21b, obtained by scanning the image with a photodetector, the deflection of the plate between the in-phase and out of phase conditionsof the two contour patterns could be estimated with little difficulty. Consequently any system that displayed the moiré deflection or difference fringe pattern directly to an operator for visual interpretation would be limited to an accuracy of $\pm$ .25 fringes.

Microdensitometer traces of the intensity distribution across the negative of fig. 21a, shown in fig. 21b, illustrate the measuring difficulties. The moiré deflection frequency was approximately a quarter of the contour frequency and it could be seen that the moiré difference pattern was not very well defined. The total modulation depth was less than 40% of that of the contour fringes. For a measuring accuracy and resolution of $\Delta/10$ the intensity profile of the moiré would be required to be known to within 15 or 20% although in this case the moiré difference fringe was only defined by 3 or 4 points per contour interval deflection. The measuring problem was alleviated to some extent by small deflection so that the moiré difference was defined by more contour fringes. But, as shown in fig. 22, for conditions where large deflections or dimensional differences were involved, the spatial frequency of the moiré difference approached the frequency of one of the contour patterns, thus measurement became extremely difficult.

3.2.4 Discussion of System Performance.

If the dimensional difference was equal to several contour depths a number of difference fringes would be seen and it would be possible to measure the difference to between ± .5 to ± .25 of the contour depth by direct visual inspection. For accuracies above this an image intensity measuring technique must be used.

For the particular application to turbine blades the maximum difference expected between a master and production component was 0.02", which represented between one and two difference fringes. The required measuring accuracy was 0.1 times the contour depth. Two typical examples of these measuring conditions are shown in fig. 23. These photographs were formed by double exposure to add the two patterns, for convenience, rather than one observed through the other, but the final result of the moiré pattern was the same. A 180° phase change has effectively been applied to one contour pattern. Fig. 23 shows a turbine blade bent in the z direction and the moiré difference where the contours were out of phase could be clearly seen. Accurate assessment of the difference at any region across the chord of the blade, apart from the out of phase region, was extremely difficult by either visual inspection or fringe intensity scans. For the case of the blade being twisted about its own axis the visual interpretation of this effect was also difficult because the moiré difference fringes were parallel to the contour fringes and there are a large number of contour fringes which tended to lead to visual confusion. Accurate assessment of this deflection was impossible. The intensity scan would give better results but because the scan technique relied upon accurate relative intensity measurements of the contour fringes the noise produced by the practical factors of surface finish, etc., would greatly reduce the accuracy of this method.

Finer contour fringes < 0.01" produced a greater visual effect of the differences but could not be used because of the depth of the blade and the diffraction effect limitations produced by the finer fringes.

3.2.5 Discussion of Overall Technique.

Although the system was attractively simple the results showed that for a practical application it had a fundamental disadvantage in that it relied upon the accurate measurement of the relative intensities of the resultant carrier fringes to estimate sub-contour differences. The computer simulation showed that the technique was capable of 0.1 fringe accuracy under ideal conditions but in a practical case of a blade the scattered light intensity could vary with surface finish across the blade or be affected by grease or dust marks. Also it relied on the linearity of the readout system. In this case the readout system would be a television camera which under the prevailing low light level conditions expected from the moiré subtraction technique would not be operating in a region where the response would be linear.

The form of the difference information moiré pattern when displayed on a monitor would be complex, as seen in fig. 23, and would be quite different from the accepted form of a moiré pattern. Because of the complexity of the patterns caused by the carrier fringes it would not be possible to use this method as a direct visual indication of shape difference either for direct assessment or an object adjustment method in which the operator adjusted the position of the object to minimize the number of moiré fringes. Some of the carrier fringes could be eliminated by electronic low pass filtering of the vidicon output but since the shape of a blade would be complex and the spatial frequency of the contours varied across the chord of the blade satisfactory electronic filtering would be difficult. Even then visual judgement of relative fringe intensity to measure sub-fringe differences would be difficult and inaccurate.

With reference to the information processing aspect of this technique this method did not indicate the direction of the difference information whether a point on the production object was closer to or further away from the master.

An additional practical limitation of the technique was formed because the contoured image was passed through the master negative to obtain the difference information. Consequently, much of the available light would be attenuated by the master negative resulting in a very low light level final image on the vidicon. Hence very sensitive vidicons would be needed to obtain reasonable signal levels at the normal T.V. scan rates. Alternatively, slow scan rate or storage systems have to be used which increases the complexity of the apparatus required. Slow scanning systems would have to be used for computer input because of the limiting digitizing rates available but even then the light levels would be very low.

The limitations of this technique are summarized as follows:-

a) the complexity of the resultant fringe pattern,

b) reliance upon relative intensity measurements to obtain accurate sub-fringe information,

c) limitation upon the rate of increase of the shape difference,

d) the practical problems of very low light levels.

These limitations resulted in the conclusion that it was not a suitable technique for application to either visual or computer based shape difference subtraction for the applications to turbine blades.

3.3 ELECTRONIC FRINGE SUBTRACTION.

This system was identical to direct optical subtraction but used an electronic method of subtracting the two contour patterns. The master contour image must be stored optically or electrically and assessed for subtraction from the production contour fringes. Since the electronic fringe subtraction also relied on relative measurement of intensity it would be prone to the same limitations and disadvantages as direct optical subtraction and would be somewhat more complex. For these reasons the technique would not be suitable for the envisaged inspection system.

3.4 ELECTRONIC/COMPUTER SHAPE SUBTRACTION.

Shape subtraction with optical contouring could only be achieved with the aid of a computer to produce any form of automatic system capable of routine application. It would compare actual dimensional shapes rather than optical information relative to the shape. Hence it would be a direct comparison for a large number of points. The principle of operation was that the shape co-ordinates of the master object were taken for a number of plane sections through the blade aerofoil parallel to the chord and stored within the computer. These were compared to the shape data of the same section of a production or distorted blade. The computer would be used to generate the difference data at any given number of points and used to manipulate this data to obtain the best fit between the two shapes to give the overall difference in the form of a difference in two directions plus an angle. The manipulation of the data would be one of the main assets of this technique over the present inspection systems. The accuracy of the shape comparison technique would be better than the contour subtraction method as it does not rely to such a great extent on absolute intensity information as the direct optical subtraction system did.

As all the data reduction in this technique would be done by the computer it would be more complex than the optical subtraction but considerably more versatile. By building up dimensional difference information in a number of planes along the blades axis and relating the planes it would be possible to produce the three-dimensional differences between the blades.

It would be possible to compare objects direct with computer design data and if linked into the Company's main computer complex would have automatic access to the design data. Hence this would eliminate the requirement for a physically made master for comparison, as was still needed by the present system.

The format of the output from the computer could be varied according to the requirement of the application, such as in the production application this could be the general difference between the blades, such as thickness bending, twisting plus detailed results of areas with localized differences above a particular limit. For a distortion the format may be required to be compatible to a theoretical computer programme.

An additional use of computer facilities could be used to store the values of the general differences between blades to obtain statistical data to analyse trends which could be used to improve production techniques.

Before studying the available methods of converting the optical information into computer co-ordinate data, or the methods of handling shape data within the computing the reliability and accuracy of the contour shape information was assessed.

3.4.1 Contour Shape Information.

The shape contour intensity distribution function as a component is scanned is given by the equation

$$I(x,y) \propto \Delta y \left[\frac{p}{2} + \frac{4p}{\pi^2} \sum_{\substack{n=1 \\ n \text{ odd}}}^{\infty} \frac{1}{n^2} \sin \frac{2\pi n}{p} \left(x - z(x,y) \tan \alpha \right) \right]$$

The clarity of this function depended upon the area of the scanning detector. The extent of this in the x direction would be fixed at p/2 to obtain maximum fringe contrast. Thus the controlling factor would be the width of the slit in the y direction. Consequently this must be as small as possible. The overall accuracy of the system depended upon the accuracy with which the peaks and troughs of the contour fringes could be located and how faithfully the practical signal follows the theoretical intensity function. The most appropriate method of examining these factors was experimentally.

3.4.2 Mechanical Scan System Accuracy.

The scan system developed for these tests was simple but an extremely effective device. The contoured image formed on the camera image plane in the system shown in fig. 11 was mechanically scanned by a photomultiplier with a small slit, approximately 0.015 x 0.005". The position of the slit provides the X and Y co-ordinates of each point with respect to the blade and the contours give the Z co-ordinate.

The photomultiplier was clamped in a lathe bed worm-driven slide unit, the worm being driven by a variable speed geared electric motor. The position of the Photomultiplier tube (P.M.T.) with respect to the Y co-ordinate was set manually by adjustment of a second lathe slide unit to which the first assembly was clamped, fig. 24. The P.M.T. was scanned in the X direction by the electric motor and its position with respect to the scan was monitored by the voltage output of a 10 turn potentiometer geared to the electric motor drive. The potentiometer output was fed to the X direction of an XY plotter and the P.M.T. output voltage applied to the Y direction. This generated an intensity versus scan position plot of the contour pattern.

The blade was set in a horizontal position in the moiré contouring rig (section 2.7.3) with the aerofoil surface facing the camera, as close to the moiré grid as possible. The grid lines were in the vertical direction and thus the angle of incidence of the grid illuminating beam in the horizontal plane. The P.M.T. was scanned vertically parallel to the grid lines to eliminate the grid noise. The slit length of 0.015" covered 3 complete periods of the grid in the image plane (100 lines per inch with a 0.5 image magnification).

With this system the scan was only recorded when the P.M.T. was moving in the upward direction so that it was loaded by gravity against the drive screw to overcome the slackness within the mechanical drive.

The photomultiplier had some degree of high frequency noise on its output in addition to the spurious noise caused by dust particles on the blade and grid which produced a random noise effect on the contour intensity trace, fig. 28. This type of noise decreased the accuracy of the location of the contour maxima and minima and could not be tolerated for computer analysis as it would result in spurious fringe counts. Consequently a low frequency pass filter was put on to the P.M.T. output calculated to transmit only the frequencies below the maximum contour frequency for the particular scan rate of the P.M.T. which was approximately 1 scan/minute. This technique worked well and gave a good noise-free trace, shown in fig. 25a, which was also suitable for computer analysis.

An examination showed that for repeat scans of the same part of the blade the X direction scan position repeatability was within ± .002". The Z direction measuring repeatability and accuracy of the contour system was within 10% of the contour depth for contours between 0.020" and 0.010" depth intervals.

The turbine blades were kinematically mounted at the fir tree root and it was possible to achieve a relocation accuracy of ± 0.001" towards the blade tip. The overall performance of the scanning system illustrated that the measuring system was sufficiently accurate for the present measuring requirements on the turbine blades.

Dimensional measurement by manually plotting the shape from the contour information, using the maxima and minima values, showed that the system was consistent and accurate. An example of this work is shown in figs 26, 27. This was an example of the comparison of a turbine blade that had been run in a test rig under engine conditions and had been thermally fatigued. This was compared to a new blade of the same type. The contour depth was 0.018" with measuring accuracy of ± .0015". The comparison of scans across three chord sections along the blade aerofoil, two of which are shown in figs 26 and 27, showed that there was little difference between the standard and run blades. There was a progressively increasing difference in the aerofoil positions towards the tip of the blades, indicating that the engine run blade had been bent backwards by approximately 0.010" at the uppermost scan. The engine run blades were also thicker by an average of 0.006". This agreed with the effects of a carbon and oxidization coating across the engine run blade which was measured to be between 0.002" and 0.005" thick. This layer was shown by the definite kink in the aerofoil shape, fig. 17, where part of it had broken away from the convex surface.

3.5 DISCUSSION.

The investigation into the methods of comparing two components to find the dimensional difference has shown that direct shape comparison would be the most suitable method of obtaining the difference information. The moiré contouring method was capable of producing the shape to an accuracy of 10% of the contour depth interval used.

For the dimensional inspection of turbine blades using optical contouring techniques a computer linked system should be used to cope with the increased quantity of data. Although this appeared a complex procedure, it would have the increased potential of being accurate to within 0.001" over the depth of the object and would have the ability to manipulate the difference information to calculate the overall differences and present the information in a form easily assimilated by the operator.

The overall system envisaged for the computer linked inspection is shown in block diagram form in fig. 28. The optical to electronic information interface would be a slow scan television camera which would provide 20 line scans of 500 information points per scan in a total time of 10 seconds. This information would be fed into a small computer for analysis and the difference information would be displayed on a Cathode Ray Tube or printed on paper. From this information the operator would either accept or reject the blade, unless the computer did the decision making for him, or specify what remedial action would be required on the blade. This system would be basically a passive system as far as the operator was concerned, as no adjustments would be required from him and so operator errors would be eliminated.

Chapter IV.

Information Processing by Computer.

4.1 INTRODUCTION.

The methods used to process the optical contour information within the computer are described in this chapter. There were two separate objectives in the computing. First, to obtain an array of shape co-ordinates within the computer memory that was accurate and reliable. Secondly, to compare this information with the design or master data so as to calculate the overall differences together with any abnormally large localized errors.

The system envisaged for the computer linked inspection has been discussed in section 3.5. The equipment used to investigate the computing aspect of this work was different from that of the overall system and is also shown in fig. 28. The information from the television system was fed into a computer type digital tape recorder. The magnetic tape was then fed directly into the IBM 360 computer system for analysis and the final output was in a printed form. This system was dictated by the lack of the availability of a small computer. However, a digital tape recorder was acquired to enable the blade data to be put into the IBM 360 system. The equipment was sufficient to investigate the feasibility of the technique.

4.2 SHAPE FORMATION FROM CONTOUR FRINGES. PROGRAMME OUTLINE.

The shape formation computer programme was required to calculate the shape of the aerofoil surface of a turbine blade from a signal generated from a scan across the contoured image. Fig. 29a shows the intensity profile of the contours on the convex surface of the blade taken by a scan along the direction of the chord. The shape represented by the contour pattern is shown in fig. 29b.

The programme used to obtain the shape information consisted of four main sub-routines:-

a) Location of intensity maximum and minimum values for each half fringe.

b) Calculation of object shape from intensity data between the intensity maximum and minimum values of each half fringe.

c) Counteraction against noise on the contour intensity signal.

d) Location of shape inversion region.

The first two sub-routines were the main part of the programme and could together calculate the basic shape of the component. As the computer had to process a real electronic signal from the optical to electronic information interface the noise effects produced on this signal had to be taken into account in the third sub-routine. The final sub-routine was a method used to locate when the direction of the shape changed as it was being scanned as shown in fig. 29b.

The programme is explained in greater detail in a block, or flow diagram form in fig. 30. The four main sub-routines are shown by the dotted lines. During the majority of the programme only the maximum and minimum location and shape calculation would be used. The computer was used to locate each half fringe and defined the maximum and minimum intensity values and their positions with respect to the scan and then calculated the shape for the measuring points between these values.

The noise generated on the intensity signal was principally produced by surface effects on the blade, i.e. scratches, dirt, rather than electronic noise. Hence the noise was inherent in any practical system for blade inspection and had to be taken into account by the computer, otherwise spurious intensity maximum and minimum values were indicated. The noise effects were only found to be critical where there were few contour fringes, i.e. where the surface was nearly parallel to the reference plane of the contouring system. Two typical intensity scans across a contoured turbine blade are shown in fig. 31 and these illustrate the noise effects that are produced on the fringe intensity.

The noise correction sub-routine was only applied over the region shown in fig. 31.

The point where the direction of the shape changed from going away from the observer to coming towards the observer, or vice versa, as the scan proceeded, occurred in the same region as the noise effects. Hence in the region of the scan the input information was examined to find the inversion point. Once located and the direction parameters changed accordingly, this sub-routine was locked out of the main programme.

Both the noise correction and shape inversion sub-routines were of necessity complex, to accommodate all the variations by which the noise and inversion point indication occurred and to ensure that false shape information did not occur. Although the sub-routines were complex only a small part of each one was used for each individual scan of the blade, so that the actual calculations performed by the computer were kept to a minimum.

The contour fringe intensity data was in the form of a digitized value of the intensity for a given position along the scan. The distance between each intensity value was equal or nearly equal depending upon the scan system used, fig. 32a, b, and the position of each point along the scan was known. The object of the information processing system was to obtain as much data as possible and as accurately as possible. Information could always be rejected later on in the process if it was not required. The amount of information used depended on the application and the component being investigated.

The contour fringes formed a series of maxima and minima with a dimensional depth separation of half the contour depth interval, fig. 29. The computer system could be used just to count these and record their positions along the scan. This would generate the shape but would only provide 20 to 50 points across the blade with an uneven distribution along the scan. There would be little detailed information in the areas where the blade's surface is nearly parallel to the reference grid as shown in fig. 32c. This would reduce the spatial resolution of the measurements to below a tolerable limit. Hence information was required between the fringe maxima and minima.

Another factor that directly affected the components' programming was the requirement to utilize the minimum quantity of storage within the computer. The system would ultimately be used in conjunction with a small on-line computer which would have only a restricted storage capacity. Increasing the storage requirements of the computer system would be expensive and its subsequently high cost would make the overall inspection device less attractive for industrial application.

The absolute values of the intensity at the peaks and troughs of the contour pattern and the overall intensity level varied across the blade, as shown in fig. 31. These overall fluctuations meant that it was not possible to calibrate distance (contour depth) with respect to any given value of absolute intensity.

The computer was used as a data processing or sorting system rather than a pure calculating machine and its logic was used to sort the incoming data before actually calculating any depth values. The computer program was written in the language PL/1 in a punched card format for use on an IBM 360 system. The use of the IBM 360 computer dictated slightly different procedures to what would be used with a small on-line computer, so that the maxim of keeping strictly to an on-line system could not be adhered to.

The method used to put the data into the IBM 360 system operated most efficiently if all the data of one scan was loaded in one step and stored as an array of a known number of values and then this array could be interrogated by the programme.

4.3 CONTOUR MAXIMUM AND MINIMUM LOCATION.

The information input of the contour fringes was in the form of an intensity or voltage value, V, and a given voltage representing the position X along the scan, VX.

The values of the intensity voltage were compared in groups of three to locate the maximum and minimum values using the procedure of an 'IF' statement.

```
IF  V(I)  >  V(I-1)  &  V(I)  >  V(I+1)   THEN GO TO  (Max. value)

                                                      .....  (61)

IF  V(I)  <  V(I-1)  &  V(I)  <  V(I+1)  THEN GO TO  (Min. value)
```

where I is the integer counter within a DO-LOOP.
For an on-line system this would be of the form

```
IF  V(2)  >  V(1)  &  V(2)  >  V(3)  THEN GO TO  -----

    V(2)  <  V(1)  &  V(2) <  V(3)  THEN GO TO  -----
```

and at the end of each comparison the group would be up-dated to include the next point, i.e.

```
    V(1)  =  V(2)  ,  V(2)  =  V(3)  ,  V(3)  =  V
```

When a maximum or minimum was located, its position in the array was located and fringe intensity stored. The computer programme is shown in Appendix 1.

4.4 BLADE SHAPE FORMATION.

The maximum and minimum location procedure was continued until both a maximum and minimum value were located. From the known values of these maximum and minimum intensity values a triangular waveform was fitted to the intensity distribution to calculate the depth z for any intermediate intensity value. The relative value of the position of the intermediate intensity point in the waveform which was proportional to the depth was of the form

$$R = [V(I)-VMIN]/[VMAX-VMIN] \quad \ldots\ldots \quad (62)$$

R = the incremental value between 0 and 1 for any intermediate position.

VMAX and VMIN = the intensities of the maximum and minimum points of fringe.

In some practical cases when the contour fringes were scanned the diffraction effects etc. spread the moiré shadow edges and the finite width of the scanning detector distorted the triangular intensity. These effects broadened the peaks and troughs of the fringes, so that a $\sin^2 V$ function was more representative of the curve. To fit this curve to the intensity distribution between the maximum and minimum values, an intermediary intensity function was used of the form

$$AINT = [V(I)-VMIN]/[VMAX-VMIN] \quad \ldots\ldots \quad (63)$$

This varied from a value of 0 to 1 as V(I) varied between the maximum and minimum limits.

The incremental position was then given by the expression

$$R = \sin^{-1} (\sqrt{AINT}) \quad \ldots\ldots \quad (64)$$

To find this value an iteration process was used by setting up an angle, calculating the value of the sine and comparing this to the root of the actual contour intensity function AINT.

This calculation was of the form

```
          C  =  SQRT(AINT) ;
          K,J  =  0 ;
          P  =  1 ;
ASIN  :  YEW  =  J/2**K ;
          P  =  P + YEW
          S  =  SIN(.7854*P) ;
          IF C-S < .001 & C-S > -.001 THEN GO TO BSIN ;
          IF C-S > 0  THEN J = 1 ;
          IF C-S < 0  THEN J = -1 ;
          K  =  K+1 ;
          GO TO ASIN ;
BSIN  :  R  =  P/2 ;
```

R was the solution of the iteration. The IF statement determined the accuracy to which the iteration was operated.

To form the component shape over the whole of the scan the peaks and troughs were counted by the normal counting procedure of

```
COUNT  =  COUNT + 1
```

The calculation of the total depth also required knowledge of whether the fringe under investigation was going from trough to peak or vice versa. For this an indicator was used.

Q = 1 for min to max (intensity increase with increasing VX)

Q = -1 for max to min (intensity decrease with increasing VX)

Finally in the depth calculation the direction of depth represented by increasing contours must be established. Whether the surface was coming towards or away from the observing system. This could not be established from the contour fringes and was preset by the computer from knowledge of the expected shape of the component. Since the system could be used to compare shapes the basic knowledge of the expected shape would be known.

This indicator was of the form

Y = 1 for increasing depth z, object going away from the observer.

Y = -1 decreasing depth Z.

The surface on a turbine blade, however, would be curved and this direction could change, which was indicated by a change in a constant from W = 1 to W = -1.

The resultant depth of the surface was given by

Z( ) = (START + (W*Y*(COUNT+R)))* DELTA *.5 ..... (65)

for Q = 1 and

Z( ) = (START + (W*Y*(COUNT+1-R)))* DELTA *.5 ..... (66)

for Q = -1.

DELTA = the contour depth of the fringes.

START = the number of contour half fringes the first point was from the reference plane.

The position of the point analysed along the blades in the X direction was calculated from either the number of the point in the array or from the X direction voltage VX and a previous calibration. The position of any point EX along the scan was given by

EX( ) = (WIDTH*(XMAX-VX( )))/(XMAX-XMIN) ..... (67)

where WIDTH was the actual width in the object plane represented by a voltage change of XMAX-XMIN. The reference point X=0 was formed at the position represented by a voltage of XMAX.

During the blade scan the computer operation was of the form where it located the position of the maximum and minimum contour intensity, noted the position of these points in the array, calculated the intensity shape value Q, then proceeded to calculate the values of the depth Z between these points. It then continued to the next maximum and minimum pair.

4.5 NOISE EFFECTS.

Sections 4.3 and 4.4 discussed the basic outline of a shape generation process which worked well under idealized conditions. However, the output signal from the optical to electronic interface was a practical signal and consequently had some noise produced by both the interface system and optical surface effects from the object.

The noise on the contour fringe intensity scan produced spurious spikes on the signal which were located by the computer as fringe maximum and/or minimum values and produced additional fringe counts. This was eliminated by a process which examined the values of the maximum and minimum voltages and rejected them if the difference between them was less than a given value. This worked well over the regions where the fringes were closely spaced and for spurious maximum and minimum indications that occurred close to the true maximum or minimum voltage values. However, much of the noise that affected the calculations occurred when the fringes were widely spaced, as shown in fig. 31.

The effects of the noise over this region was reduced by an averaging method. This region was approximately known for each scan. Let it lie between the values VX = XLIM1 and XLIM2.

When the scan reached this region a series of average values of the intensity voltage was calculated.

$$VAV(\ ) = \frac{\sum_{n=1}^{m} V(\ )}{m} \qquad \ldots\ldots \quad (68)$$

m was set between 4 and 9.

This average was taken at every 3rd or 5th information point and was stored in a separate array, as shown in appendix 1.

These average values were then interrogated in blocks of three to find the fringe maxima and minima and then the depth calculated in the normal way.

By going into this averaging routine, it was possible to miss a true maximum or minimum value close to the entry and exit points of the sub-routine. A principal cause of this was that these parameters could only be detected from the second value of the averaging array to the penultimate value since the location depended upon the IF statement

IF VAV(AA) > VAV(AA-1) & VAV(AA) > VAV(AA+1) ..... (69)

An overlapping procedure was used to overcome this problem but it introduced a possibility of one peak or trough being located twice to produce an additional count. This situation was prevented by comparing the number of the point in the input array at which the peak was found in the main programme to the number of the point in the input array at which the peak occurred in the averaging sub-routine. If they coincided within the increment between consecutive averaging points the fringe count was rejected. The point was still used to form a maximum and minimum point pair.

The averaging sub-routine was not infallible in rejecting the noise. It has been found when running the programme that spurious counts occur when noise peaks occur on the main intensity shape between the maximum and minimum regions on the averaged signal.

If these occurred on an increasing intensity slope from a minimum to maximum fringe the noise would produce a spurious maximum, then a spurious minimum and then the intensity would continue to increase. This characteristic was located by examining the intensity of the points after the spurious maximum value using the IF statement

IF VAV(AA+1) > VAV(AA+2) & VAV(AA+2) > VAV(AA+3)

THEN GO TO (MAX Calculation) ; ELSE GO TO (Reject point) ..... (70)

Equation 70 defined that unless the points after the location of the maximum point continued to decrease over the next two points as would occur in a true maximum the point would be rejected as being spurious. For the spurious point on the negative intensity slope the rejection procedure was similar.

4.6 DIRECTION INVERSION PROCEDURE.

The shape of both the concave and convex surfaces of the turbine blade involved a change of direction of the gradient of the surface with respect to the reference plane, fig. 31. The change was not directly indicated by the contour fringes themselves, but only by the reduction in the spatial frequency of the contours in the region where the surface was nearly parallel to the reference plane. It would be possible to locate this region by measuring the relative fringe spatial frequency and locating the minimum. This would not be a satisfactory method as it required knowledge of the maximum-minimum intensity pair beyond the pair over which the slope was being calculated. Hence it needed a large amount of storage within the computer as these maximum and minimum points in this region would be well separated. The increased storage would prohibit the use of this technique on a small computer.

There were two techniques that were used in conjunction with each other to locate the inversion region. These were sub-fringe location and shape gradient measurements.

4.6.1 Sub-Fringe Location.

The fringe intensity distribution of the scans taken along the chord of the blade, fig. 29, shows the inversion region as a decrease in the spatial frequency of the contours with a subsequent increase beyond the actual inversion point. In the majority of cases the point of inversion would not occur at a contour depth of Z = n*DELTA/2 where either a fringe maximum or minimum occurred but at a depth arbitrarily spaced between these values. In these cases the intensity distribution would show either a sub-maximum or sub-minimum, an example of which is shown in fig. 31b. The location of the sub-fringe gives an accurate indication of the inversion point.

When a turbine blade was being inspected the approximate region of the inversion point would be known to within 0.2 inches from the master shape information. It also occurred within the region of the noise averaging process. Hence the region of which the inversion point was expected could be set. The region was set principally to reduce the computing effort used to locate this point. A sub-fringe test was carried out when the programme was in the process of locating the maximum or minimum points for the next half-fringe step.

If a maximum was located its value was compared to the previous maximum and minimum values by the equation

SUBMAX = (VAV(AA)-VMIN)/(VMAX-VMIN) ..... (71)

IF SUBMAX < .75 THEN (Sub-fringe is located) ..... (72)

As seen above, a sub-fringe was defined if the relative height of the peak was less than 75% of the previous half-fringe parameters. This factor was used to allow for the variation of the half-fringe intensity excursion as the blades scanned,as seen in fig. 31. The factor could be varied according to the uniformity of the fringe contrast across the blade. The higher this factor was, the more accurate the distinction between a normal maximum and a sub-fringe. A similar process was used for a sub-minimum.

SUBMIN = (VAV(AA)-VMIN)/(VMAX-VMIN) ..... (73)

IF SUBMIN > .25 THEN (Sub-fringe) ..... (74)

Once the sub-fringe was located the fringe counting factor was stopped. An indicator was also used to stop the system testing for another sub-fringe once it had been located as at times it was possible to get a false location if the SUBMAX and SUBMIN limits were set too close to 1 and 0 respectively.

For a sub-maximum the computer then continued to look for a true maximum and minimum. It then went on to locate the next minimum. This minimum had the same depth value as the previous value and the sub-maximum region increased beyond the depth at these minimum values. The component's shape was then plotted between these two values.

On completing this the next half-fringe pair was found where the intensity was increasing to a maximum value. In this case inversion had already occurred and so before the shape was calculated a number of parameters were modified.

W = -1

START = START + COUNT -1

COUNT = 0

W changed the direction of the value of the depth Z with increase in contour fringes.

The START parameter, the factor which related the shape to the reference plane, was updated by adding the value of (COUNT-1) to it. This fixed the inversion point with respect to the reference plane. COUNT was then set to zero so that it could operate in the normal way of fringe counting but now the depth was going in the opposite direction. The equation of the component shape was of the form

```
Z( )  =  (START +(W*Y*(COUNT+R)))*DELTA*.5
```

Hence the depth beyond the inversion region was subtracted from the depth calculated from the updated START parameter.

A similar process was adopted for the sub-minimum fringe location. Details of both procedures are shown in Appendix 1. Many of the print-out statements (PUT EDIT) were not required in the final programme but were used for fault locations in the development of the programme and have been included in Appendix 1 to make the programme more easily followed.

4.6.2 Gradient Inversion Location.

This procedure calculated the inversion point when it occurred in the region of a full maximum or minimum contour region. The actual inversion point always occurred at either an intensity maximum or minimum, including sub-fringes, because of the depth function symmetry at the depth inversion. Consequently for inversion at a true maximum or minimum it was sufficient to be able to say whether or not the inversion was going to occur at the end of any particular half-fringe set of calculations. As with the sub-fringe effect the inversion point in test was only carried out over a specific region of the blade.

Gradient inversion location was formed by examining the rate of change of depth Z of the points immediately preceding the actual point being plotted. This could be achieved calculating the gradient between the point being plotted and its immediate predecessor in the form

```
Gradient  DZ  =  (Z(L)-Z(L-1))/(EX(L)-EX(L-1))                    .....  (75)
```

This was not sufficiently reliable under practical conditions due to the noise and slight inaccuracies within the system which caused DZ to equal zero or go negative prematurely.

To overcome this a more detailed estimation of the gradient of the shape was taken by operating a straight line fit to the blade shape for a number of points preceding the one being plotted by the method of least squares, Brownlee [39].

$$\text{Mean value of EX} = DEXB = \frac{\sum_{m=1}^{n} EX_m}{n} \quad \ldots\ldots (76)$$

$$\text{Gradient} \quad DZ = \frac{\sum_{m=1}^{n} (EX_m - DEXB) x Z_m}{\sum_{m=1}^{n} (EX_m - DEXB)^2} \quad \ldots\ldots (77)$$

This was operated for the 6 points before the point that was being plotted. The gradient DZ was compared to a given limit GRAD and if DZ < GRAD then the inversion point would occur at the end of the half-fringe being plotted. (GRAD was always positive.) When this occurred a number of parameters were reset as with the sub-fringe inversion location.

W = -1

START = START+COUNT

COUNT = 0

After this normal shape plotting was resumed.

The same method would be used if the inversion point occurred at either a maximum or minimum intensity point.

There were occasions, if the limit GRAD was set too high, when the noise in the intensity input signal triggered the inversion procedure prematurely and as the program continued a sub-fringe value would be subsequently located. In the event of this happening on the IBM 360 system the programme was made to restart with the knowledge that the inversion point would be formed by a sub-fringe. For a smaller computer the programme would be made to return to the point where the premature inversion occurred and then recalculate the shape from that point knowing that the inversion would be in a sub-fringe form.

4.7 SYSTEM REFINEMENTS.

The shape plotting programme operated from the first maximum to minimum fringe pair which left the shape of the part of the blade up to this area unknown. This was overcome by extrapolation ~~back projection plotting~~ in which a straight line fit was applied to the shape plotted from the first few contours by the method of least squares and then this was extended backwards to the edge of the blade. The edge was defined by the position in which the intensity voltage went above a given threshold value as the scan went from a dark background to the blade.

On the concave surface of the turbine blade aerofoil there was a second direction inversion region close to the leading edge. In this case the point of inversion was located by measuring the spacings between the half fringe peaks and troughs and locating the region of the maximum spacing. This was not particularly effective because of the rapid change of depth in this region and the decrease in intensity signal level as the edge was approached as seen in fig. 31. An approximation method was used in which it was assumed that the direction inversion occurred at a particular position from the leading edge and the inversion procedure was operated accordingly.

Other possible improvements to the technique depend upon the application for which the system was designed. It would be possible for the computer to control the scanning interface during the scan but this would greatly increase the complexity of the system. A simple method of controlling the number and density of the point calculations as the scan was operated would appear more practical so that the detail of the analysis of different parts of the blade could be controlled. Considering the routine application of the overall inspection system a computer must be used to control the whole inspection operation. The computer would indicate when the system was ready to accept the blade, check that the blade was loaded correctly, trigger the scanner to operate, analyse the blade and state when the cycle had been completed.

4.8 THREE-DIMENSIONAL ANALYSIS.

The turbine blade aerofoils were three-dimensional and the detailed analysis required a shape profile at a number of positions along the axis of the blade to build up the three-dimensional information. The three-dimensional link between the scans could be achieved by two methods; scanning in the direction at right angles to the normal scan and counting fringes or by having a physical marker at each scan position which relates the first point on the blade to a given reference plane.

The former method would mean scanning the blade parallel to the axis and across the grid lines of the contouring grid which would introduce a noise factor but this could be reduced by either accepting information points that occur only in between the grid lines, or just accepting the values of the intensity peaks, which would be modulated by the contour fringes. This would relate a particular value across each scan and so modify the set parameter START to a derivation of this value. By this means three-dimensional information could be built up.

The second method would perform the same function and could be produced by using a number of arms from a reference plane that were spring loaded against the surface of the blade as shown in fig. 33. The thickness of the levers was made to be equal to one contour depth interval.

4.9 TURBINE BLADE DIMENSIONAL REFERENCES.

The reference system used on turbine blades was defined by a point 'P' on or just below the bottom of the fir tree root through which the axis of the blade runs, see sketch. This point was also on a line that ran parallel to the fir tree root in a plane normal to the blade's axis. This line was defined as datum 'D'. The tip of the blade was defined by a point on the face of the shroud that would be visible in the contouring system. This point was a specific distance from the axis of the blade measured normal to the plane of datum D. The aerofoil was defined with respect to a plane (AE) parallel to the blade's axis and set at a specific angle, rotated about the point P and normal to the blade axis. The angle was dependent upon the blade design.

For inspection by optical contouring the turbine blade mounted in a kinematic mount on the base of the fir tree root to locate the reference point P and the datum line D. The axis of the blade was located by the reference point on the shroud by a point in this position on the mounting jig. The whole of the blade was then held in position kinematically with the blade's axis in a horizontal plane normal to the direction of observation.

The dimensional depth of the aerofoil was related to the reference point on the shroud by the mechanical probes as shown in fig. 33. The reference plane of the optical system was not necessarily the one which defined the aerofoil on the drawing as the blade was rotated about its axis to present the most suitable contour pattern on the aerofoil for the contouring system. This angle was set for each type of blade. It would be a simple arithmetical process within the computer to relate the aerofoil dimensions to the reference plane set by the optical system from that defined on the drawing.

The blade would be rotated about its axis through 180° to inspect

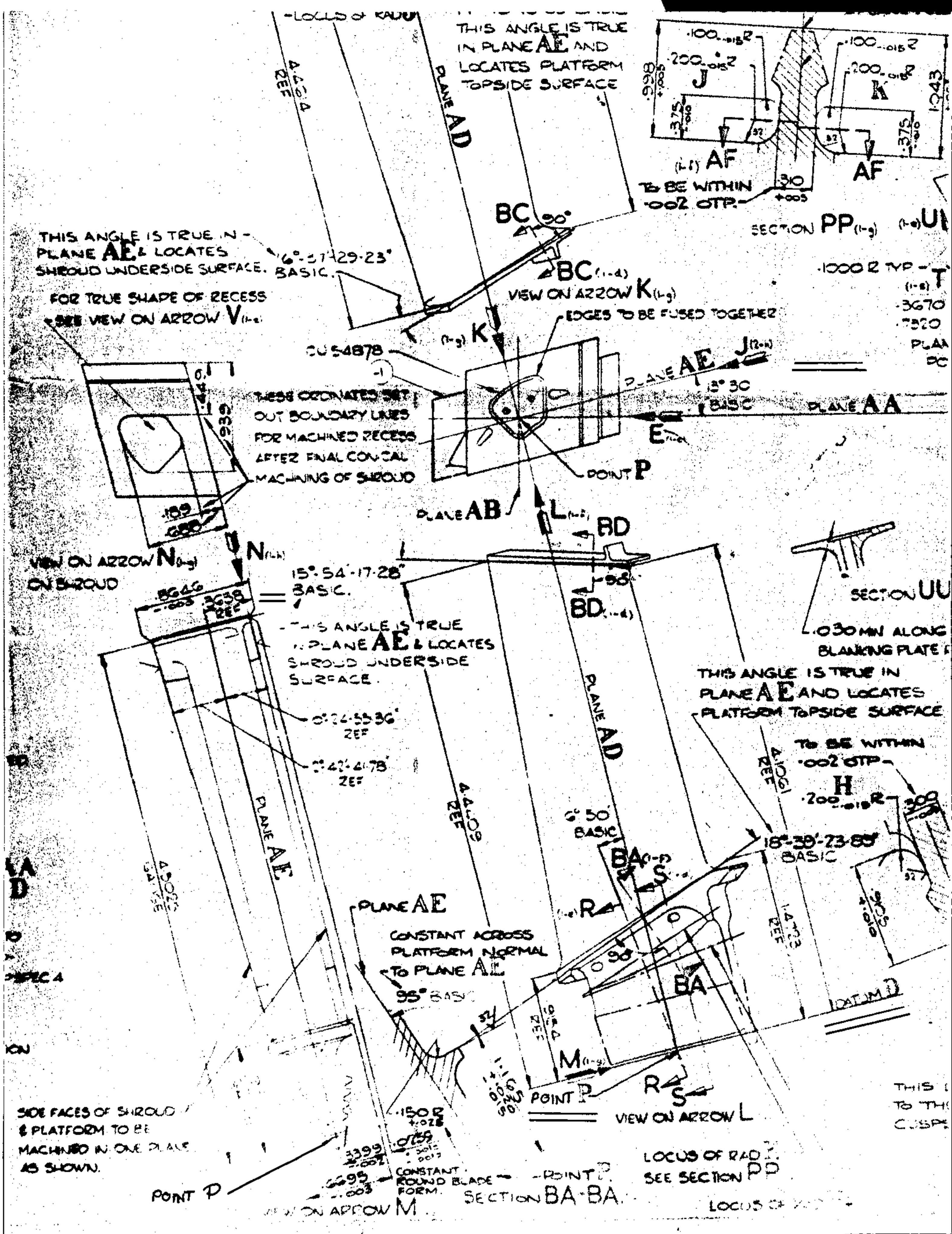

THIS ANGLE IS TRUE IN PLANE AE AND LOCATES PLATFORM TOPSIDE SURFACE
PLANE AD
TO BE WITHIN .002 DTP.
SECTION PP
THIS ANGLE IS TRUE IN PLANE AE & LOCATES SHROUD UNDERSIDE SURFACE.
16°-37'-29-23" BASIC
FOR TRUE SHAPE OF RECESS SEE VIEW ON ARROW V
VIEW ON ARROW K
EDGES TO BE FUSED TOGETHER
PLANE AE
PLANE AA
THESE ORDINATES SET OUT BOUNDARY LINES FOR MACHINED RECESS AFTER FINAL CONICAL MACHINING OF SHROUD
POINT P
PLANE AB
VIEW ON ARROW N ON SHROUD
15°-54'-17-28" BASIC.
THIS ANGLE IS TRUE IN PLANE AE & LOCATES SHROUD UNDERSIDE SURFACE.
SECTION UU
.030 MIN ALONG BLANKING PLATE
THIS ANGLE IS TRUE IN PLANE AE AND LOCATES PLATFORM TOPSIDE SURFACE
PLANE AE
CONSTANT ACROSS PLATFORM NORMAL TO PLANE AE
95° BASIC
18°-38'-23-85" BASIC
DATUM D
SIDE FACES OF SHROUD & PLATFORM TO BE MACHINED IN ONE PLANE AS SHOWN.
POINT P
CONSTANT ROUND BLADE FORM.
VIEW ON ARROW M
SECTION BA-BA.
VIEW ON ARROW L
LOCUS OF RAD P. SEE SECTION PP

the other surface of the aerofoil in a similar manner.

The basic concept of this analysis programme was straightforward but the logic within the programme to permit analysis of a practical intensity scan signal with all the possible variations and factors involved increased the overall complexity. However, all the control indicators were necessary to ensure that the programme would function correctly for the number of practical variations that occur. Details of the use of this programme is given in section 5.3.

4.10 OBJECT SHAPE COMPARISON.

It has been established that direct shape subtraction was the most satisfactory method of comparing two objects for this method of inspecting turbine blades. A number of comparison methods were investigated. These were direct depth subtraction, co-ordinate system manipulation and sectional moment effects.

4.10.1 Depth Subtraction.

This provided identical information to direct optical contour subtraction as discussed in section 3.2 but with greatly increased accuracy. The co-ordinate array of a scan across the reference object could be of the form RZ( ) and REX( ) and the corresponding scan across the production object would be of the form Z( ), EX( ). The values of the distancesalong the scan REX( ) and EX( ) did not necessarily correspond because of the variations that occurred in the rate of scan across the blade and the total number of point measurements taken with the mechanical scan system as discussed in section 4.4.

For this subtraction method for each value of EX(I) on the production shape the nearest value of REX( ) was located and the exact value of RZ( ) corresponding to the scan position EX(I) was found using an extrapolation of the form

$$\mathrm{REFZ} = \mathrm{RZ(U)} - ((\mathrm{REX(U)} - \mathrm{EX(I)}) \times \frac{(\mathrm{RZ(U)} - \mathrm{RZ(U-1)})}{(\mathrm{REX(U)} - \mathrm{REX(U-1)})} \quad \ldots\ldots \quad (78)$$

where U was the number of the point in the reference array that is the nearest value to the value EX(I) in the production array.

The difference between the shapes was given by the array

$$ERROR(I) = Z(I) - REFZ \qquad \text{.....} \quad (79)$$

This gave the point by point difference between the shapes. The difference normal to the actual surface of the blade was given by applying a cosine correction to the value of ERROR(I). The value of cosine was calculated from the shape of the surface with respect to the scan direction Z.

A linear fit to the values within the ERROR(I) array by the method of least squares gave the general trend of the difference but from this information it was not possible to obtain an accurate assessment of the overall difference between the object and its reference shape. There was not sufficient information to isolate the dimensional difference possibilities because no account had been taken of the differences in the direction of the scan. Ideally the overall difference should be given as the displacements in the x and z directions plus an angle of rotation.

4.10.2 Co-ordinate System Manipulation.

This technique was a more appropriate means of providing the data for the overall difference as a co-ordinate shift plus an angle of rotation. In this case the changes to the co-ordinate system of the production component to superimpose its shape on to that of the reference shape would be calculated. To achieve this, consider a point (x,z) on the co-ordinate system x,z, fig. 34a. This system is displaced by an amount (p,q) with respect to the reference system (XZ) and is also rotated by an angle α with respect to the reference. The point P(x,z) on the (xz) system is equivalent to the point (X,Z) on the reference co-ordinate system whose values are given by

$$X = x \cos \alpha - z \sin \alpha + p \qquad \ldots\ldots (80)$$

$$Z = x \sin \alpha + z \cos \alpha + q \qquad \ldots\ldots (81)$$

In the case of the shape of a turbine blade this had to be applied in two stages. Firstly a point on both the reference shape and production shape must be identified as identical points, fig. 34b. Such a point could be the starting point on each blade, on the trailing or leading edge. These two points would be superimposed by solving the equations

$$REX = EX + p \qquad \ldots\ldots (82)$$

$$RZ = Z + q \qquad \ldots\ldots (83)$$

for p and q.

The production shape array would then be modified by the effects of p and q. The angle α would be found by an iteration process of estimating an approximate angle through which the co-ordinate system should be rotated. Then the effects of the rotation would be examined and a better estimate of the angle made. This iteration loop would be continued until the required accuracy was achieved. The iteration function could be made to converge rapidly to minimise the number of iterations but the method has a number of fundamental faults.

(a) It was solely dependent upon the integrity of the two points at the edge of the blade for the superimposition of the two shapes. In practice these points would not always be in the same position with respect to the main part of the blade. This would be particularly true of blades that have been affected by thermal fatigue where the trailing edge may have been grossly distorted. There would be no other reference points on the blade that would be suitable unless the blade was deliberately marked. Marking the blade would not be practical for a production system.

(b) To gain more accurate information and improve on the fit obtained by superimposing the end points, additional iteration processes would be involved for both the x,z co-ordinate shifts and angle.

(c) As iteration processes were involved it would be liable to take up more computer time than a direct approach and hence increase the overall inspection time.

The practical problems of the position of the end points with respect to the main section of the blade and the number of iteration processes involved made this technique impractical in comparison to the sectional centroid technique.

4.10.3 Sectional Centroid Superimposition.

At any given scan position along the axis of the turbine blade aerofoil both the concave and convex surfaces could be scanned and linked together within the computer to form the complete section of the blade. For the whole sectional area the basic shape of the reference section and the corresponding section on the production blade would be the same. The actual shape differences would be small as in practice the production surface would be only of the order of 0.020" larger than the reference surface at any one point for a blade section around 1.0" wide and up to 0.30" maximum sectional thickness. Under these conditions the fundamental assumption could be made that the Centroids of both sections would remain in the same relative positions with respect to their surfaces. Hence for a blade section that had an overall displacement with respect to the reference section plus some localized differences the overall displacement could be calculated by superimposing its centroid on to that of the reference surface. The required co-ordinate shift would give the overall difference between the two in the x and z directions.

The angular displacement between the two could be calculated from the angular difference between the principal axes of each of the two surfaces.

In addition to these parameters the comparison of the area of the production and reference sections would give an indication of the integrated size difference between them.

To examine these properties in greater detail, consider the turbine blade section in fig. 35a. The co-ordinate system is the depth Z plotted against the position along the scan X as derived from the practical scanning system. Both the concave and convex surfaces were formed to give the complete section. This could be achieved by suitable manipulation of the surface data within the computer. The concave surface is represented by curve z_1 and z_2 represents the convex surface.

The area of the blade section is given by taking individual elements in the x direction, Massey [40] and is given by the equation:-

$$\text{Area} = \sum_{n=1}^{m} \tfrac{1}{2}\left[\left(z2_n + z2_{n+1}\right) - \left(z1_n + z1_{n+1}\right)\right]\left[x_{n+1} - x_n\right]$$

$$= \sum_{n=1}^{m} \left(\text{Area}_{dx}\right)_n \qquad \ldots\ldots \quad (84)$$

where m is the number of elements that the surface is divided into. This can also be expressed as a sum of a series of elements in the z direction.

$$\text{Area} = \sum_{n=1}^{m} \tfrac{1}{2}\left[\left(x2_n + x2_{n+1}\right) - \left(x1_n + x1_{n+1}\right)\right]\left[z_{n+1} - z_n\right]$$

$$\sum_{n=1}^{m} \left(\text{Area}_{dz}\right)_n \qquad \ldots\ldots \quad (85)$$

The position of the centroid of this area with respect to each of the two axes is calculated by taking the first moment of each element about the respective axis and dividing by the total area.

$$\bar{x} = \frac{\sum_{n=1}^{m} \left(\text{Area}_{dx}\right)_n \cdot \tfrac{1}{2}\left(x_n + x_{n+1}\right)}{\sum_{n=1}^{m} \left(\text{Area}_{dx}\right)_n} \qquad \ldots\ldots \quad (86)$$

$$\bar{z} = \frac{\sum_{n=1}^{m} \left(\text{Area}_{dz}\right)_n \cdot \tfrac{1}{2}\left(z_n + z_{n+1}\right)}{\sum_{n=1}^{m} \left(\text{Area}_{dz}\right)_n} \qquad \ldots\ldots \quad (87)$$

Using the above equation the centroid of both the reference and production section can be found with respect to the co-ordinate system of the scanning device.

~~The second movement of the surface~~, The effective radius of gyration about the two axes are given by equations

$$RX^2 = \frac{\sum_{n=1}^{m} \left(\text{Area}_{dx}\right)_n \cdot \left[\frac{1}{2}\left(x_n + x_{n+1}\right)\right]^2}{\sum_{n=1}^{m} \left(\text{Area}_{dx}\right)_n} \qquad \text{.....} \quad (88)$$

and

$$RZ^2 = \frac{\sum_{n=1}^{m} \left(\text{Area}_{dz}\right)_n \cdot \left[\frac{1}{2}\left(z_n + z_{n+1}\right)\right]^2}{\sum_{n=1}^{m} \left(\text{Area}_{dz}\right)_n} \qquad \text{.....} \quad (89)$$

The equivalent to the product of inertia over this area about the origin of the co-ordinate system would give the relation of the angular orientation of the surface with respect to the co-ordinate system. This would produce a radius of gyration of the form, Timoshenko [41],

$$RHXZ^2 = \frac{\sum_{n=1}^{m} \left(\text{Area}_{dz}\right)_n \cdot \left[\frac{1}{4}\left(x_n + x_{n+1}\right)\left(z_n + z_{n+1}\right)\right]}{\sum_{n=1}^{m} \left(\text{Area}_{dz}\right)_n} \qquad \text{.....} \quad (90)$$

The radius of gyration of the surface about any line parallel to the respective axes and a distance k from it can be calculated by the parallel axes theorem.

$$RX^2 = k^2 + RX_k^2 \qquad \text{.....} \quad (91)$$

Hence using this theorem the radius of gyration about the lines parallel to the axes through the centroid is given by

$$RXG^2 = RX^2 - \bar{X}^2 \qquad \ldots\ldots (92)$$

$$RZG^2 = RZ^2 - \bar{Z}^2 \qquad \ldots\ldots (93)$$

Similarly the radius of gyration of the product of inertia can be transferred from the origin to the centroid by the equation

$$RHXZG^2 = (RHXZ^2 - \bar{X}.\bar{Z}) \qquad \ldots\ldots (94)$$

The total radius of gyration of the section about the centroid is:-

$$R_G = (RXG^2 + RZG^2)^{\frac{1}{2}} \qquad \ldots\ldots (95)$$

If the product of inertia was taken for a series of co-ordinate systems rotated about the origin ~~of the original~~ the value of the radius of gyration will vary between a maximum and minimum value to form an ellipse, known as the ellipse of inertia. The position of the radius where the value would be either a maximum or a minimum would be known as the principal axis of inertia and occurs when the product if inertia with respect to this co-ordinate system is equal to zero. Hence the principal axes form axes of symmetry of the ~~surface.~~ cross section.

The angle, ϕ, of the principal axes with respect to the co-ordinate system xz is given by Timoshenko [36].

$$\tan 2\phi = 2 \,.\, Ixz/(I_x - I_z) \qquad \ldots\ldots (96)$$

where I_x and I_z are the inertia values about the x and z axes respectively and I_{xz} is the product of inertia.

Referring this to the computed values the angle calculated at the centroid of the surface becomes

$$\tan 2\phi = \frac{2(RHXZG)^2}{(RZG^2 - RXG^2)} \qquad \ldots\ldots \quad (97)$$

By trigonometry

$$\tan \phi = (1 + \cot^2 2\phi)^{\frac{1}{2}} - \cot 2\phi \qquad \ldots\ldots \quad (98)$$

If the angular position of the principal axes of both the production and reference surfaces are found the angular difference between these axes gives the actual angular difference between the two surfaces, fig. 36.

Hence the angular difference is given by

$$\tan \alpha = \frac{\tan \phi_{prod} - \tan \phi_{ref}}{1 + \tan \phi_{prod} \tan \phi_{ref}} \qquad \ldots\ldots \quad (99)$$

where ϕ_{ref} and ϕ_{prod} are the angles of the principal axes of the reference and production surfaces respectively.

This angle plus the co-ordinate corrections found by superimposing the centroids of the two sections would give sufficient information to describe the overall difference between any component and its master shape. To compare the shape of the production blade to its master in greater detail the co-ordinate system of the production blade should be modified according to the overall differences to superimpose the production on to master shapes within the same co-ordinate system.

To modify the production system the effect of the linear differences between the shape centroids was considered first. This formed an intermediate co-ordinate system whose origin was displaced with respect to the production co-ordinate system by (P_{int}, Q_{int})

$$\begin{aligned} P_{int} &= \bar{x}_{ref} - \bar{x}_{prod} \\ Q_{int} &= \bar{z}_{ref} - \bar{z}_{prod} \end{aligned} \qquad \ldots\ldots \quad (100)$$

$(\bar{x}_{ref}, \bar{z}_{ref})$ and $(\bar{x}_{prod}, \bar{z}_{prod})$ = the co-ordinates of the reference on production centroids respectively.

The modified co-ordinates of the production shape (x_{int}, z_{int}) were given by

$$(x_{int} = x_{prod} + P_{int} \; , \; z_{int} = z_{prod} + Q_{int}) \qquad \ldots\ldots \quad (101)$$

The displacement of the origin of the intermediate co-ordinate system produced by the angular rotation α about the centroid was given by

$$P \; = \; \bar{x}_{ref} - \bar{x}_{ref} \cos \alpha + \bar{z}_{ref} \sin \alpha \qquad \ldots\ldots \quad (102)$$

$$Q \; = \; \bar{z}_{ref} - \bar{x}_{ref} \sin \alpha - \bar{z}_{ref} \cos \alpha \qquad \ldots\ldots \quad (103)$$

$$(\bar{x}_{int} \; = \; \bar{x}_{prod} + P_{int} \; = \; \bar{x}_{ref})$$

Combining the effects of the intermediate translation and the rotational effect the co-ordinates of the production shape were modified by the equations

$$\text{XMOD( )} \; = \; [\text{EX( )} + P_{int}] \cos \alpha + [\text{Z( )} + Q_{int}] \sin \alpha - P \qquad .. \quad (104)$$

$$\text{ZMOD( )} \; = \; - [\text{EX( )} + P_{int}] \sin \alpha + [\text{Z( )} + Q_{int}] \cos \alpha - Q \qquad .. \quad (105)$$

Having established the overall differences between the production and reference blade sections and modified the production co-ordinate data accordingly the localized differences could be calculated by direct co-ordinate subtraction.

This technique could also be applied to ~~just~~ adjust the shape curve of either the concave or convex surface of the blade, if the curve was considered as an area or line with an infinitely small width. In this case the length of the curve would be equivalent to the area of the blade section. Thus

$$\text{Curve length} \; = \; \sum_{N=1}^{M} ds_N \qquad \ldots\ldots \quad (106)$$

where ds is the length of each of the m elements into which the curve is divided.

Using the present computer programme nomenclature for the Nth point in the shape co-ordinate array the value of ds between two adjacent points would be:-

$$ds_N = \left[\left(Z(N) - Z(N-1) \right)^2 + \left(EX(N) - EX(N+1) \right)^2 \right]^{\frac{1}{2}} \quad ..... \quad (107)$$

Taking the first moment about the Z axis to calculate the centroid

$$\bar{x} = \frac{\sum_{N=1}^{M} ds_N \cdot \frac{1}{2} \left(EX(N) + EX(N+1) \right)}{\sum_{N=1}^{M} ds_N} \quad ..... \quad (108)$$

Also $$\bar{z} = \frac{\sum_{N=1}^{M} ds_N \cdot \frac{1}{2} \left(Z(N) + Z(N+1) \right)}{\sum_{N=1}^{M} ds_N} \quad ..... \quad (109)$$

Similarly the second moments about the co-ordinate system axes

$$RX^2 = \frac{\sum_{N=1}^{M} ds_N \left[\frac{1}{2} \left(EX(N) + EX(N+1) \right) \right]^2}{\sum_{N=1}^{M} ds_N} \quad ..... \quad (110)$$

$$RZ^2 = \frac{\sum_{N=1}^{M} ds_N \left[\frac{1}{2} \left(Z(N) + Z(N+1) \right) \right]^2}{\sum_{N=1}^{M} ds_N} \quad ..... \quad (111)$$

and the radius of the product of inertia would be:-

$$RHXZ^2 = \frac{\sum_{N=1}^{M} ds_N \left[\frac{1}{4}\left(EX(N) + EX(N + 1)\right)\left(Z(N) + Z(N + 1)\right)\right]}{\sum_{N=1}^{M} ds_N} \quad \ldots\ldots (112)$$

Using these values and the procedure for calculating the rotational and displacement differences that have been previously discussed it would be possible to calculate the change in co-ordinate position of any point on the blade's surface, within the scan, or any point within the XZ plane.

The use of the centroid location technique for the individual shape curves enabled the problems discussed in the co-ordinate system manipulation method section 4.10.2 to be overcome.

4.10.4 Three-Dimensional Assessment.

Using the above methods of analysis it would be possible to build up an array of the values of the difference in the X and Z direction and the angular difference for each of the sections of the blade that had been scanned. Considering each of these parameters individually a linear equation fit could be applied to estimate the general trend along the axis of the blade as shown in fig. 35b. Or if more detailed information was required a spline fit could be applied to all the points in one array. In a spline fit a line would be drawn between the first two points in the graph or array. A similar line would be drawn through the second and third points. The spline would be defined as the co-ordinate of the second point in the array plus the angle between the line through the first two points and the line through the second and third points as shown in fig. 35b. The next pair of points would be considered and the values calculated and these parameters are continued for all the points in the array. The first point in the spline curve would be the co-ordinates of the first point plus the angle of the line through the first and second points with respect to the axis. Such a function would enable the deviation from the general trend to be shown clearly.

If a spline fit was constructed for the overall deflection in the Z direction of each section scanned the variation in the values of the angle ψ, as defined in fig. 35b, would indicate the overall distortion of the blade. If ψ was approximately zero for all the sections, excluding the first, this would indicate that the aerofoil was bent backwards about a point towards the blade root and the overall aerofoil was not distorted, whereas if ψ was other than zero the blade had a processive bend or curved structure. The type of bending effect on the blade would be particularly interesting when the system was being used to examine thermally stressed blades. The blade twist could be analysed in a similar manner, to measure whether the twist was progressive or not.

A more rigorous and usual spline fitting procedure would be the application of the cubic spline, Ahlberg [42]. This would apply a smoothing out procedure between the discrete points on the deflection curve by applying a polynomial equation to the points. This would have particular advantages in calculating the first and second derivatives of the deflection to form the strain and bending moments, and therefore could be effectively used for the examination of a blade that had been thermally or mechanically stressed. The cubic spline has been used in holographic strain measurement by Brandt [43].

The type of analysis in three dimensions primarily depends on the application.

4.11 COMPUTER VERIFICATION.

The hypothesis stated above was examined in greater detail using a theoretical model on the computer. A shape was formed mathematically to represent the blade section. This shape was displaced by known amounts and the point by point co-ordinates recalculated. The original shape represented the reference object and the displaced shape represented the production object. Using the area, first and second moments of the area, as described above, the distortion parameters were calculated. These values were compared to the actual displacements that had been applied to the original shape.

An elliptical shape was used as this could be generated conveniently within the computer using the equation

$$\frac{(x - p)^2}{a^2} + \frac{(y - q)^2}{b^2} = 1 \qquad \ldots\ldots \quad (113)$$

where a = 1, b = 0.4, p = 1.0, q = 0.6 to form the ellipse in approximately the same position as that of a blade section. The centre of the ellipse (p,q) was displaced and the ellipse was tilted through a small angle, and these parameters were used to calculate the new point by point co-ordinates of the now displaced shape.

The centroid and second moments calculated for the reference shape with respect to the two axes of the reference system and the components of the radius of gyration about the centroid were calculated. The program used is shown in Appendix 2.

The same set of parameters was calculated for the production surface, using interpolation technique when calculating the values of the area elements, Appendix 2. From these results the displacement was calculated and compared with the actual displacement applied. This was also applied to a line forming one half of the elliptical surface. The results of this examination are shown in Table 2, and Appendix 2.

The calculated linear and angular displacements for the single curve of half of the ellipse agreed exactly with the applied distortion for all the cases considered. There were, however, some slight differences between the calculated and applied distortion when the whole area of the ellipse was considered. These were due to the errors built up in calculating the surface area and second moments of the displaced shape when using a finite number of area elements. The calculations showed that these methods gave the overall dimensional differences in the form of co-ordinate system change as predicted in section 4.10.

Chapter V.

Experimental Results and Television Interface.

5.1 INTRODUCTION.

In this chapter the experimental work carried out on the contour image scanning system and the results obtained from the computer using contour intensity information is described. The slow scan television camera interface and digital recorder system that were used to increase the input rate of the information into the computer and the results obtained are also described.

5.2 IMPROVEMENT OF MOIRÉ CONTOUR FRINGES.

The objective of this work was to improve the quality of the contour fringe intensity traces that were obtained when the contoured image was scanned. Both the moiré shadow and fringe projection image scan techniques were studied and developed.

Much of the initial work was carried out using these techniques before the television interface was developed and a mechanical scan system was used. This has been described in section 3.4.2, and is shown in fig. 24. The quality of the contour fringe intensity profiles obtained by scanning parallel to the moiré grid lines was improved by decreasing the width of the slit, normal to the direction of the scan, to a minimum < .005" for an image to object magnification of approximately 0.95 in the observing camera. The slit length was approximately 0.020". The limit on these parameters was the noise produced on the photomultiplier as the gain was increased to accommodate the smaller signal levels. However, on a typical turbine blade aerofoil section with a slit some ·20 mm wide and ·40 mm long it is possible to obtain good quality contours at 0.015" depth interval. At 0.010" intervals the spatial frequency of the fringes was high and could not be effectively resolved by the photomultiplier slit. Further examination of the variation of fringe quality with depth interval on the turbine blade showed that if the contour depth interval was increased to the region of 0.015" to 0.020" the quality of the fringe intensity profile greatly increased and a true triangular waveform was obtainable, an example of which is shown in fig. 37. Since the intensity function followed the theoretical function more closely and the maximum and minimum intensity values of the contours were more clearly defined, it was possible to form the interfringe depth values to an accuracy of 5% of the contour depth interval and hence retain the measuring accuracy of ± 0.001" and in some cases improve on it.

Thus for the dimensional analysis of turbine blades whose total depth varied from 0.2" to 1.0" the most accurate depth information would be obtained by using a contour depth that provided a good quality fringe intensity distribution that followed the theoretical triangular intensity function rather than generating contours with a small depth interval which became difficult to resolve and the intensity distribution became distorted by diffraction and penumbra effects.

Further examination of the fringe projection/scanning method of contour generation, using the photomultiplier mechanical image scanning system, confirmed that this was a viable and attractive technique. It was possible to make good quality moiré grids with a varying spatial frequency across the grid to comply with the requirements discussed in section 2.7.6. When projected, the grid lines were focused in a plane at 45° to the optical axis of the projection system. The blade was placed in the focal plane of the projected fringes and the contouring system formed as shown in fig. 15. It was possible to obtain good quality contour fringe scans with contour depth intervals down to 0.010". The photomultiplier aperture size was found to be most effective and produce better contrast fringes if it was less than half the period of the projected fringes. Reducing the aperture size takes into account the cosine effect of the projected fringe width produced by the slope of the surface of the object.

Very good quality intensity scans were produced, as shown in fig. 38, with a contour interval of 0.010". The maximum and minimum points of the fringes were well defined and the intensity distribution was triangular. The overall variation in the intensity of the fringe peaks across the blade was less than that of the moiré shadow contouring technique. Also the clarity of the high spatial frequency fringes was better than that of the moiré shadow contouring. The image scanned in fig. 38 is shown in fig. 17.

In addition to the improvements in contour fringe quality obtained by the fringe projection system it had the purely practical advantage in handling the turbine blade in so far as the blade was not close to the actual moiré grid. This meant that more space would be available for the operator in which to handle the blade when it was being loaded and rotated to inspect both surfaces.

An investigation into the range of surface finishes which would produce reasonable contour fringes showed that the surface must have good light scattering rather than reflecting properties. The most efficient surface finish was matt white paint which could be easily applied from a spray can. The majority of turbine blade surface finishes would be suitable including the vapour blasted surface on a completed turbine blade and the blackened surface of a blade that had been run in an engine.

Examining both the moiré shadow and fringe projection methods of contouring for use in conjunction with the television interface on a routine basis, the fringe projection system was found to be the more suitable. In the television system the size of the integrating area of the scanning spot for a television tube with a resolution of 800 lines across the frame of 0.75" was approximately 0.0005". For a turbine blade an object to vidicon image demagnification of the order of 5:1 was required to enable the whole of the aerofoil section to be observed. Thus for 100 lines/inch spatial frequency of the fringes on the object (for 0.010" contour depth interval) the width of half the grid period on the vidicon was 0.001". This was twice the size of the scanning spot. Hence under these conditions the fringe projection would be the ideal form of contouring system. The moiré grid in the moiré shadow technique presented a possibility of not being able to obtain any contour fringes if the scanning line position coincided with the dark section of the moiré grid. Also because the spot size was less than the half period of the moiré grid the grid was not acting as any form of demodulation system and so was redundant. The alignment of the scan direction parallel to the grid lines was critical in both contouring systems. If the alignment was not correct for the moiré shadow method, contour information would only be obtained during part of the scan. The effect on the fringe projection system was less crucial as misalignment added a varying depth error on to the contour fringes. From these observations it was concluded that the moiré fringe projection system was the most suitable for use with the television interface.

5.3 COMPONENT TOTAL DEPTH EFFECTS.

The effects of the variation of the contour depth interval with the depth being plotted, fringe number, were investigated for the blades that were examined during the experimental work. This was basically a study of to what extent it could be assumed that the depth contour interval was constant for any contour fringe number, i.e. that the contour depth for the Nth fringe was given by equation 35, section 2.6.1.

$$z = \frac{N.p.h}{d}$$

If h was not much greater than the depth z the value of z from the reference plane was given by equation 34.

$$z = \frac{N p h}{d - Np}$$

For the laboratory contouring system h = .35.5".

The depth excursion of the majority of turbine blades that would be examined by the contouring system was less than 0.50". This represented a ± 0.25" depth excursion from the image plane of the projected grid, fig.15a, on the fringe projection/image scan contouring system. The blade under examination was always positioned so that the image plane of the projected grid was approximately midway along the total depth excursion of the blade. Hence both positive and negative values of N were used. This made best use of the depth of focus of the fringes either side of the image plane.

For a contour depth interval of 0.010" generated using a 100 cycles/inch moiré grid, p = 0.01", d = 35.6", the depth represented by the + 25th fringe on the uncorrected equation z = 0.250" and for the corrected equation z = 0.251". The resultant error was 0.001" which was within the measuring accuracy of the overall system. Hence it would not be necessary to correct the depth value against fringe number for the majority of turbine blades. If the depth excursion was increased to ± .50" the error would be 0.005" and so the correction equation would be required.

The requirement to use the corrected equation for calculating the depth z was highlighted when a model fan blade was examined for a development department within the Company. This was approximately 12" long and had a maximum depth excursion of 2.5" over the area of interest.

A nominal contour interval of 0.040" was used to examine the blade. The grid frequency was 50 cycles/inch. h = 35.5, d = 17.77. For the fringe number N = + 30 representing maximum fringe number encountered, the uncorrected depth was z = 1.200" and the corrected depth was z = 1.240". The difference was 0.040" which in terms of a percentage error was 3.3% but in terms of the actual depth dimension this was a large error for a system with an expected 0.004" measuring accuracy. Hence in this case the corrected value of depth had to be used.

It was not difficult to locate the image plane of the projected moiré grid with respect to the blade and to keep note of the number of the fringe with respect to the reference plane that was being measured. A second reference plane was formed which was N fringes in front of the imaged grid with respect to the observing optics, i.e. the fringe number N and the depth value z were negative. The second reference plane was a physical marker. A spring loaded lever was made to run from the second reference plane to the edge of the blade nearest to the observer. This was similar to the reference location probes shown in fig. 33. By counting the fringes from the second reference plane to the blade the fringe number at any part of the blade was known.

Another factor was found to affect the accuracy of the contouring system when the laboratory system was used to study objects with a large depth such as the model fan blade and this was variation in the lateral magnification of the image produced by the depth values z. These produced errors in the scan distance along the blade, i.e. distance x. This effect was the same as those that caused the non-linear effects in the production of the grids for the fringe projection technique, section 2.7.6.

Consider the conventional single lens imaging system that would represent the camera used to image the contour object on to the photomultiplier scanning plane similar to that shown in fig. 15b.

U = the distance of the image plane of the moiré grid on the object from the camera lens.

V = the distance of the image from the camera lens.

M_o = the image magnification on the optical axis.

$$M_o = \frac{V}{U}$$

The distance U would be modified by the shape of the object.

Hence $U' = U + Z$

Under these conditions the distance X of the point on the object from the axis of the optical system corresponding to a distance x from the optical axis on the scanned image is given by the function

$$X = \frac{x}{M_o}\left(1 + \frac{Z}{U}\right) \quad \ldots\ldots \quad (114)$$

For the example of the model blade the X direction error on the object along the scan from the optical axis for the 30th depth fringe was 3.3%. This represented a 0.030" error in the blade in the X direction at its edge, which was approximately 1" from the optical axis.

This direction error would not be significant in the majority of cases on the measurement of turbine blades as this would represent an X directional error of 0.003" which would be less than the effective integrating area on the object of the scanning system. However, when components were inspected the likelihood of these two factors affecting the accuracy of the results should be considered to define whether corrective procedures were necessary.

During the manual plotting of the model blade and other similar components these correction factors were conveniently applied by the use of a small computer programme on the C.P.S. teleprinter system. The fringe number and position along the resultant scan were typed in and then X and Z dimensions of the blade calculated and printed out. These corrections could also be incorporated into the main shape generation programme for use on deep objects.

The shape measurement made by contouring agreed with the manufacturing specification. Specific parts of the blade were also contoured using a difference direction of observation to reduce the overall dimensional depth and increase the measuring accuracy from 0.004" to 0.001". Details of the results cannot be included because of the advanced nature of this component.

5.4 SHAPE GENERATION BY COMPUTER.

The optical information to electronic interface used for this work was based on the photomultiplier scanning device described in section 3.4.2. This was used in conjunction with the moiré shadow method of contour generation. The photomultiplier output was digitized with the aid of a data logger and then put on to punched paper tape for input into the IBM 360 computer system.

The photomultiplier tube output and X direction potentiometer voltage were fed into two channels of an Ampex FM tape recorder taking between 3 and 6 minutes to scan the blade. The time limit was set by the data logger system. The tape recorder was used for convenience rather than moving the moiré rig to the data logger or vice versa.

The two output channels of the tape recording were replayed into the data logger via a switching system. The data logger system converted the input voltage to a frequency proportional to the voltage and counted the number of cycles over a given integration time. The number of cycles representing the voltage was digitized and punched on to paper tape. It had a speed of 2 points per second, the limitation being the paper tape punch, but it had a buffer store which enabled it to measure two points rapidly, hold one while it punched the first, then punch the second.

Using this property, a switching device was constructed which every second fed two samples of the tape recorder output in quick succession into the data logger. Hence this system enabled the two channels of the contouring system to be read at second intervals resulting in between 180 and 360 co-ordinate pairs per blade scan for analysis. This number of points was sufficient to accurately represent the contour traces.

The system was initially examined using a test object with a linear slope set at 10° to the contouring reference plane. This produced evenly spaced contours over the whole of the test surface. Both a triangular waveform fit and a $\sin^2 V$ fit were applied to the contour fringe intensity profile within the computer. The resultant shape co-ordinates derived by the computer produced a good linear shape when plotted out but the triangular waveform showed a larger deviation about the straight line than the $\sin^2 V$ fit. The integrating area used on the photomultiplier was relatively large and so reduced the intensity function of the contour fringes to an approximate $\sin^2 V$ function. Fig. 39 shows the error between the 10° slope as plotted by the computer compared to a purely theoretical 10° slope plotted against the distance along the scan using a contour depth interval of 0.020". The error increased with distance across the scan due to an inaccuracy in the calibration of the fringe depth that was used by the computer. However, the main area of interest was the deviation of the computed points from the general error curve due to the errors in the fringe intensity fit applied within the computer. This had a maximum of $\pm$ .001" representing an error of 0.05 times the contour interval and was better than initially predicted for the system.

Application of the system to turbine blades produced a clear, well-defined set of shape co-ordinates for scans across blades at several positions along the blade axis. An example of the computer co-ordinate printout is shown in Table 3. A contour depth interval of 0.016" was used together with a $\sin^2 V$ intensity function. The overall spread of the shape co-ordinates was within $\pm$ .001". An example of the calculated shapes of two scans across the concave surface of the blade is shown in fig. 40.

To examine the dimensional differencing capabilities of the technique a turbine blade was rotated by a small amount about its axes between consecutive photomultiplier scans. Two separate angles of rotation were used, 44 minutes and 1 degree 28 minutes, to simulate approximately one and two contour fringes difference at the trailing edge of the blade. The contour data was transferred from paper tape to a magnetic tape storage unit within the computer facility for ease of handling on repeated computer runs. The computer programme was extended to use the first scan as the master shape and store the information and the second and third scans were compared to the master data. Because of the nature of the recording and digitizing system, each digitized point in the scan, say the nth, did not have the same scan position as the corresponding point, the nth, in the subsequent scan. Thus, the positions along the scan were exactly matched by extrapolation between the point co-ordinates on the master object.

The shapes of the reference scan and the scan with the blade rotated through $1^\circ 28'$ is shown in fig. 41. The direct Z direction dimensional differences between the reference scan and a rotated scan is shown in fig. 42.

A straight line fit by the method of least squares was applied to the error values. The errors did not have a linear trend across the blade as shown by fig. 42 because of the cosine effect of the differences with respect to the normal to the surface of the blade and the Z direction. Fig. 42 also illustrates the information that would be obtained from any direct optical moiré subtraction system.

The method of calculating the co-ordinates of the centroid of the blade shape for a scan across either the concave or convex surface of the blade and the angle of the principal axes of the shape as discussed in section 4.7.3 was applied for the blade rotation. This was done for a number of scans at various positions along the axis of the blade.

An example of the computer output used to calculate the angle of rotation from the basic shape information is shown in Appendix 3. The first output array was that of the reference surface, i.e. the blade with zero angular rotation applied. The scan was taken across the convex surface in the chordwise direction at approximately the centre of the aerofoil. The second data array was for the blade rotated by 44'. From the two data arrays the difference in the positions of the two centroids and the angles of the principal axes were calculated as described in chapter 4. The overall difference was given as three parameters, X direction difference, Z direction difference and angular difference. The values of the various parameters such as the centroid position of the radii of gyration were also printed out mainly for information rather than direct use. The computer output of the overall differences illustrated that it was possible to obtain these values direct and they are the only values that are required to describe the overall differences between the shapes. For a production system the co-ordinate system of the production blade would be modified according to section 4.10.3 using these difference values and then a point by point subtraction done to investigate local differences. In Appendix 3 similar calculations were performed for a second angular rotation of $1^{\circ}28'$. Table 5 shows the values of the angular rotation of the blade calculated from different scans in other positions on the blade aerofoil. The computed values of the angular rotation agreed with the applied value to within 7%. These results showed that the method of calculating the general shape differences by the centroid displacement and principal axes methods operated as predicted for practical objects. It was not possible to investigate these techniques for complete blade sections and other types of blade displacement because of the difficulty of arranging for all the recording and digitizing equipment to be available at one time and the time involved for other departments in such an operation. Further investigations were made using the television interface and magnetic tape input into the computer. These are discussed in section 5.6.

5.5 SLOW SCAN TELEVISION INTERFACE.

The objective of manufacturing a television optical to electronic information interface was to speed up the computer processing times to those that are acceptable to a routine inspection system, i.e. to enable the whole inspection process to be undertaken in less than one minute. In the system envisaged for automatic inspection, the computation would be done by a small on-line computer such as a PDP8. This would be capable of handling an input speed of greater than 1000 ten bit bytes per second and thus, to form an efficient system, the optical data must be capable of being obtained at approximately the same rate. These speeds obviously precluded any form of mechanical scanning devices, which also would have the disadvantage of moving parts. Consequently, a television system would be the most probable interface device for this application.

At normal scan rates of 25 frames/second with 625 lines/frame, the information output rate for a line of 800 points of information would be 12.5 MHz. This was three orders of magnitude above the rate at which the computer could read the data and well above the maximum rate to which standard Analogue to Digital converters would operate. The information could be read out by observing the different points in sequential frames, but this would slow the system down below the required input rate. Consequently, the most efficient way of obtaining this information would be by slow scan television techniques.

The overall computer analysis system is shown in fig. 28 and due to industrial circumstances it was not possible to use a small on-line computer and so a digital magnetic tape recorder was used as a temporary storage medium between the television system and the IBM 360 computer system. Fig. 43 shows the layout of the television interface. The input data was of the form of a digitized light intensity value at each of 500 equispaced points across one line scan. This was obtained for up to 20 lines within one complete frame. The positions of these lines within the frame could be set manually. The speed of this system was set at 1000 points of information/second and was limited by the input rate of the tape recorder.

5.5.1 Television Camera.

The selection of the most suitable vidicon tube for this system was critical. The tube had to have a high spatial resolution, good spectral response in the visible and compatible with an Hg arc source, flexible slow scan facilities and low noise. A survey of available vidicon tubes, as summarized in Table 4, concluded that the Thomson CSF 9892 one inch slow scan vidicon tube was the most suitable. The tube's main attributes were as follows:-

a) High resolution 1000 TV lines in the tube centre under maximum electrode voltage conditions. The system uses electromagnetic deflection and focusing rather than electrostatic focusing and deflection, which increases the power requirements on the vidicon control circuitry over those of the more common electrostatic slow scan tubes, but the high resolution warrants its use.

b) Peak spectral response is at 430 nm and covers the whole visible spectral band. The overall sensitivity is high, to enable the system to accommodate the low light levels when scanning dull black objects.

c) The effective photographic gamma, γ, over the light input region of 0.05 to Lux-seconds is between 0.9 and 1.0

The photographic gamma in this case is the gradient of the graph of the log of the output signal versus the log of the optical exposure on the photocathode (intensity x time) similar to the Hurter-Driffield curve for photographic emulsions as discussed in section 3.2.1. When $\gamma = 1$ the output signal is directly proportional to the optical exposure, and hence optical intensity for a given exposure time. Thus the triangular intensity function of the contour fringes produces a triangular output signal from the vidicon and hence no mathematical signal corrections are required.

5.5.2 <u>Vidicon Scanning</u>.

The vidicon deflection and focusing parameters were governed by the normal deflection and focusing coils surrounding the tube. These coils were supplied with the correct voltages by power amplifiers designed to operate at the slow scan rates rather than normal video scan speeds. The vidicon was scanned in the X direction in 500 incremental steps with a linear spacing to give 500 video signal output values for digitization and storage.

The X deflection coil voltage was controlled by the following system, referring to fig. 43. The control logic sent a pulse to the scan position unit to indicate a required shift to the next position. This pulse operated a nine bit binary counter and increased the count by one. The binary counter could vary from 0 to 499. A digital to analogue converter produced a voltage proportional to the counter value which was amplified and fed into the vidicon deflection coil. This scanned the vidicon accordingly in the required 500 steps.

When the X deflection counter reached a value of 499 and was then instructed to move to the next position, the counter emitted a pulse into the Y deflection logic and then set itself to zero ready to start the next line. The Y deflection consisted of a similar five bit counter which counted the line number and supplied the Y deflection coils with the appropriate voltage via a second digital to analogue converter.

The scan system operated for 20 scans unless stopped at a particular line and point number that could be set manually in the control logic. The position of the line scans within the television frame could be set manually. There was an indicator on the control logic console which indicated the line and point number being interrogated during the scan.

5.5.3 <u>Digitizing and Recording System</u>.

The digitizing and control system was linked to a Racal Thermionic T.D.L.10,000 digital tape recorder. The control logic system, fig. 43, instructed the X,Y scan to move to the next position, allowed a time for the system to settle and then instructed the vidicon output Analogue to Digital converter to operate. The A/D converter was a 10 bit BCD system. On completion of the conversion the control logic instructed the Mixer Level change unit to record the digitized signal. The mixer level change unit put the signal on to the tape recorder in the form of three separate digits, hundreds, tens and units. This was recorded in binary form on four channels of the recorder. On recording the first digit, the recorder informed the control logic that it was ready to receive the next digit. The control logic then instructed the mixer unit and recorder to present and record the second digit. The same control loop continued to record the third digit. On completion the scan system was moved to the next position to record the next intensity value.

The limiting factor on the speed of this system was the tape recorder, which took 0.3 m.sec. to record each digit, i.e. 1 m.sec. per video signal word.

The system had an additional facility for putting normal data on to the tape in the form of a 5 digit number to identify the run. Data such as contour depth interval, START parameter, inversion limits were fed into the computer in card form.

The television system could be scanned without recording information, intermittently or continuously at a range of scan speeds. This was used for focusing the camera, general setting up and wiping the remaining signal off the photo cathode before recording optical data on the tape recorder.

5.5.4 Television System Development.

This section is subdivided into two sections, the development of the tape recorder and then the television camera, described in chronological order. The digital tape recorder and the procedures involved to read the magnetic tape into the computer for the main contouring program were examined first since the whole television system depended upon the ability to get the intensity information into the computer.

5.5.4.1 Digital Tape Recorder.

The process of recording information on to the tape recorder and then reading this into the computer suffered from a number of difficulties, some technical, but the majority were administrative or communication problems with the Company's Computer Centre. The Computer Centre within the Company is one of the largest in Europe and serves the other Divisions as well as the Derby Engine Division, plus other Companies who buy the services of the computer. Hence the computer facilities are organized to accommodate a large throughput of computer programs on a continuous production-line basis and their data input handling capabilities are organized accordingly. The magnetic tape and disc facilities are run entirely by the Computer Centre, which involves both reading and writing information on to the magnetic tapes. Consequently the Computer Centre was not readily organized to accept magnetic tape that had been written outside the computer area. The tapes normally used by the Computer Centre has an automatic magnetic labelling system, by which the computer automatically verifies that the operator is using the correct tape for the program. Also the computer information is set out in a series of blocks of a given length. The information on the tapes is read into the computer a block at a time. A block can be up to 30,000 characters long, although the usual size is 800. The computer reads the block and then checks that there are no errors within this block and that the format is correct before continuing to the next. This is principally a means of reading data quickly into the computer to minimize time wasted by data errors. If a fault is located the complete block of data is rejected and the next block is examined or the program abandoned. The action depends upon the instructions formed within the program. Both the automatic labelling and standard block sizes are not convenient for use on the television system. The block size used for the television system varied from 5 bytes to 1500 bytes and so it was not possible to define a standard block size.

A computer program run on the Company's IBM 360 system has a series of cards before the start of the program, defined as control cards, which inform the computer and its operator the type of program that is being used. In detail these state:-

a) the program language, P.L./1 or Fortran,

b) the type of program, test or production,

c) where the program is located, i.e. on cards or stored in a magnetic disc or tape,

d) additional facilities required, such as access to other programs or data on disc, tape or card outputs,

e) the number of any magnetic tape or tapes or discs or paper tape reels being used that contain input data and the format of the blocks of data.

All these control cards have to be correct before the program will run on the computer. A control and program set up sequence was devised that enabled the magnetic tape from the television system to be read into the computer. The tape was defined as unlabelled and a manual verification procedure used by the operator to check that the correct tape was being used for the program instead of the automatic verification. It was also found that the data could be read in blocks of varying lengths if the undefined blocklength control statement was used.

An additional limitation was found in the use of magnetic tape information in so far as it was only possible to run the program on the night shift operation of the computer because of other commitments during the daytime. These were caused by higher priority programs and direct linkages to the computing facilities of the other Divisions of the Company. This meant that only five computer runs could be made per week, which restricted the rate of progress on the development of the television system when using the computer.

The initial attempts to read information into the computer in the form of a constant voltage fed directly into the analogue to digital converter, fig. 43, in place of the video signal resulted in the computer readout system completely stopping without printing any characters. This was traced to the fact that the magnetic tape being used was relatively old and had become magnetically noisy and produced spurious magnetized areas which could not be decoded by the computer as a character. This was rectified by the use of a new tape.

The main problem was found to be the binary format used on the tracks of the tape recorder to form the characters. Since in the normal circumstances magnetic tapes are both written on and read by IBM peripheral equipment the actual format of character in relation to the individual tape tracks is not required for normal operation, and consequently the format was not generally known within the Computer Centre. This presented the main communication problem with the Centre.

The magnetic tape used by the recorder was standard ½" wide computer tape. The tape contained nine parallel tracks on to which the information was fed as shown in fig. 45a with a character density of 800 bytes per inch. The information from each track was staggered, as shown in fig. 45a. This enabled each track to be read separately and gave a clear indication of the beginning and end of each byte of information to ensure that the information was read accurately into the computer.

Two data formats were used for 9 track recorders with the IBM 360 system. These were Hexadecimal or Character, as shown in fig. 45b. Only the character format could be used with a program written in the P.L./1 language. Each of these nine tracks operate at the binary logic level of 0 or 1. For numerical characters in this format the tracks 0, 1, 2 and 3 are held at logic level 1 and tracks 4, 5, 6, 7 for the numerical character from 0 to 9 in the binary form. To form an alphabetic character from A to I the tracks 0 and 1 are held at level 1 and tracks 2 and 3 are held at 0. Tracks 4, 5, 6, 7 form the binary number from 1 to 9, forming the letters from A through to I. The first track on the tape, denoted as 'P', formed a parity track. With this I.B.M. system an odd parity format was used which stated that the number of tracks on the tape for each character which were set at a logic level of 1 must be odd. If this applied, the parity value was 0. If the number of tracks at level 1 was even, the parity was set at 1 to make the total number odd.

Another requirement in the format of the digitized data was the formation of definite blocks of data rather than a continuous stream, as discussed earlier in this section. This was a distinctive magnetic mark on the tape put on by the tape recorder and called an interblock gap. This was automatically applied at the end of each line of the television scan and so each data block consisted of 500 readings of the video signal, each of 3 digits forming blocks of 1500 bytes each.

In addition to the television video data a facility for putting a five digit number onto the tape manually was made as discussed in section 5.5.3. At the end of this data an interblock gap (I.B.G.) was put on to the tape, forming a block of some 5 bytes.

Using the above format it was possible to record data on to the tape recorder and read it off with the aid of the computer. There were some occasions when the recorder would either miss a digit or form some uncodable character on the tape. This was caused by some crosstalk within the Control Logic unit but was soon rectified.

Having established that it was possible to read data from the television A/D converter into the computer the control of this data by the computer was studied and formulated as shown in fig. 45c. The television scan data was preceded by a set of manual data. The first digit of the manual data block was wired up with the logic levels on tracks 2 and 3 at zero to form an alphabetic character which was set to 'A'. The remaining four digits were used as a means of identifying the television scan. The television then recorded the video intensity data for one complete frame of 20 lines. After the television scan had been recorded a second set of manual data was recorded with the first of the 5 characters set at 'B'. This completed the recording of one television frame. The next frame was repeated by the same procedure, starting with the character 'A' and ending with 'B'. At the end of the recording a block of manual data beginning with 'C' was recorded. After the insertion of the manual data containing 'A' at the beginning of each run an I.B.G. was automatically added but at the end of the scan the manual data was followed by an I.B.G. which had to be inserted by a manual operation. Any number of television frames could be recorded by following the loop as shown in fig. 45c. Each magnetic tape contained 1200 ft of tape with a packing density of 800 characters per inch and so the storage capacity was 11.5×10^6 characters. Each complete scan consisted of 30,000 characters and hence 300 complete scans could be recorded. On normal test runs between 3 and 30 frames only were used.

At the end of a complete recording a 'Tape Mark' was recorded by means of a facility on the recorder. This control signal was used to inform the computer that that was the end of the data on the tape, Otherwise the computer would run through the rest of the tape looking for data, which ~~This~~ greatly increased computer time and inconvenienced the computer operators.

The main computer program was made to read the tape from the beginning and locate the first letter 'A'. By doing this the magnetic tape was set by the program at the beginning of the first television scan and hence its exact position was known. The next four digits were read to form an identification of the scan. Following this two DO-LOOPS were used to read and store the 500 points of each of the 20 television lines. The next character immediately after the video data was the alphabetic character 'B' which was set manually. If the character 'B' occurred in the correct place on the tape the television scan data had been recorded and read correctly and so the program was made to proceed with the shape calculations. If the character was not a 'B' but was a numerical character something was wrong with the information, such as some of the characters missing, and the whole of the information to this frame was rejected and the computer was instructed to look for the next 'A' and hence the next television frame, as shown in fig. 45c. This formed a basic check on the incoming information.

Whenever the alphabetic character 'C' was located which signified the end of the recorded data the computer program was shut down.

This overall format was verified by using the manual data input and a sawtooth waveform applied to the A/D converter to simulate the video signal. Tests showed that this system operated satisfactorily when the magnetic tape input was controlled by the moiré contouring computer program.

5.5.4.2 <u>Television Camera.</u>

The construction and development of the slow scan television camera to the design discussed in section 5.5.1 revealed a fundamental problem when the camera was driven in conjunction with the digital tape recorder to record the image intensity. The output current of the video circuit was extremely low in the region of several nano amps. This current was not sufficient to produce a reasonable signal above the ambient noise level. The scan rate under these circumstances was 1 ms. per point for 500 points per line, resulting in a frame time of 312 seconds for a normal T.V. raster, which is 7500 times slower than the normal television framing rate.

The faceplate of the vidicon tube was coated with a thin layer of photo-conductive material, fig. 46a, whose conductivity was dependent upon the level of optical illumination at that point. The backplate between the tube window and the photo-conductive layer was set at a positive voltage of approximately 30 volts. The photo-conductive layer (photocathode) was scanned with the electron beam and its surface brought to the cathode potential which was less than the backplate potential of +30V. The vidicon was then exposed to the image. The illumination modified the conductivity of the individual elements of the photocathode to produce a flow of current across the layer at each element. This modified the potential distribution on the photoconductive layer, i.e. potential increased with increasing illumination. The electron beam was then rescanned across the photocathode to return the photocathode to the cathode potential and the current flow in the backplate circuit when the elements of the photocathode were recharged formed the video output signal.

The charging current was basically the same as that for a normal capacitor and had an exponential decay with time as shown in fig. 46b. When the electron beam was charging a single element of the tube for approximately 1 ms. as with the contouring television system the averaged current output would be extremely low which corresponded to the effects observed when testing the system. The scan rate was determined by the recording rate of the tape recorder and could not be increased.

The only means to overcome this problem was to use a buffer store so that the vidicon could be scanned faster and the output signal stored in the buffer and then read into the tape recorder at the normal rate. This meant redesigning and rebuilding a major part of the data handling system. A 500 times 12 bit shift register store was used as the buffer storage system.

The buffer storage enabled the point by point analysis time to be reduced from 1 ms. to 25 μs. This limit was set by the time required for the analogue to digital converter to operate. Even the 25 μs. per point was a relatively long time and was equivalent to a scan time of 7.8 seconds, which gave a specified signal to noise ratio of 10:1. During the 25 μs. taken for the A/D converter to operate the video signal still had a rapid decay. However the operation of the converter was on a sample and hold basis where the input signal was integrated for the first 40 nano seconds of the cycle and then this voltage was held while it was digitized as shown in fig. 46c. Thus the output signal was sampled before it had decayed by any appreciable amount and a reasonable signal was obtained.

Experimental tests on the completed television camera showed that the vidicon tube was extremely sensitive and operated at the low light levels dictated by the fringe projection system with the camera's 85 mm focal length lens set at f.16. However it was not possible to achieve a reasonable optical resolution across the vidicon tube under either internal or external scan conditions. On continuous internal scan the resolution was limited to approximately 100 television lines across the face of the vidicon where the tube specification was 800 television lines.

Internal scan conditions were set by frequency of the X deflection and Y deflection ramp generators and these produced a line scan in 1 ms. and some 400 lines per frame in a continuous scanning mode. The video output was displayed on an oscilloscope. The external scan was controlled by the Logic Control Unit with a line scan time of 12.5 ms.

The resolution of 100 lines was extremely low for the camera particularly for the internal scan conditions although for the external scan mode the 500 point by point sampling and aliasing effects reduced the predicted resolution of a continuous lined grid to approximately 150 lines. Neglecting the 500 discrete sampling points and displaying the video output signal from the camera directly on to an oscilloscope the resolution was still found to be approximately 100 television lines.

The lack of resolution was attributed to the spot size of the scanning electron beam being larger than anticipated. This was verified by the fact that it was not possible to produce contour fringes on a turbine blade when the fringe projection system was used to illuminate the blade for 0.020" contours. Hence the spot size was greater than half the period of the projected fringes imaged on to the vidicon. If the lack of resolution had been caused by such effects as frequency limiting on the video amplifiers the signal would have made some attempt to follow the contours as they were at an effective spatial frequency of less than 100 television lines. The spot size assumption was re-affirmed by the fact that contours could be seen on the blade when the moiré shadow contouring technique was used. The spot size was estimated to be approximately 0.004" dia. on the vidicon surface which represented a spot of approximately 0.020" dia. on the object with the camera's 5:1 image demagnification factor.

Adjustments were made to the electrical operating parameters of the vidicon tube including the alignment and electrical focusing coils but the resolution could not be improved.

Apart from the lack of resolution the camera operated as anticipated. It was possible to store data on the tube and then record the digitized intensity information on the tape recorder. The overall operation of the camera and digitizing system was verified using the moiré shadow contouring technique with a contour depth of approximately 0.030". A typical digitized line scan that was produced by this system for computer processing is shown in Table 6. An analogue plot of this data is shown in fig. 47. As seen in fig. 47 the depth contours were visible but the intensity modulation produced by the contours was low and there was a significant noise level on the overall signal. The television camera was not sufficiently reliable to be used in conjunction with the main computer program to continue the research.

After a number of unsuccessful attempts to improve the television camera, including consultations with the U.K. representatives of the tube manufacturers, the vidicon tube designers in France were contacted. They confirmed that a spot enlarging effect would occur when the tube was run in a slow scan mode and hence degrade the tube resolution.

The effective spot enlargement was due to the relatively long time that the scanning electron beam was incident on any one spot on the face of the photocathode. When the electron beam was scanning a line and replacing the charge lost on the face of the photocathode, the electrons migrated radially from the point of incidence of the electron beam. Hence the electron beams charging influence ~~perpetuated~~ permeated along the surface of the photoconductive layer as well as directly through the layer. This produced an effective enlargement of electron beam at the photocathode. The slower the electron beam scanning rate, the more time the charge had to spread and hence the greater the spot size. At the scanning rate used when digitizing the image intensity information the 0.004" spot size that was observed was considered normal by the tube's design engineers.

Consequently it would not be possible to improve the resolution of the slow scan television interface when operating it in this particular slow scan mode.

To achieve optimum resolution the vidicon must be operated at the normal scanning rate of 25 frames per sec. at 625 lines. Thus a line would be scanned in 64 μs. and the time available to digitize each of the 500 points on the line scan would be 0.12 μs. This would require an A/D converter that could operate at 8 MHz. There are commercially available A/D converters that operate up to 4 MHz or 15 MHz such as the Micro-Consultants Ltd. AN-DI 802 VID. 10 bit converter at 4 MHz and the AN-DI-RAD-A 8 bit converter at 15 MHz.

There appeared no fundamental reason why it should not be possible to run the television system at close to the normal framing rate in conjunction with the digital tape recorder. The system would be controlled by the camera rather than the logic control unit in so far as the camera would operate in the standard continuous mode at the full frame resolution of 625 lines and the interface unit would be instructed by the camera when to digitize and store the nth line. When this line was recorded on the tape the next line (i.e. (n+30)th line of the TV frame) would be processed until the complete 20 lines were recorded.

Digitizing a single T.V. line fast would be preferable to processing the 500 points in sequence frame by frame as this would take a long time, 20 seconds/line, and there would be possible exposure time and illuminating intensity variations from frame to frame that would reduce the accuracy of the contour intensity function across the blade.

From this work it was concluded that the achieved resolution of the television interface of 100 television lines was not sufficient but that it would be possible to increase the resolution to an acceptable value by further electronic development. However it would not be possible to carry out this development within a sufficiently short time to be included in this thesis.

To continue the research into the optical contouring technique and to enable a continuing influx of turbine blades and research aerofoil sections from other departments of the Company to be examined the logic control unit and the digital tape recorder were linked to the photomultiplier mechanical scanning system. The control logic unit was slowed down to digitize the photomultiplier output signal every 120 ms. so as to complete the 500 point cycle in 60 seconds. The photomultiplier was arranged to scan across the blade in just less than 60 seconds. The photomultiplier mechanical scan speed was constant to within 0.4% and was sufficient to assume that each of the 500 data points were equi-spaced along the length of the scan.

This interface system worked extremely well and enabled the contour intensity information to be recorded onto the digital tape recorder in exactly the same format as used for the full television system including the manual data inserts at the beginning and end of each frame, fig. 45c. The scans across the blade using the fringe projection system were similar to those shown in fig. 38 and were noise free apart from the inherent optical noise produced by dirt on the surface of the blades. An example of the digitized data fed into the computer for analysis is shown in Table 7. For normal testing purposes three scans per aerofoil surface or frame were used although for some components five scans were taken. These limits were used to keep the data recording time and computer program time to a minimum to conserve processing expenditure.

5.6 TEST RESULTS.

A number of tests were carried out using the photomultiplier mechanical scan and magnetic tape recorder system in addition to the experimental results described in section 5.4 to extend the experimental confirmation of the computer linked optical contouring technique. In addition to these tests the interface system was used to measure the aerofoil shape of a number of blades for potential users of the technique within the Company.

For this experimental work a number of modifications were made to the main computer program from that shown in Appendix 1.

It was not possible to simplify the shape generation program to any great extent as the surface noise effects produced by the dirt on the surface of the blade was still prevalent and had to be accommodated. The program was made more efficient and its size reduced slightly by subdividing the inversion parameter change and restart parameter change sections into separate procedures or subroutines which were then called when required within the main program.

To accommodate the complete frame of information from the television camera or photomultiplier of up to 20 lines some of the parameters were defined as two-dimensional arrays. These were principally the input data, shape data Z and RZ and the centroid and principal axis data of both the individual surface line shapes and the whole sections. Each of these arrays had to be defined separately at the start of the program to generate the correct storage areas within the computer. However when using the program a varying number of lines per frame were used to conserve computer costs and to enable the extent of these arrays to be varied easily a computing procedure known as a controlled variable array was used.

In this case the array was defined in a declare statement as controlled:-

```
DCL (V(*,*), Z(*,*), RZ(*,*)) CONTROLLED ---
```

The number of lines to be used within the actual program was obtained from a single data card and denoted as 'LINES'. Then the main arrays were set up by an allocation statement

```
ALLOCATE V(LINES, 500) , Z(LINES, 170) , RZ(LINES, 170) ;
```

The values of the second dimension of the array, 500, and 170, were the number of points within the line scan and the number of points at which the dimensional information was calculated.

Using this system the computer storage could be set up for any particular experimental run by the use of only one number on a data card. This saved having redundant computer storage space within the program and hence reduced costs as the storage requirements form part of the running expenses. An example of the use of the controlled variable for a one-dimensional array can be seen at the beginning of Appendix 1.

For the dimensional shape calculations of the blade aerofoil a number of data points less than 500 across the aerofoil would be adequate. The 500 measuring points were still required to define the contour intensity with sufficient accuracy. For these tests a number of approximately 150 was considered a reasonable number giving a data point every 0.010" for an average blade.

This was achieved by taking every third point of the scan for the depth calculation. This was most conveniently done by using the 'FLOOR' function within the computer. This was preferable to the use of a normal counting system as it was not known where within the scan the blade surface started or where the contour peaks were located but the number of the point within the Z array gave the X co-ordinate.

The 'FLOOR' function gave the integer part of any value, i.e. FLOOR(1.33) = 1. Hence the depth calculation section of the main program, Appendix 1, (statement 258) was modified as follows:-

```
CALA : DO L = NN TO MM;
       AL   = L/3;
       BL   = FLOOR(AL);
       IF BL ¬ = AL THEN GO TO CALEND;                    ... (115)
       ELSE DO; (Calculate Z dimension)
```

Hence the IF statement defined that if the number L was not completely divisible by 3 the Z calculation was not performed.

Using this technique it was possible to divide the 500 point array by any number to give the required number of shape data points by changing divisor in the 'AL' statement.

The retro-plotting technique discussed in section 4.7 to complete the dimensional shape of the blade right up the edges were included and this worked well.

The overall methods of calculating the moments of complete sections of the blade were simplified from those used on the mathematical model as shown in Appendix 2. These parameters were calculated by a closed loop method in so far as the blade section was a completely enclosed and self-contained area. The calculation started at one point, i.e. the trailing edge of the blade on the convex surface as shown in fig. 35a and traversed around the closed loop in a clockwise sense. The area and moments of element enclosed between the curve between the two element points and the co-ordinate systems axes were calculated rather than the element of the blade section. As the elements were taken around the closed loop the values became negative for the elements on the concave surface giving only the parameters for the area within the closed loop. This overcame the difficulty in matching the X and Z co-ordinates of the two surfaces when calculating the dX and dZ element moments as shown in Appendix 2.

Consider the blade section in fig. 35a where the closed loop calculation starts at the point A and proceeds round the loop in a clockwise direction to return to A. For an element between the nth and (n + 1)th points the area under the curve with respect to the X axis is given by

$$\text{Area} = \tfrac{1}{2}(Z_n + Z_{n+1}) \cdot (X_{n+1} - X_n) \qquad \ldots (116)$$

Proceeding round the loop along the convex surface of the blade $X_{n+1} > X_n$, hence the area elements have a positive value and along the concave surface $X_{n+1} < X_n$ and the elements are negative. Hence summing the whole of the loop defined by N points the area within the loop was obtained.

$$\text{Section Area} = \tfrac{1}{2}\sum_{n=1}^{N-1} (Z_n + Z_{n+1}) \cdot (X_{n+1} - X_n) \qquad \ldots (117)$$

The first and second moments of the section about both the X and Z axes and the product of inertia were found using this technique.

The manual data inserted on the magnetic tape before each frame was used to identify the frame by a number and to inform the computer on the type of scan being taken, as shown by the use of the REF parameter in Appendix 1. In this case the parameter REF had four discrete values:-

REF = 0 ----- Convex surface, Reference data

REF = 1 ----- Concave surface, Reference data

REF = 2 ----- Convex surface, Production data

REF = 3 ----- Concave surface, Production data

Using these identifiers it was possible to control the program to set up the parameters of the reference blade and then those of the production components and compare the production centroid location and angle of the principle axis to the reference blade's parameters to find the overall differences as described in section 4.10.

The experimental results obtained using a 3" long turbine blade and the fringe projection contouring gave a dimensional accuracy of $\pm$ 0.0015" for a 0.015" contour depth interval. An example of the analogue trace of a scan that was digitized and fed into the computer is shown in fig. 48. The noise in the region of the inversion point was optical noise produced on the surface of the blade rather than electronic noise within the photomultiplier and signal amplifiers. This was similar to the scans produced in the previous experimental work as was illustrated in fig. 38. The computer analysis and printout of a typical line scan across the convex surface of the blade is shown in Appendix 4. The photomultiplier output was amplified to give an analogue voltage from 0 to 10 volts into the A/D converter and when digitized and recorded formed a number from 0 to 999. The digitized photomultiplier output was printed at the beginning of the computer program as seen in Appendix 4. A number of printout statements were included in the main program for fault location purposes. These printout statements give an indication of the operation of the program.

The full program was tested by rotating the turbine blade through a small angle about the blade's axis. This was the most stringent test that involved the whole shape program as the angle of rotation was calculated from the difference in the angle of the principal axis of the reference and production surfaces rather than any direct X and Z direction shifts that only had a real effect upon the location of the edges of the blade with respect to the scan and the 'START' parameter.

The results for the comparison of the convex surface of the blade rotated through a small angle gave similar results to those discussed in section 5.4 and Table 5. This confirmed the overall accuracy of the calculated rotation to the actual applied rotation to be better than 10% as had been previously obtained. An example of the results obtained are shown in Table 8. The accuracy obtained at these small angles was particularly good since the direct effect of a shape error of $\pm$ .0015" at the edges of the blade would produce a 0.2 degree error about the centroid of the surface resulting in a 20% error for a 1° rotation.

Three scans were taken across both the convex and concave surfaces of the blade, in the region of the blade root, centre and tip. A set of scans was taken on the convex and concave surfaces of the blade to set up the reference parameters for both the line shapes of the surfaces and the completed sections that were formed by fitting the convex and concave surfaces together. Similar scans were taken for the blade rotated through a number of small angles to form the production blade data. The angular differences between the production and reference shapes were calculated. A sample of the results obtained is shown in Table 8. Small angles were used of less than 3° as these were considered to be within the possible range expected on production components.

The results show a good agreement between the calculated angles for the various blade sections for both the line shapes and sectional shapes within an accuracy of better than 10%. The agreement between the calculations of the blade's sectional areas for the reference and production conditions shown in Table 8 indicated that the sectional parameter calculations were consistent and accurate.

The results obtained and described in this section and section 5.4 demonstrated that the computer linked optical contouring operated as predicted to give the overall difference between the aerofoil surfaces of a turbine blade in a simple form of two orthogonal linear shift parameters and the angular difference. The accuracy of the shape information was within the predicted one tenth of the contour depth used.

More detailed analysis of the differences between the blades could be obtained by straightforward manipulations of the data within the computer as discussed in section 4.10 since all the basic information to do this was available.

The ultimate type of result obtained would depend upon the application.

Chapter VI.

Discussion and Conclusions.

6.1 INTRODUCTION.

This research has demonstrated that computer linked optical contouring was a feasible technique for inspecting the aerofoil sections of aero engine compressor and turbine blades. The system was accurate to within $\pm$.001" for a turbine blade that had a dimensional depth of between 0.3 and 1.0 inches. The system was capable of being used as an automatic inspection system on a routine basis. The information produced by this system was as accurate as the present Calliperscope and Point Gauging methods and produced more detailed information over a greater area of the blade than the latter methods. In this chapter the concept of the overall system is discussed together with the possible ways of utilizing the technique. Finally, the conclusions drawn from this research are formed.

6.2 DISCUSSION.

The information output from the computer for this technique could be made to suit the particular application and produced data on two levels, (a) the overall differences between the components and (b) details of the localized differences after condition (a) had been applied to the shape being inspected.

It was not possible to produce a purely visual inspection system for turbine blades using contouring techniques such as a pure moiré fringe comparison on a television monitor because of the complexity of the resultant moiré pattern and the limited amount of data that it provided. Hence the computer linked system must be used as described.

The technique could also be applied to the accurate measurement of complex distortion of turbine blades produced by engine condition type tests. Information of these distortions to this accuracy and detail had not previously been possible and hence the application of the optical contouring system to this type of analysis greatly increased the potential uses of the technique. The computer aspect of the device enabled dimensional difference data to be presented in a form compatible to any theoretical computer program that was being used to study the blade.

6.2.1 Contour Generation.

Both the moiré shadow and moiré fringe projection/scanning techniques produced good results suitable for turbine blade inspection. The fringeprojection was more appropriate for use with the television interface and computer. It did not, however, produce any visible impression of contour fringes. The intensity distribution obtained in practice followed the theoretical triangular intensity function extremely well and from some scan examples examined it was possible to measure the shape function to better than 10% of the contour depth, resulting in an increase in measuring accuracy by 2 to 3 times.

The fringe projection/television system would be well suited to routine application since both the projection optics and the television camera would be well away from the blade being inspected. Hence they would not be liable to be damaged while loading and unloading the blade and there would be sufficient room to construct a kinematic mounting system for the blade that also rotated the blade through 180° to inspect both the concave and convex surfaces of the blade. If operating in a particularly harsh environment, the optics could be completely hermetically sealed from their surroundings.

6.2.2 Television Interface.

The overall concept of the television interface with the magnetic tape recorder worked well and it was possible to record 20 television lines within approximately 10 seconds as originally predicted.

The basic limitation of the interface was the lack of resolution when the television system was operated in a slow scan mode. This was a function of the vidicon tube as discussed in section 5.5.4.2. The resolution could be improved by increasing the scan speed up to that of the normal scanning rate of 25 frames per second of 625 lines per frame and performing the digitization of one line within 64 μs. with the aid of a fast A/D converter and a buffer store. These modifications were technically possible and formed an electronic development task rather than fundamental research into the system. As discussed in section 5.5.4.2 it was not possible to carry out these modifications before the completion of this thesis.

The work carried out on the television system showed that it was the correct technique to be used to feed the contour fringe data into a computer either by direct access into a small on line computer or, as was done for this research, fed into the Company's main computer complex via a digital tape recorder. The system had the speed required to obtain the data within 10 seconds and the recording rate of the tape recorder formed the limiting factor rather than the television system. Hence there was room for possible improvements in these speeds as computer technology improved.

The system would be particularly suitable for routine application as it would be compact and easy to maintain.

6.2.3 Information Output.

The present output format of the data using the IBM 360 computer was in a paper printout form providing both the general differences between the components and the localized differences formed after the inspected components shape co-ordinates have been modified by the overall difference parameters. The exact form of this output depended upon the application;

in some cases of inspection it could be a direct go no-go statement, whereas other cases would require details of the localized differences.

The localized differences could be presented in a paper printout form in three ways.

(a) Direct list of co-ordinates and errors.

(b) Outline of blade with errors tabulated in relevant position.

(c) Error contour map.

Method (a) would be straightforward. Method (b) would give a direct impression of the location and values of the errors. A basic outline of the blade would be formed on the printout by the computer. The area within the outline would be divided into a matrix and at any point where the error was greater than a given value, defined by the tolerance envelope, the actual error would be printed. Points where the error was within the tolerance envelope would be left blank. Hence one could obtain a visual impression of the errors over the whole blade. The error contour map (c) would be a slight simplification of (b). Here for a given value of the error a number or character would be printed. The whole matrix would be scanned and the error printed out. This could either be of a line contour form, where a character would be printed if the error was exactly say, 2, 4, 6, 8, x 10^{-3} inches, or an area contour, where a given character would be printed for any error between 0 and 2 x 10^{-3} inches, or between 2 and 4 x 10^{-3} inches and so on. Both would give a good visual impression of the errors. The area contour printout would be the most appropriate method for general use.

If used on a routine production inspection basis, the printout could be displayed on a C.R.T. display to give a fast, clear and easily observable display without the operator having to handle a sheet of paper.

For distortion measurements the difference information could be stored directly on a disc or magnetic tape for easy access for subsequent computer programs as well as a printout form for normal analysis.

6.2.4 Routine Application.

One of the main attributes of the computer linked inspection system was the ability to compare an object to design data rather than requiring a physically made master object. This represented a considerable saving in the cost of manufacture of the master component. Also, the master had a tolerance envelope of ±.002" in its manufacture, which would reduce the accuracy of any inspection system. This saving would become increasingly important in the development of any aero engine, when the blade design was being constantly improved and the blades manufactured in small quantities.

All the turbine and compressor blades were designed with the aid of the computer. The detailed drawings and specifications were produced from the computer data. The basic and detailed design information was stored on either disc or tape within the I.B.M.360 system. This design information for any blade could be easily accessed within the computer complex, given the disc or tape number and access code. Hence the precise shape information would be readily available and could be made compatible to the contour inspection system by some simple arithmetic manipulation and then used as the reference information. Thus the cost of changing the blade that was being inspected would be reduced to reprogramming the computer to obtain the correct reference data as opposed to a complete change in the mechanical probe of the point gauging system that was used at present.

To reduce the cost and increase the efficiency of the optical contouring system the digitizing and computer system would be used on a time sharing basis by a number of inspection units, between 3 and 5 units, each with their own fringe projection and television interface. To operate this complex the whole system would be controlled by the computer where the operator loads the component and presses a button to indicate the system is ready. The computer would check the mounting of the blade, scan the contoured image, process the data, and finally present the data and indicate that the inspection cycle was complete.

6.2.5 Additional Applications.

In addition to the two basic applications in production inspection and blade distortion measurement, the technique had been applied to a number of dimensional analysis measurements of aero engine components. These measurements principally used the fringe projection/scanning system. Some blade measurements were done using the moiré shadow contouring method. The applications included the dimensional analysis of approximately fifty research blade aerofoil sections to provide the overall dimensional shape and some modified sets of nozzle guide vanes. The ability to project the grid fringes directly on to the object's surface proved a particularly valuable asset for measurement on inaccessible surfaces. The measurements were mainly performed using manual shape plotting. These applications are now being continued and are being extended.

The practical applications showed that the technique could be used on a number of diverse components and situations and so increased the overall potential of the system. A number of potential applications of the system included the dimensional analysis of component dies to provide a more detailed analysis than used at present by clock gauging. The results could be compared to the computer design data. Also included would be the measurement of sections of small engine casings. The range of object size could be extended using the fringe projection system to large objects, engine casings, provided that the contour depth interval and overall object depth was kept within the resolution limits of the television camera. Using this principle, there would be a number of applications for the technique outside the aero engine industry.

Some applications would require modification to the system, particularly the contour programming aspect to accommodate the points of depth inversion that occur. The principal objectives for the development of the system on some components would be to simplify the contour analysis system so as to operate mainly on the contour peaks and troughs and only use the contour intermediate calculations where necessary so as to use a minimum of computer storage space. These parameters depend upon the component and the amount of detailed information required.

6.3 CONCLUSIONS.

This programme of research has investigated the improvement in inspection methods for aero engine components using a computer linked optical contouring technique and from this work the following conclusions have been shown.

The computer linked optical contouring technique was a practical method of improving the inspection of compressor and turbine blades aerofoil sections. This technique significantly increased the amount of data that could be obtained on the aerofoils and achieved a measuring accuracy of ±.001". The dimensional data obtained within the computer could be processed to calculate the difference between two components in the form of an overall difference in two orthogonal directions and an angle of rotation plus any localized differences as required by the particular application. The information could be presented to an operator in an easily assimilated form.

The use of a computer to process the dimensional information would relieve the operator of much of the burden of handling a large amount of optical data and in some cases the decision-making responsibilities. The computerized inspection system would be particularly compatible with existing design and production technology as much of the design work was computer orientated.

The overall system could be used for either inspection of turbine bladesduring production or to measure the distortions of blades caused by thermal fatigue in engine tests.

REFERENCES.

1. B. S. Hockley

A Holographic Method of Analysis of Compressor, Turbine Blades and Discs.

1969 M.Tech. Thesis, Loughborough University of Technology.

2. B. S. Hockley and J. N. Butters

Holography as a Routine Method of Vibration Analysis.

1970 Jn. Mech. Eng. Sc. Vol. 12 No. 1 p.37.

3. B. S. Hockley

Large Amplitude Vibration Analysis by Phase Modulation Holography.

1972 British Patent Application No. 50634/72.

4. B. S. Hockley

Holographic Visualization of Large Amplitude Vibration using Reference Beam Phase Modulation.

1973 Jn. Physics E. Sc. Instrum. Vol. 6 p.377.

5. B. S. Hockley

Non-Destructive Testing by Holography.

1972 Brit. Jn. of N.D.T. July/August.

6. E. Archbold, J. M. Burch, A. E. Ennos

The Application of Holography to the Comparison of Cylinder Bores.

J. Sc. Instrum. Vol. 44, p.489, 1967.

7. B. P. Hildebrand and K. A. Haines

Multiple-Wavelength and Multiple-Source Holography Applied to Contour Generation.

1967 Jn. Opt. Soc. Am. Vol. 57 No. 2 p.155.

8. N. Shiotake et al.

Holographic Generation of Contour Map of Diffusely Reflecting Surface by Using Immersion Method.

1968 Japanese Jn. Appl. Phys. Vol. 7 No. 8 p.904.

9. D. M. Meadows, W. O. Johnson and J. B. Allen
Generation of Surface Contours by Moire Patterns.
1970 Applied Optics Vol. 9, No. 4, p.942.

10. S. S. Carlisle and A. R. Bugden
Some Trends in the Development of Automatic Inspection and Testing.
1970 Metron. Vol. 2 No. 8 p.273.

11. C. Watkins
Computerized Inspection of Components.
1969 Automated Inspection for Defects and Dimensions p.89.
Adam Hilger, London.

12. S. Aveyard and K. Whinney
Multipoint Electronic Gauging Machine for Measurement of Turbine Blade Aerofoil.
1969 Automated Inspection for Defects and Dimensions,
Adam Hilger, London.

13. Ferranti Cordax Inspection Aids Colour C.R.T. Production 1972.
Ferranti International News, Spring 1972.

14. K. A. Haines and B. P. Hildebrand
Interferometric Measurements on Diffuse Surfaces by Holographic Techniques.
1966 IEEE Trans. Instrumentation and Measurement. Vol. 15 No. 4 p.149.

15. J. S. Zelenka and J. R. Varner
A New Method for Generating Depth Contours Holographically.
1968 Applied Optics Vol. 7 No. 10 p.2107.

16. M. Born and E. Wolf
Principles of Optics.
1964 Pergamon Press, Oxford.

17. J. M. Burch

Interferometry with Scattered Light.

1970 Optical Instruments and Techniques, Howe Dickson, Oriel Press, Newcastle-upon-Tyne. p.222-229.

18. J. M. Burch

Laser Speckle Metrology.

1971 S.P.I.E. Proceedings Vol. 25 "Developments in Holography."

19. E. N. Leith, C. M. Vest and J. R. Varner

Investigation of Holographic Testing Techniques.

1970 Semi-annual Report 2420-9-P (AD 705-220) University of Michigan.

20. K. Biedermann, N. E. Malin

Combining Hypersensitization and Rapid In-Situ Processing for Time Average Observation in Real-Time Hologram Interferometry.

1970 Jn. Phys. E. Sc. Instr. Vol. 3 p.669.

21. J. S. Zelenka and J. R. Varner

Multiple-Index Holographic Contouring.

1969 Applied Optics Vol. 8 No. 7 p.1431.

22. H. Horvath

The Refractive Index of Freon 12.

1967 Applied Optics Vol. 6 No. 6 p.1140.

23. J. R. Partington

An Advanced Treatise on Physical Chemistry Vol. 4.

1953 Longmans, London.

24. P. S. Theocaris

Moiré Fringe in Strain Analysis.

1969 Pergamon Press, New York.

25. H. Takosaki

Moiré Topography.

1970 Applied Optics Vol. 9 No. 6 p.1467.

26. J. B. Allen and D. M. Meadows

Removal of Unwanted Patterns from Moire Contour Maps by Grid Translation Techniques.

1971 Applied Optics Vol. 10 No. 1 p.210.

27. J. M. Burch and R. W. E. Cook

A New Method for Comparing a Diffusely Reflecting Component Against a Holographically Recorded Master Shape.

1968 The Engineering Uses of Holography Proceedings p.449.

Cambridge University Press.

28. K. Rektorys

Survey of Applicable Mathematics.

1969 Iliffe Books Ltd, London.

29. R. S. Longhurst

Geometrical and Physical Optics (Second Edition)

1967 Longman, London.

30. J. Der-Hovanesian and Y. Y. Hung

Moiré Contour-Sum Contour Difference, and Vibration Analysis of Arbitrary Objects.

1971 Applied Optics Vol. 10 No. 12 p.2734.

31. R. E. Brooks and L. O. Heflinger

Moiré Gauging Using Optical Interference Patterns.

1969 Applied Optics Vol. 8 No. 5 p.935.

32. F. S. Chen, J. T. LaMacchia and D. B. Fraser

Holographic Storage in Lithium Niobate.

1968 Applied Phys. Letters Vol. 13 No. 7 p.223.

33. L. H. Lin and H. L. Beauchamp
Write-Read-Erase in-Situ Optical Memory Using Thermoplastic Holograms.
1970 Applied Optics Vol. 9 No. 9 p.2088.

34. J. C. Bellamcy et al.
In-Situ Double Exposure Interferometry Using Photoconductive Thermoplastic Film.
1971 Applied Optics Vol. 10 No. 6 p.1458.

35. J. A. Leendertz
Interferometric Displacement Measurement on Scattering Surfaces Utilizing Speckle Effect.
1970 Jn. of Phys. E. Sci. Instrum. Vol. 3 p.214.

36. J. N. Butters and J. A. Leendertz
Holographic and Video Techniques Applied to Engineering Measurement
1971 Measurement and Control Vol. 4 No. 12 p.349.

37. A. Macovski, S. D. Ramsey and L. F. Schaefer
Time-Lapse Interferometry and Contouring using Television Systems.
1971 Applied Optics Vol. 10 No. 12 p.2722.

38. J. N. Butters
Speckle Pattern Interferometry using Video Techniques.
1970 Presented at the S.P.I.E. 15th Annual Technical Symposium Sept. 1970 Anaheim California.

39. K. A. Brownlee
Statistical Theory of Methodology in Science and Engineering.
(Second Edition) 1965 J. Wiley, New York.

40. H. S. W. Massey and H. Kastelman
Ancillary Mathematics.
1959 Pitman - London.

41. S. Timoshenko

Strength of Materials (Part 1.)

1955 O. Van Nostrand, New York.

42. J. H. Ahlberg, E. N. Nilson and J. L. Walsh

The Theory of Splines and Their Applications.

1967 Academic Press, New York.

43. G. B. Brandt and L. H. Taylor

Holographic Strain Analysis using Spline Functions.

Proceedings on the Engineering Application of Holography Symposium

1972 Feb. 16th-17th Los Angeles, California.

Acknowledgements

The author gratefully acknowledges the encouragement and advice given throughout this work by Professor J.N.Butters (Loughborough University of Technology) and Mr R.J.Hill (Head of Advanced Research, Rolls-Royce (1971) Ltd). The author also wishes to thank Mr M. Sadler and Mr C. Haxell for the design and development of the slow scan television camera and the digital tape recorder control and interface system, and Mrs N. Heseltine for typing the manuscript.

Thanks are also given to Rolls-Royce (1971) Ltd for the facilities to carry out this research.

TABLE 1. Comparison of the Optical Contouring Techniques examined for Turbine Blade Inspection.

Technique	Contour Depth Interval (inches)	Measuring Accuracy (Fraction of contour depth)	Fringe Contrast	Light Source	Contour Recording Medium	Ease of Operation	Comments	Conclusions
Double Wavelength Illumination (Argon Laser)	.0005 - .001	1/4	Reasonable	Argon Laser	Photo Plate	Good	Contours too fine for blades. System difficult to set up.	Not suitable for use with an optical to computer interface.
Double wave-length. (Dye laser) *	2×10^{-5} - .1	1/4	Reasonable	Dye Laser	Photo Plate	Good	Requires accurate setting up.	
Double Refractive Index	.001 - .5	1/4	Good	Argon Laser	Photo Plate	Slow	Good results. Loading workpiece and gas too slow.	Not applicable for routine work.
L.S.P. Video Recording *	2×10^{-5} - .1	1/4	Fair	Dye Laser	Video tape/disc	Unknown	Low spatial resolution.	Shows good potential
Moiré Fringe	.01 - .1	1/20	Good	Hg Arc	Not required	Real time	Equipment simple	Suitable for visual observation and mechanical scanning.
Projected Moiré Fringes	.01 - .1	1/20	Very Good	Hg Arc	Not required	Real time	Very good results	Suitable for use with image scanning.

* Estimated performance from experimental work on associated methods.

TABLE 2. Computer Calculated Displacements of a Simulated (Elliptical) Object.

Applied Displacement for the Point (1,0.6) on the reference surface.			Calculated Displacement of the production surface (With respect to the point (1,0.6) on the reference surface.)					
			Surface Line			Surface Section		
x Displ.	y Displ.	Angle	x Displ.	y Displ.	Angle	x Displ.	y Displ.	Angle
0.000	0.000	5° 0'	0.000	0.000	5° 1'	0.001	0.0005	4° 51'
0.100	0.100	5° 0'	0.100	0.100	5° 1'	0.102	0.100	4° 52'
0.100	0.100	3° 0'	0.100	0.100	3° 0'	0.100	0.102	2° 58'
0.100	0.050	3° 0'	0.100	0.049	3° 0'	0.100	0.051	2° 58'
0.100	0.100	1° 0'	0.100	0.100	1° 0'	0.100	0.100	1° 1'
0.100	0.050	1° 0'	0.100	0.050	1° 0'	0.100	0.0505	1° 1'
0.100	0.100	0° 30'	0.100	0.100	0° 30'	0.100	0.100	0° 30'

TABLE 3 - 1

An Example of the Printout from the Computer for the Blade Shape Calculated from Contour Fringes.

POINTS NUMBER	EX VALUE	Z VALUE
1	0.00000	0.00000
2	0.00001	0.00000
3	0.00000	0.00000
4	0.00000	0.00000
5	-0.00448	0.00001
6	-0.00065	0.00462
7	0.00317	0.00812
8	0.00784	0.01183
9	0.01204	0.01580
10	0.01540	0.01601
11	0.01951	0.01980
12	0.02380	0.02173
13	0.02725	0.02412
14	0.03099	0.02891
15	0.03509	0.03201
16	0.03920	0.03484
17	0.04312	0.03775
18	0.04648	0.04012
19	0.05040	0.04353
20	0.05339	0.04627
21	0.05628	0.04801
22	0.05899	0.05129
23	0.06207	0.05375
24	0.06524	0.05612
25	0.06925	0.05989
26	0.07317	0.06401
27	0.07663	0.06630
28	0.08092	0.07087
29	0.08484	0.07212
30	0.08876	0.07720
31	0.09259	0.08001
32	0.09697	0.08477
33	0.10080	0.08812
34	0.10547	0.09184
35	0.10929	0.09601
36	0.11349	0.09796
37	0.11723	0.10144
38	0.12152	0.10412
39	0.12535	0.10784
POINT NUMBER	EX VALUE	Z VALUE

TABLE 3 - 2

POINT NUMBER	EX VALUE	Z VALUE
40	0.12945	0.11201
41	0.13337	0.11359
42	0.13739	0.11723
43	0.14187	0.12012
44	0.14588	0.12355
45	0.14952	0.12595
46	0.15437	0.12801
47	0.15848	0.13152
48	0.16193	0.13416
49	0.16548	0.13612
50	0.17061	0.13947
51	0.17388	0.14209
52	0.17705	0.14401
53	0.18135	0.14752
54	0.18443	0.14980
55	0.18751	0.15212
56	0.19059	0.15362
57	0.19367	0.15550
58	0.19600	0.15744
59	0.19908	0.16001
60	0.20207	0.16116
61	0.20487	0.16297
62	0.20692	0.16450
63	0.20991	0.16634
64	0.21289	0.16812
65	0.21523	0.17053
66	0.21849	0.17259
67	0.22157	0.17495
68	0.22521	0.17601
69	0.22839	0.17895
70	0.23212	0.18133
71	0.23604	0.18412
72	0.24033	0.18691
73	0.24416	0.18972
74	0.24845	0.19201
75	0.25275	0.19506
76	0.25667	0.19781
77	0.26105	0.20012
78	0.26497	0.20317
79	0.26927	0.20594

TABLE 3 - 3

POINT NUMBER	EX VALUE	Z VALUE
80	0.27328	0.20801
81	0.27748	0.21106
82	0.28093	0.21356
83	0.28551	0.21612
84	0.28943	0.21867
85	0.29400	0.22127
86	0.29717	0.22401
87	0.30156	0.22522
88	0.30557	0.22761
89	0.30996	0.22984
90	0.31397	0.23212
91	0.31808	0.23419
92	0.32135	0.23636
93	0.32573	0.23858
94	0.32984	0.24001
95	0.33273	0.24214
96	0.33675	0.24391
97	0.34104	0.24591
98	0.34477	0.24812
99	0.34841	0.25003
100	0.35280	0.25198
101	0.35560	0.25353
102	0.35849	0.25469
103	0.36036	0.25601
104	0.36419	0.25730
105	0.36727	0.25900
106	0.36960	0.26069
107	0.37268	0.26194
108	0.37557	0.26375
109	0.37847	0.26412
110	0.38117	0.26645
111	0.38444	0.26833
112	0.38780	0.27011
113	0.39125	0.27201
114	0.39461	0.27304
115	0.39825	0.27477
116	0.40208	0.27662
117	0.40469	0.27894
118	0.40955	0.28012
119	0.41328	0.28275

TABLE 3 - 4

POINT NUMBER	EX VALUE	Z VALUE
120	0.41776	0.28478
121	0.42149	0.28686
122	0.42579	0.28801
123	0.43008	0.29064
124	0.43363	0.29286
125	0.43848	0.29612
126	0.44165	0.29662
127	0.44557	0.29841
128	0.45024	0.30042
129	0.45453	0.30225
130	0.45817	0.30401
131	0.46191	0.30566
132	0.46527	0.30719
133	0.46965	0.30864
134	0.47329	0.31012
135	0.47815	0.31212
136	0.48067	0.31275
137	0.48337	0.31462
138	0.48692	0.31589
139	0.49093	0.31730
140	0.49355	0.31833
141	0.49653	0.32001
142	0.50036	0.32037
143	0.50241	0.32187
144	0.50549	0.32302
145	0.50839	0.32409
146	0.51184	0.32558
147	0.51436	0.32694
148	0.51735	0.32812
149	0.52071	0.32956
150	0.52313	0.33025
151	0.52519	0.33094
152	0.52789	0.33208
153	0.53125	0.33318
154	0.53387	0.33412
155	0.53797	0.33502
156	0.54040	0.33601
157	0.54311	0.33735
158	0.54647	0.33855
159	0.55020	0.33970

TABLE 3 - 5

POINT NUMBER	EX VALUE	Z VALUE
160	0.55319	0.34106
161	0.55748	0.34212
162	0.56149	0.34412
163	0.56476	0.34512
164	0.56905	0.34708
165	0.57269	0.34839
166	0.57717	0.34962
167	0.58137	0.35088
168	0.58539	0.35201
169	0.58912	0.35343
170	0.59276	0.35469
171	0.59668	0.35578
172	0.60060	0.35687
173	0.60555	0.35812
174	0.60993	0.36012
175	0.61413	0.36087
176	0.61759	0.36203
177	0.62225	0.36280
178	0.62608	0.36384
179	0.63075	0.36498
180	0.63439	0.36602
181	0.63877	0.36681
182	0.64241	0.36773
183	0.64671	0.36801
184	0.65100	0.36969
185	0.65529	0.37087
186	0.65884	0.37158
187	0.66201	0.37202
188	0.66528	0.37242
189	0.66845	0.37297
190	0.67181	0.37330
191	0.67499	0.37419
192	0.67844	0.37599
193	0.68115	0.37599
194	0.68395	0.37599
195	0.68665	0.37601
196	0.69029	0.37601
197	0.69375	0.37744
198	0.69757	0.37825
199	0.70047	0.37892

TABLE 3 - 6

POINT NUMBER	EX VALUE	Z VALUE
200	0.70317	0.37942
201	0.70672	0.38022
202	0.71120	0.38123
203	0.71512	0.38202
204	0.71904	0.38305
205	0.72343	0.38273
206	0.72660	0.38245
207	0.73117	0.38497
208	0.73547	0.38446
209	0.73957	0.38491
210	0.74340	0.38569
211	0.74788	0.38643
212	0.75124	0.38686
213	0.75553	0.38777
214	0.76001	0.38834
215	0.76449	0.38881
216	0.76841	0.38903
217	0.77196	0.38950
218	0.77523	0.39050
219	0.77952	0.39106
220	0.78363	0.39072
221	0.78829	0.39162
222	0.79249	0.39199
223	0.79585	0.39437
224	0.80061	0.39419
225	0.80444	0.39403
226	0.80780	0.39412
227	0.81191	0.39477
228	0.81349	0.39478
229	0.81713	0.39442
230	0.82087	0.39441
231	0.82348	0.39470
232	0.82684	0.39466
233	0.82908	0.39453
234	0.83235	0.39478
235	0.83440	0.39487
236	0.83711	0.39480
237	0.84075	0.39498
238	0.84280	0.39537
239	0.84457	0.39542

TABLE 3 - 7

POINT NUMBER	EX VALUE	Z VALUE
240	0.84756	0.39519
241	0.84989	0.39491
242	0.85363	0.39508
243	0.85624	0.39492
244	0.85857	0.39450
245	0.86109	0.39419
246	0.86548	0.39456
247	0.86819	0.39431
248	0.87136	0.39344
249	0.87444	0.39344
250	0.87827	0.39369
251	0.88200	0.39344
252	0.88676	0.39287
253	0.89040	0.39262
254	0.89479	0.39237
255	0.89861	0.39199
256	0.90272	0.39199
257	0.90673	0.39199
258	0.91121	0.38984
259	0.91513	0.38956
260	0.91849	0.38956
261	0.92297	0.38848
262	0.92717	0.38698
263	0.93128	0.38477
264	0.93576	0.38503
265	0.93931	0.38412
266	0.94351	0.38486
267	0.94827	0.38355
268	0.95191	0.38334
269	0.95527	0.38352
270	0.95788	0.38321
271	0.96161	0.38295
272	0.96488	0.38221
273	0.96796	0.38158
274	0.97067	0.38102
275	0.97337	0.38042
276	0.97664	0.37992
277	0.97963	0.37966
278	0.98140	0.37931
279	0.98448	0.37847

POINT NUMBER	EX VALUE	Z VALUE
280	0.98653	0.37794
281	0.98896	0.37803
282	0.99148	0.37812
283	0.99223	0.37709
284	0.99540	0.37587
285	0.99736	0.37462
286	0.99755	0.37462
287	0.99755	0.37444
288	1.00305	0.37237
289	1.00287	0.37231
290	1.00511	0.37230
291	1.00837	0.37139
292	1.01099	0.37070
293	1.01351	0.37045
294	1.01575	0.37014
295	1.01799	0.36914
296	1.02144	0.36799
297	1.02536	0.36612
298	1.02760	0.36508
299	1.03040	0.36464
300	1.03404	0.36331
301	1.03749	0.35987
302	1.04263	0.35841
303	1.04785	0.35653
304	1.05159	0.35598
305	1.05672	0.35498
306	1.06083	0.35199
307	1.06568	0.35025
308	1.07025	0.34773
309	1.07875	0.34387
310	1.08341	0.34178
311	1.08733	0.34089
312	1.08985	0.34037
313	1.09396	0.33861
314	1.09769	0.33599
315	1.10208	0.33502
316	1.10600	0.33437
317	1.10927	0.33417
318	1.11263	0.33267
319	1.11655	0.33116

TABLE 3 - 8

TABLE 4. Slow Scan Vidicon Comparison.

M'facturing Company	Type No.	Focusing & deflection system.	Spectral Response Peak (nm)	Maximum Resolution (Centre)	Modulation Depth at 400 TV Lines (Slow Scan Rate)	Typical Light Input (Lux-S)	Dark Current (nA)	% age Signal Remaining After 10 secs	Cost	Additions Required
English* Electric	V8034	Electro-magnetic	610	700	50	2.7	8.0	90	£180	Focusing & deflection coils £50.
EMI	9745	Electro-static	490	600	40	1 (Estimated)	10.0	Not specified	÷ £100	None
R.C.A.	4500	Electro-magnetic	610	700	50	2.5	8.0	95	-	Coils £50
Thomson-CSF	TH9892	Electro-magnetic	430	1000	50 at 500 TV lines	1.0	0.6	99	£250	Coils £50
Westinghouse	WL4384	Electro-static	400	700	40	1.0	0.2	95	£320	None
Westinghouse	WX5111	Electro-magnetic	400	700	40	1.0	0.2	95	-	Coils

* Listed in alphabetical order.

TABLE 5. Example of computed values for the centroid shift for a rotation applied to the blade.

AEROFOIL	SCAN POSITION	APPLIED ROTATION	COMPUTED VALUES OF DIFFERENCES OF THE CENTROIDS.		
Surface Scanned		(degrees)	X SHIFT	Z SHIFT	ANGULAR DIFFERENCE (degrees)
Convex	Centre	0.73	0.000	0.001	0.70
Convex	Centre	1.47	- 0.005	0.005	1.50
Concave	Centre	0.73	0.001	- 0.003	0.78
Concave	Centre	1.47	- 0.001	- 0.005	1.54
Concave	Bottom	0.73	0.006	- 0.005	0.69
Concave	Bottom	1.47	0.009	- 0.008	1.42

TABLE 6. Computer Printout of a Digitized Line Scan Recorded by the Television Interface System.

				LINE NUMBER =	4	218	208	209	207	209	207	206	205	207	203	207	207	207	207	207	243
243	243	243	243	243	243	207	207	240	203	203	203	201	181	181	181	181	190	190	198	198	178
178	178	178	178	139	218	208	209	206	207	207	207	201	203	183	203	203	183	203	201	183	183
181	191	191	190	198	178	198	178	178	178	178	99	178	178	178	99	98	178	178	178	178	178
178	178	178	178	218	218	218	218	208	218	218	139	208	214	208	218	208	139	209	208	139	207
189	209	201	207	203	203	201	181	181	181	181	181	181	181	181	180	190	190	190	190	190	190
190	198	198	198	290	278	298	338	319	339	403	398	419	470	482	479	499	506	496	480	482	469
489	524	546	557	549	539	559	560	550	516	535	541	563	607	639	672	658	632	640	600	540	508
450	437	444	448	472	492	509	549	579	641	678	696	727	750	759	782	789	798	828	820	830	800
763	772	793	802	783	790	791	800	782	779	799	799	799	800	799	788	800	803	827	809	799	809
810	768	760	736	708	678	648	622	598	548	520	481	431	406	403	425	442	468	483	503	519	566
589	599	678	701	699	719	728	708	680	650	600	537	491	460	440	440	422	450	469	502	499	573
599	638	639	658	630	600	528	504	439	460	427	450	439	479	519	559	597	620	625	608	555	530
483	439	427	448	439	477	521	539	557	579	583	568	529	502	468	434	441	455	473	498	558	583
599	600	580	518	480	450	428	399	456	478	489	547	579	600	557	530	500	458	449	455	479	496
536	569	582	580	540	509	481	462	439	443	439	480	479	509	519	550	511	498	488	458	453	477
489	499	533	550	554	500	462	460	440	435	439	479	538	519	527	530	479	458	427	438	458	472
498	529	509	495	468	440	419	420	437	439	501	493	498	468	423	400	378	388	429	468	469	490
480	430	394	389	387	399	440	449	458	438	412	380	380	378	367	380	362	327	298	278	278	278
198	178	178	99	178	214	218	218	218	218	218	218	208	208	209	207	209	207	207	207	207	187
203	203	201	201	183	290	280	290	290	290	290	298	278	278	278	278	278	278	278	278	278	278
278	238	239	239	219	239	239	239	239	306	308	239	308	308	307	307	309	308	309	307	219	309
239	309	347	383	399	499	599	687	769	857	933	999	999	999	999	999	999	999	999	999	999	999

LINE READ & STORED

TABLE 7. Computer Printout of a Digitized Line Scan Recorded by the Photomultiplier/Magnetic Tape Recorder System.

			LINE NUMBER =		2	29	38	33	37	29	35	31	40	38	29	40	29	29	34	33	49
177	265	252	231	235	287	355	390	349	293	255	251	277	342	400	411	359	305	253	239	255	311
395	441	417	377	315	262	238	251	301	365	441	433	382	317	268	233	245	291	365	432	433	383
312	255	229	255	311	385	442	448	415	347	269	248	248	285	349	422	462	442	392	345	282	251
255	308	375	440	468	445	387	309	257	242	265	329	398	452	460	425	370	292	249	239	262	327
393	448	461	413	360	295	248	231	238	292	365	440	471	460	391	341	269	229	228	267	342	415
453	462	423	365	289	235	217	251	303	385	451	487	482	433	373	298	249	223	243	282	348	417
488	499	462	415	340	269	229	235	251	308	385	451	495	482	431	269	303	248	223	239	288	355
415	475	493	465	415	342	275	238	220	231	275	341	398	460	483	491	455	387	323	268	228	220
233	283	339	398	462	482	465	415	361	292	249	225	231	280	342	401	441	463	472	448	398	341
285	244	222	225	253	298	355	422	469	487	495	465	413	355	300	255	228	232	262	309	368	428
461	482	488	455	417	382	323	269	248	238	247	269	315	368	415	453	485	495	495	468	438	398
348	299	268	243	229	237	263	301	340	372	415	449	477	482	488	475	449	409	375	345	309	282
257	251	248	253	271	293	315	329	367	401	432	465	482	502	507	509	511	505	492	469	448	422
389	362	338	315	299	282	265	266	262	268	263	288	289	309	325	341	362	377	407	417	431	445
462	471	488	498	511	505	509	522	537	541	538	535	525	522	505	502	507	515	529	528	515	501
491	500	501	508	505	505	495	498	495	511	508	509	522	525	519	515	525	548	539	522	515	525
522	515	520	499	485	471	457	438	407	380	355	327	298	282	257	262	270	291	311	341	385	420
451	471	477	462	445	402	365	315	280	255	249	262	305	342	391	431	439	421	375	321	265	238
242	295	348	405	415	388	335	257	229	249	321	375	382	351	275	223	242	305	365	380	328	262
222	261	325	351	305	241	225	285	338	311	232	220	275	302	245	211	253	262	211	215	245	197
197	222	180	193	171	162	128	105	120	115	111	85	71	57	55	57	55	60	55	51	48	51
54	48	48	51	48	48	45	45	45	43	41	42	45	45	42	42	40	38	38	38	41	38

LINE READ & STORED

TABLE 8. Blade Angles of Rotation Calculated from Contour Information.

Rotation applied to blade. (degrees) ± .05	Angular rotation calculated for the convex surface. (degrees)			Angular rotation calculated for the concave surface. (degrees)			Angular rotation calculated for the whole blade section. (degrees)			Blade Section Area (inches^2)		
	Towards root	Centre	Towards tip	Towards root	Centre	Towards tip	Towards root	Centre	Towards tip	Towards root	Centre	Towards tip
o Reference	-	-	-	-	-	-	-	-	-	0.143	0.123	0.105
1.00	1.05	0.99	0.94	1.07	0.98	0.92	1.05	0.90	0.95	0.148	0.123	0.107
1.50	1.48	1.60	1.46	1.61	1.55	1.43	1.50	1.47	1.47	0.141	0.129	0.104
2.00	2.05	1.99	2.03	2.01	1.93	1.85	2.04	1.96	1.91	0.151	0.132	0.113
2.50	2.65	2.51	2.48	2.43	2.56	2.59	2.45	2.49	2.65	0.144	0.128	0.108

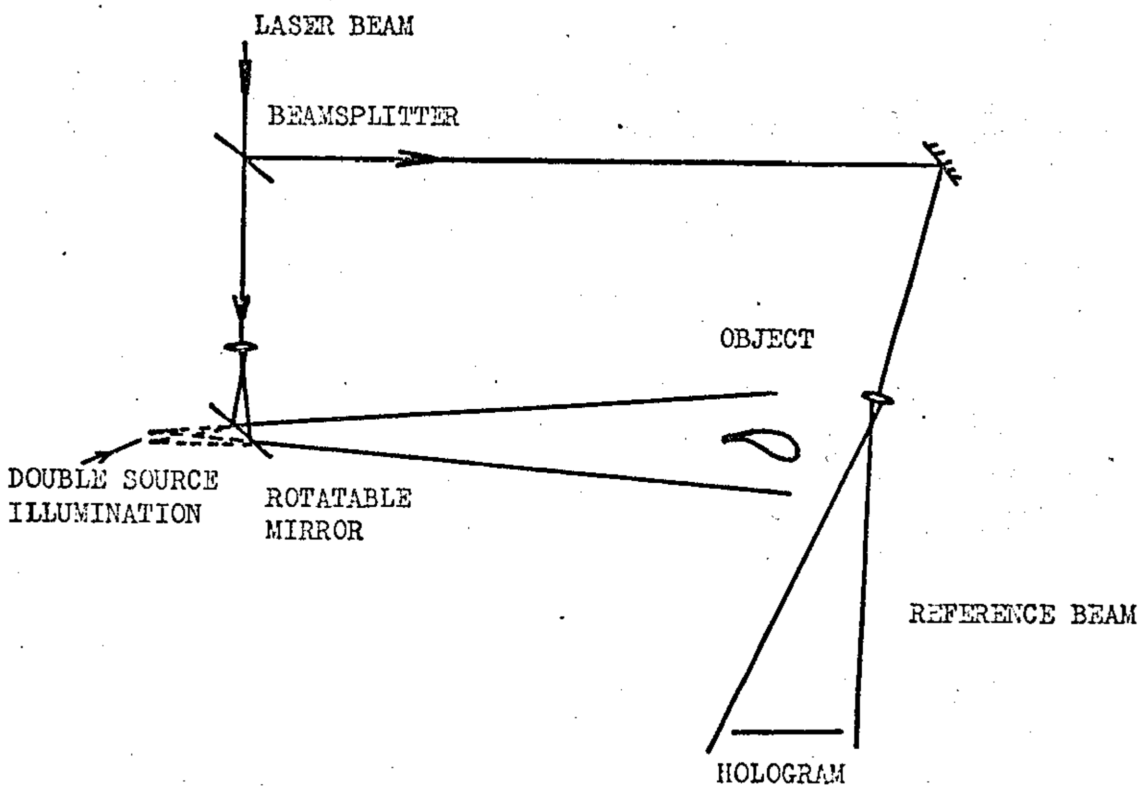

a) Schematic diagram of the optical arrangement.

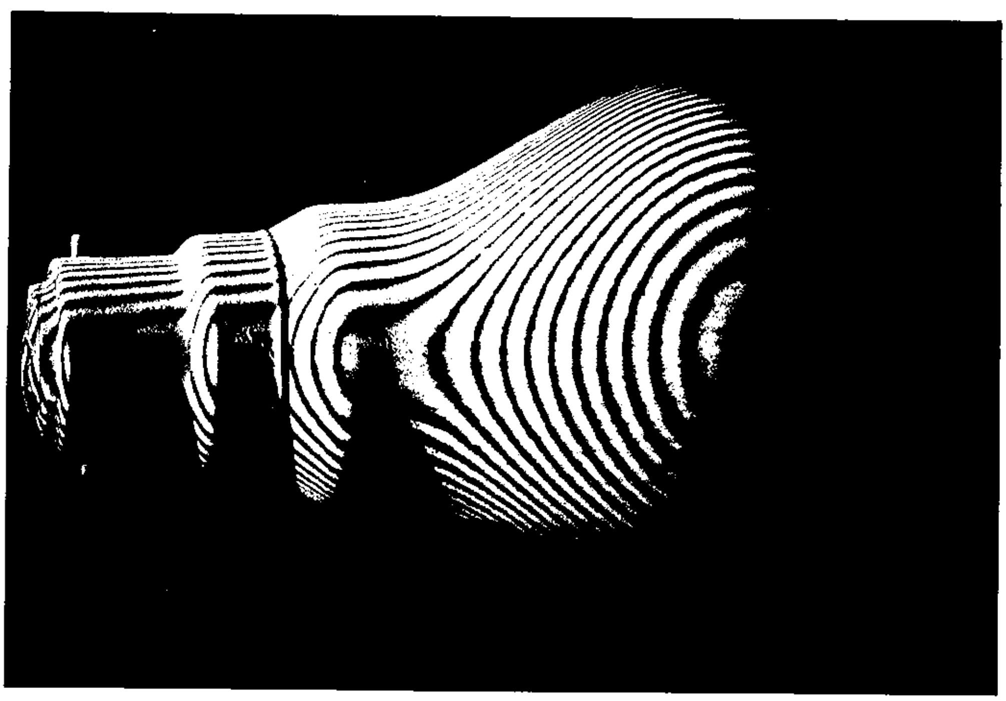

b) Example of two source contouring (depth interval = 1.5 mm.)

FIG. 1. HOLOGRAM SYSTEM FOR THE GENERATION OF DEPTH CONTOURS BY THE TWO SOURCE METHOD.

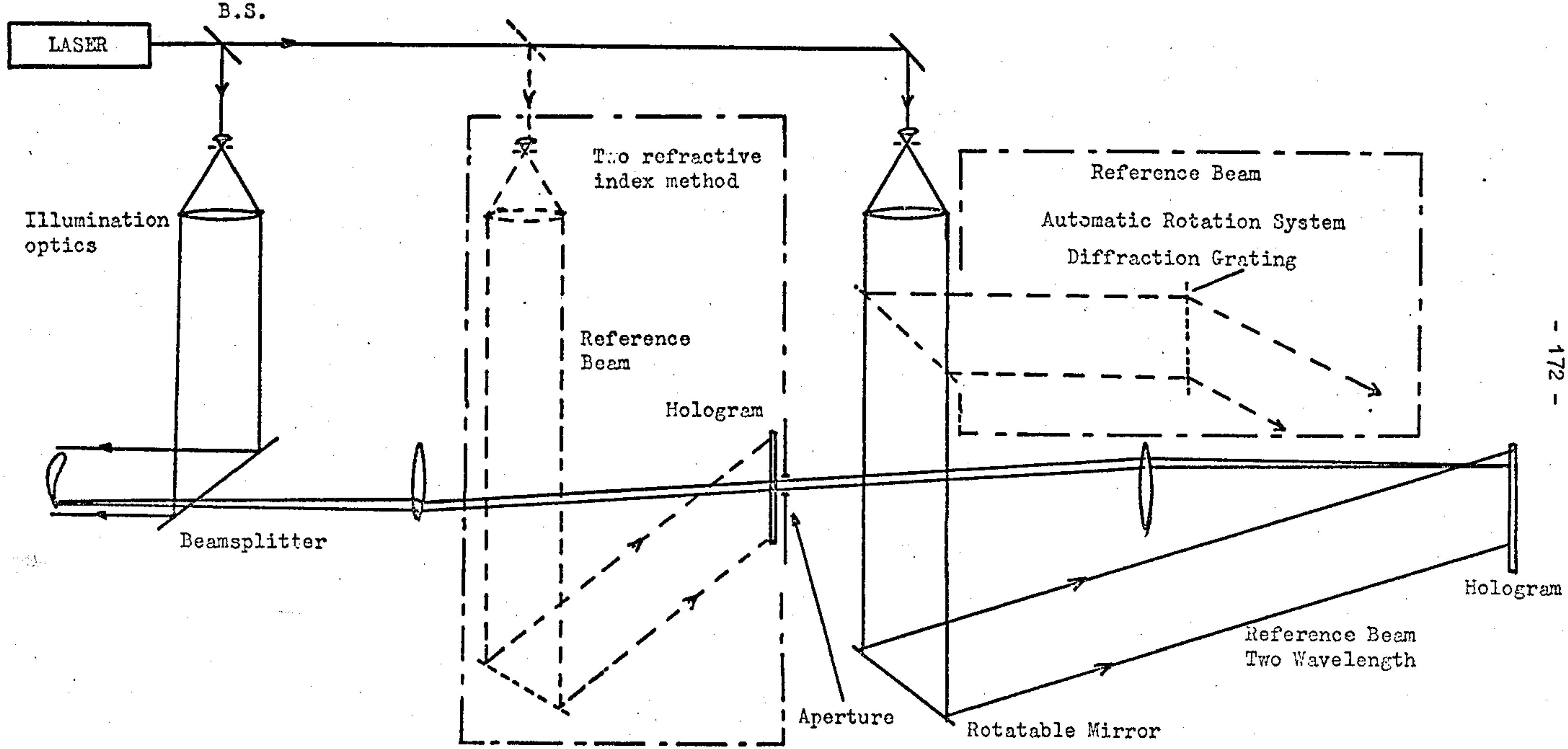

FIG. 2. TELECENTRIC IMAGING ARRANGEMENT FOR OPTICAL CONTOURING.

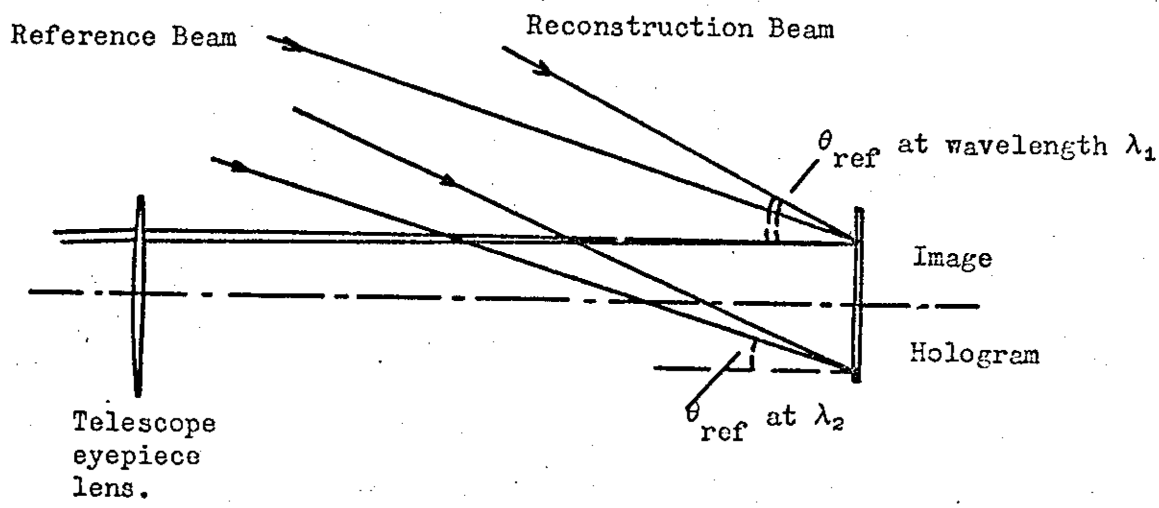

a) Reference and Reconstruction Beam Angles for Two Wavelength Contouring.

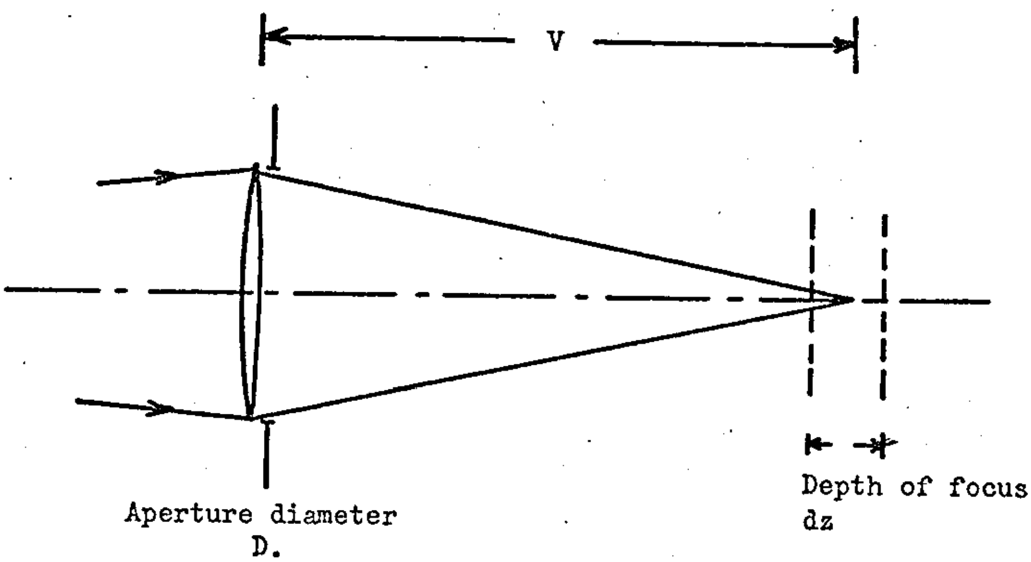

b) Depth of Focus on a Single Lens Imaging System.

FIG. 3.

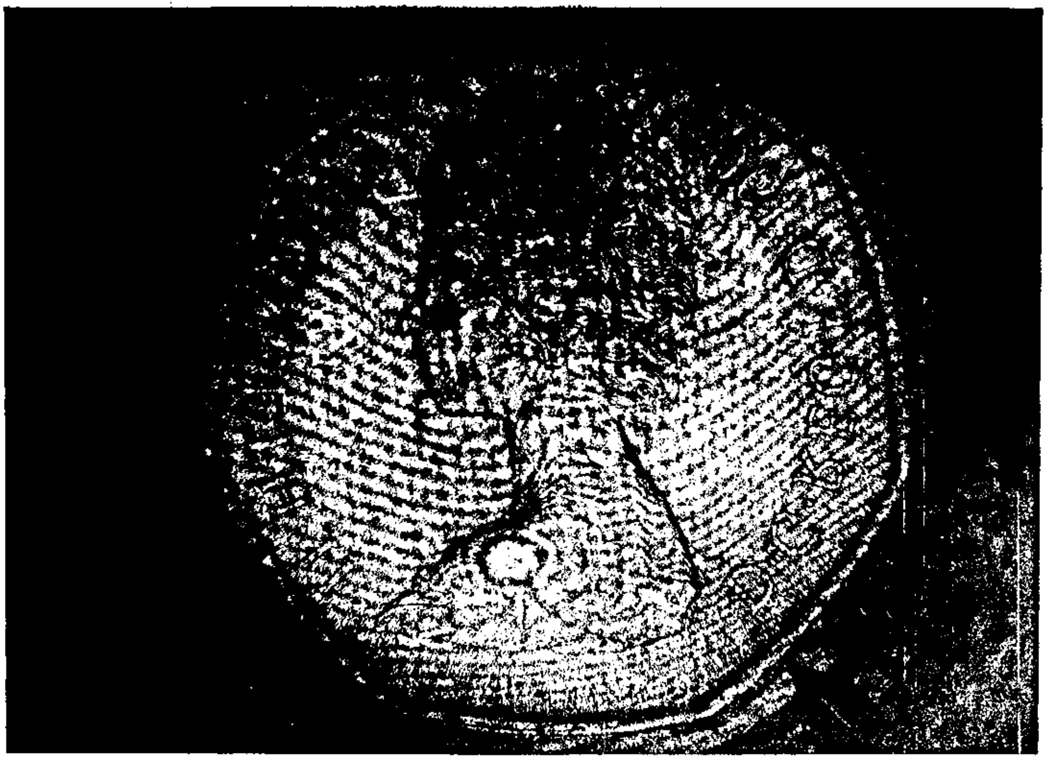

a) COIN

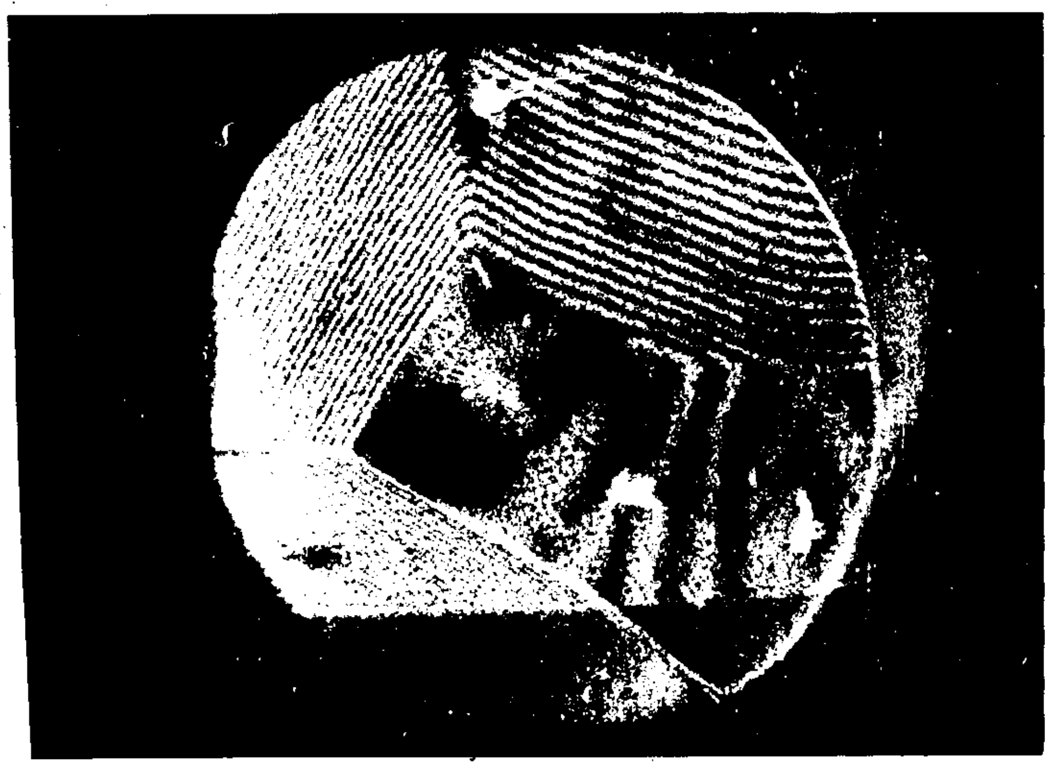

b) TEST OBJECT

FIG. 4. EXAMPLES OF TWO WAVELENGTH CONTOURING.

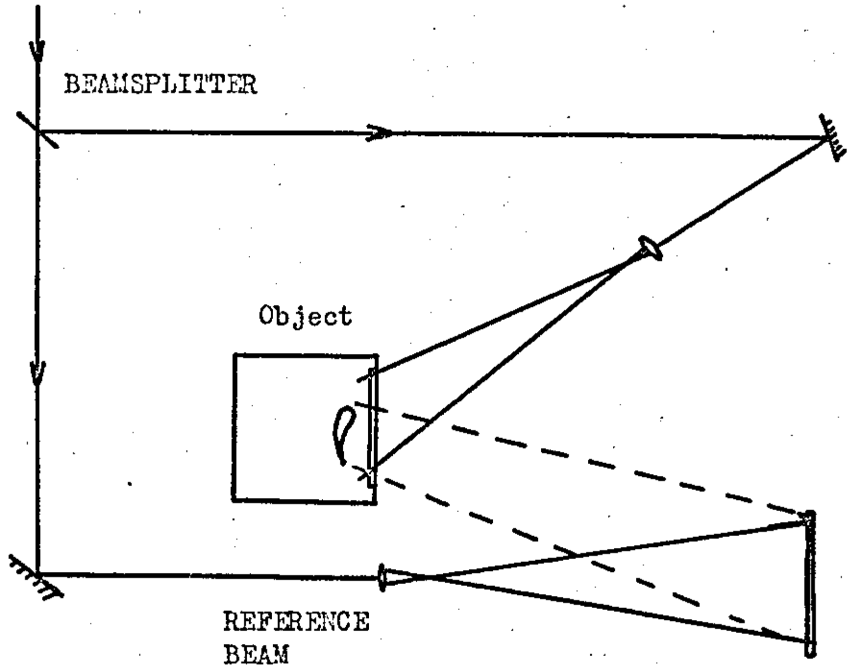

a) Schematic diagram for the optical arrangement

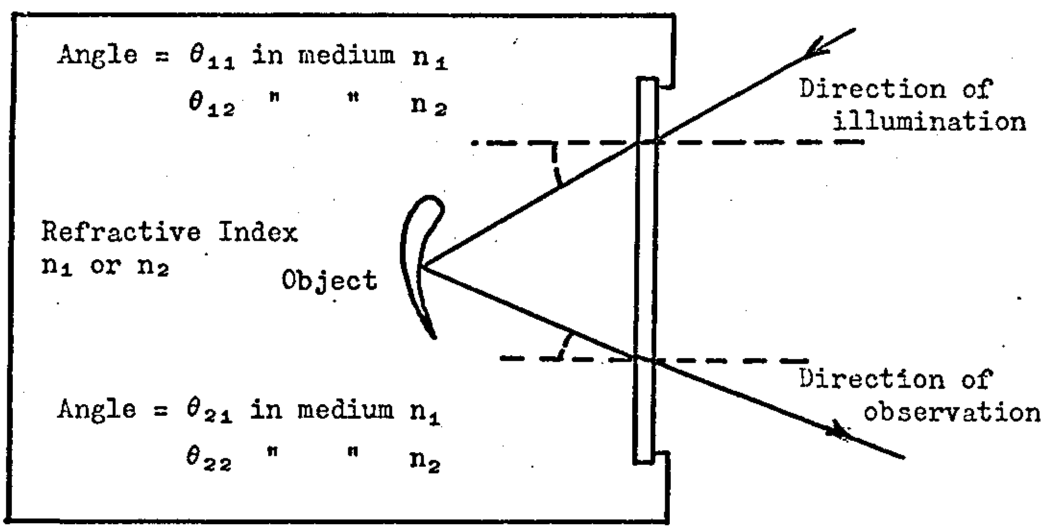

b) Optical path arrangement for the object within an enclosed chamber.

FIG. 5. TWO REFRACTIVE INDEX HOLOGRAPHIC CONTOURING

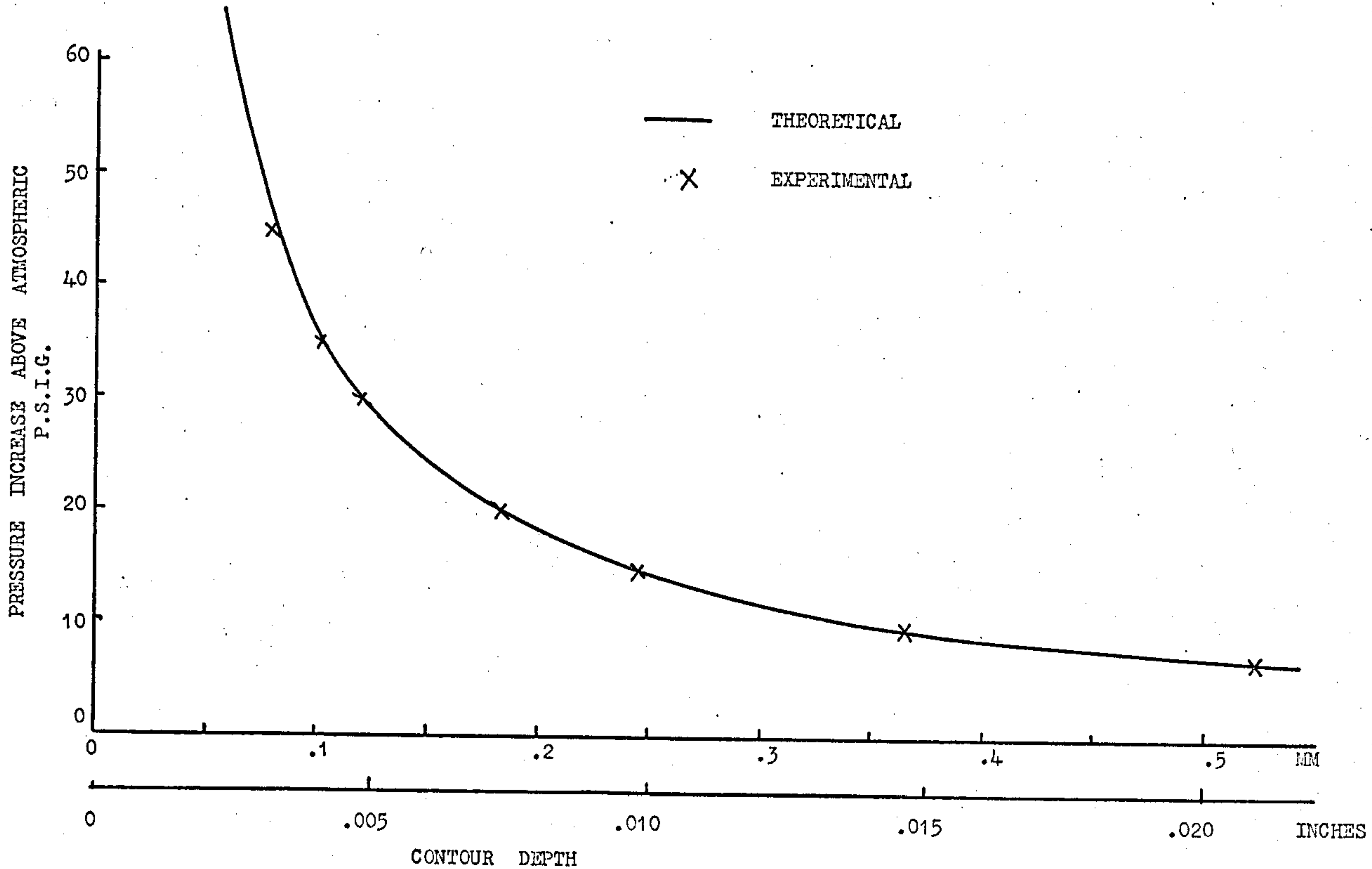

FIG. 6. CONTOUR DEPTH INTERVAL IN 'FREON 12' VERSUS PRESSURE INCREASE.

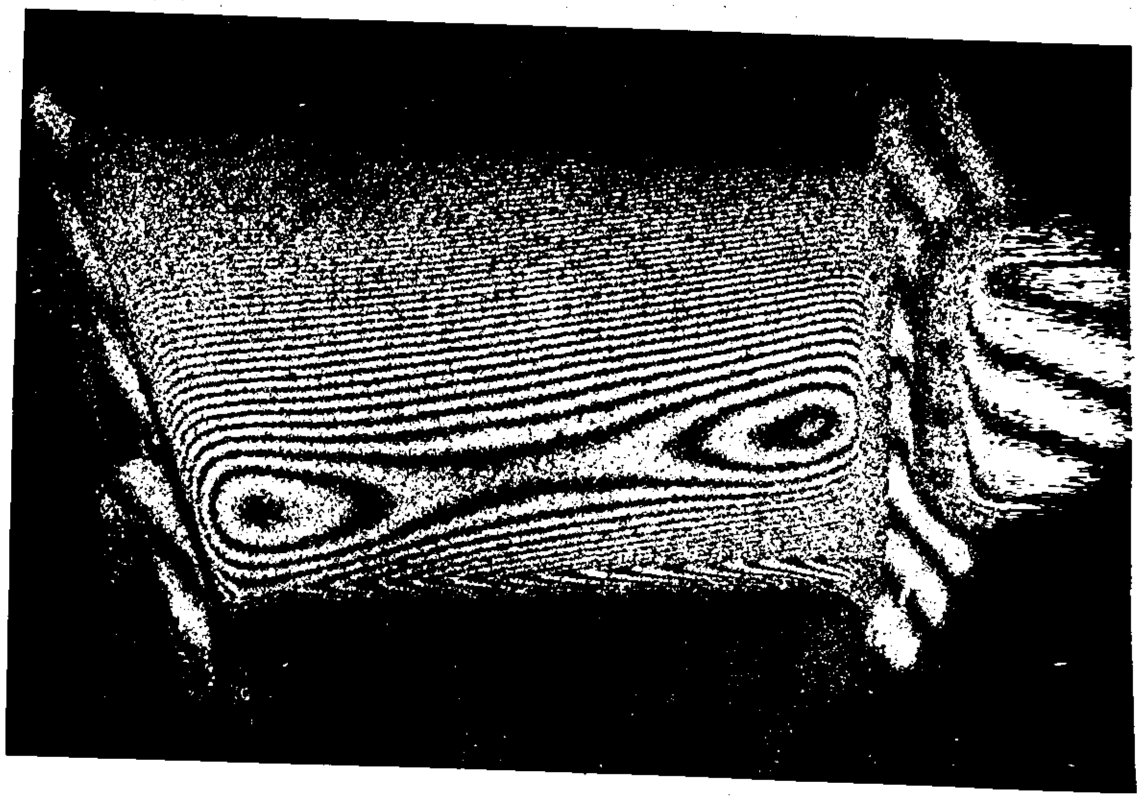

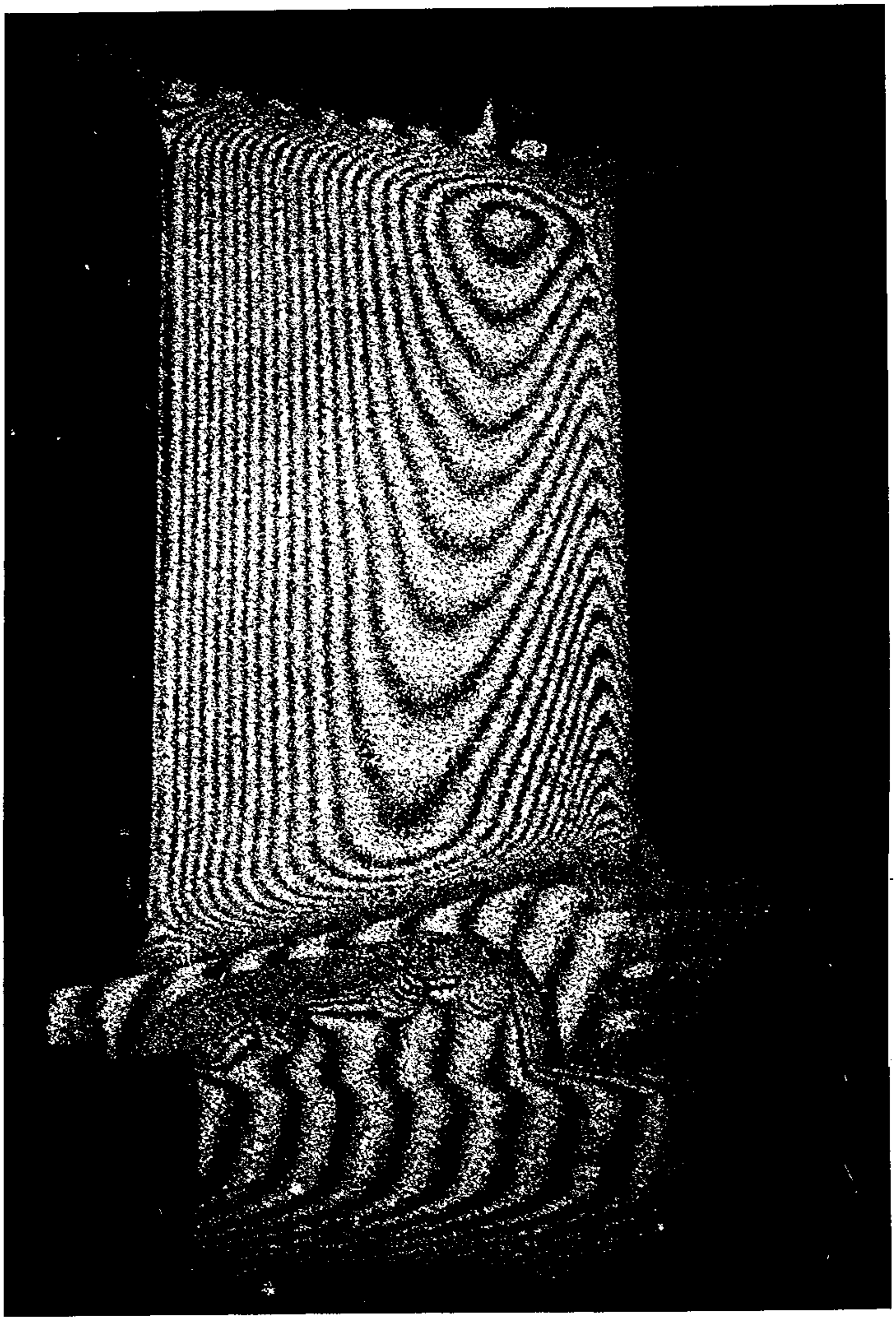

FIG. 7. DOUBLE REFRACTIVE INDEX CONTOURS ON A SMALL TURBINE BLADE (DEPTH INTERVAL = 0.010).

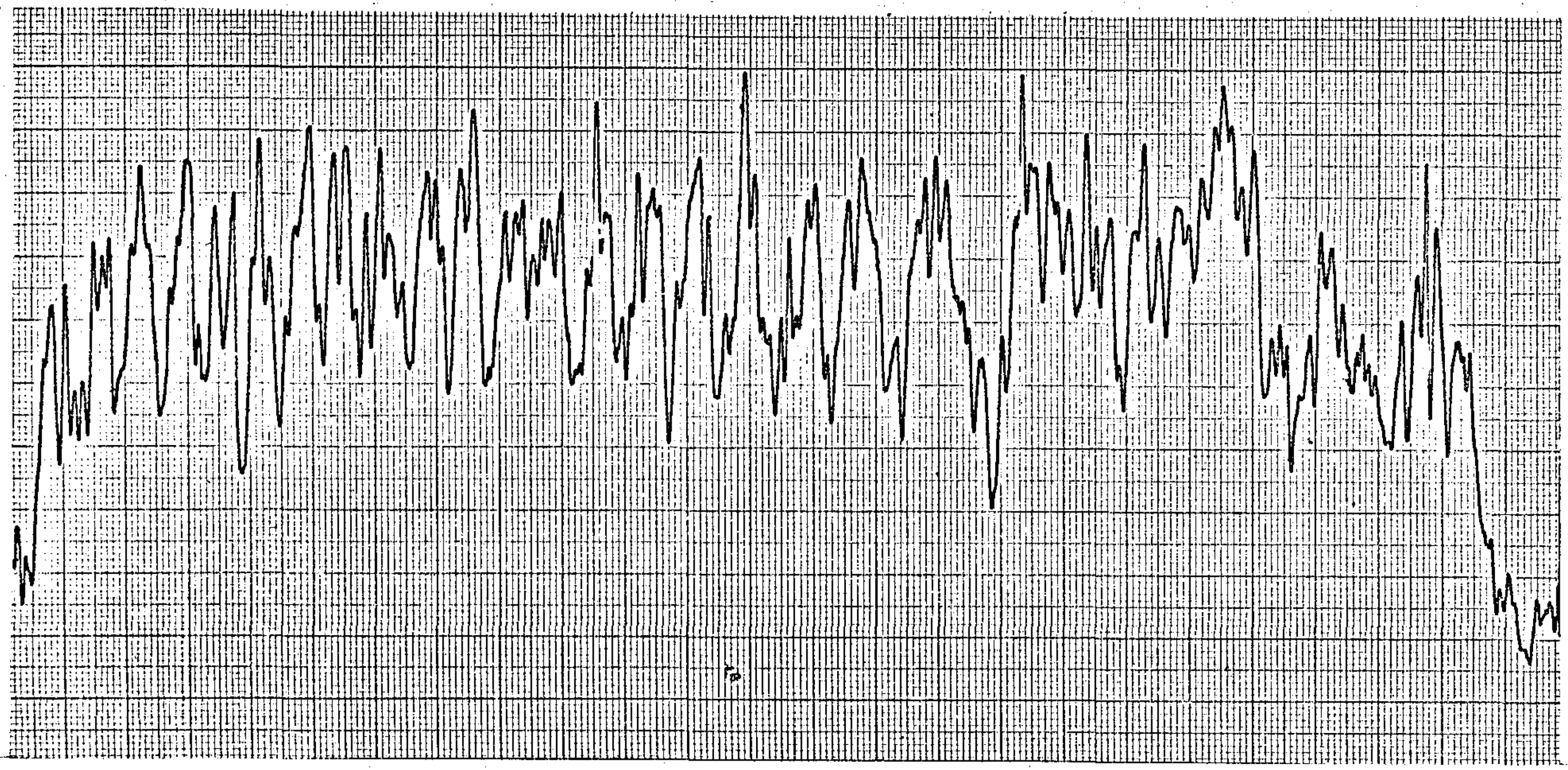

FIG. 9. MICRODENSITOMETER TRACE ACROSS A HOLOGRAPHICALLY CONTOURED BLADE. APERTURE F.40

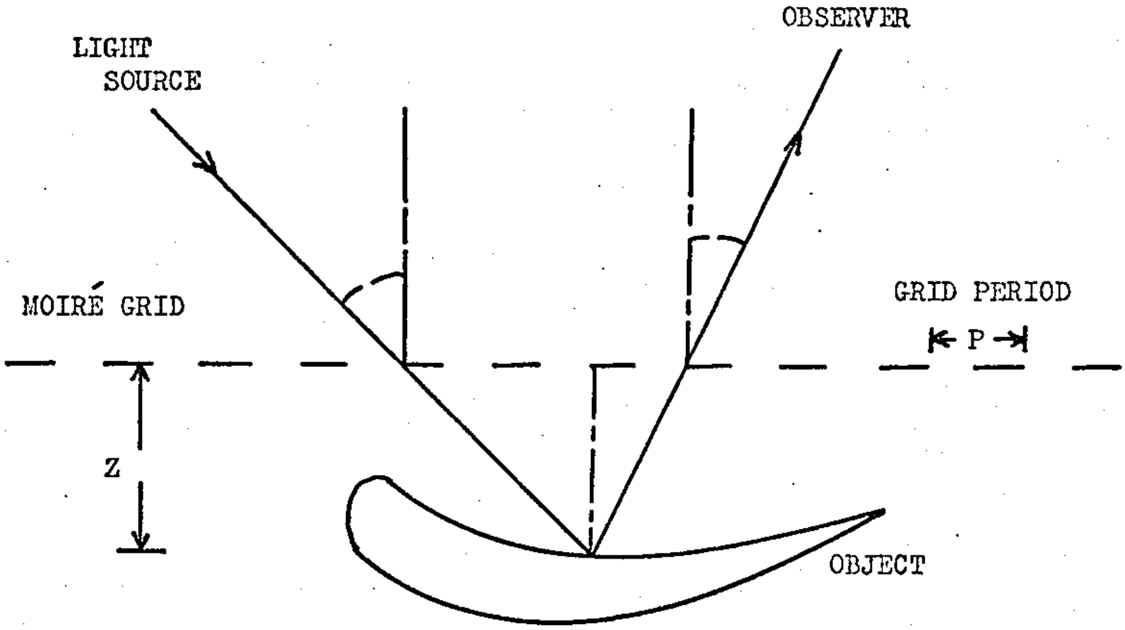

A. SOURCE & OBSERVER AT INFINITY

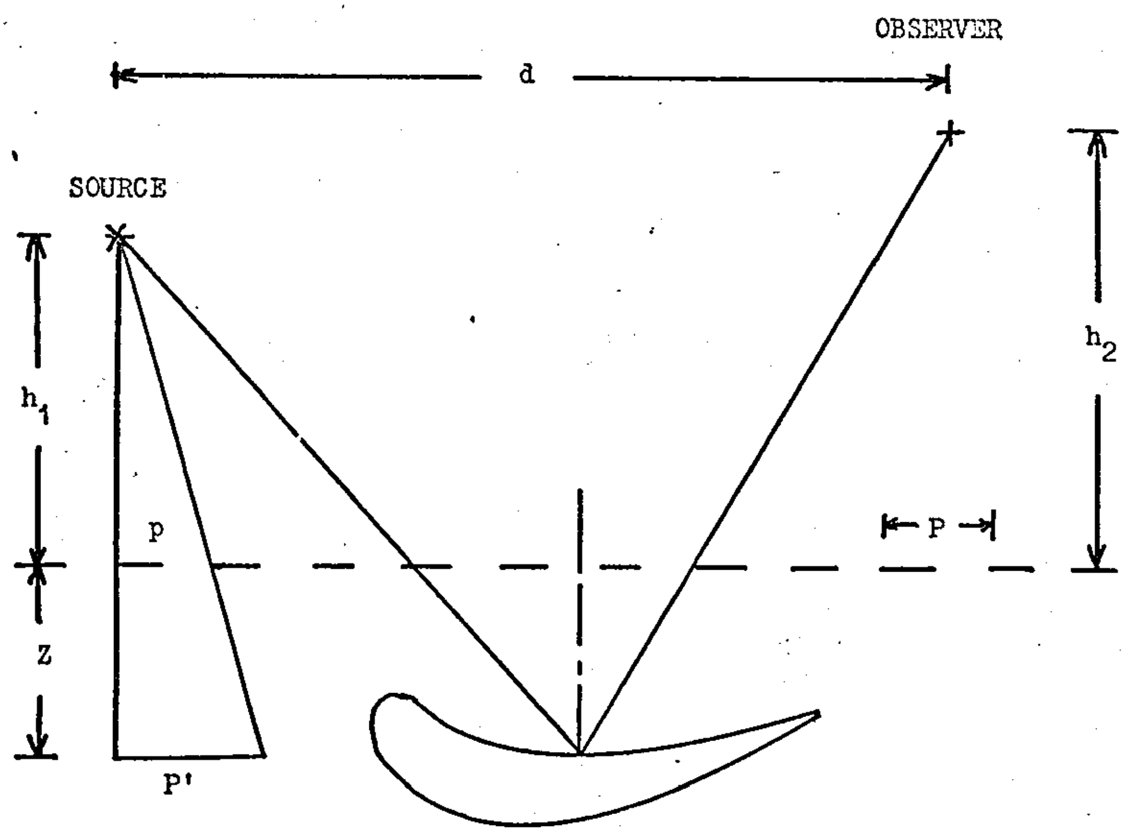

B. FINITE SOURCE & OBSERVER DISTANCES

FIG. 10. MOIRÉ FRINGE CONTOURING

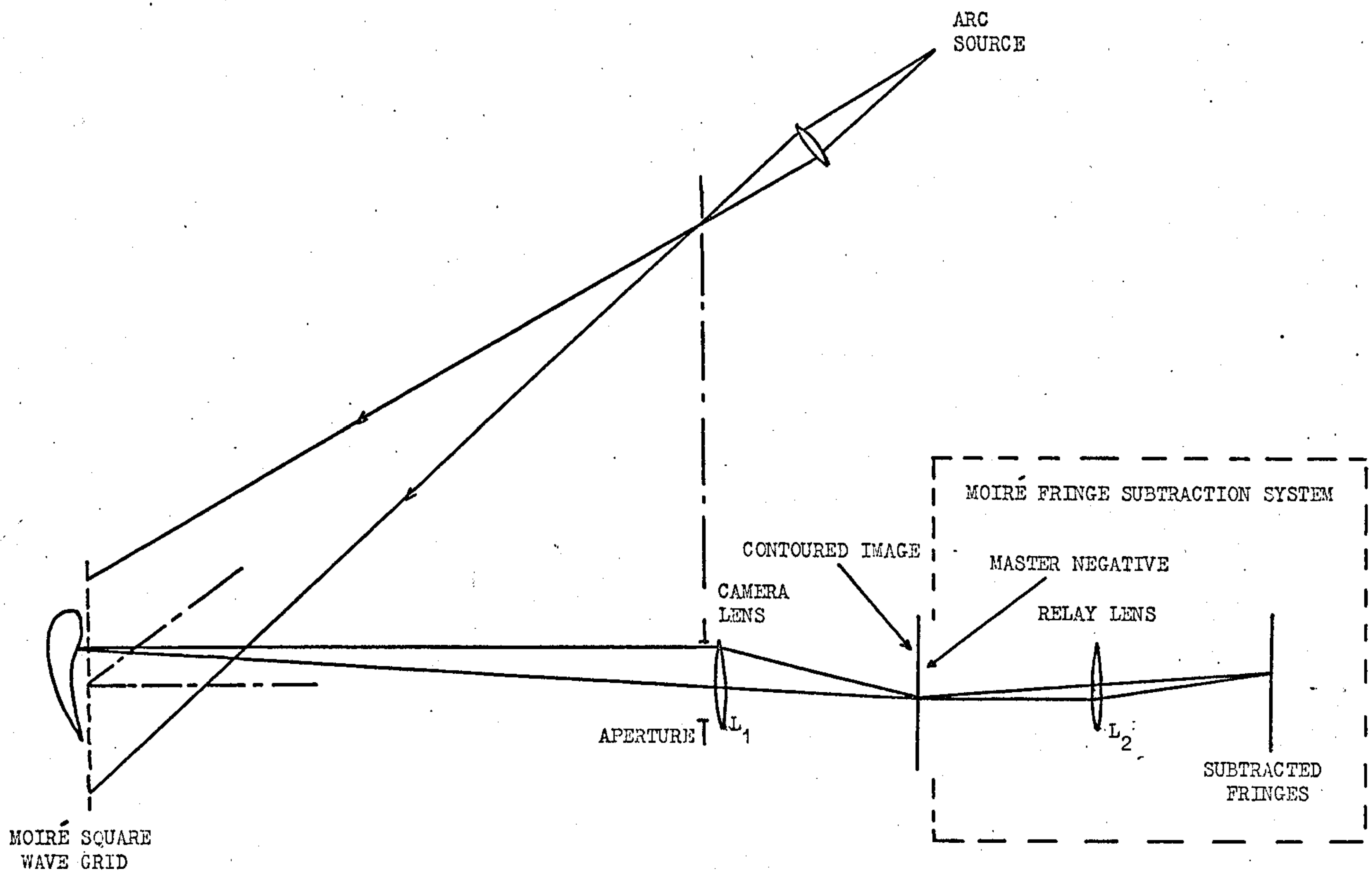

FIG. 11. MOIRÉ SHADOW CONTOURING AND IMAGE SUBTRACTION SYSTEM.

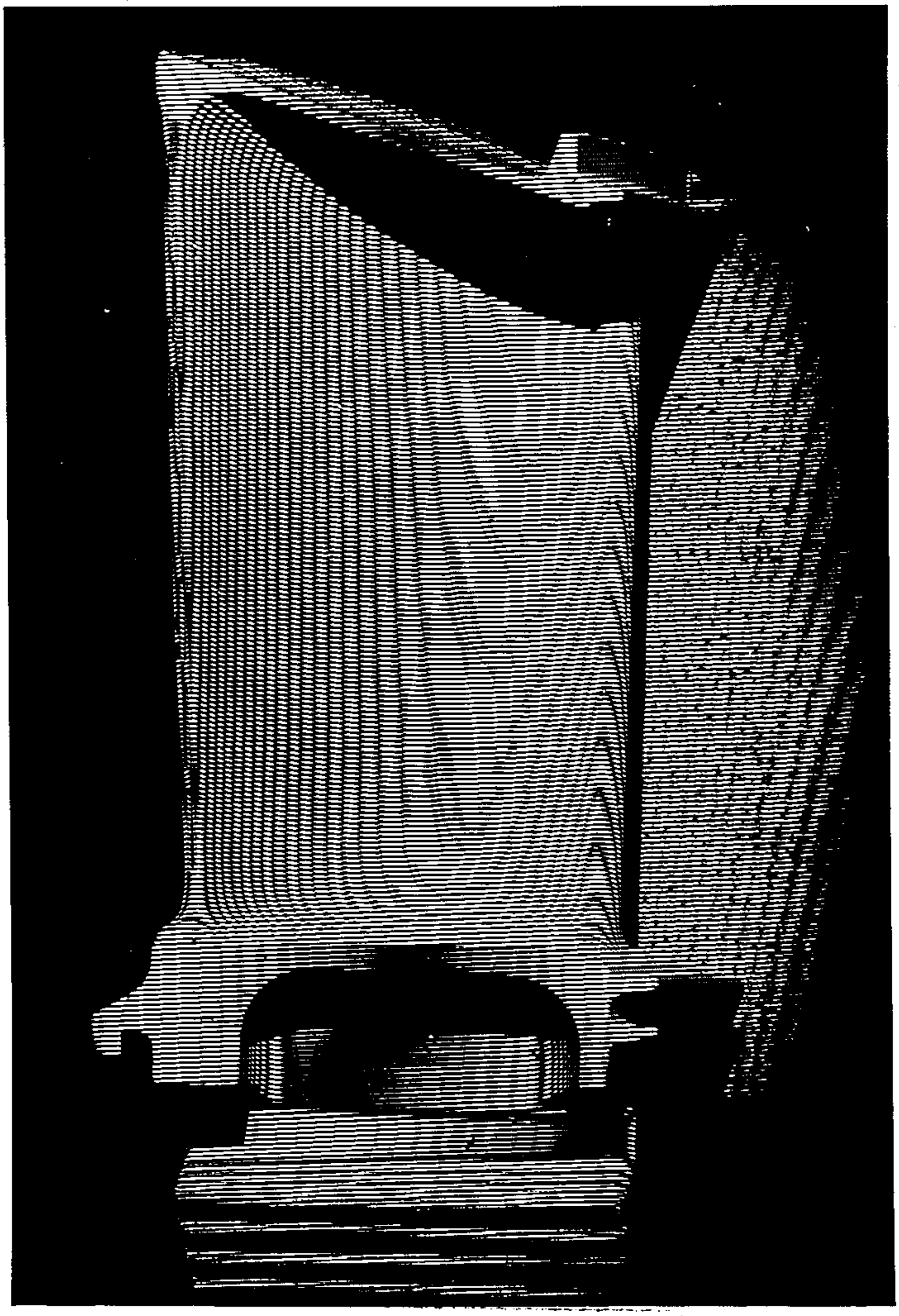

FIG. 12. MOIRÉ SHADOW DEPTH CONTOURS ON A TURBINE BLADE.

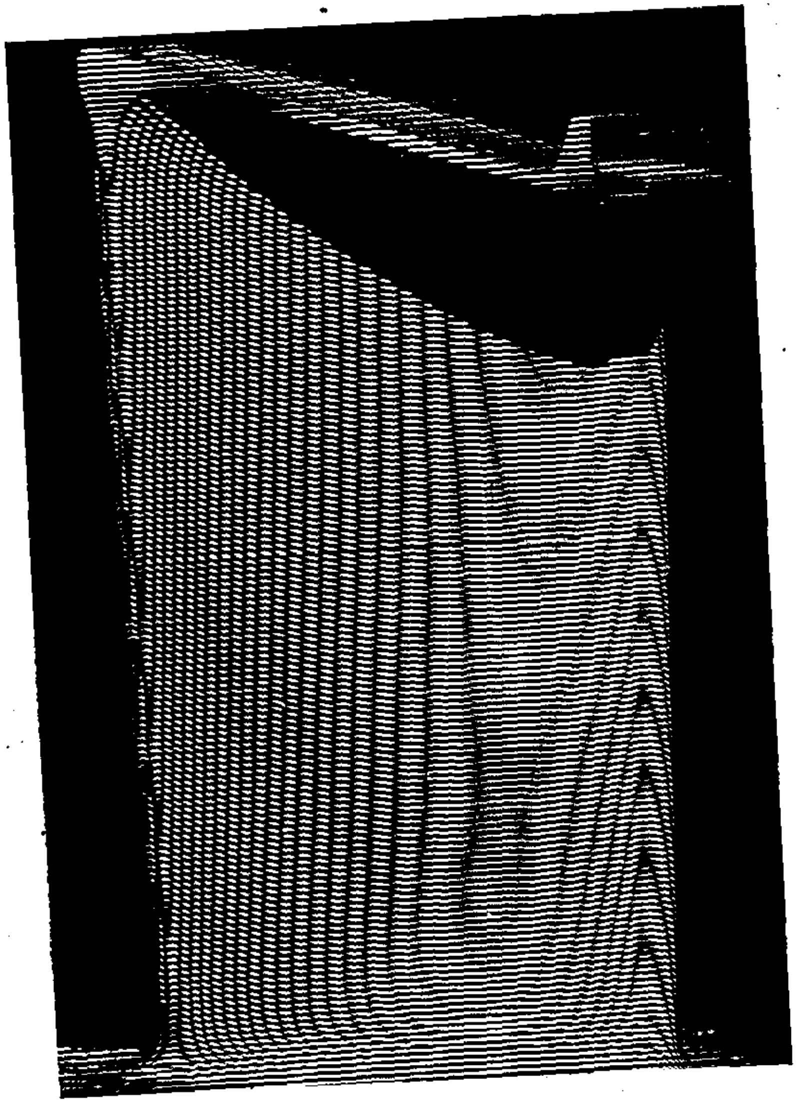

(a) GRID STATIONARY

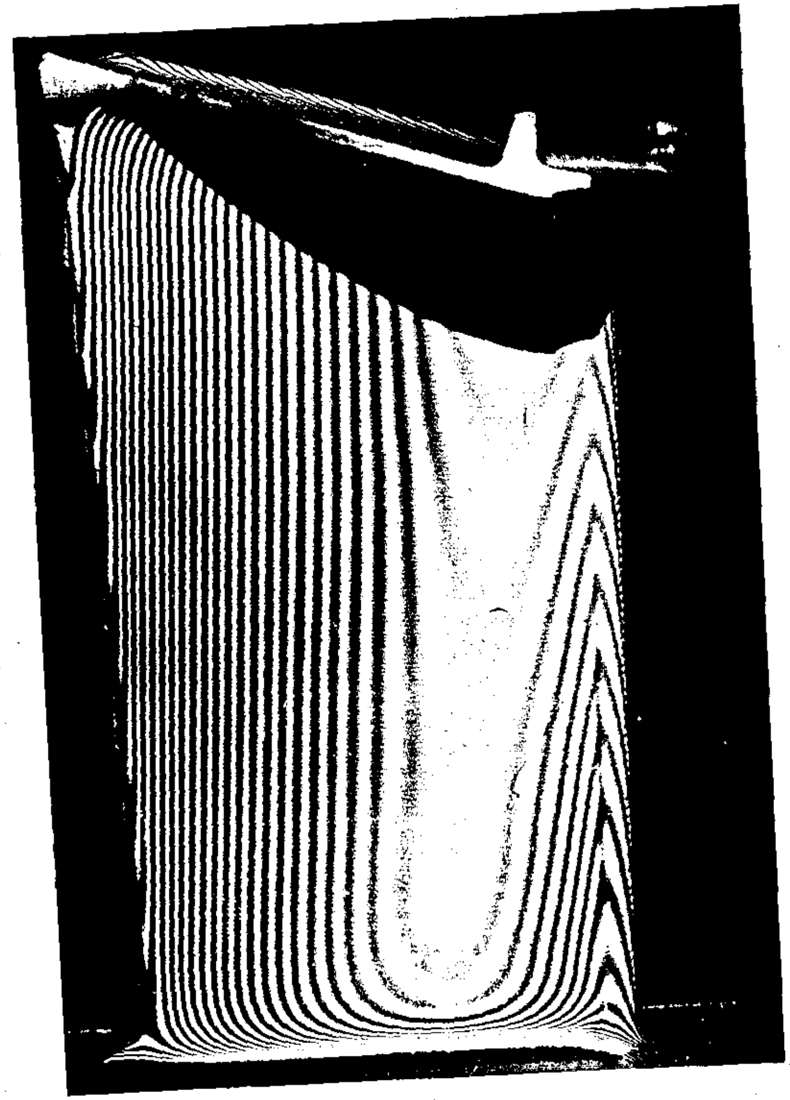

(b) GRID MOVING

FIG. 13.. EFFECTS OF GRID MOVEMENT ON MOIRÉ SHADOW CONTOURS.

a) Grid stationary

(Grid lines parallel to blade axis.)

b) Grid moving in the direction of scan when the negative was formed.

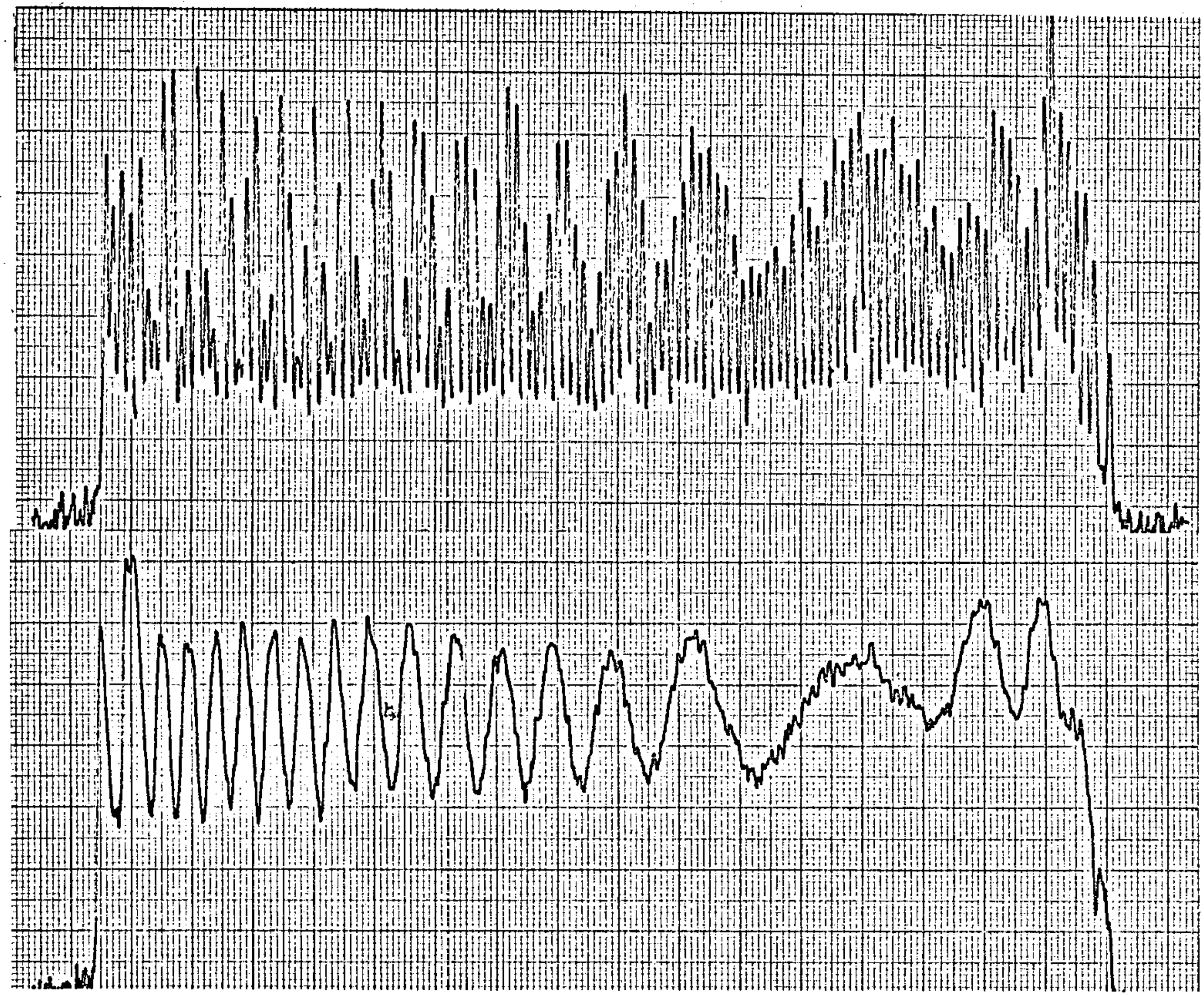

FIG. 14. MICRODENSITOMETER TRACES ACROSS A NEGATIVE OF A CONTOURED TURBINE BLADE (MOIRÉ SHADOW CONTOURS).

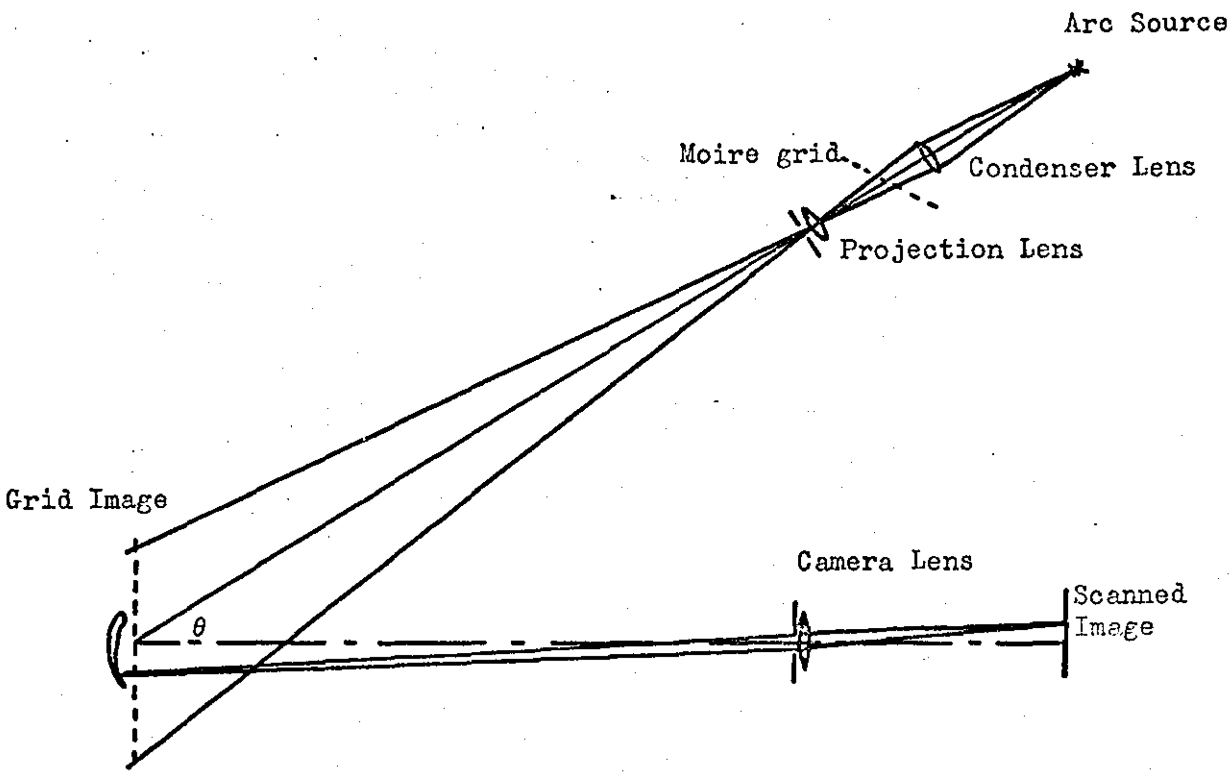

a) Optical Arrangement.

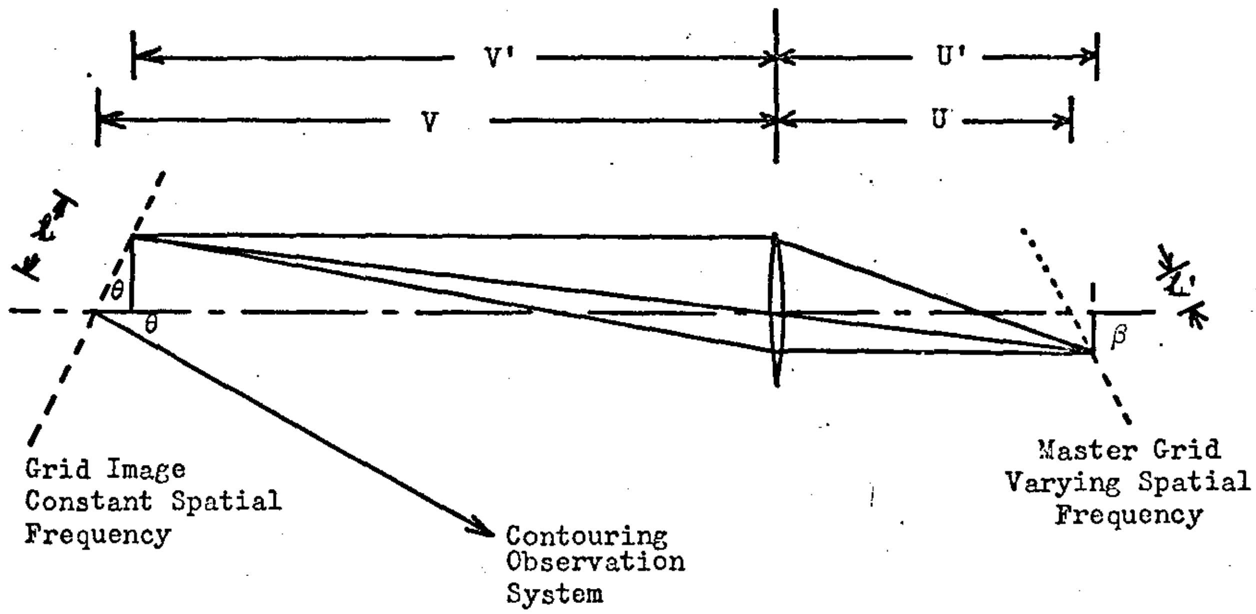

b) Production of a Moiré Grid Image with a Linear Spatial Frequency at an angle θ to the axis.

FIG. 15. FRINGE PROJECTION / SCAN CONTOURING SYSTEM.

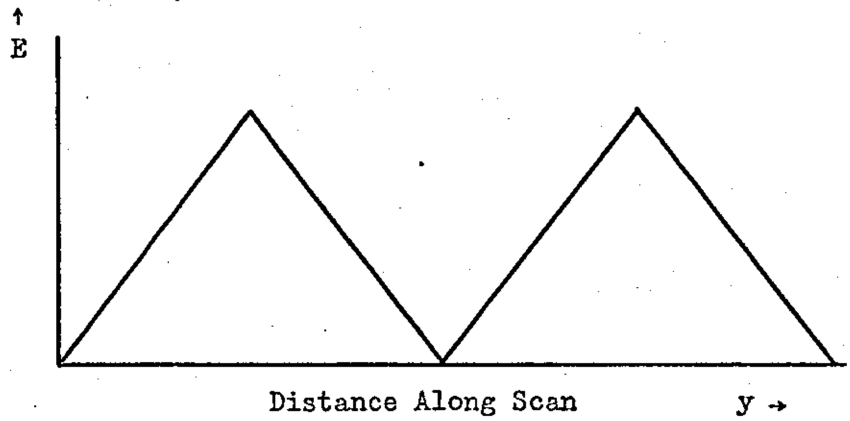

a) Triangular Wave Function.

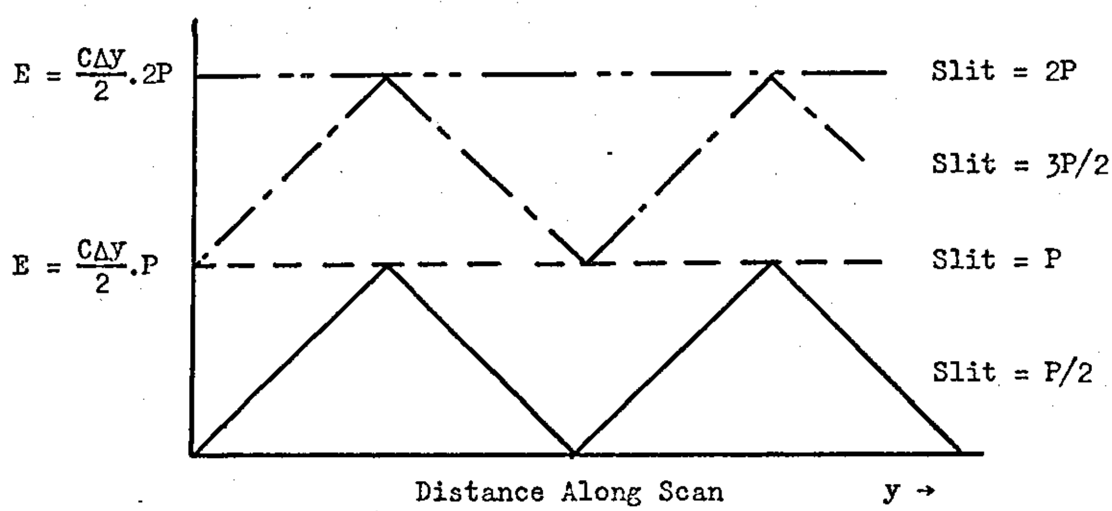

b) Intensity function with various slit widths.

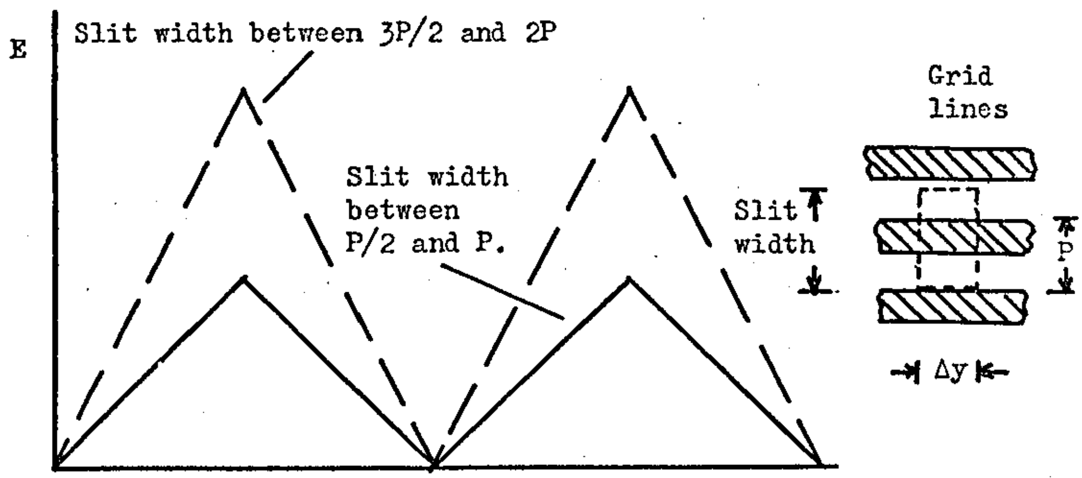

c) Intensity function - Grid in Observing Optics.

FIG. 16. CONTOUR INTENSITY FUNCTIONS.

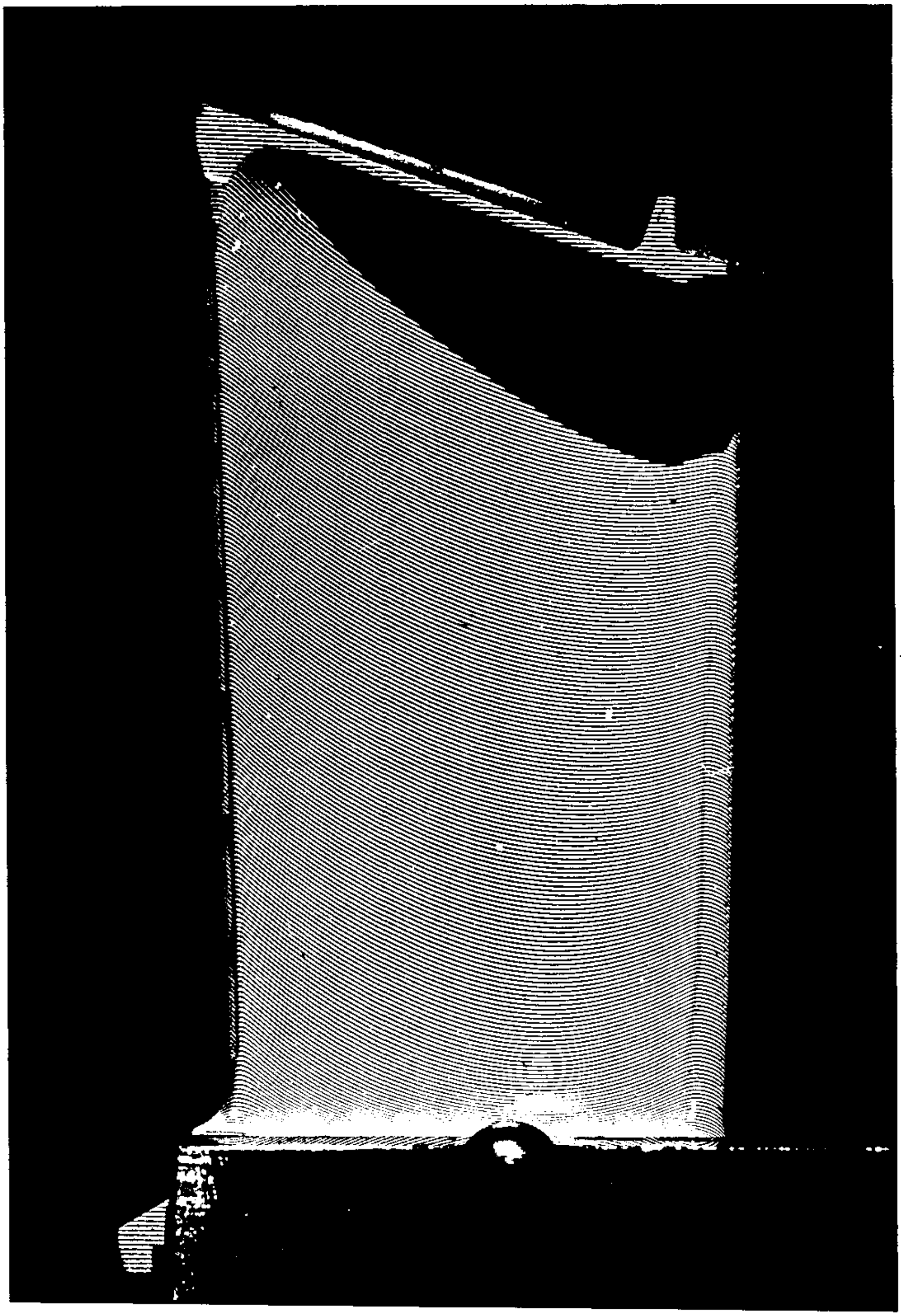

FIG. 17. FRINGES PROJECTED ON TO A TURBINE BLADE.
EQUIVALENT CONTOUR DEPTH = 0.010"
(PHOTOGRAPH MAGNIFICATION = 2.5:1)

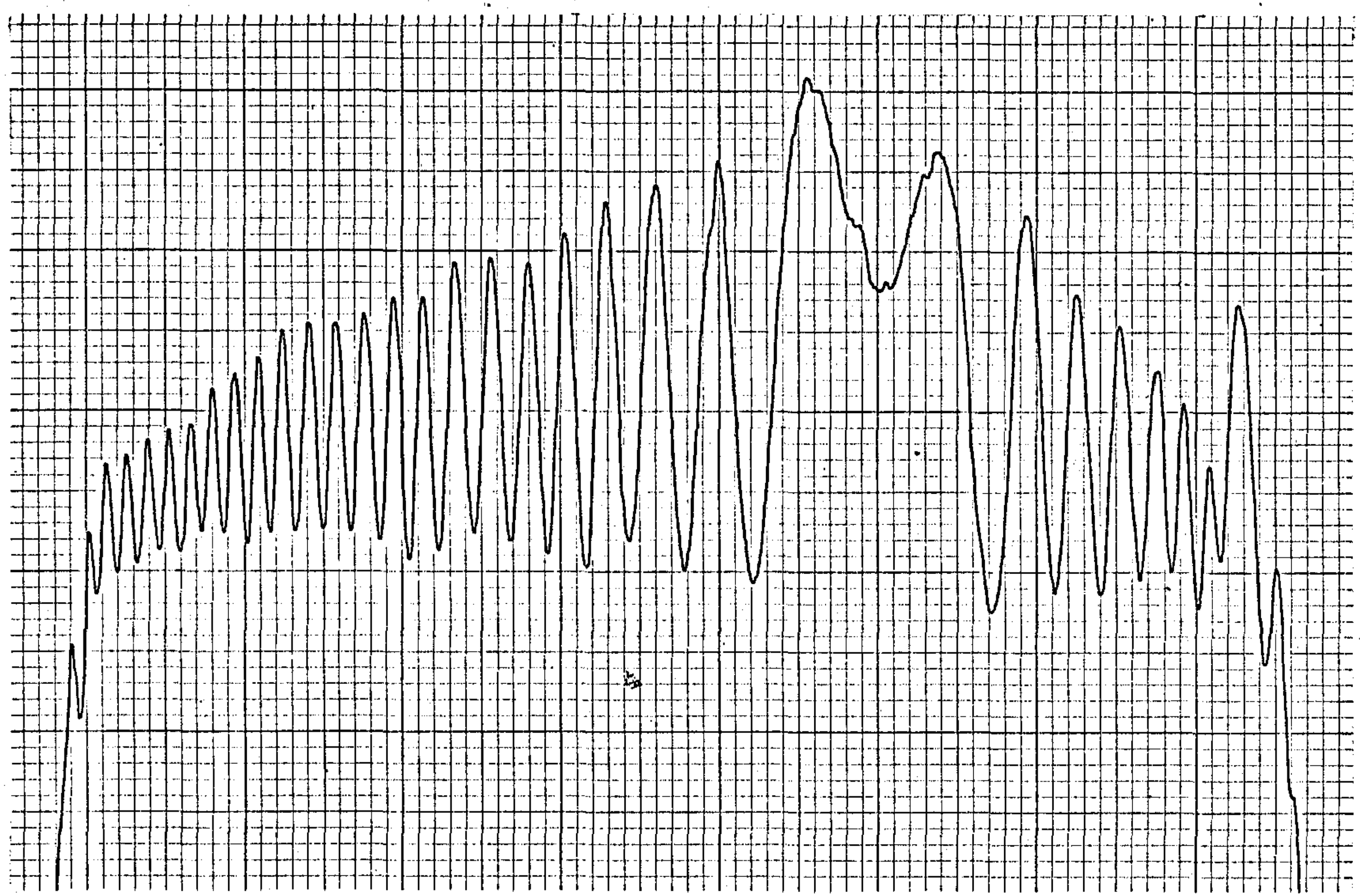

FIG. 18. DEPTH CONTOUR SCAN USING MOIRÉ PROJECTED FRINGES.

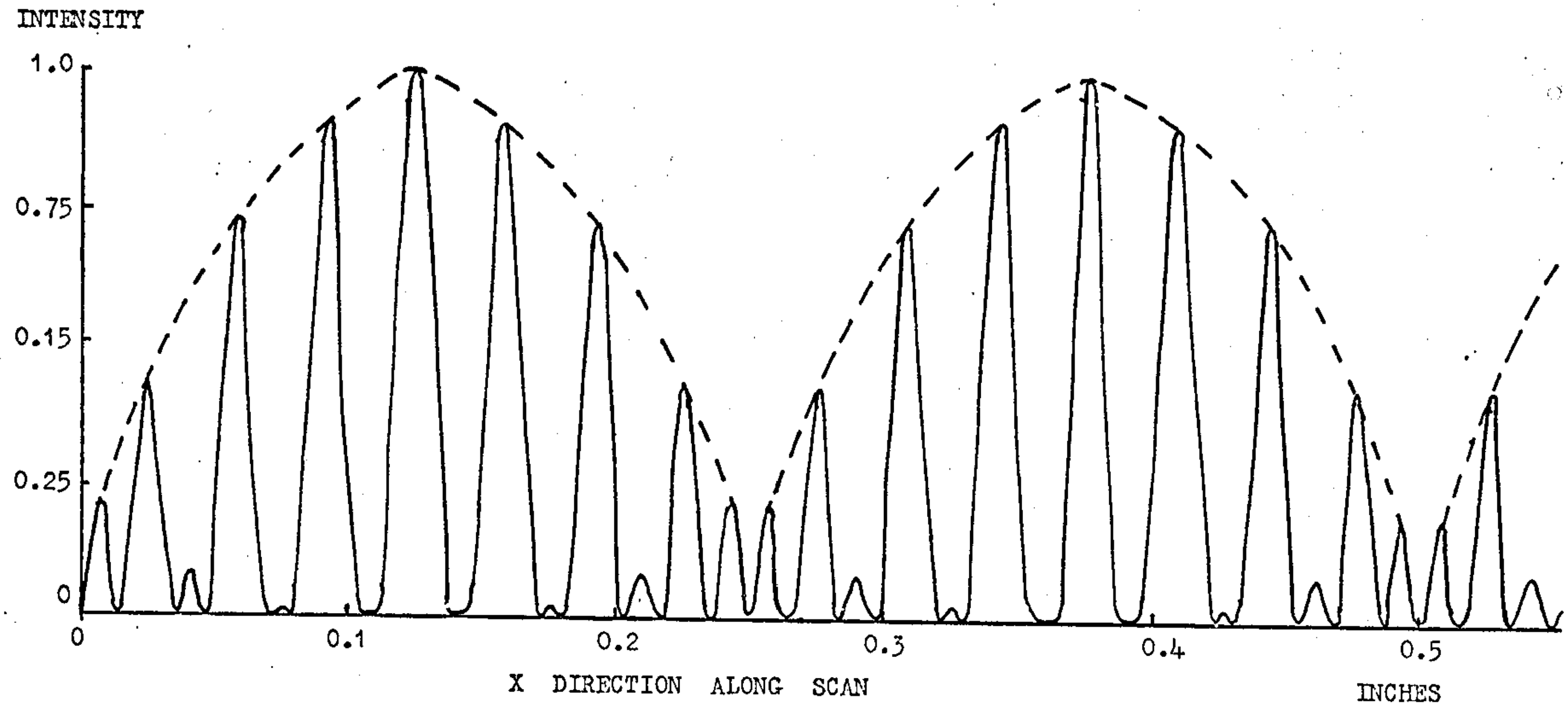

FIG. 19. COMPUTER SIMULATED MOIRÉ DIFFERENCE FRINGES FOR TWO LINEAR SLOPES.

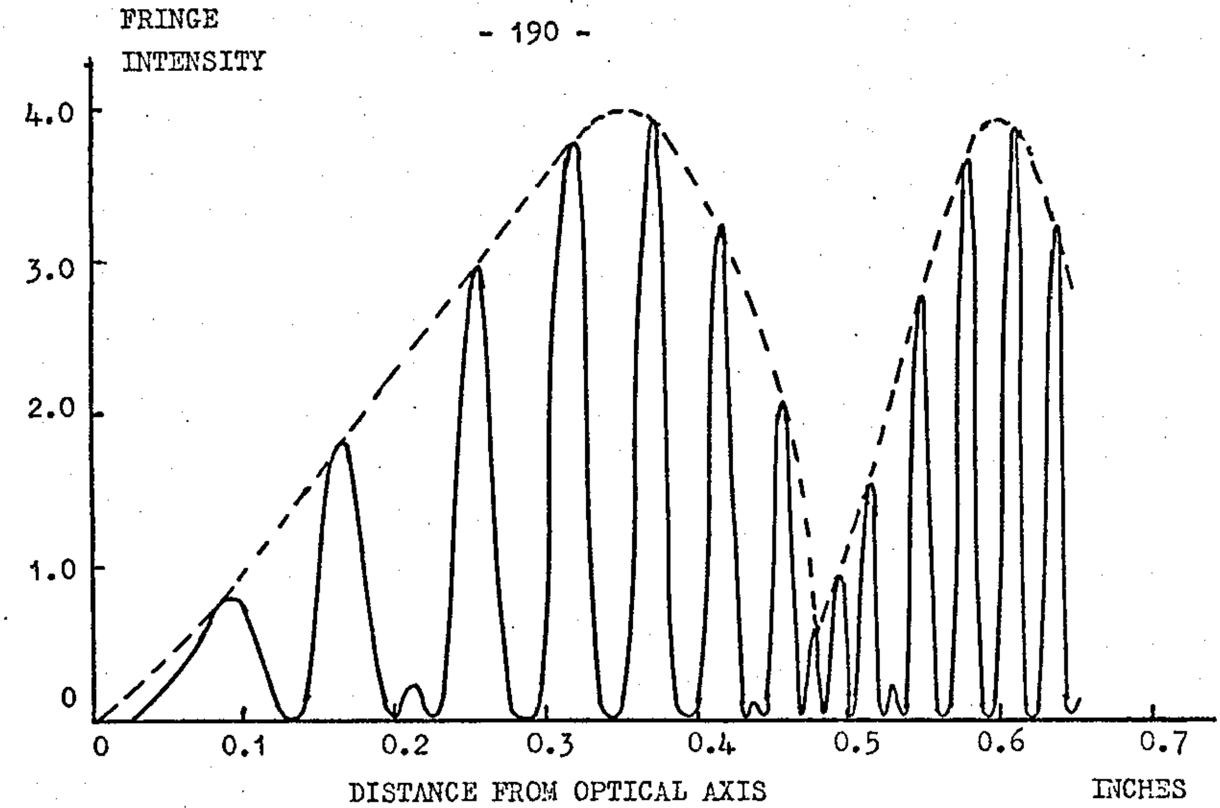

(A) COMPUTER GENERATED SUBTRACTED MOIRÉ FRINGE PATTERN. (ELLIPTICAL OBJECT)

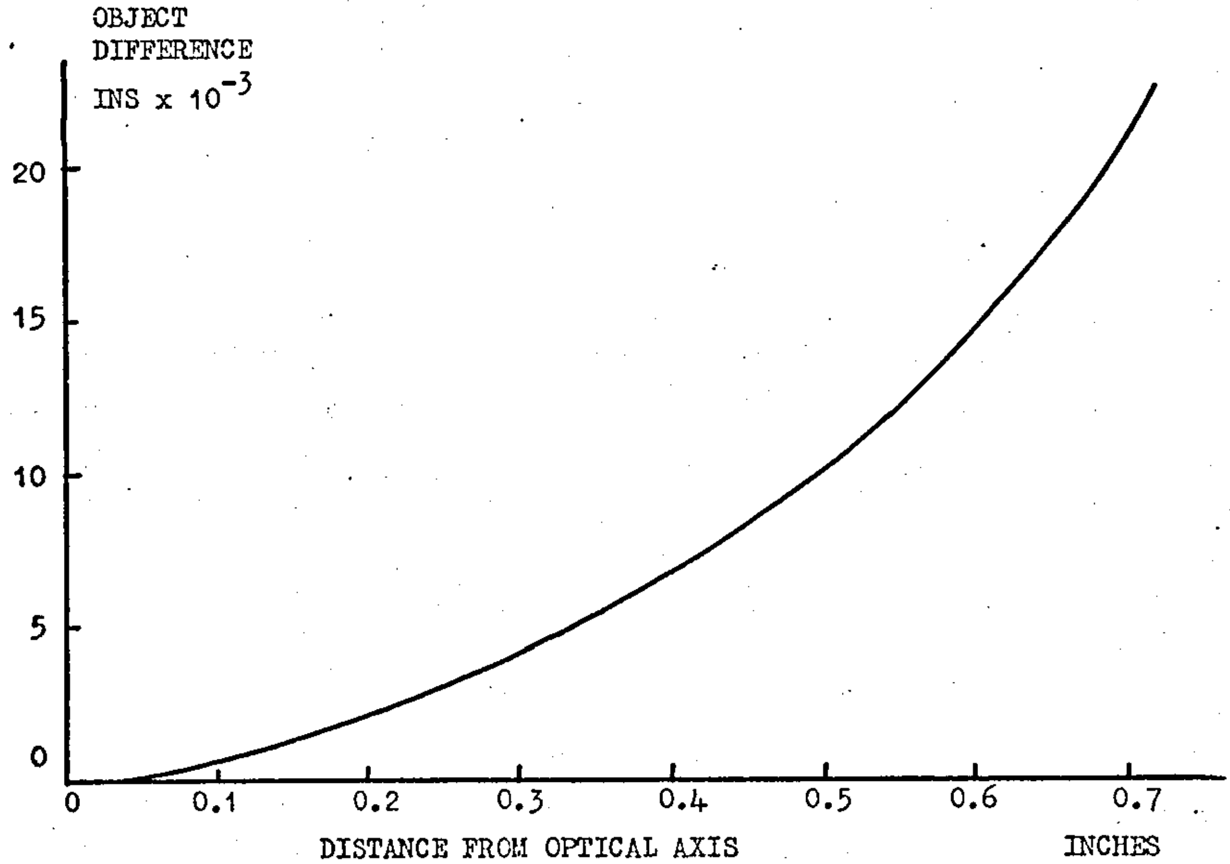

(B) MOIRÉ DIFFERENCE PLOT.

FIG. 20. COMPUTER SIMULATED MOIRÉ PATTERN ANALYSIS OF ELLIPTICAL OBJECTS.

(A) Moiré pattern of subtracted contour fringes for a deflected plate.

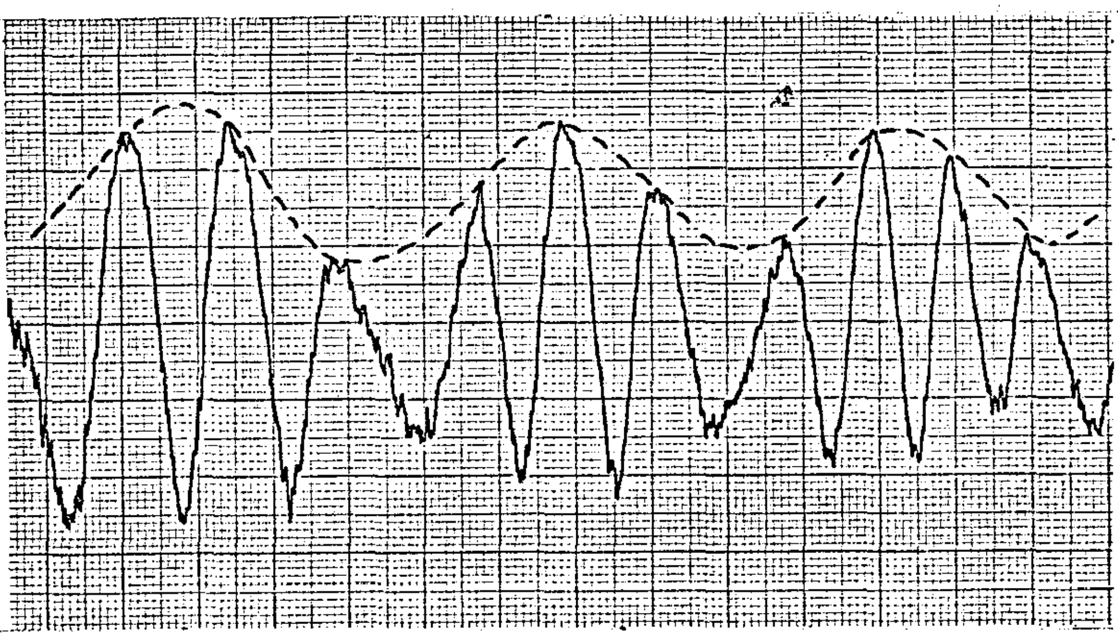

(B) Microdensitometer trace of fringe intensity.

FIG. 21. MOIRÉ FRINGE SUBTRACTION.

(CONTOUR FREQUENCY TO MOIRÉ FRINGE FREQUENCY RATIO ÷ 4:1)

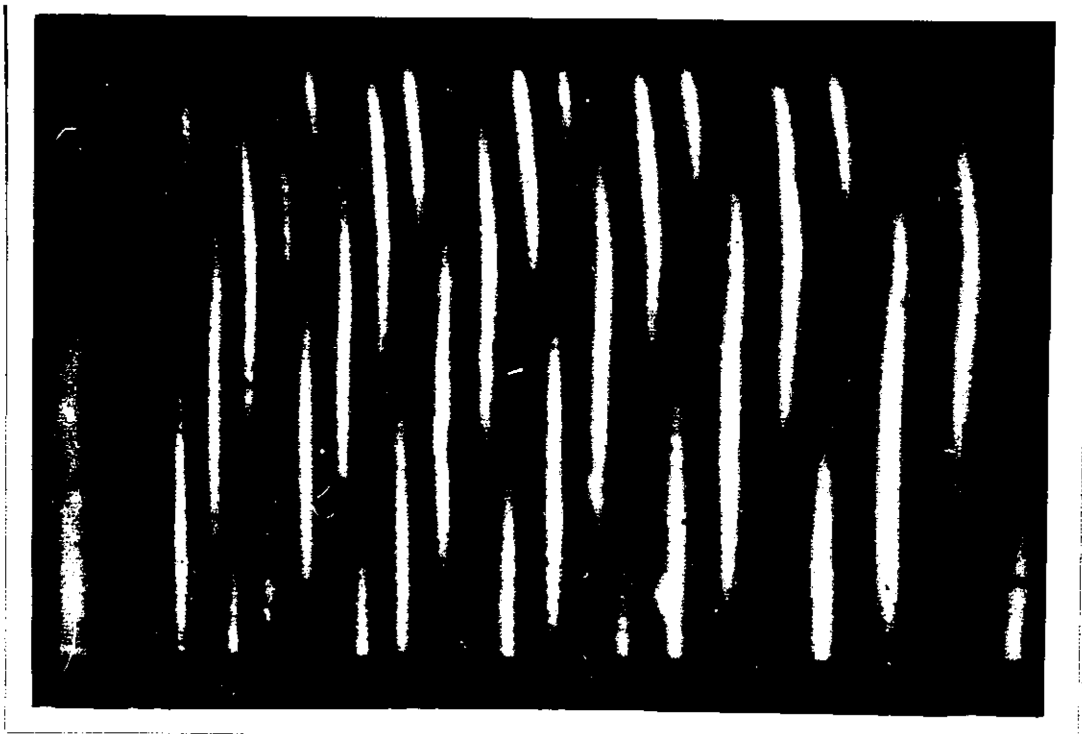

(A) Moiré pattern of subtracted contour fringes for a deflected plate.

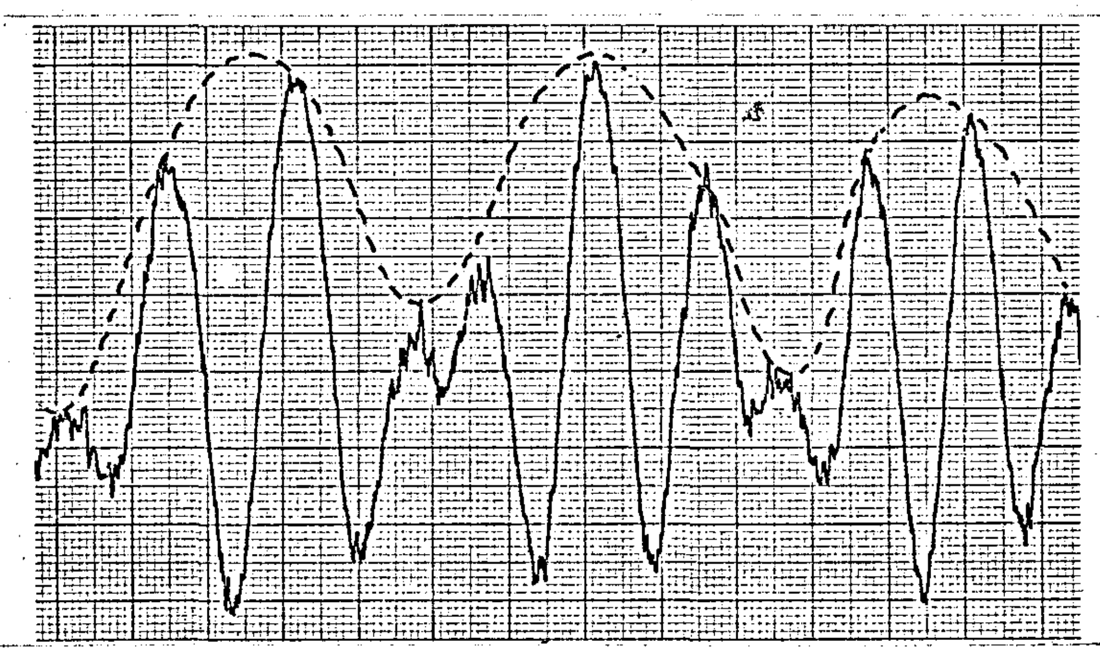

(B) Microdensitometer trace of fringe intensity.

FIG. 22. MOIRÉ FRINGE SUBTRACTION.

(CONTOUR FREQUENCY TO MOIRÉ FRINGE FREQUENCY RATIO ÷ 2.5:1)

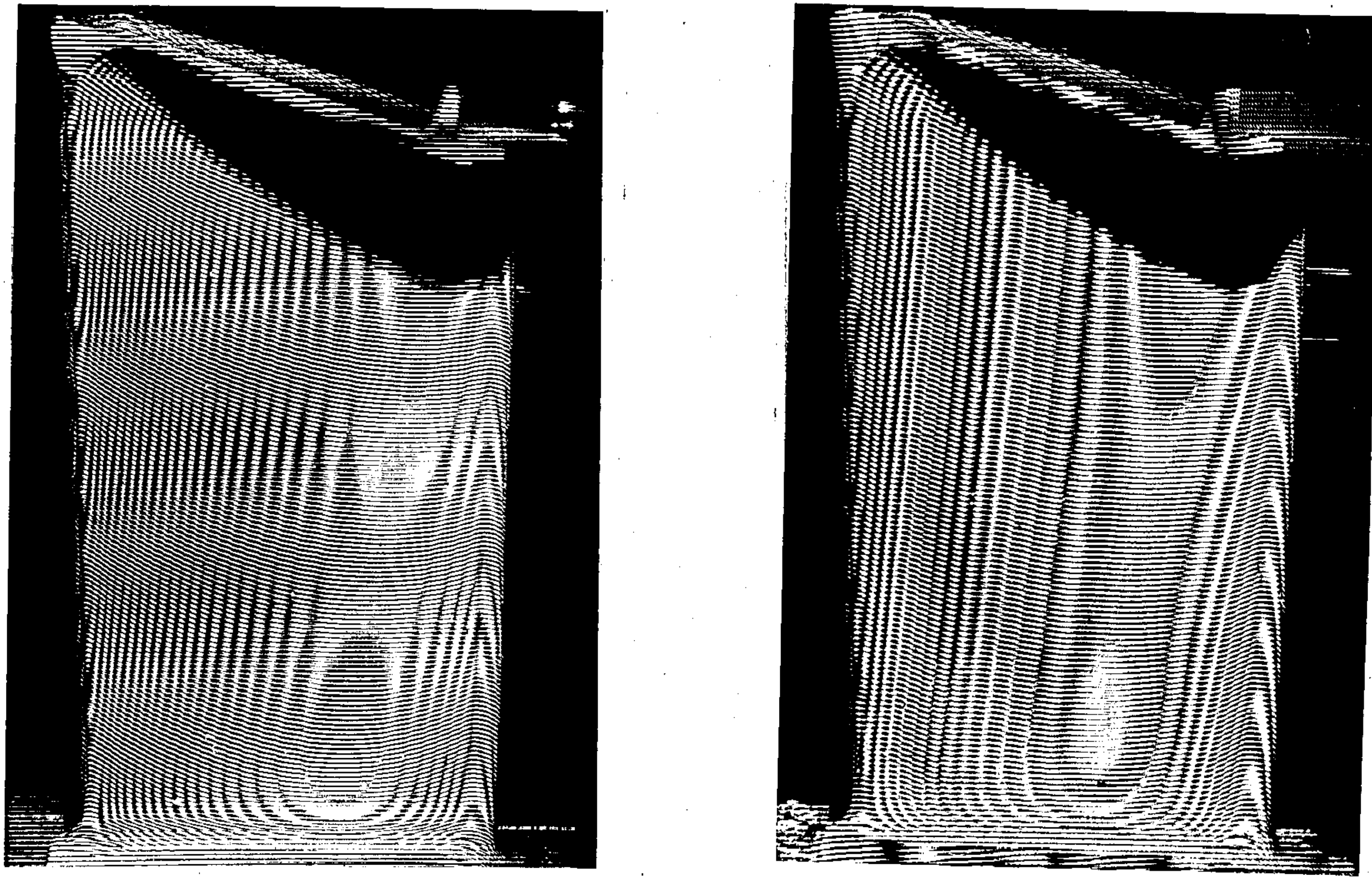

(a) BLADE BENDING (b) BLADE TWIST

FIG. 23. MOIRÉ FRINGE DIFFERENCES FOR A DEFLECTED TURBINE BLADE.

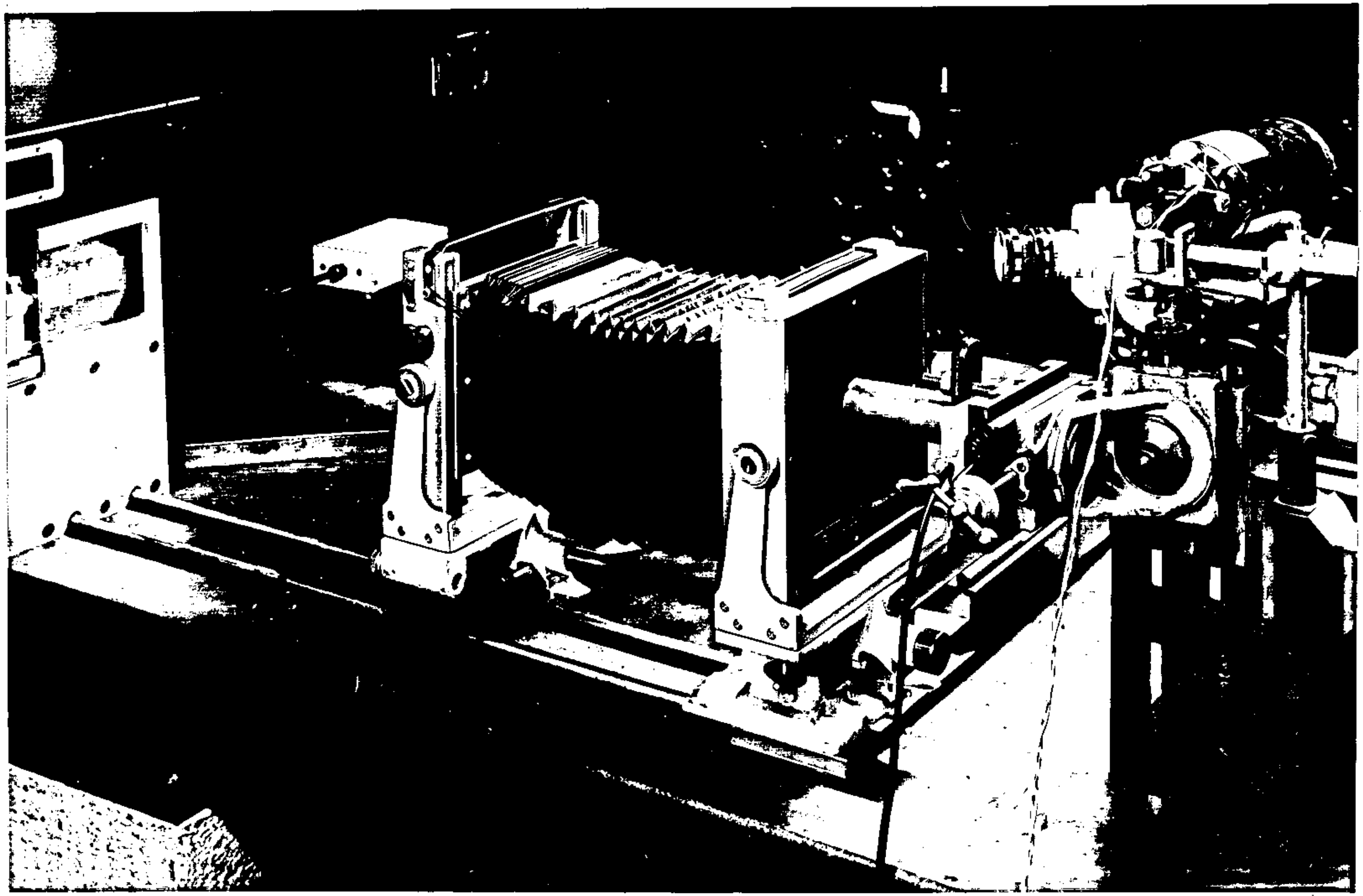

FIG. 24. MECHANICAL PHOTOMULTIPLIER SCANNING UNIT FOR MOIRÉ CONTOURING.

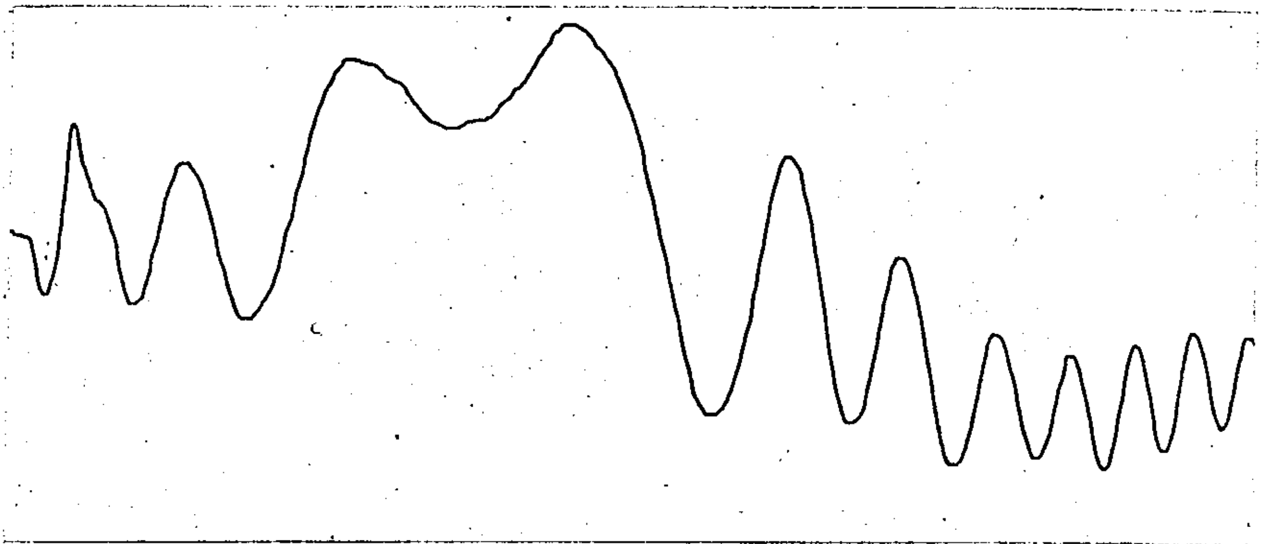

(A) With low pass filtering.

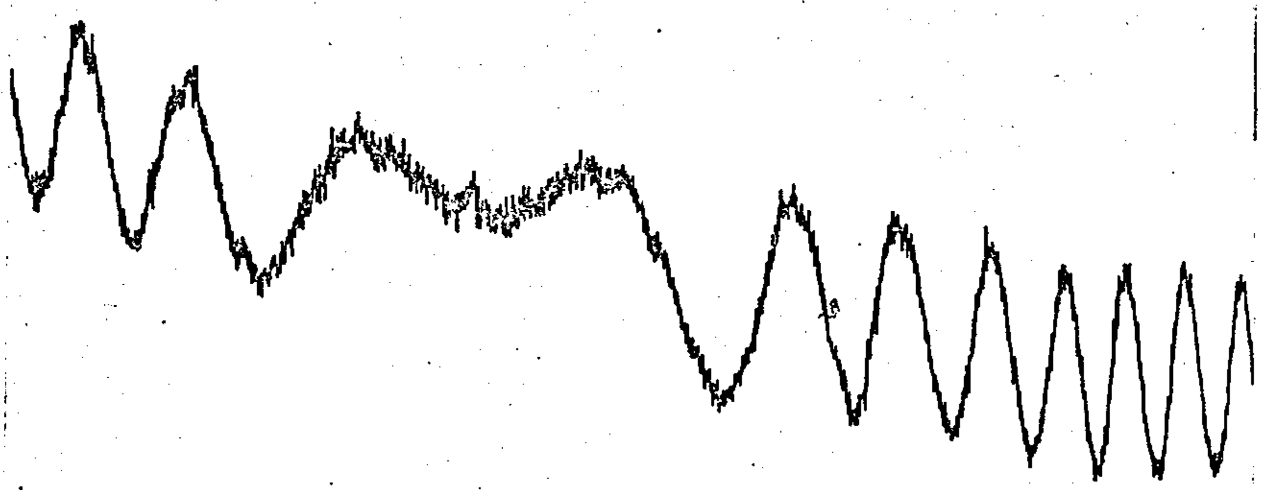

(B) Without filtering.

FIG. 25. THE USE OF LOW PASS ELECTRONIC FILTERING TO ELIMINATE NOISE ON THE CONTOURING SIGNAL.

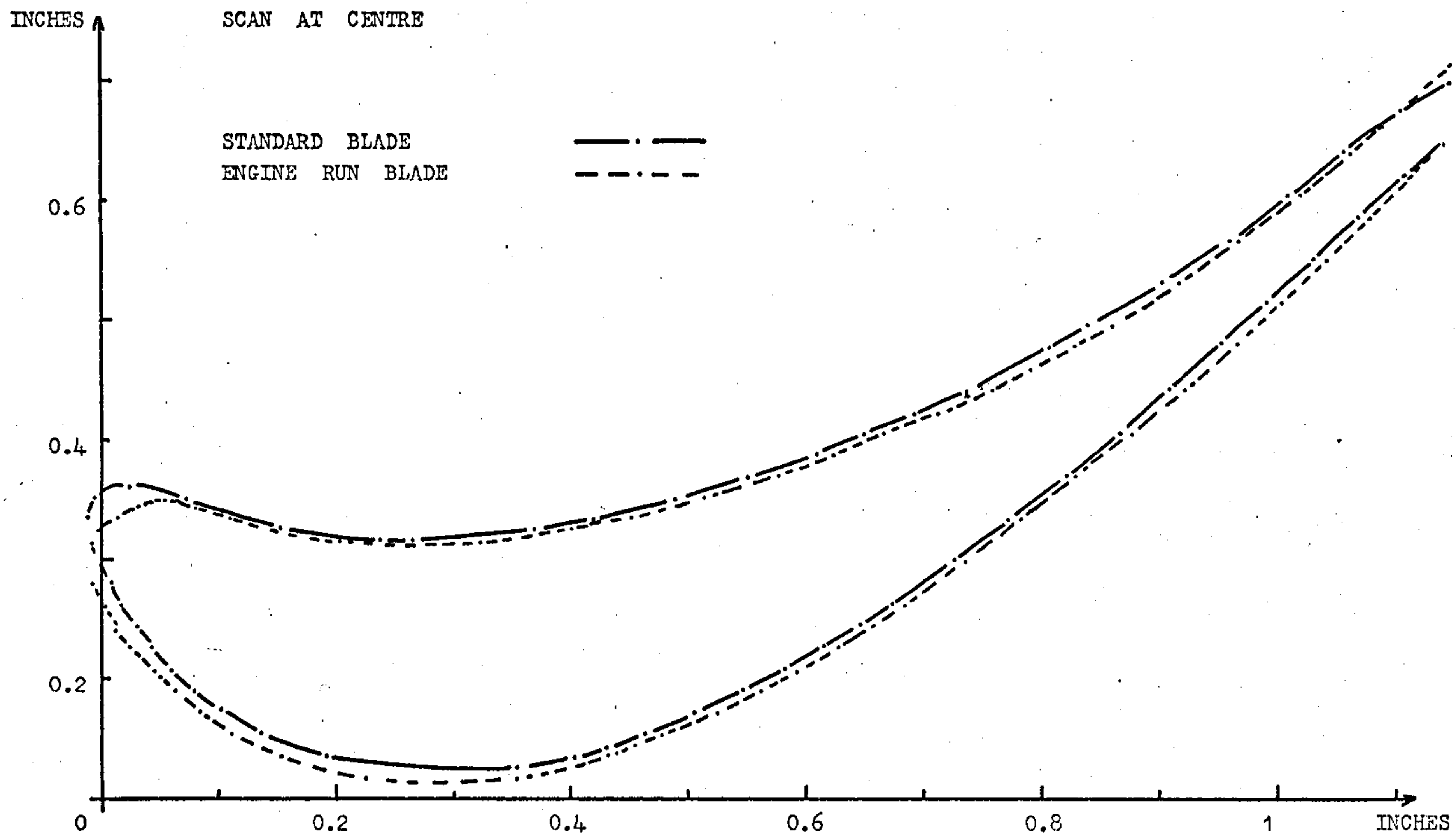

FIG. 26. BLADE COMPARISON BEFORE AND AFTER ENGINE RUNS (CENTRE).

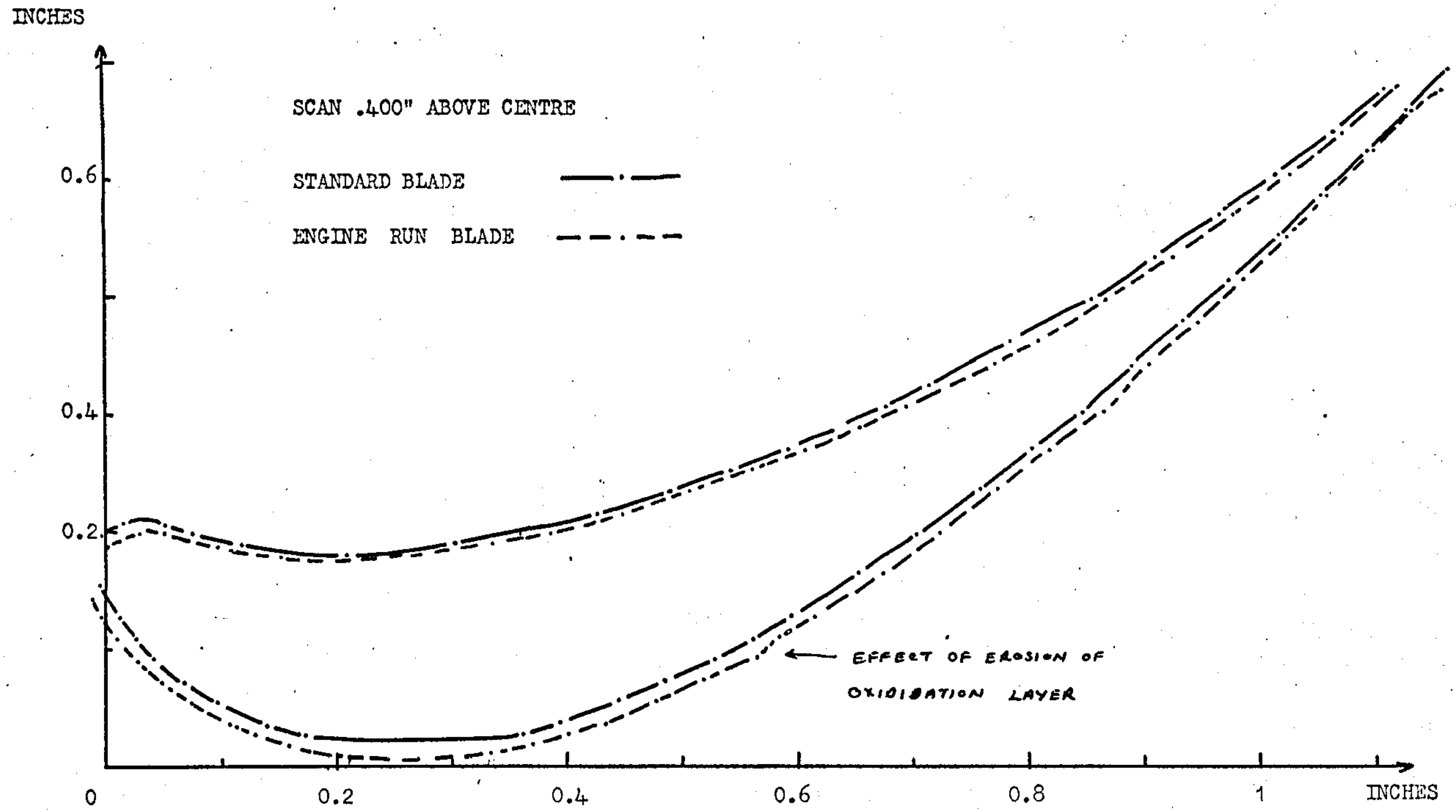

FIG. 27. BLADE COMPARISON BEFORE AND AFTER ENGINE RUNS (ABOVE CENTRE).

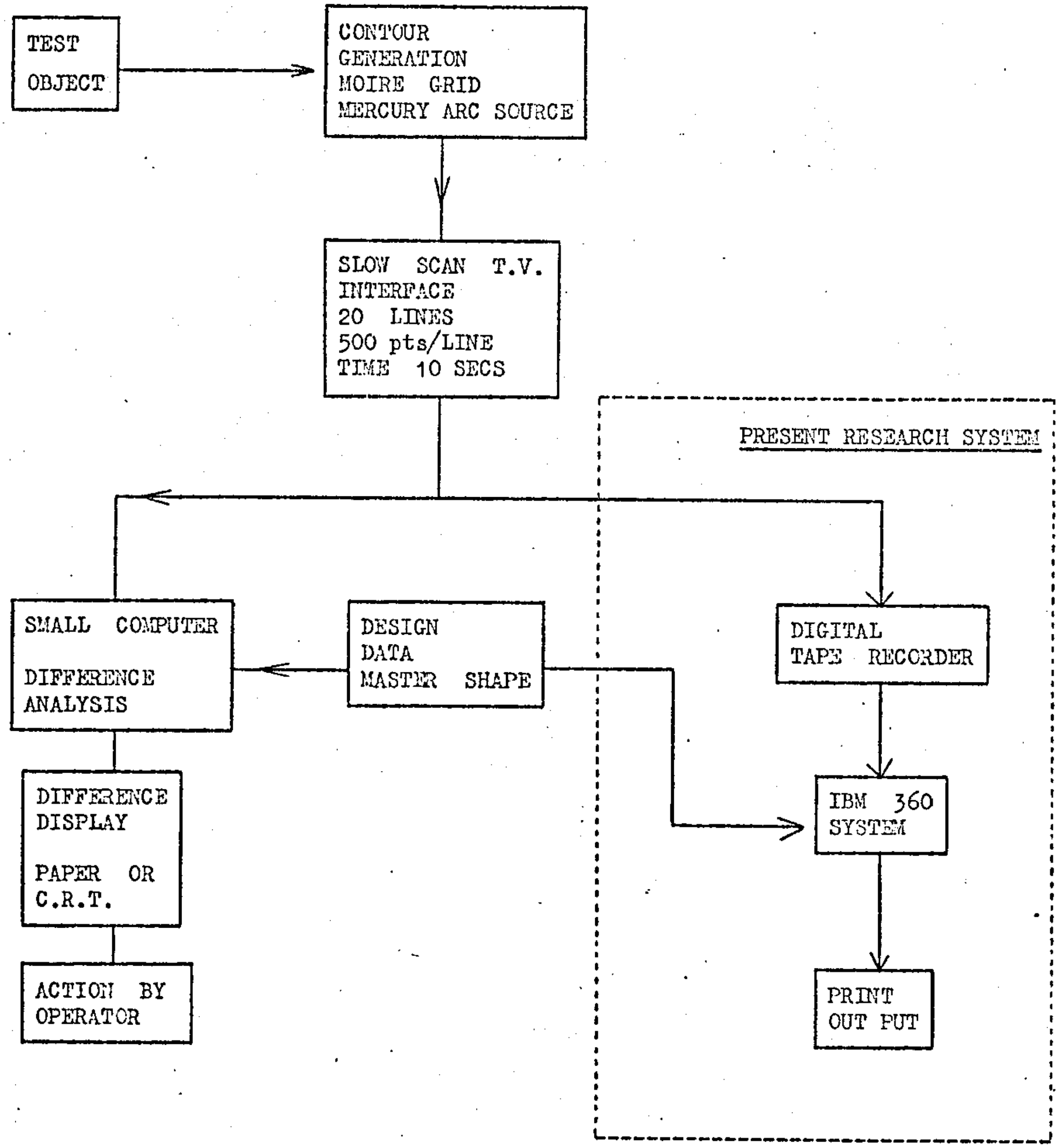

FIG. 28. BLOCK DIAGRAM OF THE OVERALL DIMENSIONAL INSPECTION SYSTEM.

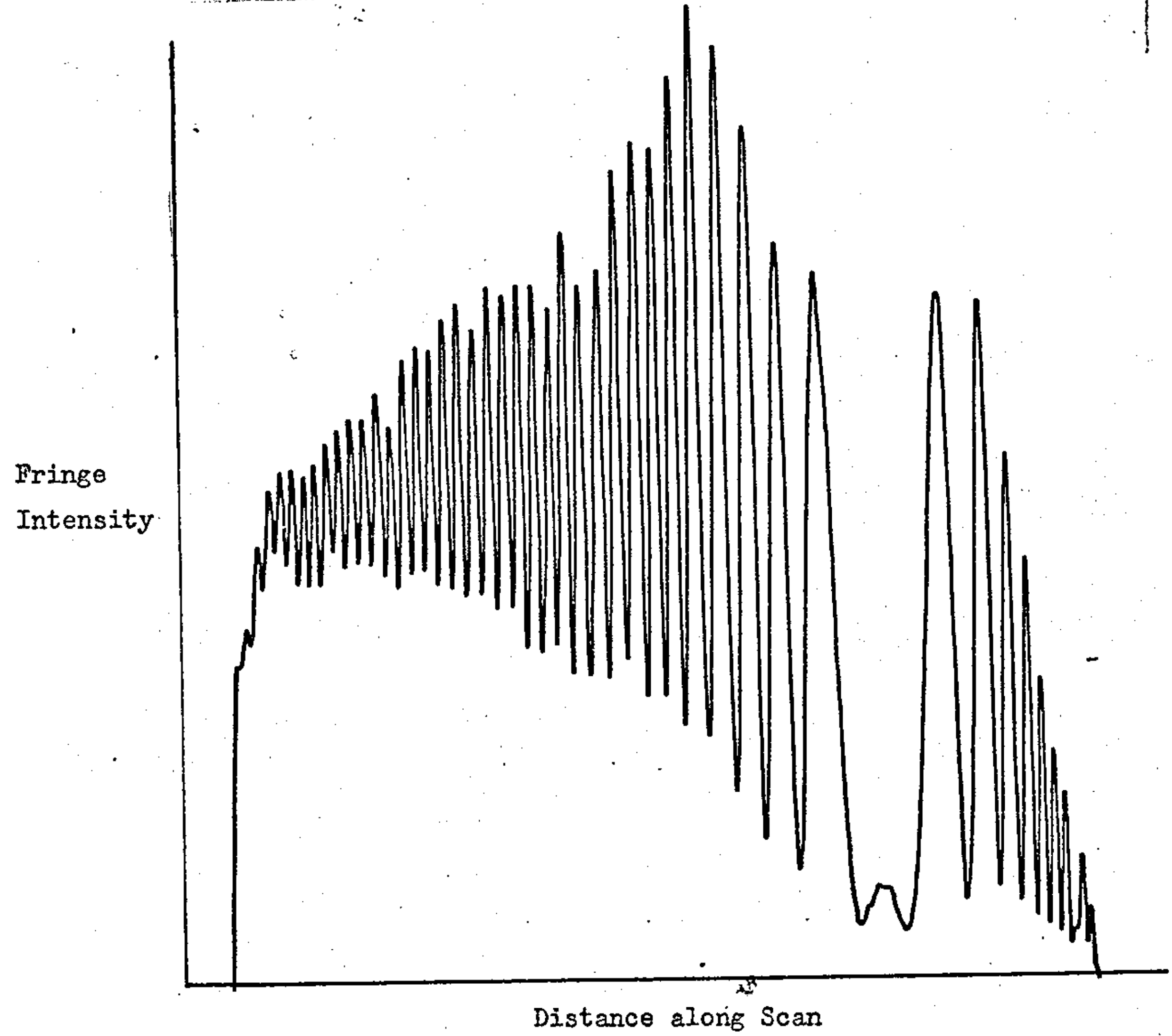

a) Intensity scan across a contoured image of the blade. (Contour interval = 0.016")

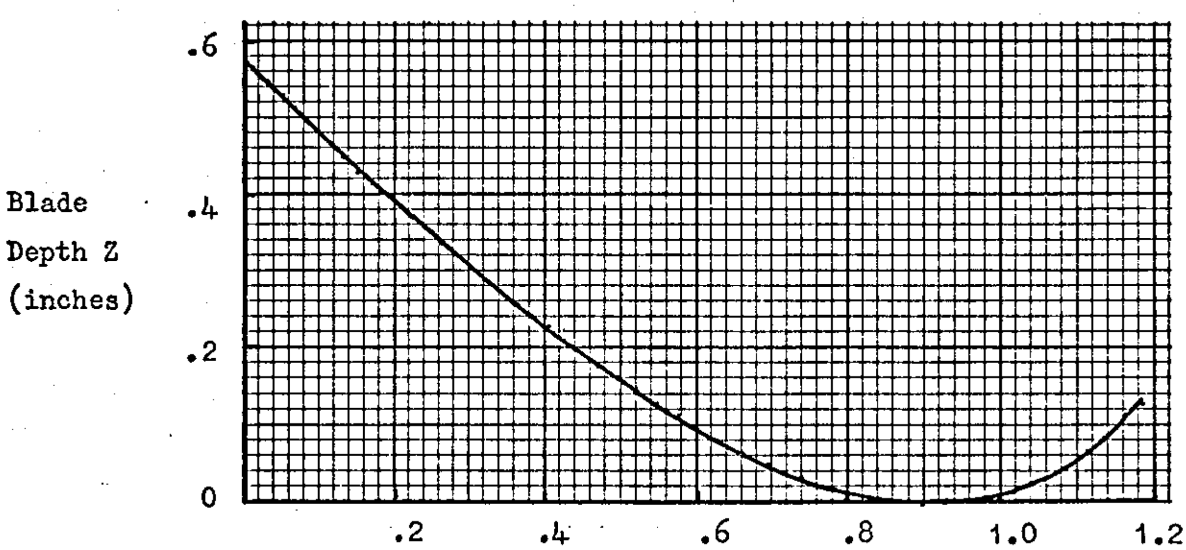

b) Blade shape.

FIG. 29. SHAPE OF THE CONVEX SURFACE OF A TURBINE BLADE CALCULATED FROM THE CONTOUR FRINGES.

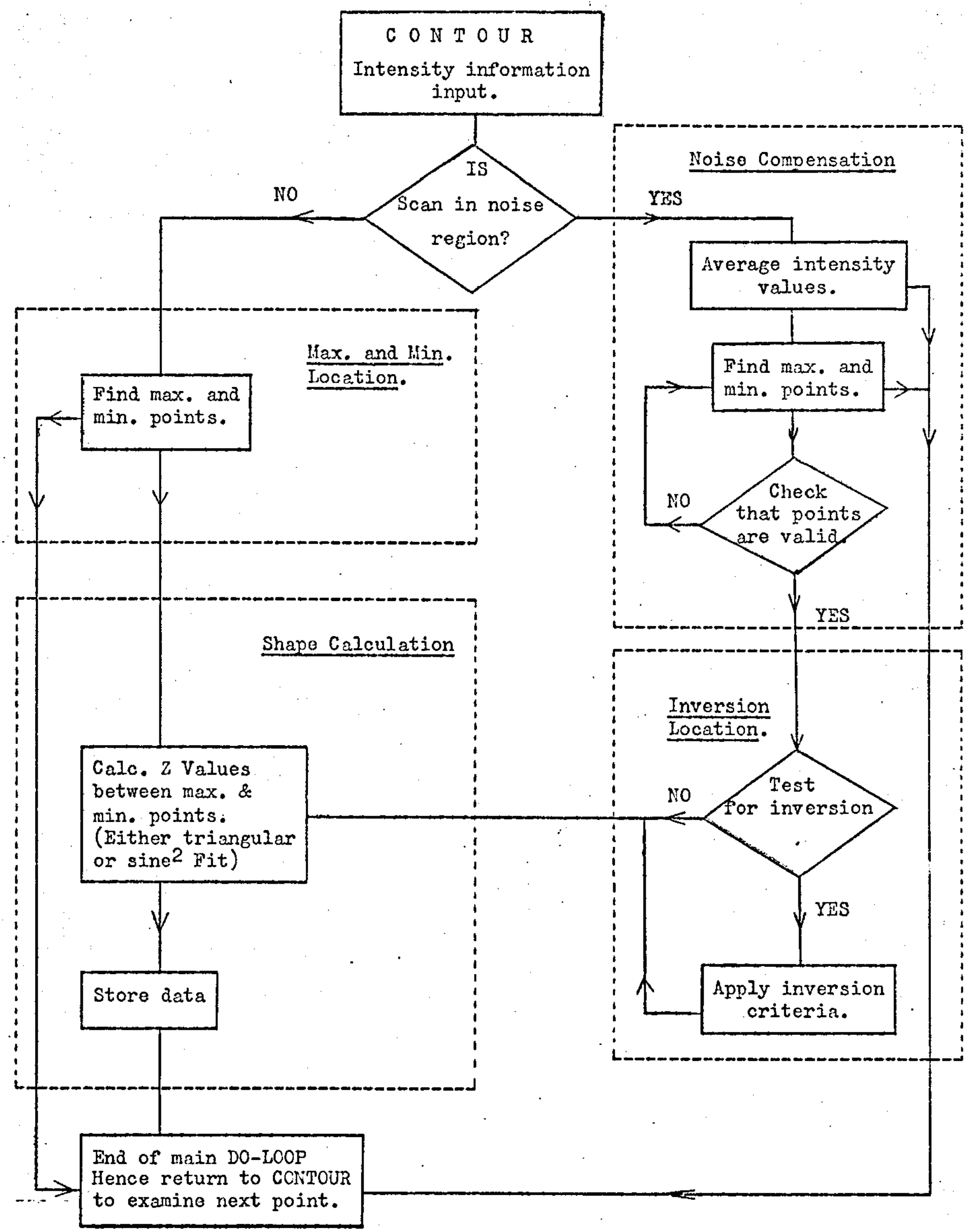

FIG. 30. BLOCK DIAGRAM OF SHAPE GENERATION COMPUTER PROGRAMME.

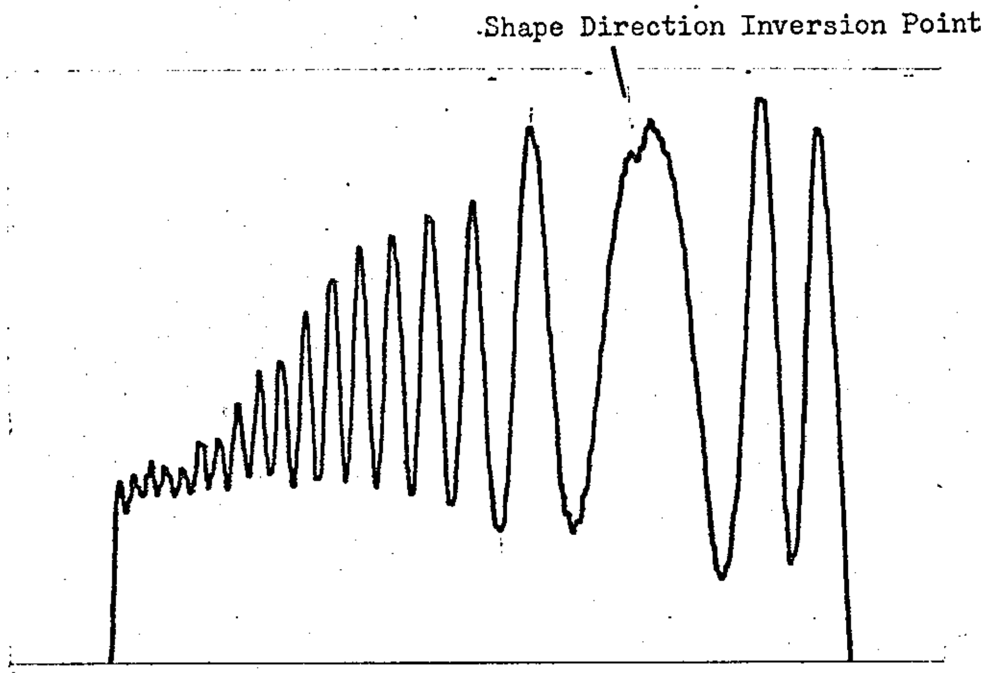

(A) Scan concave surface.

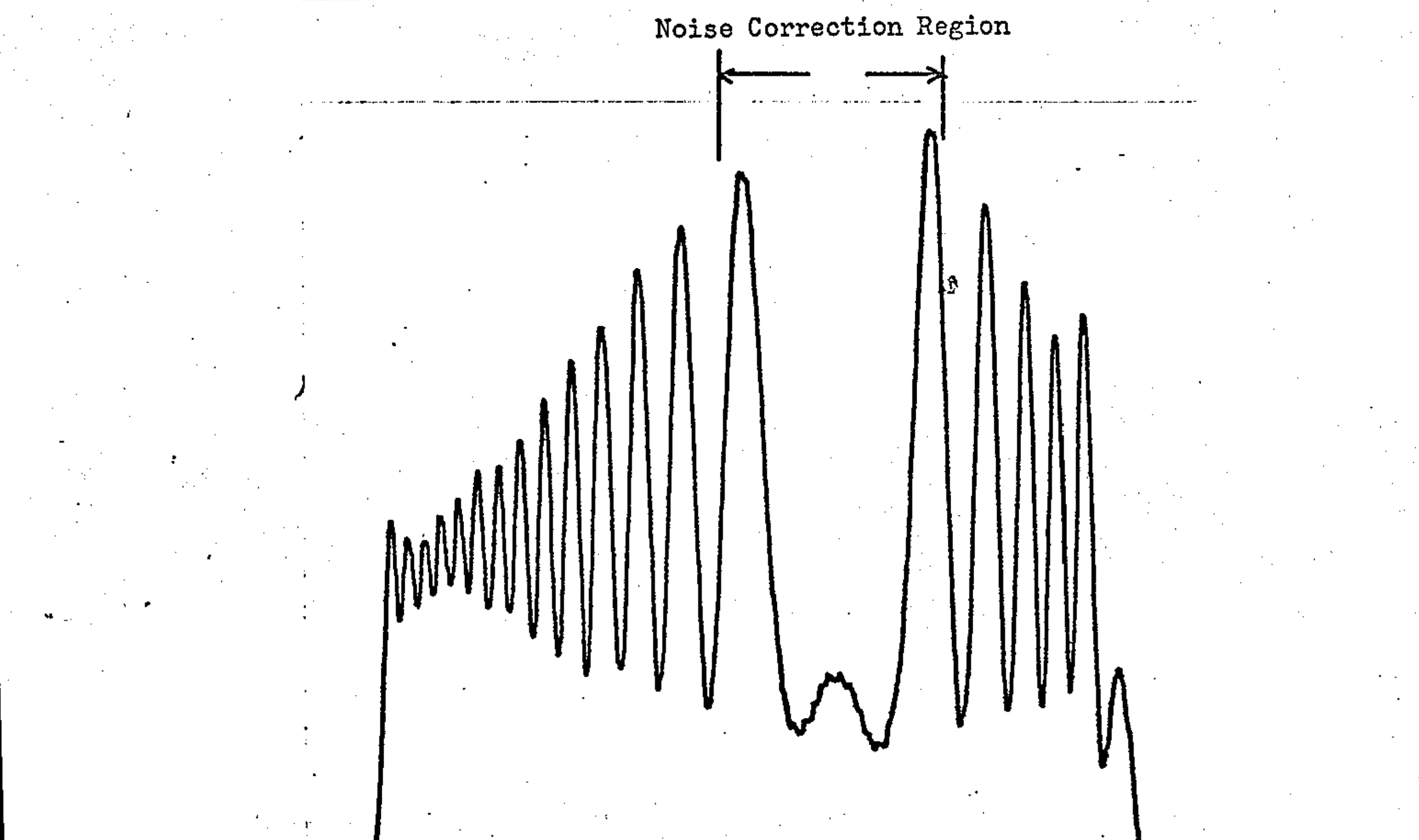

(B) Scan with subfringe effect.

FIG. 31. TYPICAL TURBINE BLADE SCANS USED FOR COMPUTER ANALYSIS.

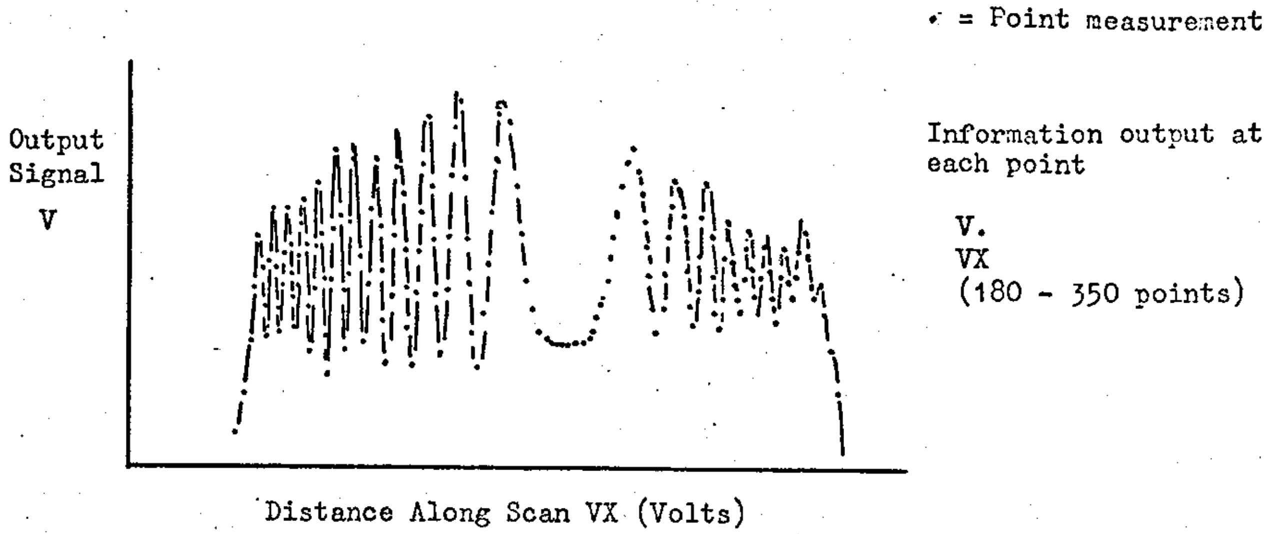

(a) Mechanical Scan.

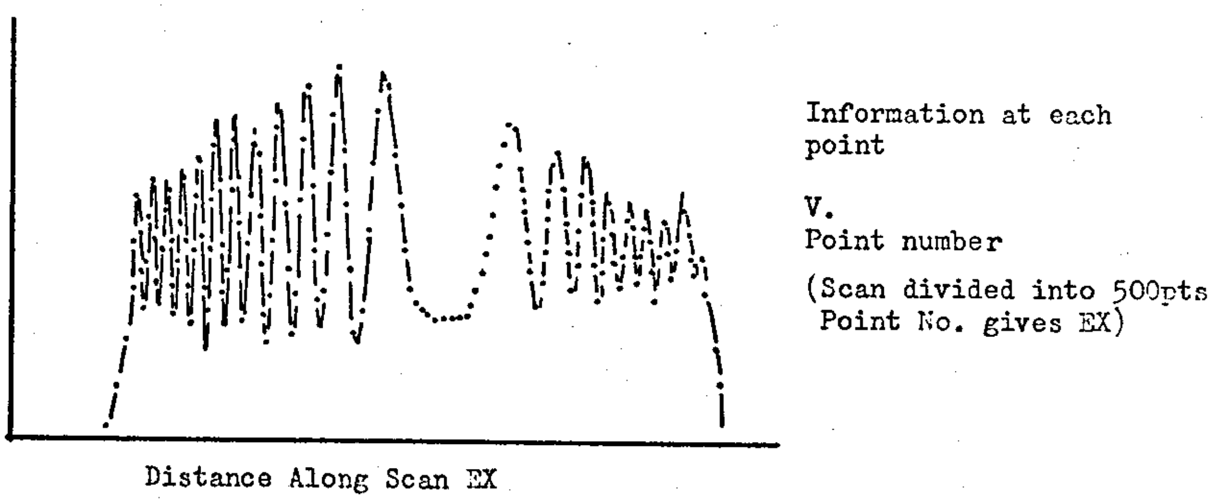

(b) Slow Scan Television.

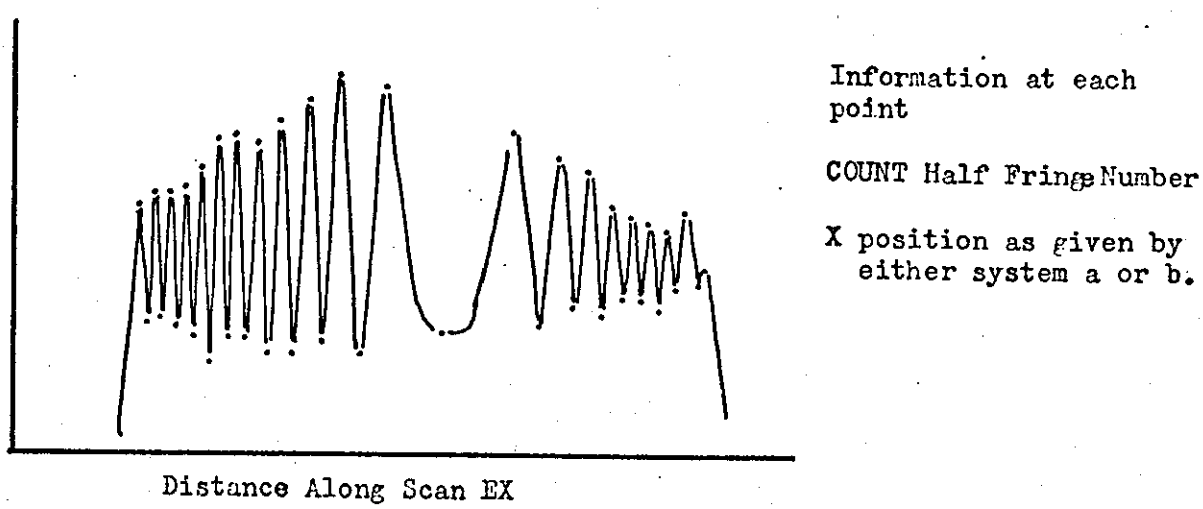

(c) Maximum and Minimum Point Location.

FIG. 32. AVAILABLE TYPES OF DIGITIZED INFORMATION FROM THE CONTOUR FRINGES.

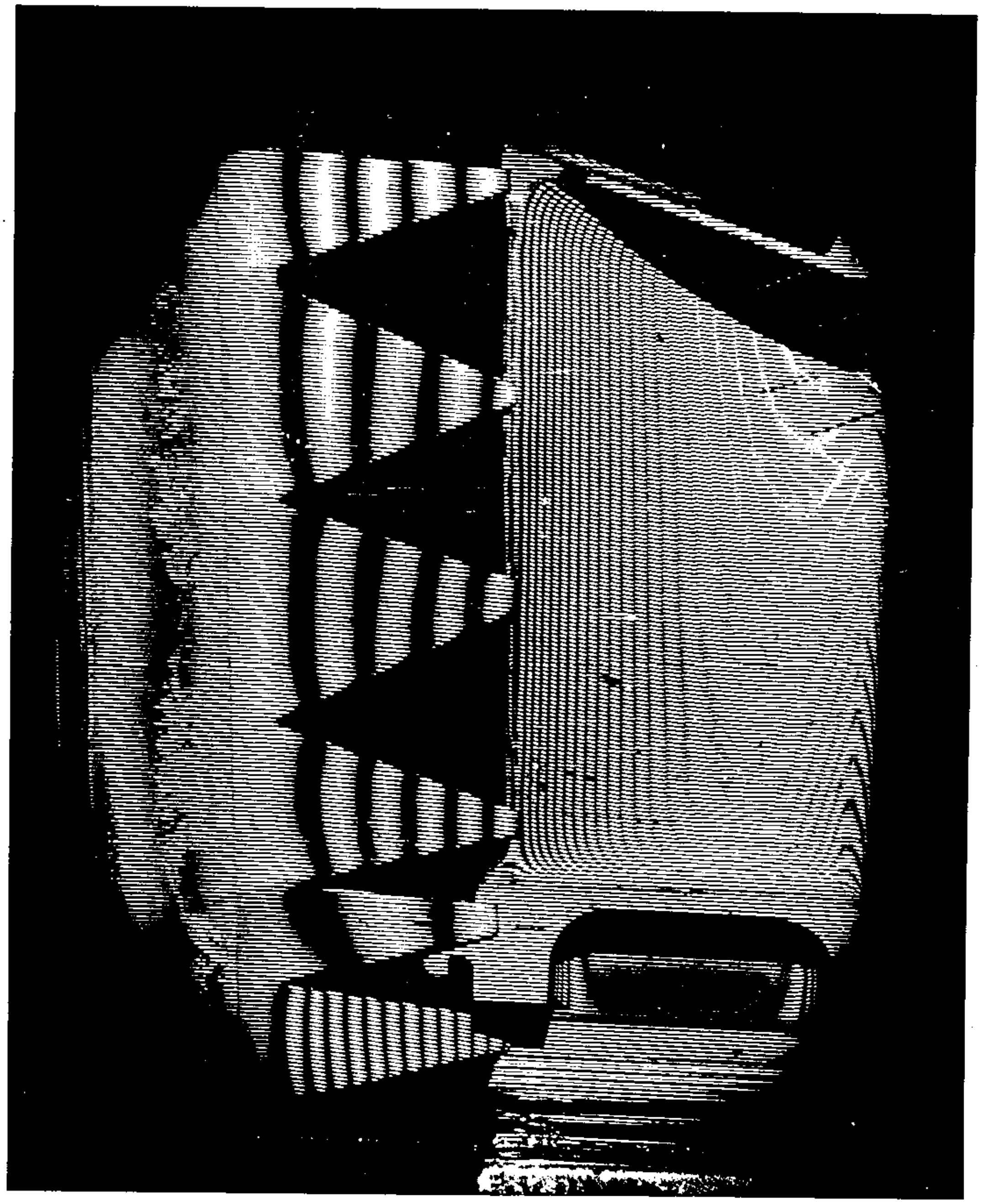

FIG. 33. MECHANICAL REFERENCE PLANE LOCATION FOR VARIOUS PARTS OF THE TURBINE BLADE.

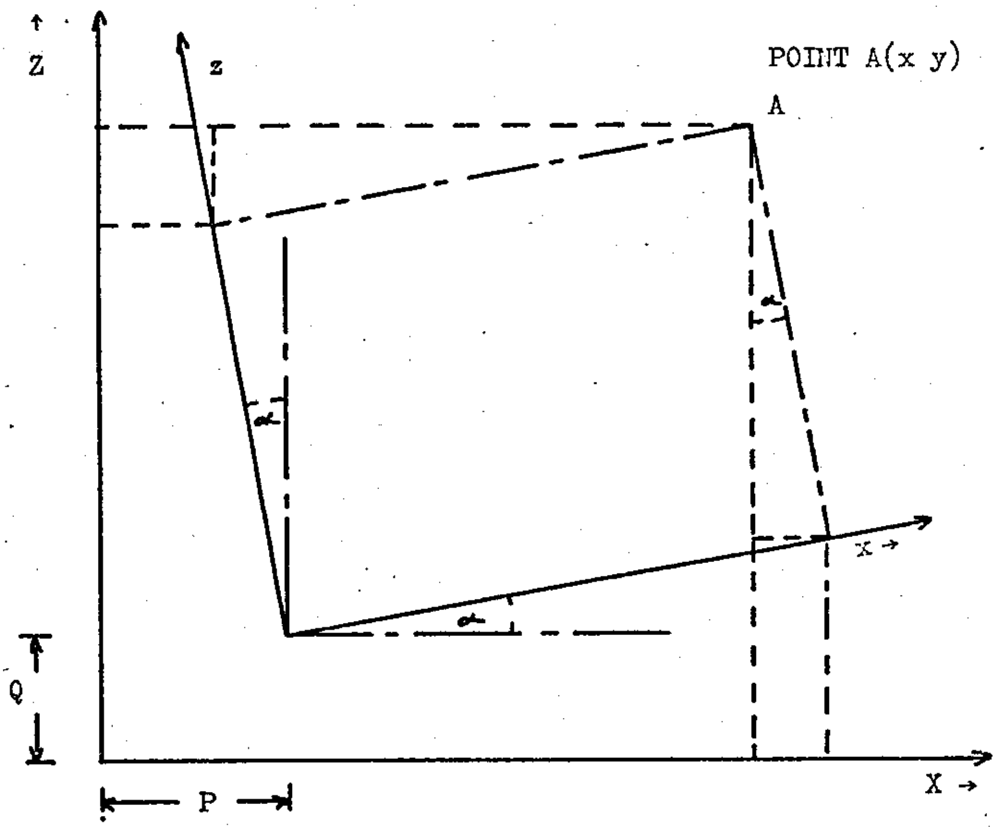

FIG. 34a. CHANGE OF CO-ORDINATE AXES.

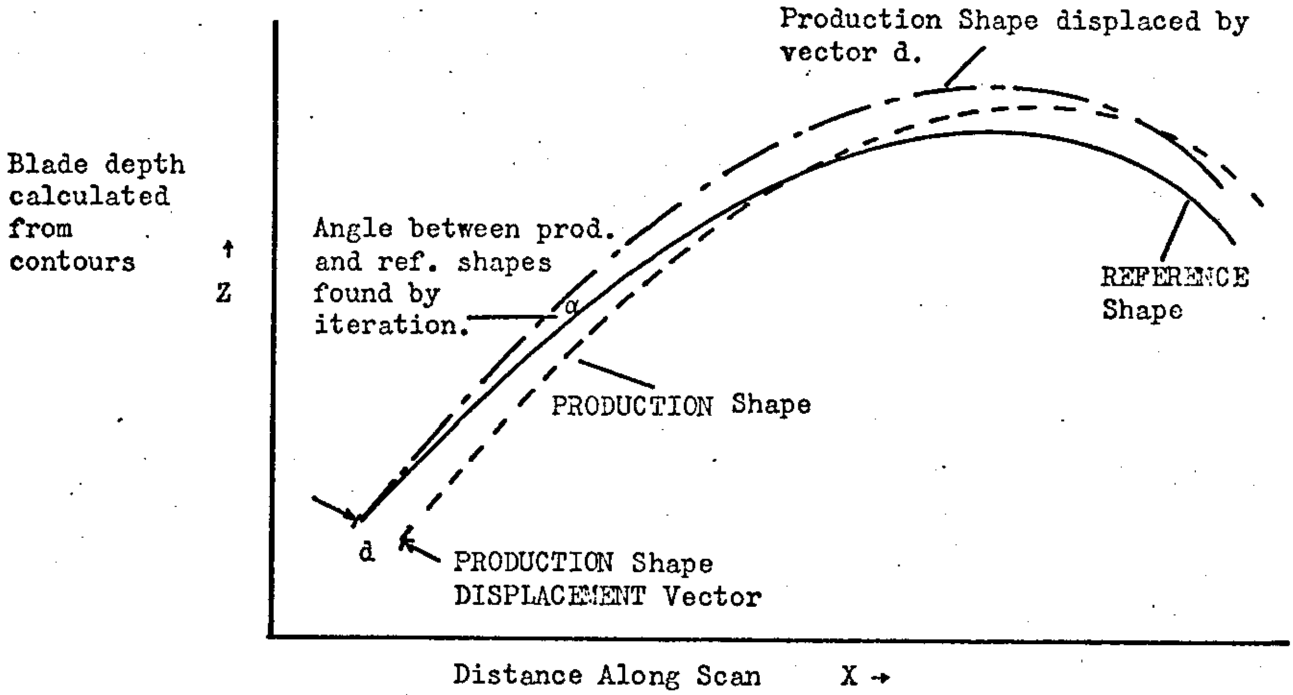

FIG. 34b. BLADE SHAPE FITTING BY ITERATION.

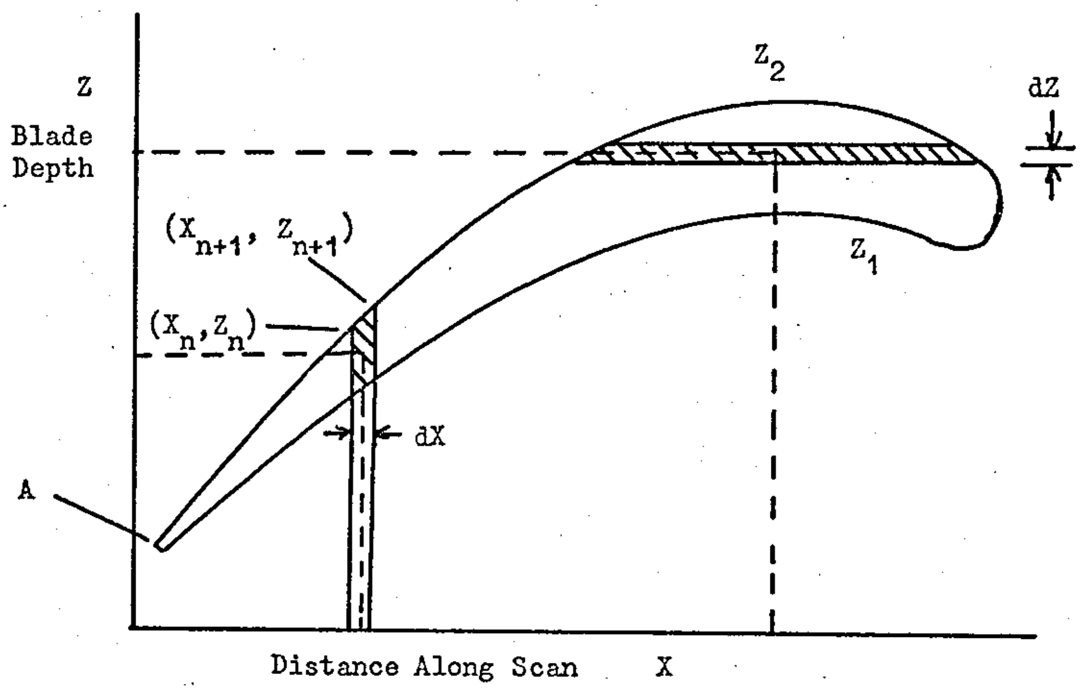

FIG. 35(a). MOMENTS OF A BLADE SECTION.

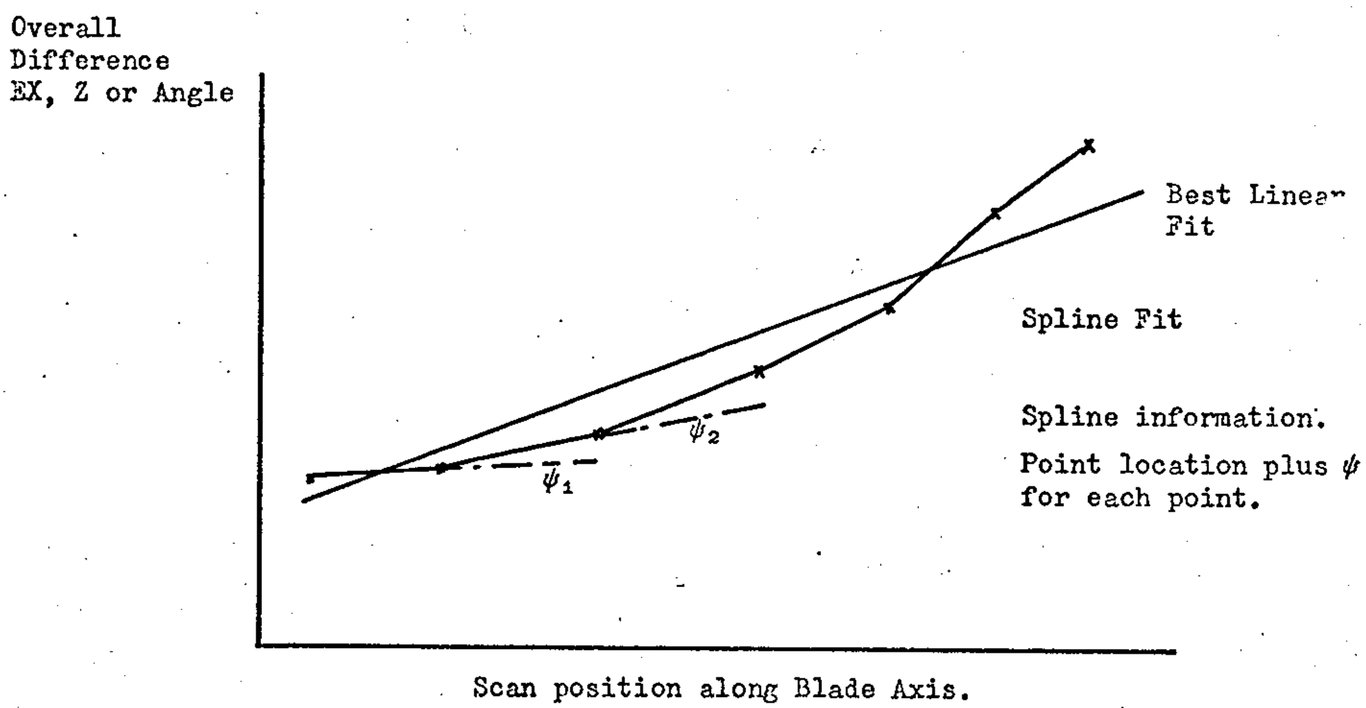

FIG. 35(b). LINEAR AND SPLINE FITS TO DATA.

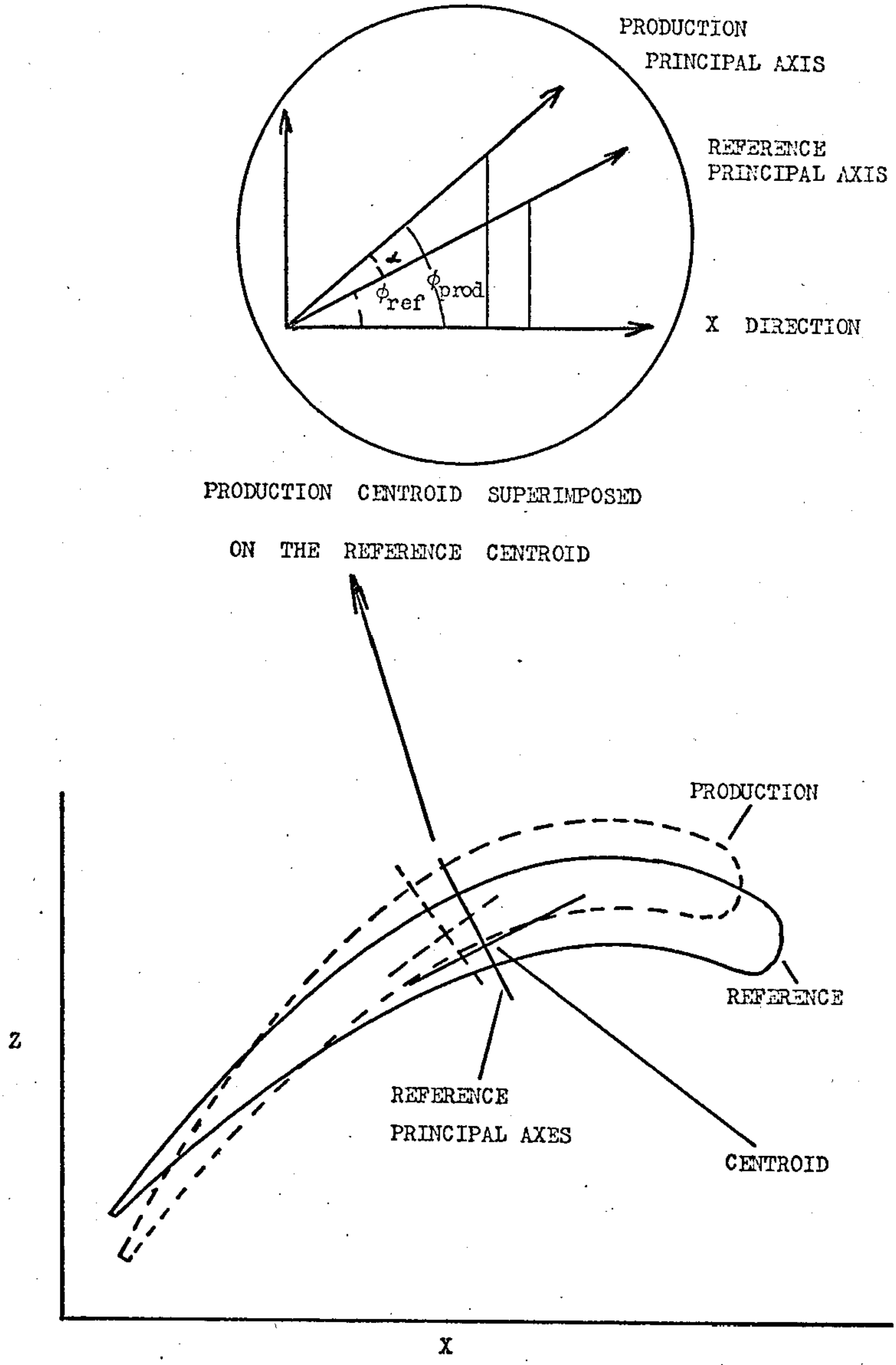

FIG. 36. COMPARISON OF BLADE SECTION CENTROIDS AND PRINCIPAL AXES.

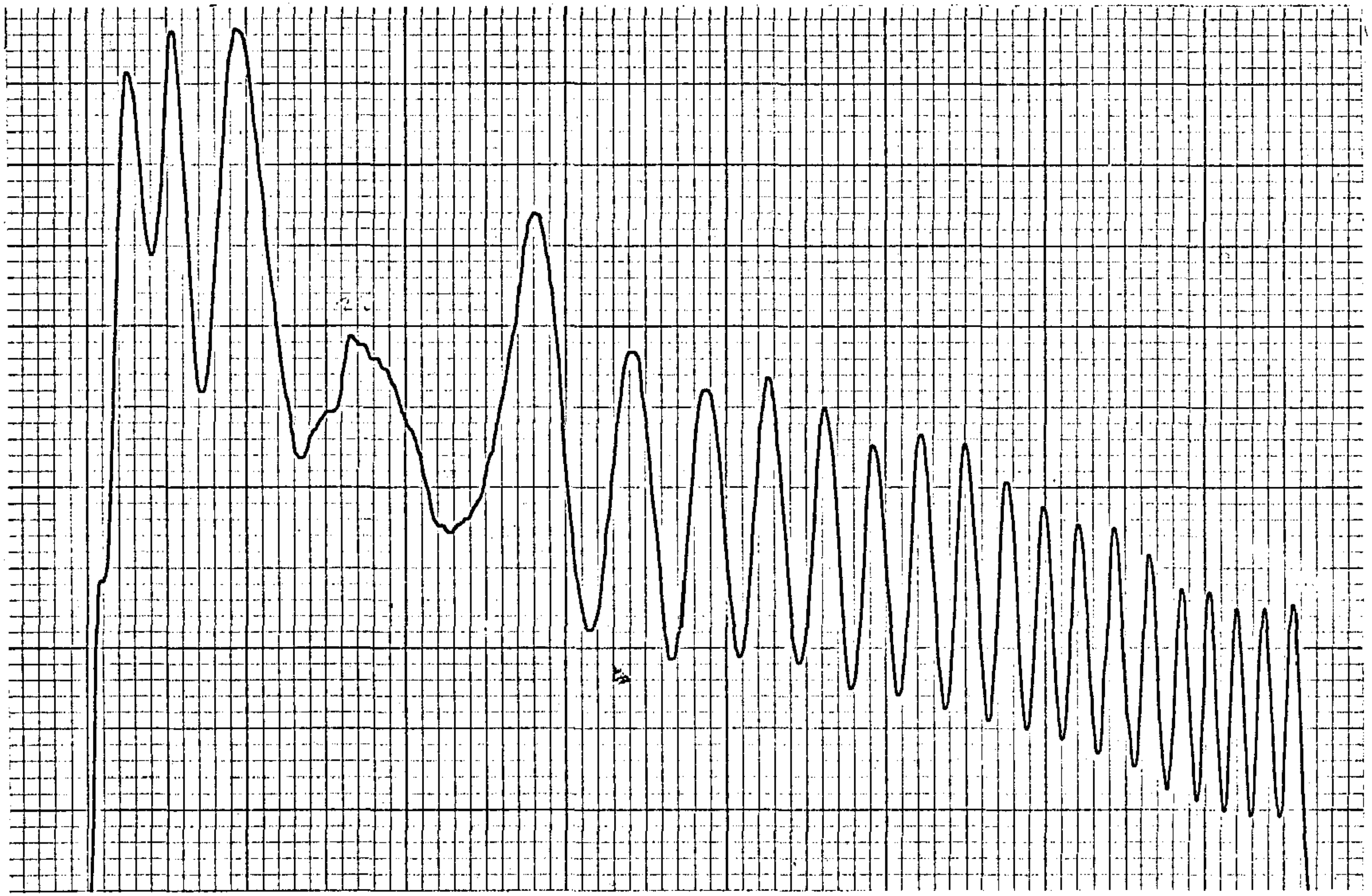

FIG. 37. TYPICAL GOOD QUALITY MOIRE SHADOW CONTOURS ACROSS A TURBINE BLADE. (CONTOUR DEPTH = 0.02")

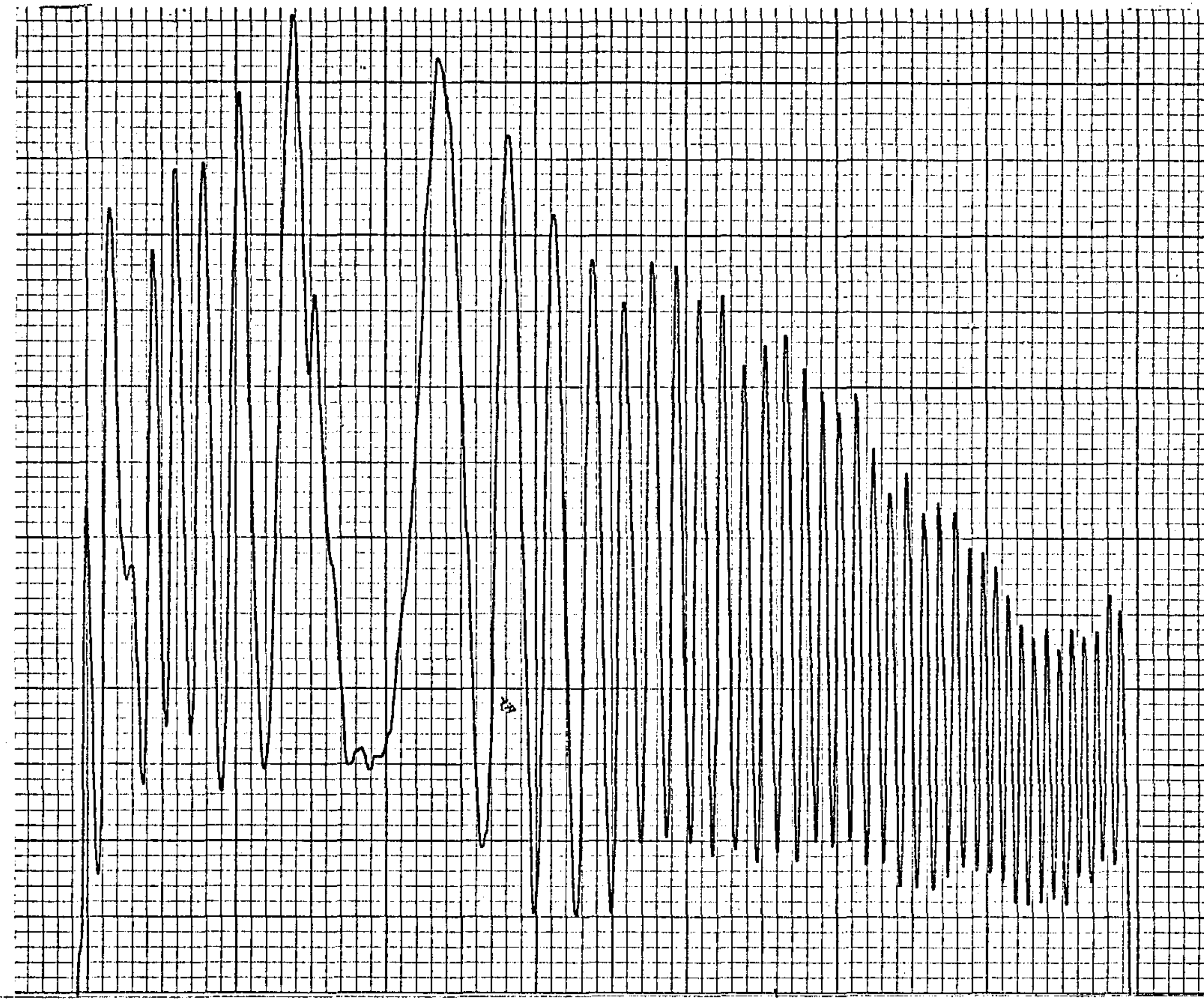

FIG. 38. TYPICAL GOOD QUALITY CONTOUR FRINGES USING THE FRINGE PROJECTION/SCAN TECHNIQUE. (CONTOUR DEPTH INTERVAL = 0.010")

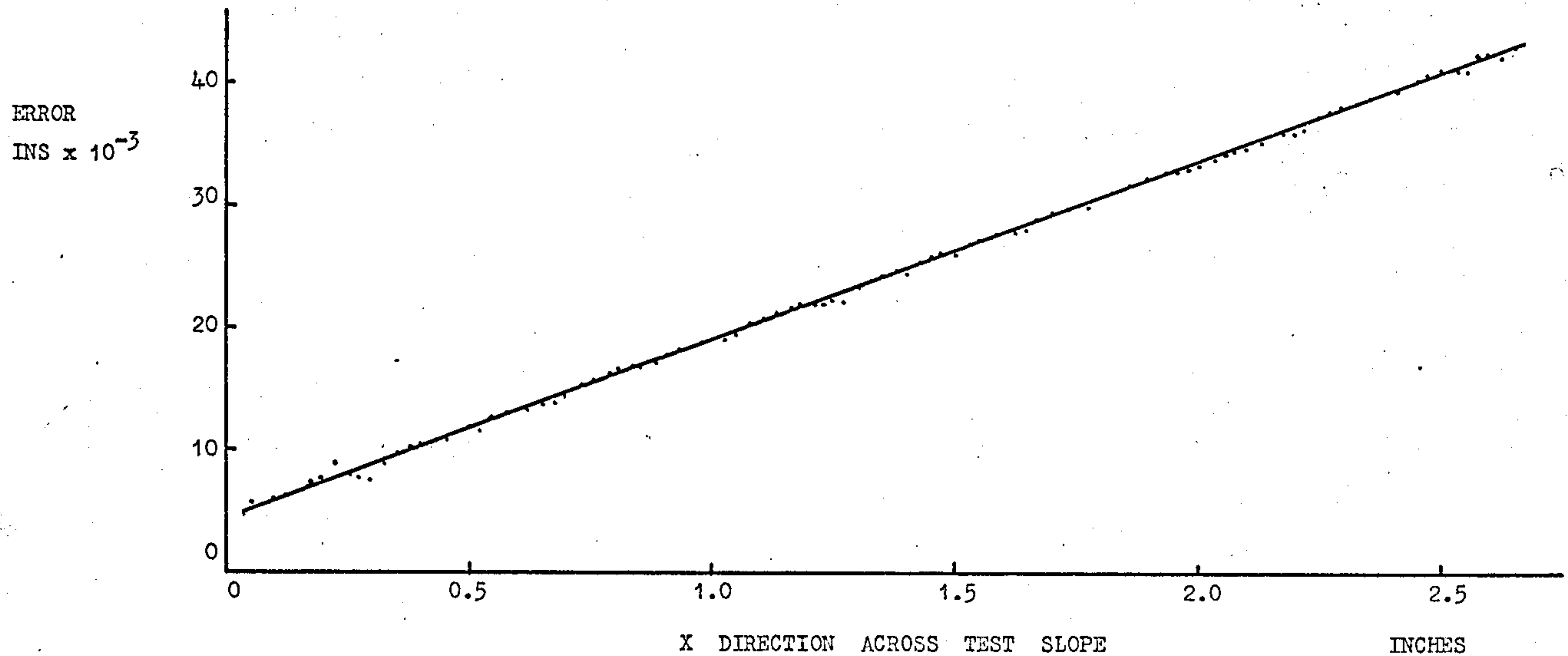

FIG. 39. COMPUTED ERROR PLOT ON A 10° SLOPE. CONTOUR INTERVAL = 0.02".

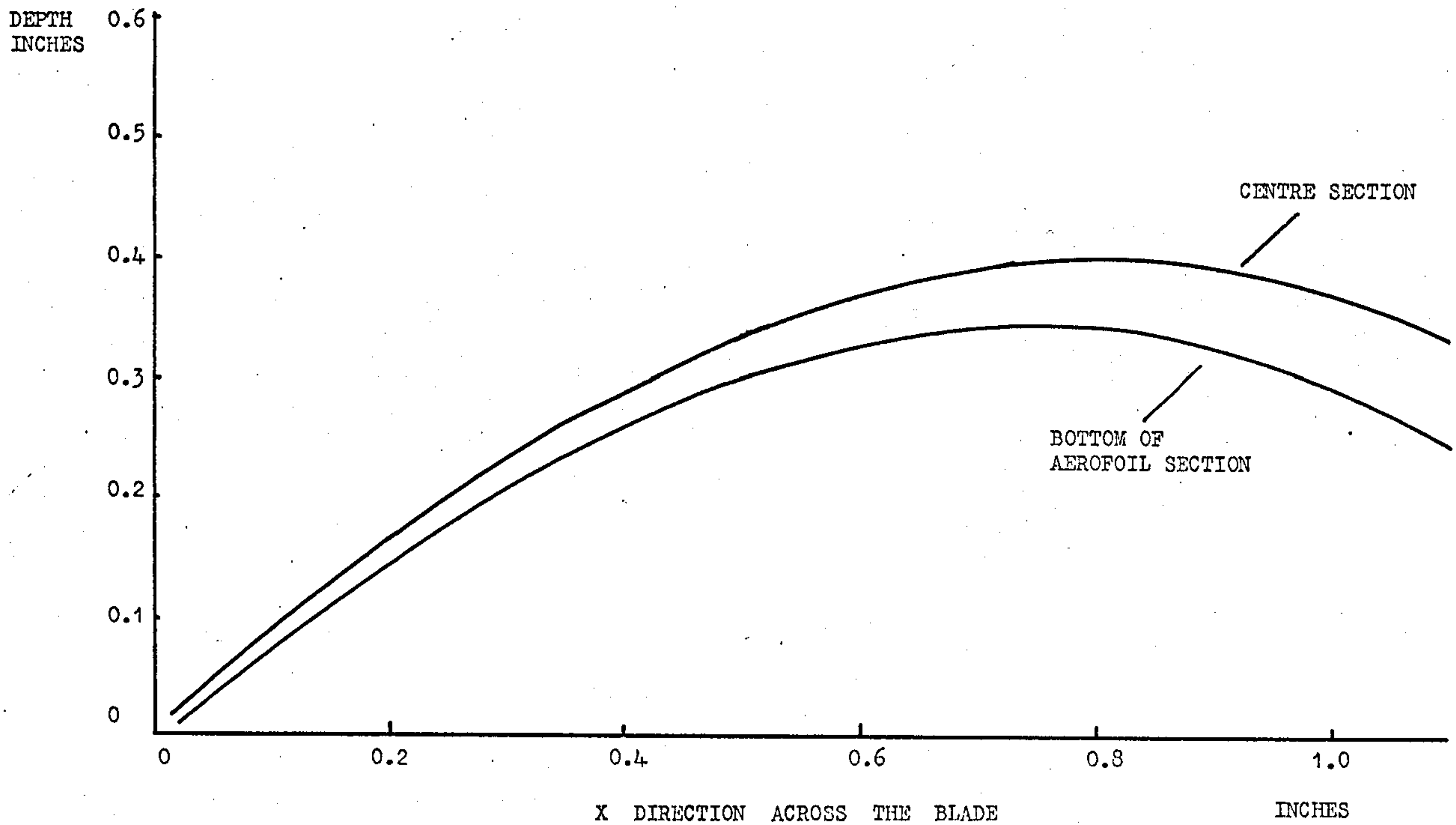

FIG. 40. COMPUTER CALCULATED SHAPE ACROSS TWO SECTIONS OF A BLADE. CONCAVE SURFACE.

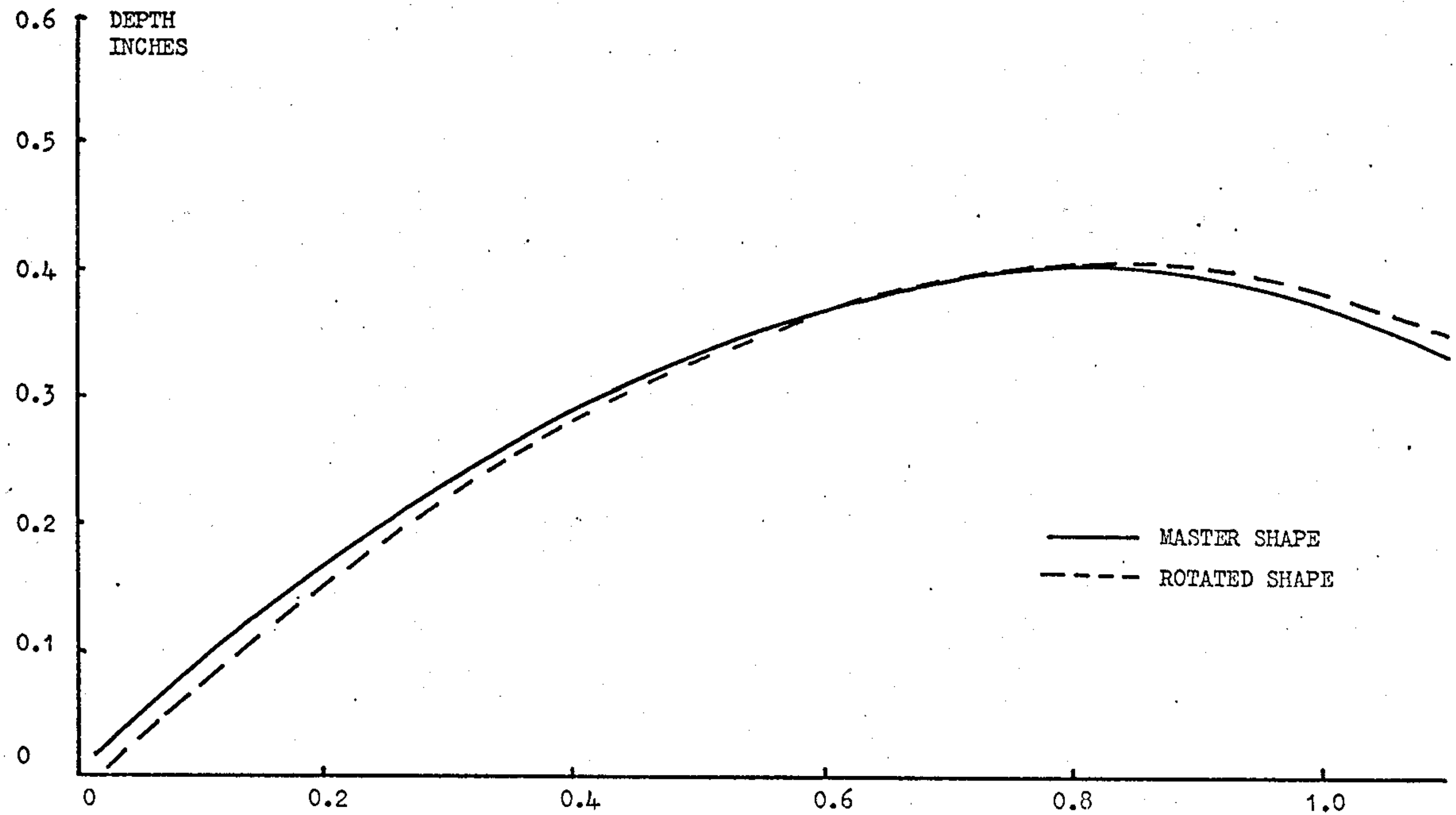

FIG. 41. COMPUTER CALCULATED SHAPES FOR THE MASTER AND ROTATED BLADE CONCAVE SURFACE.

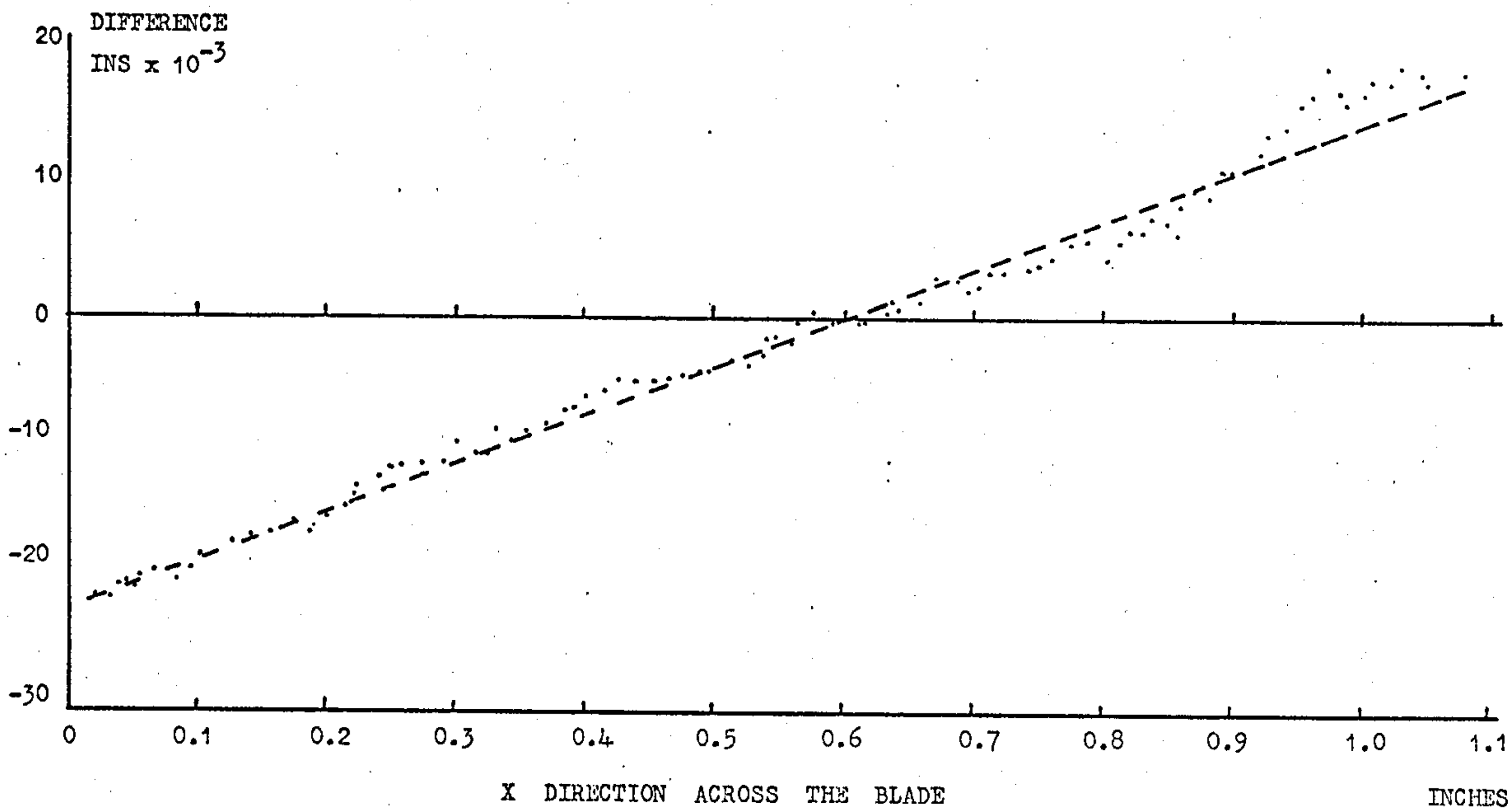

FIG. 42. COMPUTED SHAPE DIFFERENCES MEASURED ALONG THE Z AXIS.

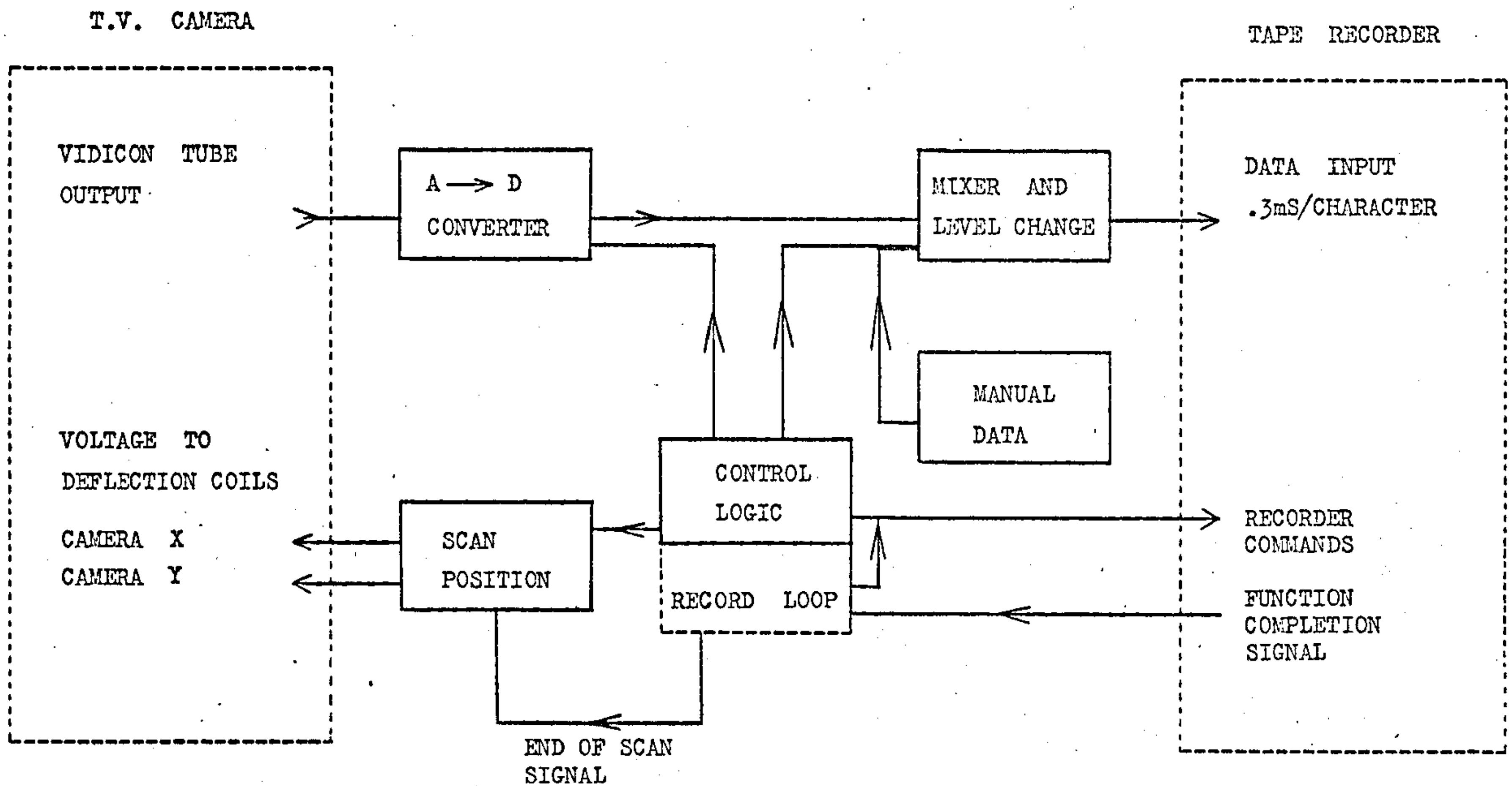

FIG. 43. TELEVISION INTERFACE FUNCTION - BLOCK DIAGRAM

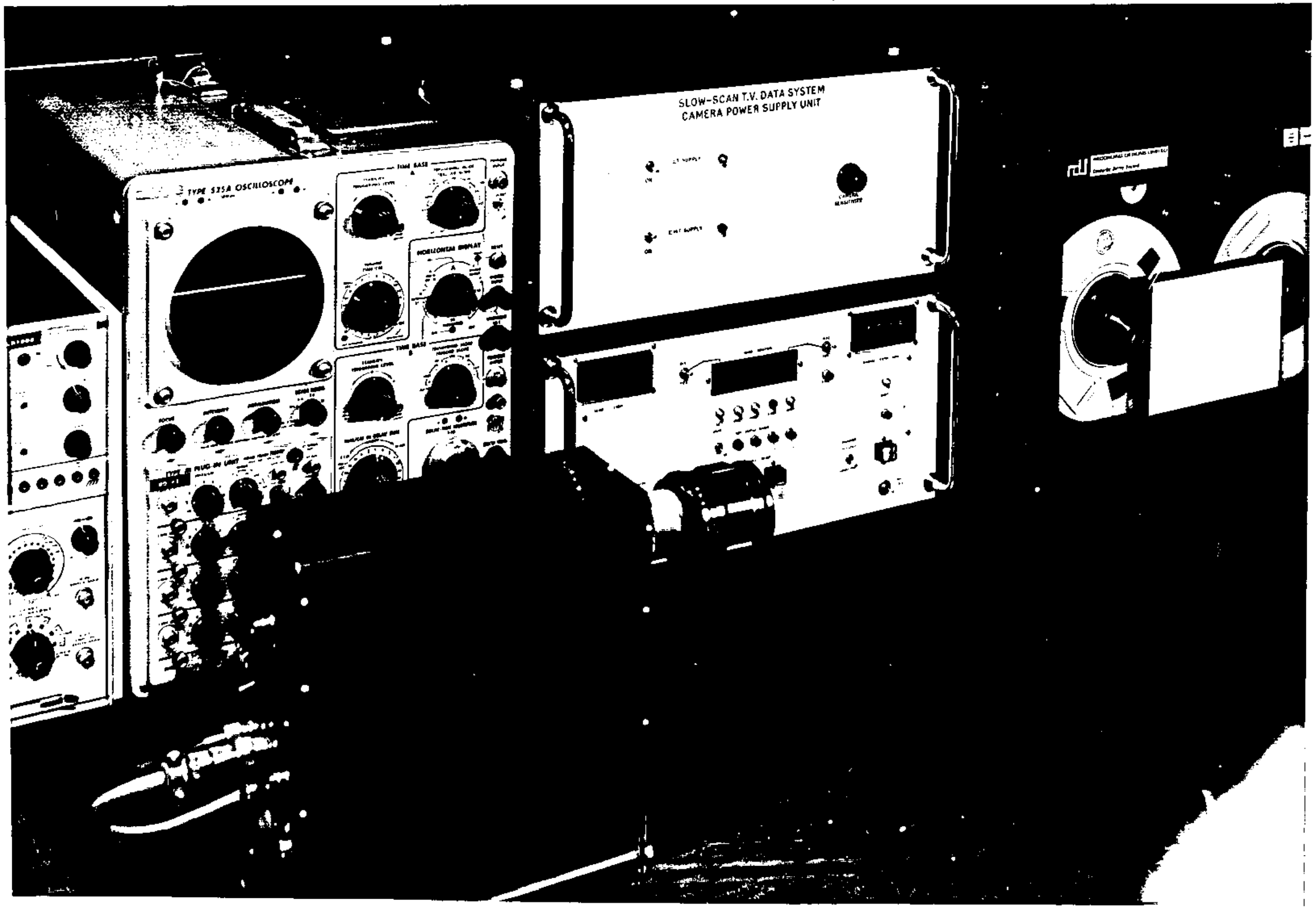

FIG. 44. TELEVISION INTERFACE UNIT FOR MOIRÉ CONTOURING.

Track No.	Allocation for B.C.D.	Beginning of Byte	
5	4^s	X	X
7	1	X	X
3	-	X	X
P	Parity	X	X
2	-	X	X
1	-	X	X
0	-	X	X
6	2^s	X	X
4	8^s	X	X

Tape Width

End of Byte   Tape Length

a) Recording Format.

Track No.	P	0	1	2	3	4	5	6	7	
Hexadecimal Character	1/0	0	0	0	0	B.C.D. Number				
Numerical Character,	1/0	1	1	1	1	B.C.D. Number				
Alphabetic Letters A to I.	1/0	1	1	0	0	Number				

b) Recording Code.

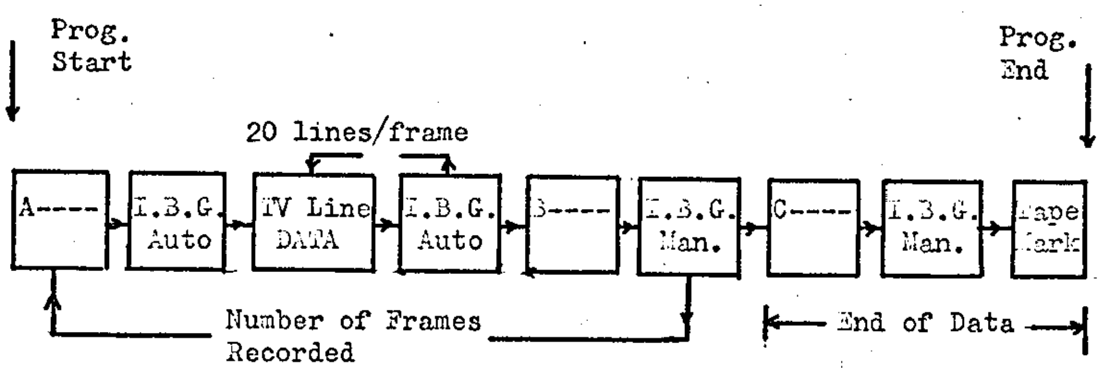

c) Recording Procedure - Block Diagram.

FIG. 45. MAGNETIC TAPE RECORDING FORMATS.

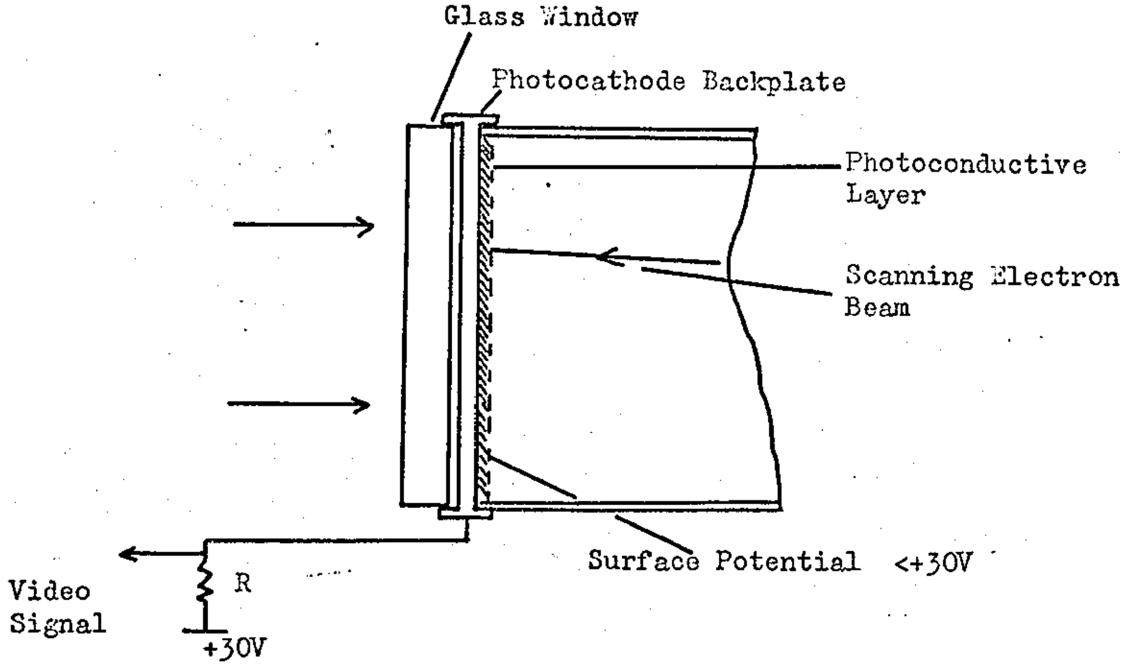

a) Operation of Vidicon at the Photocathode.

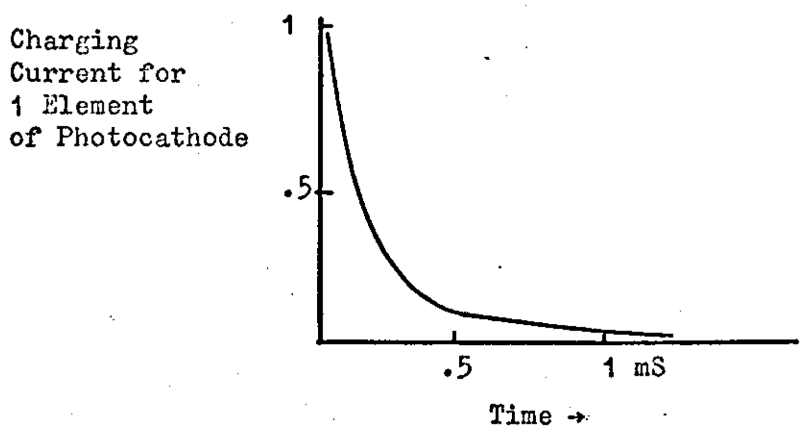

b) Effective Signal Decay with Time.

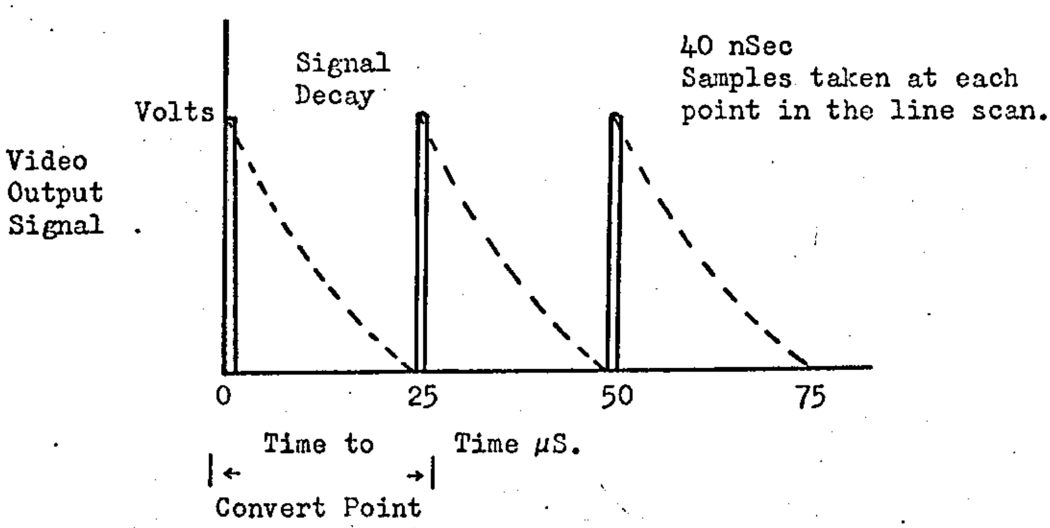

c) Samples Taken by A/D Converter.

FIG. 46. TELEVISION CAMERA OPERATION.

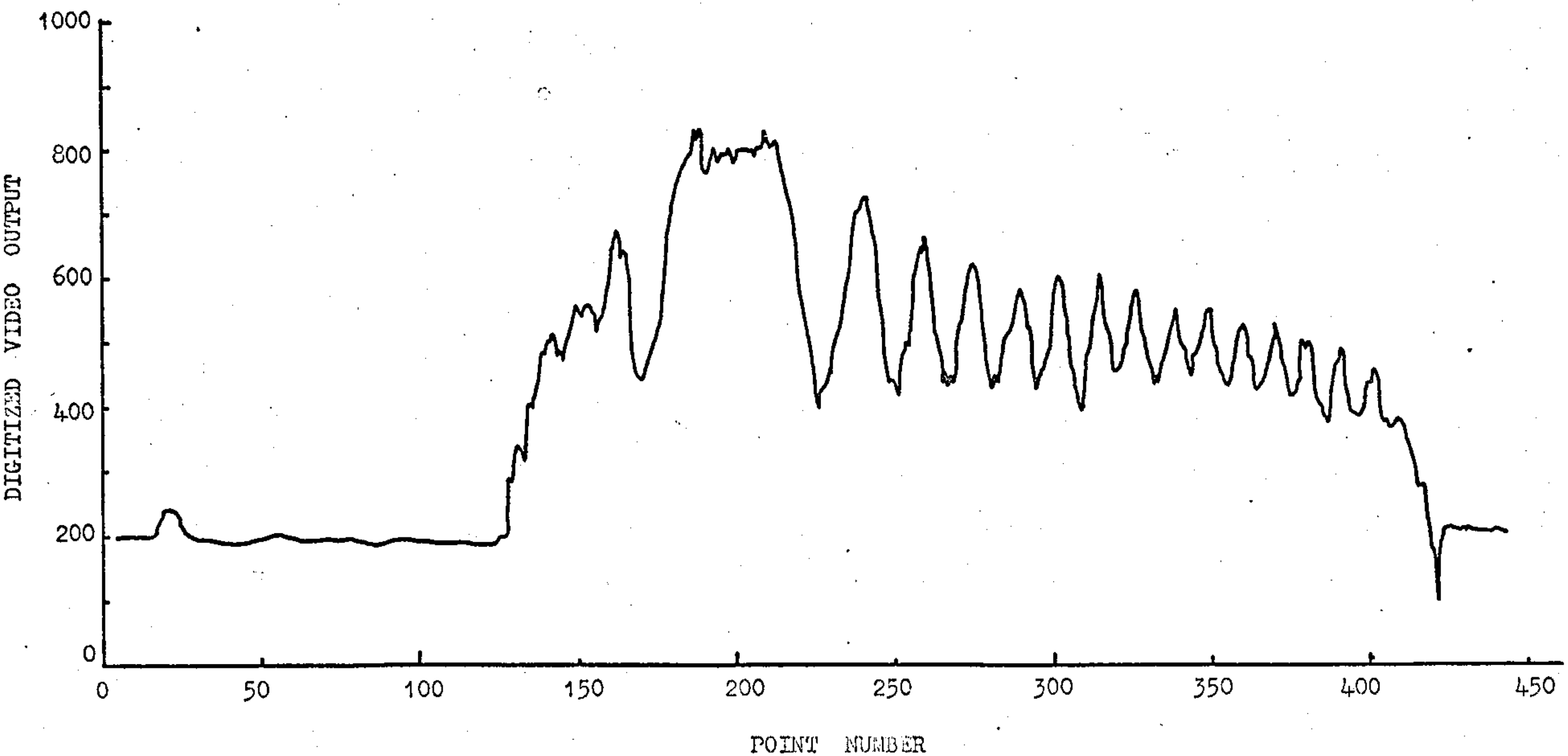

FIG. 47. PLOT OF THE DIGITIZED VIDEO OUTPUT FROM THE TELEVISION SYSTEM.

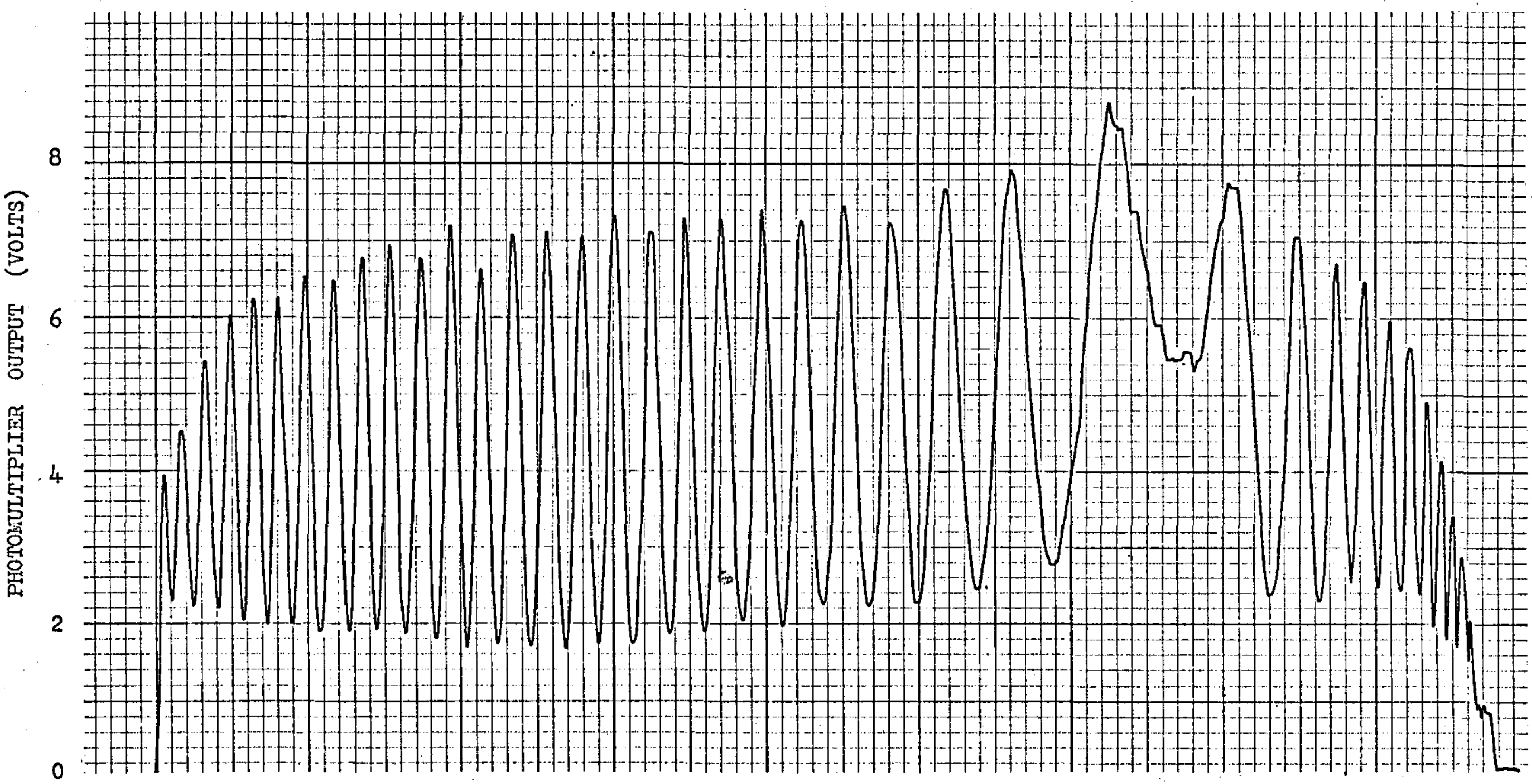

FIG. 48. AN EXAMPLE OF A SCAN RECORDED BY THE PHOTOMULTIPLIER/MAGNETIC TAPE RECORDER SYSTEM FOR COMPUTER ANALYSIS (CONTOUR DEPTH INTERVAL 0.015").

SOURCE LISTING

```
STMT LEV NT

                             /*  APPENDIX ONE:  BLADE SHAPE FROM CONTOUR FRINGES  */       A010S749
   1      0  HOLO      : PROC OPTIONS (MAIN) ;                                         A025S749
   2   1  0               DCL MP(20) FLOAT  ;                                          A033S749
   3   1  0               DCL ASTART FIXED BINARY  ;                                   A034S749
   4   1  0               DCL (ISUB1,ISUB2) FIXED BINARY  ;                            A041S749
   5   1  0               DCL APO FIXED BINARY  ;                                      A042S749
   6   1  0               DCL APOINT FIXED BINARY  ;                                   A043S749
   7   1  0               DCL Y FIXED BINARY  ;                                        A044S749
   8   1  0               DCL (POINTS,START,COUNT,AA,AV,Q,T,AVSTAT) FIXED BINARY ;     A045S749
   9   1  0               DCL (IMAX,IMIN) FIXED BINARY ;                               A046S749
  10   1  0               DCL (VX(*),V(*),Z(*),EX(*)) CONTROLLED  ;                    A047S749
  11   1  0               DCL (REX(*),RZ(*)) CONTROLLED  ;                             A048S749
  12   1  0               DCL RUN CHAR(10) EXT  ;                                      A049S749
  13   1  0               DCL (LIM1,LIM2) FLOAT ;                                      A050S749
  14   1  0               DCL IDENT CHAR(9) EXT  ;                                     A051S749
  15   1  0               DCL D CHAR(1) EXT  ;                                         A052S749
  16   1  0               DCL INDIC CHAR(1)      ;                                     A053S749
  17   1  0               DCL VAV(*) CONTROLLED  ;                                     A055S749
  18   1  0               DCL CARDST (30) CHAR (80)  ;                                 A056S749
  19   1  0               Y = 1  ;                                                     A057S749
  20   1  0               DCL CARD CHAR (80) EXT  ;                                    A058S749
  21   1  0               DCL TEST CHAR (9) DEFINED CARD POSITION (1) ;                A059S749
  22   1  0               DCL BW CHAR (20) DEFINED CARD POSITION (60) ;                A060S749
  23   1  0               DCL INPT FILE INPUT  ;                                       A061S749
  24   1  0               DCL ERR1 CHAR (21) INIT ('FIRST CHARACTER NOT A') ;          A062S749
  25   1  0               DCL ERR2 CHAR (14) INIT ('ERROR IN BLOCK')  ;                A063S749
  26   1  0               ON CONV GO TO REPEAT ;                                       A064S749
  27   1  0               ON ENDFILE (SYSIN) GO TO P2  ;                               A065S749
  28   1  0               II = 0B  ;                                                   A066S749
  29   1  0  VDATA     : GET FILE (INPT) EDIT(D) (A(1)) ; /* TO FIND FIRST A */        A100S749
  30   1  0               IF D = 'A' THEN GO TO ABLK ;                                 A101S749
```

```
STMT LEV NT

  31    1  0                  PUT EDIT (ERR1) (SKIP(3),X(10),A(21)) ;                       A102S749
  32    1  0  REPEAT     :  GET FILE (INPT) EDIT (D) (A(1)) ;                                 A103S749
  33    1  0                  IF D ¬= 'A' THEN GO TO REPEAT  ;                                A104S749
  34    1  0  ABLK       :  INDIC = 'A' ;                                                     A105S749
  35    1  0                  GET FILE (INPT) EDIT (IDENT,RUN) (A(9),A(10)) ;                 A106S749
  36    1  0                  PUT EDIT ('IDENT =',IDENT,'RUN =',RUN)(PAGE,SKIP(10),X(15),     A107S749
                              A,A(9),X(15),A,A(10)) ;                                         A108S749
  37    1  0                  GET FILE (INPT) EDIT (POINTS,DELTAA,LIM1,LIM2)(E(4,0),          IN01S749
                              E(8,0),E(8,0),E(8,0)) ;                                         IN02S749
  38    1  0                  GET FILE (INPT) EDIT(XMAX,XMIN,WIDTHA,DIFMIN,START)             IN03S749
                              (E(8,0),E(8,0),E(8,0) ,E(8,0),E(4,0)) ;                         IN04S749
  39    1  0                  GET FILE (INPT) EDIT (XLIM1,XLIM2,GRADA)(E(8,0),E(8,0),         IN05S749
                              E(8,0))  ;                                                      IN06S749
  40    1  0                  GET FILE (INPT) EDIT (REF) (E(1,0))  ;                          IN08S749
  41    1  0                  GRAD = GRADA*.0001 ;                                            IN10S749
  42    1  0                  IF REF = 2 THEN DO  ;                                           IN40S749
  43    1  1                    FREE REX,RZ  ;                                                IN60S749
  44    1  1                    REF = 0  ;                                                    IN80S749
  45    1  1                    END  ;                                                        IN90S749
  46    1  0                  ALLOCATE VX(POINTS),V(POINTS),Z(POINTS),EX(POINTS)  ;           AD01S749
  47    1  0                  IF REF = 0 THEN DO ;                                            AD02S749
  48    1  1                    ALLOCATE RZ(POINTS),REX(POINTS)  ;                            AD03S749
  49    1  1                    END  ;                                                        AD04S749
  50    1  0                  APO = POINTS*.40  ;                                             AD05S749
  51    1  0                  APOINT = FLOOR(APO)  ;                                          AD06S749
  52    1  0                  ALLOCATE VAV(APOINT)  ;                                         AD08S749
  53    1  0  STCAL      :  DELTA = DELTAA*.0001 ;                                            AD10S749
  54    1  0                  WIDTH = WIDTHA*.0001 ;                                          AD20S749
  55    1  0                  JJ = 0B  ;                                                      AD30S749
  56    1  0                  Z,EX = 0 ;                                                      AD40S749
  57    1  0                  DO T = 1 TO POINTS ;                                            A109S749
  58    1  1                  GET FILE (INPT) EDIT (VX(T),V(T)) (E(8,0),E(8,0)) ;             A110S749
  59    1  1                  END ;                                                           A111S749
  60    1  0                  GET FILE (INPT) EDIT (D) (A(1)) ;                               A112S749
```

```
STMT LEV NT

 61   1  0            IF D ¬= 'B' THEN GO TO ERROR1  ;                          A113S749
 62   1  0            GO TO P1 ;                                                A114S749
 63   1  0  ERROR1    : PUT EDIT (ERR2,INDIC,'TEST =',IDENT) (SKIP(2),X(10),A(14),AB01S749
                      X(20),A(1),X(20),A,A(9)) ;                                AB02S749
 64   1  0            PUT EDIT ('CHARACTER D =',D)(SKIP,X(10),A,A(1)) ;         AB04S749
 65   1  0  AGIN    : GET FILE (INPT) EDIT (D) (A(1)) ;                         AB06S749
 66   1  0            JJ = JJ+1B ;                                              AB08S749
 67   1  0            PUT EDIT ('CHARACTER D =',D) (SKIP,X(10),A,A(1)) ;        AB10S749
 68   1  0            IF JJ = 10 THEN GO TO P1 ;                                AB12S749
 69   1  0            IF D ¬= 'B' THEN GO TO AGIN ;                             AB14S749
 70   1  0            GO TO P1   ;        /* TO BE USED ONLY ON TEST RUNS  */   AB16S749
                      /* ON PRODUCTION RUNS LOOK FOR NEXT A */                  AB18S749
 71   1  0  P1      : GET EDIT (CARDST(II+1B))(A(80)) ;                         AC02S749
 72   1  0            II = II+1B  ;                                             AC04S749
 73   1  0            IF II < 30 THEN GO TO P1 ;                                AC06S749
 74   1  0  P2      : CARDTOT = II  ;                                           AC08S749
 75   1  0  LOOK    : DO II = 1 TO CARDTOT ;                                    AC10S749
 76   1  1              CARD = CARDST(II)   ;                                   AC11S749
 77   1  1            IF TEST = IDENT THEN DO ;                                 AC12S749
 78   1  2              PUT EDIT ('CORRECT CARD AND TAPE FOUND II =',II)        AC14S749
                        (SKIP (5),X(10),A,F(3,0)) ;                             AC16S749
 79   1  2              PUT EDIT (BW) (SKIP(2),X(10),A(20)) ;                   AC18S749
 80   1  2              END ;                                                   AC20S749
 81   1  1            END LOOK ;                                                AC22S749
                      /* PRINTOUT OF MAIN INPUT CONSTANTS  */                   A118S749
 82   1  0            PUT EDIT ('HOLOGRAPHIC CONTOURING PROGRAMME',             A120S749
                      'INPUT CONSTANTS','POINTS =',POINTS,'DELTA =',DELTA,      A130S749
                      'LIM1=',LIM1,'LIM2 =',LIM2)(PAGE,X(30),A,SKIP(2),X(20),   A140S749
                      A,SKIP(2),X(15),A,F(5,1),X(15),A,F(6,3),SKIP(3),X(15),    A150S749
                      A,F(6,0),X(15),A,F(6,0)) ;                                A160S749
 83   1  0            PUT EDIT ('NOISE LIMIT','DIFMIN =',DIFMIN)(SKIP(4),X(20), A161S749
                      A,SKIP,X(10),A,F(4,0)) ;                                  A162S749
 84   1  0            PUT EDIT ('START PARAMETER =',START)(SKIP(2),X(20),A,     A163S749
                      F(6,2)) ;                                                 A164S749
```

```
STMT LEV NT

  85   1  0            PUT EDIT ('XMAX =',XMAX,'XMIN =',XMIN)(SKIP(2),X(20),A,       A166S749
                       F(6,0),X(30),A,F(6,0)) ;                                     A167S749
  86   1  0            PUT EDIT ('COMPONENT WIDTH',WIDTH)(SKIP(2),X(15),A,F(9,5));   A168S749
  87   1  0            PUT EDIT ('DIRECTION INDICATOR=',Y)(SKIP(4),X(9),A,F(3,0));   AE10S749
  88   1  0            PUT EDIT ('X DIRECTION INVERSION REGION ','XLIM1 =',XLIM1,    AE20S749
                       'XLIM2 =',XLIM2)(SKIP(3),X(10),A,X(10),A,F(7,0),X(10),A,     AE30S749
                       F(7,0))  ;                                                   AE40S749
  89   1  0            PUT EDIT ('RUN TYPE 0 = REF 1 = SUBTRACT REF =',REF)          AE50S749
                       (SKIP(2),X(5),A,F(3,0))  ;                                   AE60S749
  90   1  0            IMAX = 1  ;                                                  A180S749
  91   1  0            IMIN = 1  ;                                                  A182S749
  92   1  0            ISUB1 = 1  ;                                                 A184S749
  93   1  0            ISUB2 = 1  ;                                                 A186S749
  94   1  0            ISMAX,ISMIN = 0  ;                                           A188S749
  95   1  0            ISUBF = 0  ;                                                 A189S749
  96   1  0            AV = 1 ;                                                     A190S749
  97   1  0            AA = 1 ;                                                     A195S749
  98   1  0            COUNT = -2  ;                                                A200S749
  99   1  0            IPK,IAPK = 5  ;                                              A201S749
 100   1  0            W = 1 ;                                                      A205S749
 101   1  0            IIND = 0  ;                                                  A207S749
 102   1  0            ASTART = START  ;                                            A208S749
                       /*  START OF MAIN PROGRAMME  */                              A209S749
                       /* TO FIND MAX & MIN */                                      A210S749
 103   1  0  CONTOR  : DO I = 2 TO (POINTS-1)  ;                                    A220S749
 104   1  1            IF IIND = 1 THEN GO TO PEAK  ;                               A225S749
 105   1  1            IF VX(I) > LIM1 & VX(I) < LIM2 THEN GO TO AVCAL ;            A230S749
 106   1  1  PEAK    : IF V(I) > V(I-1) & V(I) > V(I+1) THEN GO TO LAB2 ;           A240S749
 107   1  1            IF V(I) < V(I-1) & V(I) < V(I+1) THEN GO TO LAB1 ;           A250S749
 108   1  1            GO TO LAB4  ;                                                A260S749
                     /* AVERAGE CALCULATION  */                                     A300S749
 109   1  1  AVCAL   : IF AV = 1 THEN AVSTAT = I - 6  ;                             A310S749
 110   1  1            IF AV = 1 THEN I = I - 6 ;                                   A315S749
 111   1  1            VAV(AV) = (V(I-3)+V(I-2)+V(I-1)+V(I)+V(I+1)+V(I+2)           A320S749
```

```
STMT LEV NT

                              +V(I+3))/7  ;                                          A330S749
 112   1  1                   I = I + 2  ;                                           A360S749
 113   1  1                   AV = AV+1 ;                                            A370S749
 114   1  1                   IF AV < 6 THEN GO TO AVCAL  ;                          A375S749
 115   1  1                   IF VX(I) > LIM2 THEN GO TO AVLP ;                      A380S749
 116   1  1                   IF VX(I) < LIM1 THEN GO TO AVLP ;                      A385S749
 117   1  1                   GO TO AVCAL ;                                          A386S749
 118   1  1  AVLP       : AA = AA+1 ;                                                A390S749
 119   1  1                   I = (AA-1)*2+AVSTAT  ;                                 A391S749
 120   1  1                   IF AA = AV - 1 THEN IIND = 1  ;                        A392S749
 121   1  1                   IF AA = AV- 1 THEN I = I - 6  ;                        A393S749
 122   1  1                   IF AA = AV-1 THEN GO TO LAB4 ;                         A395S749
                              /*  TO FIND MAX AND MIN OF AVERAGE VALUES  */          A397S749
 123   1  1                   IF VAV(AA) > VAV(AA-1) & VAV(AA) > VAV(AA+1) THEN GO TO    A400S749
                              AVMAX ;                                                A410S749
 124   1  1                   IF VAV(AA) < VAV(AA-1) & VAV(AA) < VAV(AA+1) THEN GO TO    A420S749
                              AVMIN ;                                                A430S749
 125   1  1                   GO TO AVLP ;                                           A440S749
                              /* INVESTIGATION FOR SPURIOUS MAX PRODUCED BY NOISE */ A442S749
 126   1  1  AVMAX      : IF AA+3 > AV THEN GO TO AVMAX2  ;                          A446S749
 127   1  1                   IF AA< 3 THEN GO TO AVMAX2  ;                          A446S749
 128   1  1                   IF VAV(AA+1) > VAV(AA+2) & VAV(AA+2) > VAV(AA+3) THEN GO TO A447S749
 129   1  1                   AVMAX1 ; ELSE GO TO AVEND  ;                           A448S749
 130   1  1  AVMAX1     : IF VAV(AA-1) > VAV(AA-2) & VAV(AA-2) > VAV(AA-3) THEN GO TO  A448S749
 131   1  1                   AVMAX2 ; ELSE GO TO AVEND  ;                           A449S749
                              /*  SUBMAX LOCATION  */                                A449S749
 132   1  1  AVMAX2     : IF ISUBF = 1 THEN GO TO SMAX  ;                            A450S749
 133   1  1                   IF VX(I) > XLIM2 THEN GO TO SMAX  ;                    A450S749
 134   1  1                   IF VX(I) < XLIM1 THEN GO TO SMAX;                      A451S749
 135   1  1                   SUBMAX = (VAV(AA)-VMIN)/(VMAX-VMIN) ;   /* SUBFRINGE */    A452S749
                              /* INVERSION ERROR CORRECTION  */                      AF10S749
 136   1  1                   IF SUBMAX < .75 & ISMIN = 1 THEN DO  ;                 AF15S749
 137   1  2                   PUT EDIT ('SUBMAX FRINGE ALSO FOUND SUB =',SUBMAX,'AA =',  AF20S749
                              AA) (SKIP(10),X(10),A,F(6,3),X(20),A,F(3,0))  ;        AF25S749
```

```
STMT LEV NT

 138   1  2            PUT EDIT ('PROGRAM TO RESTART ISUB1 =',ISUB1)          AF30S749
                       (PAGE,SKIP,X(30),A,F(4,0)) ;                           AF35S749
 139   1  2            IMAX,IMIN = 1 ;                                        AF40S749
 140   1  2            ISUB2,AV = 1 ;                                         AF41S749
 141   1  2            AA,W = 1 ;                                             AF42S749
 142   1  2            ISMIN,ISMAX = 0 ;                                      AF45S749
 143   1  2            ISUBF,IIND = 0 ;                                       AF46S749
 144   1  2            COUNT = -2 ;                                           AF50S749
 145   1  2            I = 2 ;                                                AF55S749
 146   1  2            START = ASTART ;                                       AF60S749
 147   1  2            GO TO LAB4 ;                                           AF65S749
 148   1  2            END ;                                                  AF70S749
 149   1  1            IF SUBMAX < .75 THEN DO ;                              A454S749
 150   1  2              ISUB1 = -1 ;                                         A455S749
 151   1  2              IMIN = -1 ;                                          A456S749
 152   1  2              ISUBF = 1 ;                                          A457S749
 153   1  2              PUT EDIT ('SUB FRINGE PEAK ','SUB =',SUBMAX,'AA =',AA) A458S749
                         (SKIP(5),X(10),A,X(10),A,F(6,3),X(10),A,F(3,0)) ;    A460S749
 154   1  2              ISMAX = 1 ;                                          A461S749
 155   1  2              GO TO AVEND ;                                        A462S749
 156   1  2              END ;                                                A464S749
 157   1  1  SMAX     : VMAX = VAV(AA) ;                                      A468S749
 158   1  1            IF IPK-I < 2 & I -IPK < 2 THEN COUNT = COUNT - 1 ;     A468S749
 159   1  1            IAPK = I ;                                             A468S749
 160   1  1            IF (VMAX-VMIN) < DIFMIN & COUNT > 0 THEN GO TO AVEND ; A469S749
 161   1  1            COUNT = COUNT+1 ;                                      A470S749
 162   1  1            GO TO AMAX ;                                           A480S749
                       /* INVESTIGATION FOR SPURIOUS MIN PRODUCED BY NOISE */ A481S749
 163   1  1  AVMIN    : IF AA+3 > AV THEN GO TO AVMIN2 ;                      A481S749
 164   1  1            IF AA< 3 THEN GO TO AVMIN2 ;                           A481S749
 165   1  1            IF VAV(AA+1) <VAV(AA+2) & VAV(AA+2) < VAV(AA+3) THEN GO TO A482S749
 166   1  1            AVMIN1 ; ELSE GO TO AVEND ;                            A483S749
 167   1  1  AVMIN1   : IF VAV(AA-1) < VAV(AA-2) & VAV(AA-2) < VAV(AA-3) THEN GO TO A483S749
 168   1  1            AVMIN2 ; ELSE GO TO AVEND ;                            A484S749
```

```
STMT LEV NT

                         /* SUBMIN LOCATION */                                        A484S749
 169    1  1  AVMIN2   : IF ISUBF = 1 THEN GO TO SMIN  ;                              A485S749
 170    1  1             IF VX(I) > XLIM2 THEN GO TO SMIN  ;                          A486S749
 171    1  1             IF VX(I) < XLIM1 THEN GO TO SMIN  ;                          A487S749
 172    1  1             SUBMIN = (VAV(AA)-VMIN)/(VMAX-VMIN) ;          /* SUBFRINGE*/A492S749
                         /* INVERSION ERROR CORRECTION */                             AG10S749
 173    1  1             IF SUBMIN > .25 & ISMAX = 1 THEN DO  ;                       AG15S749
 174    1  2             PUT EDIT ('SUBMIN FRINGE ALSO FOUND SUB =',SUBMIN,'AA =',    AG20S749
                         AA) (SKIP(10),X(10),A,F(6,3),X(20),A,F(3,0))  ;              AG25S749
 175    1  2             PUT EDIT ('PROGRAM TO RESTART ISUB1 =',ISUB1)                AG30S749
                         (PAGE,SKIP,X(30),A,F(4,0))  ;                                AG35S749
 176    1  2             IMAX,IMIN = 1  ;                                             AG40S749
 177    1  2             ISUB2,AV = 1  ;                                              AG41S749
 178    1  2             AA,W = 1  ;                                                  AG42S749
 179    1  2             ISMIN,ISMAX = 0  ;                                           AG45S749
 180    1  2             ISUBF,IIND = 0  ;                                            AG46S749
 181    1  2             COUNT = -2  ;                                                AG50S749
 182    1  2             I = 2  ;                                                     AG55S749
 183    1  2             START = ASTART  ;                                            AG60S749
 184    1  2             GO TO LAB4  ;                                                AG65S749
 185    1  2             END  ;                                                       AG70S749
 186    1  1             IF SUBMIN > .25 THEN DO ;                                    A494S749
 187    1  2               ISUB1 = -1  ;                                              A495S749
 188    1  2               IMAX = -1  ;                                               A496S749
 189    1  2               ISUBF = 1  ;                                               A497S749
 190    1  2               PUT EDIT ('FRINGE SUBMINN','SUBMIN =',SUBMIN,'AA =',AA)    A498S749
                           (SKIP(5),X(10),A,X(10),A,F(6,3),X(10),A,F(3,0)) ;          A500S749
 191    1  2               ISMIN = 1  ;                                               A501S749
 192    1  2               GO TO AVEND ;                                              A502S749
 193    1  2               END ;                                                      A504S749
 194    1  1  SMIN     : VMIN = VAV(AA)  ;                                            A508S749
 195    1  1             IF IPK-I < 2 & I -IPK < 2 THEN COUNT = COUNT - 1  ;          A508S749
 196    1  1             IAPK = I  ;                                                  A508S749
 197    1  1             IF (VMAX-VMIN) < DIFMIN & COUNT > 0 THEN GO TO AVEND  ;      A509S749
```

```
STMT LEV NT

 198   1  1              COUNT = COUNT+1 ;                                       A510S749
 199   1  1              GO TO AMIN ;                                            A520S749
 200   1  1  LAB1      : COUNT = COUNT+1 ;                                       A530S749
 201   1  1              IF IAPK-I < 2 & I-IAPK < 2 THEN COUNT = COUNT - 1  ;    A535S749
 202   1  1              IPK = I   ;                                             A537S749
 203   1  1              VMIN = V(I) ;                                           A540S749
 204   1  1              PUT EDIT ('VMIN =',VMIN,'I =',I,'COUNT =',COUNT)(SKIP,  A550S749
                         X(10),A,F(6,0),X(10),A,F(5,1),X(15),A,F(4,1)) ;         A560S749
 205   1  1  AMIN      : IF IMAX = -1 THEN N = M   ;                             A562S749
 206   1  1              IF IMIN = -1 THEN N = I   ;                             A565S749
 207   1  1              IF IMIN = 1 THEN M = I   ;                              A570S749
                         /*  PARAMETERS RESET FOR INVERSION AT A SUBMIN  */      A571S749
 208   1  1              IF IMAX = -1 THEN DO   ;                                A572S749
 209   1  2                W = -1    ;                                           A573S749
 210   1  2                START = START + COUNT - 1   ;                         A574S749
 211   1  2                COUNT = 0   ;                                         A575S749
 212   1  2                IMAX = 1   ;                                          A576S749
 213   1  2                PUT EDIT ('INVERSION POINT AT SUBMIN START =',START)  A577S749
                           (SKIP(5),A,F(4,0))   ;                                A578S749
 214   1  2                END   ;                                               A579S749
                         /*  PARAMETERS RESET FOR INVERSION AT A MAX  */         A580S749
 215   1  1              IF ISUB2 = -1 THEN DO ;                                 A580S749
 216   1  2              START = START + COUNT   ;                               A581S749
 217   1  2                COUNT = 0   ;                                         A582S749
 218   1  2                W = -1   ;                                            A583S749
 219   1  2                ISUB1 = -1   ;                                        A584S749
 220   1  2                ISUB2 = 1   ;                                         A585S749
 221   1  2                PUT EDIT ('INVERSION POINT AT MAX  START =',START)    A586S749
                           (SKIP(5),X(20),A,F(4,0))   ;                          A587S749
 222   1  2                END   ;                                               A588S749
 223   1  1              IF COUNT < 0 THEN GO TO LAB4   ;                        A589S749
 224   1  1              GO TO LAB3 ;                                            A590S749
 225   1  1  LAB2      : COUNT = COUNT+1 ;                                       A600S749
 226   1  1              IF IAPK-I < 2 & I-IAPK < 2 THEN COUNT = COUNT - 1  ;    A605S749
```

```
STMT LEV NT

 227   1  1                 IPK = I   ;                                                    A607S749
 228   1  1                 VMAX = V(I) ;                                                  A610S749
 229   1  1                 PUT EDIT ('VMAX =',VMAX,'I =',I,'COUNT =',COUNT)(SKIP,         A620S749
                            X(10),A,F(6,0),X(10),A,F(5,1),X(10),A,F(5,1)) ;                A630S749
 230   1  1  AMAX         : IF IMIN = -1 THEN M = N  ;                                     A632S749
 231   1  1                 IF IMAX = -1 THEN M = I  ;                                     A635S749
 232   1  1                 IF IMAX = 1 THEN N = I  ;                                      A640S749
                            /*  PARAMETERS RESET FOR INVERSION AT A SUBMAX  */             A641S749
 233   1  1                 IF IMIN = -1 THEN DO  ;                                        A642S749
 234   1  2                   W = -1  ;                                                    A643S749
 235   1  2                   START = START + COUNT - 1  ;                                 A644S749
 236   1  2                   COUNT = 0  ;                                                 A645S749
 237   1  2                   IMIN = 1  ;                                                  A646S749
 238   1  2                   PUT EDIT ('INVERSION POINT AT SUBMAX START =',START)         A647S749
                              (SKIP(5),X(20),A,F(4,0))  ;                                  A648S749
 239   1  2                  END  ;                                                        A649S749
                            /*  PARAMETERS RESET FOR INVERSION AT A MIN  */                A650S749
 240   1  1                 IF ISUB2 = -1 THEN DO ;                                        A650S749
 241   1  2                 START = START + COUNT  ;                                       A651S749
 242   1  2                   COUNT = 0  ;                                                 AS51S749
 243   1  2                   W = -1  ;                                                    A652S749
 244   1  2                   ISUB1 = -1  ;                                                A653S749
 245   1  2                   ISUB2 = 1  ;                                                 A654S749
 246   1  2                   PUT EDIT ('INVERSION POINT AT MIN  START =',START)           A655S749
                              (SKIP(5),X(20),A,F(4,0))  ;                                  A656S749
 247   1  2                   END  ;                                                       A657S749
 248   1  1                 IF COUNT < 0 THEN GO TO LAB4  ;                                A658S749
                            /* NOISE INVESTIGATION  */                                     A659S749
 249   1  1  LAB3         : IF (VMAX-VMIN) < DIFMIN THEN COUNT = COUNT-2 ;                 A659S749
 250   1  1                 IF (VMAX-VMIN) < DIFMIN THEN GO TO AVEND ;                     A660S749
 251   1  1                 IF N > M THEN GO TO LABA ;                                     A670S749
 252   1  1                 NN = N ;                                                       A680S749
 253   1  1                 MM = M ;                                                       A690S749
 254   1  1                 Q = -1 ;                                                       A700S749
```

```
STMT LEV NT

 255   1  1                 GO TO CALA  ;                                                A710S749
 256   1  1  LABA         : NN = M ;                                                     A720S749
 257   1  1                 MM = N ;                                                     A730S749
 258   1  1                 Q = 1 ;                                                      A740S749
                            /* TO PLOT COMPONENT SHAPE */                                A750S749
                            /* APPLICATION OF A SINE SQUARED FIT */                      A760S749
 259   1  1  CALA         : DO L = NN TO MM ;                                            A780S749
 260   1  2                 AINT = (V(L)-VMIN)/(VMAX-VMIN) ;                             A790S749
 261   1  2                 IF AINT < 0 THEN AINT = - AINT  ;                            A795S749
 262   1  2                 C = SQRT(AINT) ;                                             A800S749
 263   1  2                 K,J = 0 ;                                                    A820S749
 264   1  2                 P = 1 ;                                                      A830S749
 265   1  2  ASIN         : YEW = J/2**K  ;                                              A840S749
 266   1  2                 P = P + YEW  ;                                               A850S749
 267   1  2                 S = SIN(.7854*P) ;                                           A860S749
 268   1  2                 IF C-S < .001 & C-S > -.001 THEN GO TO BSIN ;                A870S749
 269   1  2                 IF C-S > 0 THEN J = 1 ;                                      A880S749
 270   1  2                 IF C-S < 0 THEN J = -1 ;                                     A890S749
 271   1  2                 K = K+1 ;                                                    A900S749
 272   1  2                 IF K = 10 THEN GO TO BSIN ;                                  A910S749
 273   1  2                 GO TO ASIN ;                                                 A920S749
 274   1  2  BSIN         : R = P/2 ;                                                    A925S749
                            /* TOCALCULATE BLADE SHAPE */                                B010S749
 275   1  2                 IF Q = -1 THEN GO TO LABC ;                                  B020S749
 276   1  2                 Z(L) = (START+(W*Y*(COUNT+R)))*DELTA*.5  ;                   B030S749
 277   1  2                 GO TO LABD ;                                                 B040S749
 278   1  2  LABC         : Z(L) = (START+(W*Y*(COUNT+1-R)))*DELTA*.5  ;                 B050S749
 279   1  2  LABD         : EX(L) = (WIDTH*(XMAX-VX(L)))/(XMAX-XMIN) ;                   B058S749
 280   1  2                 IF W = -1 THEN GO TO CALEND ;                                B101S749
 281   1  2                 IF VX(L) < XLIM1 THEN GO TO CALEND  ;                        B102S749
 282   1  2                 IF VX(L) > XLIM2 THEN GO TO CALEND  ;                        B103S749
                           /* LINEAR FIT TO FIND SHAPE GRADIENT:  DIRECTION INVERSION*/  BB05S749
 283   1  2                 IF ISUB1 = -1 THEN GO TO CALEND  ;                           BB10S749
 284   1  2                 DEXB = (EX(L)+EX(L-1)+EX(L-2)+EX(L-3)+EX(L-4))/5 ;           BB12S749
```

```
STMT LEV NT

 285   1  2               DSUM=((EX(L)-DEXB)*Z(L)+(EX(L-1)-DEXB)*Z(L-1)+(EX(L-2)-DEXB)BB13S749
                          *Z(L-2)+(EX(L-3)-DEXB)*Z(L-3)+(EX(L-4)-DEXB)*Z(L-4)) ;      BB14S749
 286   1  2               DSQU = (((EX(L)-DEXB)**2+(EX(L-1)-DEXB)**2+(EX(L-2)-DEXB)   BB15S749
                          **2+(EX(L-3)-DEXB)**2+(EX(L-4)-DEXB)**2)) ;                 BB16S749
 287   1  2               DZ = DSUM/DSQU  ;                                           BB17S749
 288   1  2               IF DZ < GRAD & DZ > -GRAD THEN DO  ;                        BB20S749
 289   1  3                 ISUB1 = -1  ;                                             BB30S749
 290   1  3                 ISUB2 = -1  ;                                             BB40S749
 291   1  3                 ISMIN = 1  ;                                              BB44S749
 292   1  3                 ISMAX = 1  ;                                              BB46S749
 293   1  3                 PUT EDIT ('INVERSION POINT EX =',EX(L)) (SKIP(5),X(20),   BB48S749
                            A,F(9,5))  ;                                              BB49S749
 294   1  3                 END  ;                                                    BB50S749
 295   1  2  CALEND     : END CALA ;                                                  B115S749
 296   1  1  AVEND      : IF AA < AV-1 THEN GO TO AVLP ;                              B120S749
 297   1  1  LAB4       : END CONTOR ;                                                B130S749
 298   1  0               PUT EDIT ('POINTS NUMBER','EX VALUE','Z VALUE')             B132S749
                          (PAGE,X(20),A,X(20),A,X(20),A)  ;                           B133S749
 299   1  0               PUT EDIT ((T,EX(T),Z(T) DO T = 1 TO POINTS))                B134S749
                          (SKIP,X(25),F(4,0),X(24),F(9,5),X(20),F(9,5)) ;             B135S749
                          /* CALCULATION OF CENTROID & RADII OF GYRATION */           P010S749
 300   1  0               PLIN = 0  ;                                                 P015S749
 301   1  0               XM1,XM2,ZM1,ZM2,H1 = 0  ;                                   P020S749
 302   1  0  LICAL      : DO T = 12 TO (POINTS - 12)  ;                               P040S749
 303   1  1               DSQ = (EX(T+1)-EX(T))**2 + (Z(T+1)-Z(T))**2  ;              P060S749
 304   1  1               IF DSQ = 0 THEN GO TO LICEND  ;                             P080S749
 305   1  1               DS = SQRT(DSQ)  ;                                           P100S749
 306   1  1               PLIN = PLIN + DS  ;                                         P120S749
 307   1  1               XM1 = XM1 + (.5*DS*(EX(T+1)+EX(T)))  ;                      P145S749
 308   1  1               XM2 = XM2 + (.25*DS*(EX(T+1)+EX(T))**2)  ;                  P160S749
 309   1  1               ZM1 = ZM1 + (.5*DS*(Z(T+1)+Z(T))) ;                         P180S749
 310   1  1               ZM2 = ZM2 + (.25*DS*(Z(T+1)+Z(T))**2)  ;                    P200S749
 311   1  1               H1 = H1 + (.25*DS*(EX(T+1)+EX(T))*(Z(T+1)+Z(T))) ;          P220S749
 312   1  1  LICEND     : END LICAL  ;                                                P240S749
```

```
STMT LEV NT

 313   1  0          XBAR = XM1/PLIN  ;                                          P260S749
 314   1  0          RADX = XM2/PLIN;                                            P280S749
 315   1  0          ZBAR = ZM1/PLIN  ;                                          P300S749
 316   1  0          RADZ = ZM2/PLIN  ;                                          P320S749
 317   1  0          XRAD = SQRT(RADX)  ;                                        P340S749
 318   1  0          XROOT = (RADX-XBAR**2)  ;                                   P360S749
 319   1  0          IF XROOT < 0 THEN XROOT = -XROOT  ;                         P362S749
 320   1  0          XRG = SQRT(XROOT )  ;                                       P364S749
 321   1  0          ZRAD = SQRT(RADZ)  ;                                        P380S749
 322   1  0          ZROOT = (RADZ-ZBAR**2)  ;                                   P400S749
 323   1  0          IF ZROOT < 0 THEN ZROOT = -ZROOT  ;                         P402S749
 324   1  0          ZRG = SQRT ( ZROOT )  ;                                     P404S749
 325   1  0          HXZ = H1/PLIN  ;                                            P420S749
 326   1  0          HBAR = (HXZ-XBAR*ZBAR)  ;                                   P440S749
 327   1  0          PTAN = 2*HBAR/(XRG**2-ZRG**2)  ;                            P460S749
 328   1  0          PUT EDIT ('CURVE LENGTH =',PLIN,'XBAR =',XBAR,'ZBAR =',ZBAR)P500S749
                     (PAGE,SKIP(10),X(10),A,F(9,5),SKIP(2),X(10),A,F(9,5),X(20), P520S749
                     A,F(9,5)) ;                                                 P540S749
 329   1  0          PUT EDIT ('RAD OF G X SQ =',RADX,'XRAD =',XRAD,'XRG =',XRG) P560S749
                     (SKIP(5),X(10),A,F(9,5),X(10),A,F(9,5),X(10),A,F(9,5)) ;    P580S749
 330   1  0          PUT EDIT ('RAD OF G Z SQ =',RADZ,'ZRAD =',ZRAD,'ZRG =',ZRG) P600S749
                     (SKIP(5),X(10),A,F(9,5),X(10),A,F(9,5),X(10),A,F(9,5)) ;    P620S749
 331   1  0          PUT EDIT ('CROSS TERM =',HXZ,'HBAR =',HBAR,                 P640S749
                     'TWICE ANGLE OF P AXES =',PTAN)(SKIP(5),X(10),A,F(9,5),     P680S749
                     X(10),A,F(9,5),SKIP(2),X(10),A,F(9,5)) ;                    P700S749
                     /* REFERENCE SHAPE DATA  */                                 P750S749
 332   1  0          IF REF = 0 THEN DO  ;                                       P800S749
 333   1  1          RXBAR = XBAR  ;                                             P820S749
 334   1  1          RZBAR  = ZBAR  ;                                            P840S749
 335   1  1          RXRAD = XRAD  ;                                             P860S749
 336   1  1          RXRG = XRG  ;                                               P880S749
 337   1  1          RZRAD = ZRAD  ;                                             P900S749
 338   1  1          RZRG  = ZRG  ;                                              P920S749
 339   1  1          RTAN = PTAN  ;                                              P940S749
```

```
STMT LEV NT

 340   1  1                 PUT EDIT ('REF DATA SET ')(SKIP(2),X(5),A)  ;               P960S749
 341   1  1                 GO TO FRED  ;                                                P980S749
 342   1  1                 END  ;                                                       P990S749
                            /* DIFFERENCE CALCULATION */                                 Q020S749
 343   1  0                 XSHIFT = RXBAR - XBAR  ;                                     Q040S749
 344   1  0                 ZSHIFT = RZBAR - ZBAR  ;                                     Q060S749
 345   1  0                 DIFTAN = (PTAN -RTAN)/(1+PTAN*RTAN)  ;                       Q080S749
 346   1  0                 DTAN = SQRT(1 +1/(DIFTAN**2)) - 1/DIFTAN  ;                  Q100S749
 347   1  0                 ANGL  = 57.3066*DTAN  ;                                      Q120S749
 348   1  0                 PUT EDIT ('DIFFERENCE PARAMETERS','XSHIFT =',XSHIFT,         Q140S749
                            'ZSHIFT =',ZSHIFT)(PAGE,SKIP(10),X(30),A,SKIP(2),X(10),      Q180S749
                            A,F(9,5),X(20),A,F(9,5)) ;                                   Q190S749
 349   1  0                 PUT EDIT ('DIFTAN =',DIFTAN,'ANGULAR DIFFERENCE =',ANGL)     Q200S749
                            (SKIP(5),X(10),A,F(9,5),SKIP(5),X(10),A,F(9,5)) ;            Q220S749
 350   1  0  FRED         : FREE VX,V,Z,EX,VAV  ;                                        T020S749
 351   1  0                 GO TO VDATA  ;                                               T040S749
 352   1  0  FINISH       : END HOLO  ;                                                  T060S749
```

```
                                                ATTRIBUTE AND CROSS-REFERENCE TABLE

DCL NO.      IDENTIFIER                         ATTRIBUTES AND REFERENCES

8            AA         AUTOMATIC ALIGNED BINARY FIXED(15,0)
                        97, 118, 118, 119, 120, 121, 122, 123, 123, 123, 123, 124, 124, 124, 124, 126, 127, 128, 128, 128
                        128, 130, 130, 130, 130, 135, 137, 141, 153, 157, 163, 164, 165, 165, 165, 165, 167, 167, 167,
                        167, 172, 174, 178, 190, 194, 296

34           ABLK       /* STATEMENT LABEL CONSTANT */
                        30

65           AGIN       /* STATEMENT LABEL CONSTANT */
                        69

********     AINT       AUTOMATIC ALIGNED DECIMAL /* SINGLE */ FLOAT(6)
                        260, 261, 261, 261, 262

230          AMAX       /* STATEMENT LABEL CONSTANT */
                        162

205          AMIN       /* STATEMENT LABEL CONSTANT */
                        199

********     ANGL       AUTOMATIC ALIGNED DECIMAL /* SINGLE */ FLOAT(6)
                        347, 349

5            APO        AUTOMATIC ALIGNED BINARY FIXED(15,0)
                        50, 51

6            APOINT     AUTOMATIC ALIGNED BINARY FIXED(15,0)
                        51, 52

265          ASIN       /* STATEMENT LABEL CONSTANT */
                        273
```

DCL NO.	IDENTIFIER	ATTRIBUTES AND REFERENCES
3	ASTART	AUTOMATIC ALIGNED BINARY FIXED(15,0) 102, 146, 183
8	AV	AUTOMATIC ALIGNED BINARY FIXED(15,0) 96, 109, 110, 111, 113, 113, 114, 120, 121, 122, 126, 140, 163, 177, 296
109	AVCAL	/* STATEMENT LABEL CONSTANT */ 105, 114, 117
296	AVEND	/* STATEMENT LABEL CONSTANT */ 129, 131, 155, 160, 166, 168, 192, 197, 250
118	AVLP	/* STATEMENT LABEL CONSTANT */ 115, 116, 125, 296
126	AVMAX	/* STATEMENT LABEL CONSTANT */ 123
130	AVMAX1	/* STATEMENT LABEL CONSTANT */ 128
132	AVMAX2	/* STATEMENT LABEL CONSTANT */ 126, 127, 130
163	AVMIN	/* STATEMENT LABEL CONSTANT */ 124
167	AVMIN1	/* STATEMENT LABEL CONSTANT */ 165
169	AVMIN2	/* STATEMENT LABEL CONSTANT */ 163, 164, 167
8	AVSTAT	AUTOMATIC ALIGNED BINARY FIXED(15,0)

```
DCL NO.    IDENTIFIER                     ATTRIBUTES AND REFERENCES

                     109, 119

274        BSIN      /* STATEMENT LABEL CONSTANT */
                     268, 272

22         BW        DEFINED CARD POSITION(60) UNALIGNED CHARACTER(20)
                     79

********   C         AUTOMATIC ALIGNED DECIMAL /* SINGLE */ FLOAT(6)
                     262, 268, 268, 269, 270

259        CALA      /* STATEMENT LABEL CONSTANT */
                     255

295        CALEND    /* STATEMENT LABEL CONSTANT */
                     280, 281, 282, 283

20         CARD      EXTERNAL STATIC UNALIGNED CHARACTER(80)
                     21, 22, 76

18         CARDST    (30) AUTOMATIC UNALIGNED CHARACTER(80)
                     71, 76

********   CARDTOT   AUTOMATIC ALIGNED DECIMAL /* SINGLE */ FLOAT(6)
                     74, 75

103        CONTOR    /* STATEMENT LABEL CONSTANT */

8          COUNT     AUTOMATIC ALIGNED BINARY FIXED(15,0)
                     98, 144, 158, 158, 160, 161, 161, 181, 195, 195, 197, 198, 198, 200, 200, 201, 201, 204, 210, 211
                     216, 217, 223, 225, 225, 226, 226, 229, 235, 236, 241, 242, 248, 249, 249, 276, 278

15         D         EXTERNAL STATIC UNALIGNED CHARACTER(1)
```

```
DCL NO.     IDENTIFIER                    ATTRIBUTES AND REFERENCES

                        29, 30, 32, 33, 60, 61, 64, 65, 67, 69

********    DELTA       AUTOMATIC ALIGNED DECIMAL /* SINGLE */ FLOAT(6)
                        53, 82, 276, 278

********    DELTAA      AUTOMATIC ALIGNED DECIMAL /* SINGLE */ FLOAT(6)
                        37, 53

********    DEXB        AUTOMATIC ALIGNED DECIMAL /* SINGLE */ FLOAT(6)
                        284, 285, 285, 285, 285, 285, 286, 286, 286, 286, 286

********    DIFMIN      AUTOMATIC ALIGNED DECIMAL /* SINGLE */ FLOAT(6)
                        38, 83, 160, 197, 249, 250

********    DIFTAN      AUTOMATIC ALIGNED DECIMAL /* SINGLE */ FLOAT(6)
                        345, 346, 346, 349

********    DS          AUTOMATIC ALIGNED DECIMAL /* SINGLE */ FLOAT(6)
                        305, 306, 307, 308, 309, 310, 311

********    DSQ         AUTOMATIC ALIGNED DECIMAL /* SINGLE */ FLOAT(6)
                        303, 304, 305

********    DSQU        AUTOMATIC ALIGNED DECIMAL /* SINGLE */ FLOAT(6)
                        286, 287

********    DSUM        AUTOMATIC ALIGNED DECIMAL /* SINGLE */ FLOAT(6)
                        285, 287

********    DTAN        AUTOMATIC ALIGNED DECIMAL /* SINGLE */ FLOAT(6)
                        346, 347

********    DZ          AUTOMATIC ALIGNED DECIMAL /* SINGLE */ FLOAT(6)
                        287, 288, 288
```

```
DCL NO.     IDENTIFIER                      ATTRIBUTES AND REFERENCES


63          ERROR1    /* STATEMENT LABEL CONSTANT */
                      61

24          ERR1      AUTOMATIC UNALIGNED INITIAL CHARACTER(21)
                      31

25          ERR2      AUTOMATIC UNALIGNED INITIAL CHARACTER(14)
                      63

10          EX        (*) CONTROLLED ALIGNED DECIMAL /* SINGLE */ FLOAT(6)
                      46, 56, 279, 284, 284, 284, 284, 284, 285, 285, 285, 285, 285, 286, 286, 286, 286, 286, 293, 299,
                      303, 303, 307, 307, 308, 308, 311, 311, 350

352         FINISH    /* STATEMENT LABEL CONSTANT */


********    FLOOR     BUILTIN
                      51

350         FRED      /* STATEMENT LABEL CONSTANT */
                      341

********    GRAD      AUTOMATIC ALIGNED DECIMAL /* SINGLE */ FLOAT(6)
                      41, 288, 288

********    GRADA     AUTOMATIC ALIGNED DECIMAL /* SINGLE */ FLOAT(6)
                      39, 41

********    HBAR      AUTOMATIC ALIGNED DECIMAL /* SINGLE */ FLOAT(6)
                      326, 327, 331

1           HOLO      EXTERNAL ENTRY RETURNS(ALIGNED DECIMAL /* SINGLE */ FLOAT(6)) OPTIONS(MAIN)
```

```
DCL NO.     IDENTIFIER                 ATTRIBUTES AND REFERENCES

********    HXZ        AUTOMATIC ALIGNED DECIMAL /* SINGLE */ FLOAT(6)
                       325, 326, 331

********    H1         AUTOMATIC ALIGNED DECIMAL /* SINGLE */ FLOAT(6)
                       301, 311, 311, 325

********    I          AUTOMATIC ALIGNED BINARY FIXED(15,0)
                       103, 105, 105, 106, 106, 106, 106, 107, 107, 107, 107, 109, 110, 110, 111, 111, 111, 111, 111,
                       111, 111, 112, 112, 115, 116, 119, 121, 121, 133, 134, 145, 158, 158, 159, 170, 171, 182, 195,
                       195, 196, 201, 201, 202, 203, 204, 206, 207, 226, 226, 227, 228, 229, 231, 232

********    IAPK       AUTOMATIC ALIGNED BINARY FIXED(15,0)
                       99, 159, 196, 201, 201, 226, 226

14          IDENT      EXTERNAL STATIC UNALIGNED CHARACTER(9)
                       35, 36, 63, 77

********    II         AUTOMATIC ALIGNED BINARY FIXED(15,0)
                       28, 71, 72, 72, 73, 74, 75, 76, 78

********    IIND       AUTOMATIC ALIGNED BINARY FIXED(15,0)
                       101, 104, 120, 143, 180

9           IMAX       AUTOMATIC ALIGNED BINARY FIXED(15,0)
                       90, 139, 176, 188, 205, 208, 212, 231, 232

9           IMIN       AUTOMATIC ALIGNED BINARY FIXED(15,0)
                       91, 139, 151, 176, 206, 207, 230, 233, 237

16          INDIC      AUTOMATIC UNALIGNED CHARACTER(1)
                       34, 63

23          INPT       EXTERNAL FILE INPUT
                       29, 32, 35, 37, 38, 39, 40, 58, 60, 65
```

```
DCL NO.     IDENTIFIER                      ATTRIBUTES AND REFERENCES

********    IPK        AUTOMATIC ALIGNED BINARY FIXED(15,0)
                       99, 158, 158, 195, 195, 202, 227

********    ISMAX      AUTOMATIC ALIGNED BINARY FIXED(15,0)
                       94, 142, 154, 173, 179, 292

********    ISMIN      AUTOMATIC ALIGNED BINARY FIXED(15,0)
                       94, 136, 142, 179, 191, 291

********    ISUBF      AUTOMATIC ALIGNED BINARY FIXED(15,0)
                       95, 132, 143, 152, 169, 180, 189

4           ISUB1      AUTOMATIC ALIGNED BINARY FIXED(15,0)
                       92, 138, 150, 175, 187, 219, 244, 283, 289

4           ISUB2      AUTOMATIC ALIGNED BINARY FIXED(15,0)
                       93, 140, 177, 215, 220, 240, 245, 290

********    J          AUTOMATIC ALIGNED BINARY FIXED(15,0)
                       263, 265, 269, 270

********    JJ         AUTOMATIC ALIGNED BINARY FIXED(15,0)
                       55, 66, 66, 68

********    K          AUTOMATIC ALIGNED BINARY FIXED(15,0)
                       263, 265, 271, 271, 272

********    L          AUTOMATIC ALIGNED BINARY FIXED(15,0)
                       259, 260, 276, 278, 279, 279, 281, 282, 284, 284, 284, 284, 284, 285, 285, 285, 285, 285, 285,
                       285, 285, 285, 285, 286, 286, 286, 286, 286, 293

256         LABA       /* STATEMENT LABEL CONSTANT */
                       251
```

```
DCL NO.    IDENTIFIER           ATTRIBUTES AND REFERENCES

278        LABC      /* STATEMENT LABEL CONSTANT */
                     275

279        LABD      /* STATEMENT LABEL CONSTANT */
                     277

200        LAB1      /* STATEMENT LABEL CONSTANT */
                     107

225        LAB2      /* STATEMENT LABEL CONSTANT */
                     106

249        LAB3      /* STATEMENT LABEL CONSTANT */
                     224

297        LAB4      /* STATEMENT LABEL CONSTANT */
                     108, 122, 147, 184, 223, 248

302        LICAL     /* STATEMENT LABEL CONSTANT */


312        LICEND    /* STATEMENT LABEL CONSTANT */
                     304

13         LIM1      AUTOMATIC ALIGNED DECIMAL /* SINGLE */ FLOAT(6)
                     37, 82, 105, 116

13         LIM2      AUTOMATIC ALIGNED DECIMAL /* SINGLE */ FLOAT(6)
                     37, 82, 105, 115

75         LOOK      /* STATEMENT LABEL CONSTANT */


********   M         AUTOMATIC ALIGNED BINARY FIXED(15,0)
```

DCL NO.	IDENTIFIER	ATTRIBUTES AND REFERENCES
		205, 207, 230, 231, 251, 253, 256
********	MM	AUTOMATIC ALIGNED BINARY FIXED(15,0) 253, 257, 259
2	MP	(20) AUTOMATIC ALIGNED DECIMAL /* SINGLE */ FLOAT(6)
********	N	AUTOMATIC ALIGNED BINARY FIXED(15,0) 205, 206, 230, 232, 251, 252, 257
********	NN	AUTOMATIC ALIGNED BINARY FIXED(15,0) 252, 256, 259
********	P	AUTOMATIC ALIGNED DECIMAL /* SINGLE */ FLOAT(6) 264, 266, 266, 267, 274
106	PEAK	/* STATEMENT LABEL CONSTANT */ 104
********	PLIN	AUTOMATIC ALIGNED DECIMAL /* SINGLE */ FLOAT(6) 300, 306, 306, 313, 314, 315, 316, 325, 328
8	POINTS	AUTOMATIC ALIGNED BINARY FIXED(15,0) 37, 46, 46, 46, 46, 48, 48, 50, 57, 82, 103, 299, 302
********	PTAN	AUTOMATIC ALIGNED DECIMAL /* SINGLE */ FLOAT(6) 327, 331, 339, 345, 345
71	P1	/* STATEMENT LABEL CONSTANT */ 62, 68, 70, 73
74	P2	/* STATEMENT LABEL CONSTANT */ 27

```
DCL NO.     IDENTIFIER   ATTRIBUTES AND REFERENCES

8           Q            AUTOMATIC ALIGNED BINARY FIXED(15,0)
                         254, 258, 275

********    R            AUTOMATIC ALIGNED DECIMAL /* SINGLE */ FLOAT(6)
                         274, 276, 278

********    RADX         AUTOMATIC ALIGNED DECIMAL /* SINGLE */ FLOAT(6)
                         314, 317, 318, 329

********    RADZ         AUTOMATIC ALIGNED DECIMAL /* SINGLE */ FLOAT(6)
                         316, 321, 322, 330

********    REF          AUTOMATIC ALIGNED DECIMAL /* SINGLE */ FLOAT(6)
                         40, 42, 44, 47, 89, 332

32          REPEAT       /* STATEMENT LABEL CONSTANT */
                         26, 33

11          REX          (*) CONTROLLED ALIGNED DECIMAL /* SINGLE */ FLOAT(6)
                         43, 48

********    RTAN         AUTOMATIC ALIGNED DECIMAL /* SINGLE */ FLOAT(6)
                         339, 345, 345

12          RUN          EXTERNAL STATIC UNALIGNED CHARACTER(10)
                         35, 36

********    RXBAR        AUTOMATIC ALIGNED DECIMAL /* SINGLE */ FLOAT(6)
                         333, 343

********    RXRAD        AUTOMATIC ALIGNED DECIMAL /* SINGLE */ FLOAT(6)
                         335

********    RXRG         AUTOMATIC ALIGNED DECIMAL /* SINGLE */ FLOAT(6)
```

DCL NO.	IDENTIFIER	ATTRIBUTES AND REFERENCES
		336
11	RZ	(*) CONTROLLED ALIGNED DECIMAL /* SINGLE */ FLOAT(6) 43, 48
********	RZBAR	AUTOMATIC ALIGNED DECIMAL /* SINGLE */ FLOAT(6) 334, 344
********	RZRAD	AUTOMATIC ALIGNED DECIMAL /* SINGLE */ FLOAT(6) 337
********	RZRG	AUTOMATIC ALIGNED DECIMAL /* SINGLE */ FLOAT(6) 338
********	S	AUTOMATIC ALIGNED DECIMAL /* SINGLE */ FLOAT(6) 267, 268, 268, 269, 270
********	SIN	BUILTIN 267
157	SMAX	/* STATEMENT LABEL CONSTANT */ 132, 133, 134
194	SMIN	/* STATEMENT LABEL CONSTANT */ 169, 170, 171
********	SQRT	BUILTIN 262, 305, 317, 320, 321, 324, 346
8	START	AUTOMATIC ALIGNED BINARY FIXED(15,0) 38, 84, 102, 146, 183, 210, 210, 213, 216, 216, 221, 235, 235, 238, 241, 241, 246, 276, 278
53	STCAL	/* STATEMENT LABEL CONSTANT */

```
DCL NO.    IDENTIFIER                 ATTRIBUTES AND REFERENCES

********   SUBMAX    AUTOMATIC ALIGNED DECIMAL /* SINGLE */ FLOAT(6)
                     135, 136, 137, 149, 153

********   SUBMIN    AUTOMATIC ALIGNED DECIMAL /* SINGLE */ FLOAT(6)
                     172, 173, 174, 186, 190

********   SYSIN     EXTERNAL FILE
                     27, 71

********   SYSPRINT  EXTERNAL FILE STREAM OUTPUT PRINT
                     31, 36, 63, 64, 67, 78, 79, 82, 83, 84, 85, 86, 87, 88, 89, 137, 138, 153, 174, 175, 190, 204,
                     213, 221, 229, 238, 246, 293, 298, 299, 328, 329, 330, 331, 340, 348, 349

8          T         AUTOMATIC ALIGNED BINARY FIXED(15,0)
                     57, 58, 58, 299, 299, 299, 299, 302, 303, 303, 303, 303, 307, 307, 308, 308, 309, 309, 310, 310,
                     311, 311, 311, 311

21         TEST      DEFINED CARD POSITION(1) UNALIGNED CHARACTER(9)
                     77

10         V         (*) CONTROLLED ALIGNED DECIMAL /* SINGLE */ FLOAT(6)
                     46, 58, 106, 106, 106, 106, 107, 107, 107, 107, 111, 111, 111, 111, 111, 111, 111, 203, 228, 260,
                     350

17         VAV       (*) CONTROLLED ALIGNED DECIMAL /* SINGLE */ FLOAT(6)
                     52, 111, 123, 123, 123, 123, 124, 124, 124, 124, 128, 128, 128, 128, 130, 130, 130, 130, 135, 157
                     165, 165, 165, 165, 167, 167, 167, 167, 172, 194, 350

29         VDATA     /* STATEMENT LABEL CONSTANT */
                     351

********   VMAX      AUTOMATIC ALIGNED DECIMAL /* SINGLE */ FLOAT(6)
                     135, 157, 160, 172, 197, 228, 229, 249, 250, 260
```

```
DCL NO.    ICENTIFIER           ATTRIBUTES AND REFERENCES

********   VMIN      AUTOMATIC ALIGNED DECIMAL /* SINGLE */ FLOAT(6)
                     135, 135, 160, 172, 172, 194, 197, 203, 204, 249, 250, 260, 260

10         VX        (*) CONTROLLED ALIGNED DECIMAL /* SINGLE */ FLOAT(6)
                     46, 58, 105, 105, 115, 116, 133, 134, 170, 171, 279, 281, 282, 350

********   W         AUTOMATIC ALIGNED DECIMAL /* SINGLE */ FLOAT(6)
                     100, 141, 178, 209, 218, 234, 243, 276, 278, 280

********   WIDTH     AUTOMATIC ALIGNED DECIMAL /* SINGLE */ FLOAT(6)
                     54, 86, 279

********   WIDTHA    AUTOMATIC ALIGNED DECIMAL /* SINGLE */ FLOAT(6)
                     38, 54

********   XBAR      AUTOMATIC ALIGNED DECIMAL /* SINGLE */ FLOAT(6)
                     313, 318, 326, 328, 333, 343

********   XLIM1     AUTOMATIC ALIGNED DECIMAL /* SINGLE */ FLOAT(6)
                     39, 88, 134, 171, 281

********   XLIM2     AUTOMATIC ALIGNED DECIMAL /* SINGLE */ FLOAT(6)
                     39, 88, 133, 170, 282

********   XMAX      AUTOMATIC ALIGNED DECIMAL /* SINGLE */ FLOAT(6)
                     38, 85, 279, 279

********   XMIN      AUTOMATIC ALIGNED DECIMAL /* SINGLE */ FLOAT(6)
                     38, 85, 279

********   XM1       AUTOMATIC ALIGNED DECIMAL /* SINGLE */ FLOAT(6)
                     301, 307, 307, 313

********   XM2       AUTOMATIC ALIGNED DECIMAL /* SINGLE */ FLOAT(6)
```

```
DCL NO.     IDENTIFIER                        ATTRIBUTES AND REFERENCES

                        301, 308, 308, 314

********    XRAD        AUTOMATIC ALIGNED DECIMAL /* SINGLE */ FLOAT(6)
                        317, 329, 335

********    XRG         AUTOMATIC ALIGNED DECIMAL /* SINGLE */ FLOAT(6)
                        320, 327, 329, 336

********    XROOT       AUTOMATIC ALIGNED DECIMAL /* SINGLE */ FLOAT(6)
                        318, 319, 319, 319, 320

********    XSHIFT      AUTOMATIC ALIGNED DECIMAL /* SINGLE */ FLOAT(6)
                        343, 348

7           Y           AUTOMATIC ALIGNED BINARY FIXED(15,0)
                        19, 87, 276, 278

********    YEW         AUTOMATIC ALIGNED DECIMAL /* SINGLE */ FLOAT(6)
                        265, 266

10          Z           (*) CONTROLLED ALIGNED DECIMAL /* SINGLE */ FLOAT(6)
                        46, 56, 276, 278, 285, 285, 285, 285, 285, 299, 303, 303, 309, 309, 310, 310, 311, 311, 350

********    ZBAR        AUTOMATIC ALIGNED DECIMAL /* SINGLE */ FLOAT(6)
                        315, 322, 326, 328, 334, 344

********    ZM1         AUTOMATIC ALIGNED DECIMAL /* SINGLE */ FLOAT(6)
                        301, 309, 309, 315

********    ZM2         AUTOMATIC ALIGNED DECIMAL /* SINGLE */ FLOAT(6)
                        301, 310, 310, 316

********    ZRAD        AUTOMATIC ALIGNED DECIMAL /* SINGLE */ FLOAT(6)
                        321, 330, 337
```

DCL NO.	IDENTIFIER	ATTRIBUTES AND REFERENCES
********	ZRG	AUTOMATIC ALIGNED DECIMAL /* SINGLE */ FLOAT(6) 324, 327, 330, 338
********	ZROOT	AUTOMATIC ALIGNED DECIMAL /* SINGLE */ FLOAT(6) 322, 323, 323, 323, 324
********	ZSHIFT	AUTOMATIC ALIGNED DECIMAL /* SINGLE */ FLOAT(6) 344, 348

AGGREGATE-LENGTH TABLE

DCL. NO.	IDENTIFIER	LVL	DIM	OFFSET	EL. LGTH.	TOT. LGTH.
18	CARDST	1	1		80	2400
10	EX	1	1		4	A
46	EX	1	1		4	A
2	MP	1	1		4	80
11	REX	1	1		4	A
48	REX	1	1		4	A
11	RZ	1	1		4	A
48	RZ	1	1		4	A
10	V	1	1		4	A
46	V	1	1		4	A
17	VAV	1	1		4	A
52	VAV	1	1		4	A
10	VX	1	1		4	A
46	VX	1	1		4	A
10	Z	1	1		4	A
46	Z	1	1		4	A

DCL. NO.	IDENTIFIER	LVL	DIM	OFFSET	EL. LGTH.	TOT. LGTH.

SUM OF CONSTANT LENGTHS 2480

STORAGE REQUIREMENTS

BLOCK, SECTION OR STATEMENT	TYPE	BLOCK LENGTH	(HEX)	DSA SIZE	(HEX)
HOLO	PROCEDURE BLOCK			2520	9D8
26	ON UNIT			488	1E8
27	ON UNIT			488	1E8
HOLO	DICTIONARY	11452	2CBC		
HOLO	LINK EDIT STUB	320	140		
HOLO	STATIC INTERNAL	728	2D8		

```
COMPILER DIAGNOSTIC MESSAGES PRODUCED FOR THIS COMPILATION

ERROR ID L   STMT    MESSAGE DESCRIPTION


WARNING DIAGNOSTICS


IEN0023I W   31, 36, 63, 64, 67, 78, 79, 82, 83, 84, 85, 86, 87, 88, 89, 137, 138, 153, 174, 175, 190, 204, 213, 221,
                     229, 238, 246, 293, 298, 299, 328, 329, 330, 331, 340, 348, 349   NO 'FILE' OR 'STRING' OPTION
                     SPECIFIED FOR 'PUT' STATEMENT. 'FILE(SYSPRINT)' ASSUMED.

IEN0022I W   71      NO 'FILE' OR 'STRING' OPTION SPECIFIED FOR 'GET' STATEMENT. 'FILE(SYSIN)' ASSUMED.


END OF COMPILER DIAGNOSTIC MESSAGES


TRANSLATE TIME          0.13 MINS
```

TOTAL TIME 0.13 MINS

****
****
****

```
STMT LEVEL NEST

                                /* APPENDIX TWO:  SIMULATED CONTOUR SHAPE FITTING */
  1              SIMCAL   : PROC OPTIONS (MAIN)  ;                                          A040S749
  2     1                   DCL X(250),RY1(250),RY2(250),PY1(250),PX2(250)  ;                A060S749
  3     1                   DCL PX1(250),PY2(250),YD(250),RDX1(250),RDX2(250)  ;             A080S749
  4     1                   DCL EX(250),EY1(250),EY2(250)  ;                                 A100S749
  5     1                   DCL PYA(250),XA(250),XB(250) ;                                   A120S749
  6     1                   DCL (U,T) FIXED BINARY  ;                                        A140S749
  7     1                   DCL R FIXED BINARY  ;                                            A145S749
  8     1                   KK = 0  ;                                                        A150S749
  9     1        DATA     : GET EDIT (A,B,P,Q)(X(14),F(6,4),X(14),F(6,4),X(14),F(6,4),       A160S749
                            X(14),F(6,4))  ;                                                 A170S749
 10     1                   GET EDIT (SR,TR,AL)(X(14),F(6,4),X(14),F(6,4),X(34),F(6,5));A180S749
                            /* INPUT & DISTORTION PARAMETERS OF THE ELLIPSE */               A190S749
 11     1                   PUT EDIT ('INPUT PARAMETERS','A =',A,'B =',B,'P =',P,            A200S749
                            'Q =',Q,'SHIFT PARAMETERS ','X DIRECTION SR =',SR,               A220S749
                            'Y DIRECTION TR =',TR)(PAGE,SKIP(5),X(30),A,SKIP,X(10),          A240S749
                            A,F(9,5),X(20),A,F(9,5),SKIP(3),X(10),A,F(9,5),X(20),            A260S749
                            A,F(9,5),SKIP(5),X(20),A,SKIP(2),X(10),A,F(9,5),X(20),A,         A280S749
                            F(9,5)) ;                                                        A300S749
 12     1                   PUT EDIT('ANGLE OF ROTATION =',AL)(SKIP(2),X(10),A,F(9,5)); A301S749
 13     1                   BL = 57.3066*AL  ;                                               A320S749
 14     1                   PUT EDIT ('ANGLE OF ROTATION IN DEGREES =',BL)                   A340S749
                            (SKIP(2),X(10),A,F(9,5)) ;                                       A360S749
 15     1                   ZX = P*COS(AL) - Q*SIN(AL)  ;                                    A400S749
 16     1                   ZY = P*SIN(AL) + Q*COS(AL)  ;                                    A410S749
 17     1                   SR = P - ZX + SR  ;                                              A420S749
 18     1                   TR = Q - ZY + TR  ;                                              A430S749
 19     1                   PUT EDIT ('SR =',SR,'TR =',TR)(SKIP(2),X(10),A,F(9,5),           A440S749
                            X(30),A,F(9,5))  ;                                               A450S749
                            /* TO CALCULATE REFERENCE AND PRODUCTON  SHAPE  */               B020S749
 20     1                   I = 0  ;                                                         B025S749
 21     1        SCAL     : DO XK = 0 TO 2.00 BY .01  ;                                      B030S749
 22     1    1              I = I + 1  ;                                                     B035S749
 23     1    1              X(I) = XK  ;                                                     B040S749
 24     1    1              AA =(1 -((X(I)-P)/A)**2)  ;                                      B060S749
 25     1    1              IF AA < 0 THEN GO TO SCEND  ;                                    B080S749
```

```
STMT LEVEL NEST
                              /* APPENDIX TWO:  SIMULATED CONTOUR SHAPE FITTING */
  1               SIMCAL    : PROC OPTIONS (MAIN)  ;                                        A040S749
  2     1                     DCL X(250),RY1(250),RY2(250),PY1(250),PX2(250)  ;             A060S749
  3     1                     DCL PX1(250),PY2(250),YD(250),RDX1(250),RDX2(250)  ;          A080S749
  4     1                     DCL EX(250),EY1(250),EY2(250)  ;                              A100S749
  5     1                     DCL PYA(250),XA(250),XB(250) ;                                A120S749
  6     1                     DCL (U,T) FIXED BINARY  ;                                     A140S749
  7     1                     DCL R FIXED BINARY  ;                                         A145S749
  8     1                     KK = 0  ;                                                     A150S749
  9     1         DATA      : GET EDIT (A,B,P,Q)(X(14),F(6,4),X(14),F(6,4),X(14),F(6,4),    A160S749
                              X(14),F(6,4))  ;                                              A170S749
 10     1                     GET EDIT (SR,TR,AL)(X(14),F(6,4),X(14),F(6,4),X(34),F(6,5));A180S749
                              /* INPUT & DISTORTION PARAMETERS OF THE ELLIPSE */            A190S749
 11     1                     PUT EDIT ('INPUT PARAMETERS','A =',A,'B =',B,'P =',P,         A200S749
                              'Q =',Q,'SHIFT PARAMETERS ','X DIRECTION SR =',SR,            A220S749
                              'Y DIRECTION TR =',TR)(PAGE,SKIP(5),X(30),A,SKIP,X(10),       A240S749
                              A,F(9,5),X(20),A,F(9,5),SKIP(3),X(10),A,F(9,5),X(20),         A260S749
                              A,F(9,5),SKIP(5),X(20),A,SKIP(2),X(10),A,F(9,5),X(20),A,      A280S749
                              F(9,5)) ;                                                     A300S749
 12     1                     PUT EDIT('ANGLE OF ROTATION =',AL)(SKIP(2),X(10),A,F(9,5)); A301S749
 13     1                     BL = 57.3066*AL  ;                                            A320S749
 14     1                     PUT EDIT ('ANGLE OF ROTATION IN DEGREES =',BL)                A340S749
                              (SKIP(2),X(10),A,F(9,5)) ;                                    A360S749
 15     1                     ZX = P*COS(AL) - Q*SIN(AL)  ;                                 A400S749
 16     1                     ZY = P*SIN(AL) + Q*COS(AL)  ;                                 A410S749
 17     1                     SR = P - ZX + SR  ;                                           A420S749
 18     1                     TR = Q - ZY + TR  ;                                           A430S749
 19     1                     PUT EDIT ('SR =',SR,'TR =',TR)(SKIP(2),X(10),A,F(9,5),        A440S749
                              X(30),A,F(9,5))  ;                                            A450S749
                              /* TO CALCULATE REFERENCE AND PRODUCTON  SHAPE  */            B020S749
 20     1                     I = 0  ;                                                      B025S749
 21     1         SCAL      : DO XK = 0 TO 2.00 BY .01  ;                                   B030S749
 22     1     1               I = I + 1  ;                                                  B035S749
 23     1     1               X(I) = XK  ;                                                  B040S749
 24     1     1               AA =(1 -((X(I)-P)/A)**2)  ;                                   B060S749
 25     1     1               IF AA < 0 THEN GO TO SCEND  ;                                 B080S749
```

```
STMT LEVEL NEST

 53     1     1              RYM1 = RYM1 + (.5*DS*(RY2(R)+RY2(R+1)))   ;                     K220S749
 54     1     1              RYM2 = RYM2 +( .25*DS*(RY2(R)+RY2(R+1))**2)   ;                 K240S749
 55     1     1              RH1 = RH1 + (.25*DS*(X(R+1)+X(R))*(RY2(R)+RY2(R+1))) ;          K260S749
 56     1     1              PDSQ = (PX2(R+1)-PX2(R))**2 + (PY2(R+1)-PY2(R))**2  ;           K300S749
 57     1     1              IF PDSQ = 0 THEN GO TO LICEND  ;                                K320S749
 59     1     1              PDS = SQRT(PDSQ)  ;                                             K340S749
 60     1     1              PLIN = PLIN + PDS  ;                                            K360S749
 61     1     1              PXM1 =PXM1 + (.5*PDS*(PX2(R+1)+PX2(R))) ;                       K380S749
 62     1     1              PXM2 =PXM2 + (.25*PDS*(PX2(R+1)+PX2(R))**2)  ;                  K400S749
 63     1     1              PYM1 =PYM1 +(.5*PDS*(PY2(R+1)+PY2(R))) ;                        K420S749
 64     1     1              PYM2 =PYM2 + (.25*PDS*(PY2(R+1)+PY2(R))**2)  ;                  K440S749
 65     1     1              PH1 = PH1 +(.25*DS*(PX2(R+1)+PX2(R))*(PY2(R+1)+PY2(R))) ;       K450S749
 66     1     1    LICEND  : END LICAL  ;                                                    K460S749
 67     1                    RLXB = RXM1/RLIN  ;                                             K500S749
 68     1                    RXAD = RXM2/RLIN  ;                                             K520S749
 69     1                    RLYB = RYM1/RLIN  ;                                             K540S749
 70     1                    RYAD = RYM2/RLIN  ;                                             K560S749
 71     1                    XRADL = SQRT(RXAD)  ;                                           K580S749
 72     1                    XRG = SQRT(RXAD-RLXB**2)  ;                                     K600S749
 73     1                    YRADL = SQRT(RYAD)  ;                                           K620S749
 74     1                    YRG = SQRT(RYAD-RLYB**2)  ;                                     K640S749
 75     1                    RHXY = RH1/RLIN  ;                                              K642S749
 76     1                    RHBAR = (RHXY - RLXB*RLYB)  ;                                   K644S749
 77     1                    RTAN2 = 2*RHBAR/(XRG**2-YRG**2)  ;                              K646S749
 78     1                    PUT EDIT ('REF LINE','LENGTH =',RLIN,'XBAR =',RLXB,             K660S749
                             'YBAR =',RLYB)(PAGE,SKIP(10),X(20),A,SKIP,X(10),A,F(9,5),       K680S749
                             X(20),A,F(9,5),X(20),A,F(9,5)) ;                                K700S749
 79     1                    PUT EDIT ('RAD OF G X SQ =',RXAD,'XRADL =',XRADL,               K720S749
                             'XRG =',XRG)(SKIP(5),X(10),A,F(9,5),X(20),A,F(9,5),X(20),       K740S749
                             A,F(9,5)) ;                                                     K760S749
 80     1                    PUT EDIT ('RAD OF G Y SQ =',RYAD,'YRADL =',YRADL,               K780S749
                             'YRG =',YRG)(SKIP(2),X(10),A,F(9,5),X(20),A,F(9,5),X(20),       K800S749
                             A,F(9,5)) ;                                                     K820S749
 81     1                    PUT EDIT ('CROSS PRODUCT RHXY =',RHXY,'RHBAR =',RHBAR,          K830S749
```

```
STMT LEVEL NEST

                  'TWICE ANGLE TAN-1 =',RTAN)(SKIP(5),X(10),A,F(9,5),X(20),   K832S749
                  A,F(9,5),SKIP,X(10),A,F(9,5)) ;                             K834S749
 82     1         PLXB = PXM1/PLIN  ;                                         L020S749
 83     1         PXAD = PXM2/PLIN  ;                                         L040S749
 84     1         PLYB = PYM1/PLIN  ;                                         L060S749
 85     1         PYAD = PYM2/PLIN  ;                                         L080S749
 86     1         XPADL = SQRT(PXAD)  ;                                       L100S749
 87     1         XPG = SQRT(PXAD - PLXB**2)  ;                               L120S749
 88     1         YPADL = SQRT(PYAD)  ;                                       L140S749
 89     1         YPG = SQRT(PYAD - PLYB**2)  ;                               L160S749
 90     1         PHXY = PH1 / PLIN  ;                                        L166S749
 91     1         PHBAR = (PHXY - PLXB*PLYB)  ;                               L168S749
 92     1         PTAN2 = 2*PHBAR/(XPG**2-YPG**2)  ;                          L170S749
 93     1         PUT EDIT ('PROD LINE','LENGTH =',PLIN,'PXBAR =',PLXB,       L180S749
                  'PYBAR =',PLYB)(PAGE,SKIP(10),X(20),A,SKIP,X(10),A,F(9,5),  L200S749
                  X(20),A,F(9,5),X(20),A,F(9,5)) ;                            L220S749
 94     1         PUT EDIT ('RAD OF G Y SQ =',PXAD,'XPADL =',XPADL,           L240S749
                  'XPG =',XPG)(SKIP(5),X(10),A,F(9,5),X(20),A,F(9,5),X(20),   L280S749
                  A,F(9,5)) ;                                                 L300S749
 95     1         PUT EDIT ('RAD OF G YSQ =',PYAD,'YPADL =',YPADL,'YPG =',YPG)L320S749
                  (SKIP,X(10),A,F(9,5),X(20),A,F(9,5),X(20),A,F(9,5)) ;       L340S749
 96     1         PUT EDIT ('CROSS PRODUCT PHXY =',PHXY,'PHBAR =',PHBAR,      L360S749
                  'TWICE ANGLE TAN-1 =',PTAN2)(SKIP(5),X(10),A,F(9,5),X(20),  L370S749
                  A,F(9,5),SKIP,X(10),A,F(9,5)) ;                             L380S749
                  /* TO CALCULATE OVERALL DIFFERENCES */                      L400S749
 97     1         XSHIFT = PLXB-RLXB  ;                                       L500S749
 98     1         YSHIFT = PLYB-RLYB  ;                                       L520S749
 99     1         DFTN  = (PTAN2-RTAN2)/(1+PTAN2*RTAN2)  ;                    L590S749
100     1         DFT = SQRT(1+1/(DFTN**2))-1/DFTN  ;                         L592S749
101     1         DANGL = 57.3066*DFT  ;                                      L594S749
102     1         PUT EDIT ('LINE CENTROID') (SKIP(4),X(20),A) ;              L596S749
103     1         PUT EDIT ('SHIFT PARAMETERS','XSHIFT =',XSHIFT,'YSHIFT =',  L600S749
                  YSHIFT)(SKIP(2),X(20),A,SKIP,X(10),A,F(9,5),X(20),A,F(9,5));L640S749
104     1         PUT EDIT ('ANGULAR DIFFERENCE IN DEGREES =',DANGL)(SKIP(5), L680S749
```

```
STMT LEVEL NEST

                          X(10),A,F(9,5)) ;                                          L700S749
 105      1               PP = RLXB - RLXB*COSD(DANGL) + RLYB*SIND(DANGL) ;          L800S749
 106      1               QQ = RLYB - RLXB*SIND(DANGL) - RLYB*COSD(DANGL) ;          L820S749
 107      1               XIN = P*COSD(DANGL) - Q*SIND(DANGL) + PP ;                 L840S749
 108      1               YIN = P*SIND(DANGL) + Q*COSD(DANGL) + QQ ;                 L850S749
 109      1               CXSH = XIN + XSHIFT - P ;                                  L860S749
 110      1               CYSH = YIN + YSHIFT - Q ;                                  L880S749
 111      1               PUT EDIT ('EFFECTIVE SHIFT OF SECTIONAL CENTROID',         L890S749
                          'XSHIFT = ',CXSH,'YSHIFT =',CYSH)                          L900S749
                          (SKIP(2),X(10),A,SKIP,X(10),A,F(9,5),X(20),A,F(9,5)) ;     L910S749
                          /* SHAPE FITTING BETWEEN REF & PROD:  COMPLETE SECTIONS */ B400S749
 112      1               IF KK = 1 THEN GO TO PROCAL  ;                             B450S749
                          /* TO CALCULATE MNTS ONREF OBJECT DX ELEMENTS  */          B500S749
 114      1               RAREA,RMNT1,RMNT2 = 0  ;                                   B520S749
 115      1               XRXY = 0  ;                                                B530S749
 116      1               DO IA = 1 TO 200  ;                                        B540S749
 117      1    1          DELR = ((RY2(IA)+RY2(IA+1)) - (RY1(IA)+RY1(IA+1)))*.005  ; B560S749
 118      1    1          RAREA = RAREA + DELR  ;                                    B580S749
 119      1    1          RMNT1 = RMNT1 + (DELR*(X(IA)+.005))  ;                     B600S749
 120      1    1          RMNT2 = RMNT2 + (DELR*((X(IA)+.005)**2)) ;                 B620S749
 121      1    1          XRXY = XRXY + (.5*DELR*(X(IA)+.005)*(RY2(IA)+RY1(IA))) ;   B630S749
 122      1    1          END  ;                                                     B640S749
 123      1               XBAR = RMNT1/RAREA  ;                                      B660S749
 124      1               RAD2 = RMNT2/RAREA  ;                                      B680S749
 125      1               XRAD2 = SQRT(RAD2)  ;                                      B700S749
 126      1               XRADG = SQRT(RAD2 - XBAR**2)  ;                            B720S749
 127      1               XR = XRXY/RAREA  ;                                         B720S749
 128      1               PUT EDIT ('ELLIPSE SECTIONS: SHIFT PARAMETER CALCULATIONS') B730S749
                          (PAGE,SKIP(3),X(30),A) ;                                   B735S749
 129      1               PUT EDIT ('SURFACE AREA =',RAREA,'C OF G XBAR =',XBAR,     B740S749
                          'RAD OF G SQ =',RAD2,'XRAD2 =',XRAD2,'XRADG =',XRADG)      B760S749
                               (SKIP(5),X(10),A,F(9,5),SKIP(2),X(10),A,F(9,5),       B780S749
                          SKIP(2),A,F(9,5),X(20),A,F(9,5),X(10),A,F(9,5))  ;         B800S749
 130      1               PUT EDIT ('CROSS PRODUCT =',XR)(SKIP(2),X(10),A,F(9,5)) ;  B820S749
```

```
STMT LEVEL NEST

                                /*  TO CALCULATE MNTS ON REF OBJECT: DY ELEMENTS  */          C010S749
131     1                       IB = 0  ;                                                    C024S749
132     1          DYCAL      : DO XL = .2 TO 1.00 BY .005  ;                                C030S749
133     1     1                 IB = IB + 1  ;                                               C040S749
134     1     1                 YD(IB) = XL  ;                                               C050S749
135     1     1                 DA = (1-((YD(IB)-Q)/B)**2)  ;                                C060S749
136     1     1                 IF DA = 0 THEN DO  ;                                         C070S749
138     1     2                 GO TO DYEND  ;                                               C090S749
139     1     2                 END  ;                                                       C096S749
140     1     1                 IF DA < 0 THEN DA = -DA  ;                                   C098S749
142     1     1                 DROOT = A*SQRT(DA)  ;                                        C120S749
143     1     1                 RDX1(IB) = P - DROOT  ;                                      C140S749
144     1     1                 RDX2(IB) = P + DROOT  ;                                      C160S749
145     1     1    DYEND      : END DYCAL  ;                                                 C180S749
146     1                       YRAR,YRMNT1,YRMNT2 = 0  ;                                    C200S749
147     1                       YRXY = 0  ;                                                  C210S749
148     1          YELA       : DO IC = 1 TO 160  ;                                          C220S749
149     1     1                 YEL = (RDX2(IC)+RDX2(IC+1)-RDX1(IC)-RDX1(IC+1)) ;            C224S749
150     1     1                 IF YEL = 0 THEN DO  ;                                        C226S749
152     1     2                 PUT EDIT ('YEL = 0 IC =',IC)(SKIP,X(10),A,F(4,0)) ;          C228S749
153     1     2                 GO TO YELEND  ;                                              C230S749
154     1     2                 END  ;                                                       C231S749
155     1     1                 YDELR = .0025*YEL  ;                                         C240S749
156     1     1                 YRAR  = YRAR + YDELR  ;                                      C260S749
157     1     1                 YRMNT1 = YRMNT1 + (YDELR*(YD(IC)+.0025)) ;                   C280S749
158     1     1                 YRMNT2 = YRMNT2 + (YDELR*((YD(IC)+.0025)**2)) ;              C300S749
159     1     1                 YRXY = YRXY +(.5*YDELR*(YD(IC)+.0025)*(RDX2(IC)+RDX1(IC))); C305S749
160     1     1    YELEND     : END YELA  ;                                                  C320S749
161     1                       YBAR  = YRMNT1/YRAR  ;                                       C340S749
162     1                       RYD2 = YRMNT2/YRAR  ;                                        C360S749
163     1                       YRAD2 = SQRT(RYD2)  ;                                        C380S749
164     1                       YRADG = SQRT(RYD2 - YBAR**2)  ;                              C400S749
165     1                       YR = YRXY/YRAR  ;                                            C410S749
166     1                       RHB = (XR - XBAR*YBAR)  ;                                    C410S749
```

```
STMT LEVEL NEST

 167    1                   RT2 = 2*RHB/(XRADG**2-YRADG**2)  ;                                  C412S749
 168    1                   PUT EDIT ('DY ELEMENTS AREA =',YRAR,'C OF G YBAR',YBAR,             C420S749
                            'RAD OF G SQ =',RYD2,'YRAD2 =',YRAD2,'YRADG =',YRADG)               C440S749
                            (SKIP(9),X(10),A,F(9,5),SKIP,X(10),A,F(9,5),X(10),A,F(9,5),         C460S749
                            SKIP,X(10),A,F(9,5),X(20),A,F(9,5))  ;                              C480S749
 169    1                   PUT EDIT ('TWICE ANGLE OF PRINCIPAL AXIS =',RT2) (SKIP(5),          C490S749
                            X(10),A,F(9,5)) ;                                                   C500S749
 170    1                   PUT EDIT ('CROSS PRODUCT =',YR)(SKIP(2),X(10),A,F(9,5)) ;           C520S749
                            /* PRODUCTION COMPONENT   */                                        D020S749
                            /* TO CALCULATE MNTS  */                                            D025S749
 171    1         PROCAL  : KK = 1  ;                                                           D030S749
                            /* DX ELEMENTS  */                                                  D040S749
 172    1                   CMIN = 9  ;                                                         D042S749
 173    1                   CMAX = 0  ;                                                         D043S749
 174    1                   DO MM = 1 TO 199 BY 3  ;                                            D045S749
 175    1     1             IF MM > 190 THEN GO TO MAXI  ;                                      D045S749
 177    1     1             XMIN = MIN(PX1(MM),PX1(MM+1),PX1(MM+2),CMIN)  ;                     D046S749
 178    1     1             CMIN = XMIN  ;                                                      D048S749
 179    1     1   MAXI    : XMAX = MAX(PX1(MM),PX1(MM+1),PX1(MM+2),CMAX)  ;                     D047S749
 180    1     1             CMAX = XMAX  ;                                                      D049S749
 181    1     1             END  ;                                                              D050S749
 182    1                   L = 0  ;                                                            D055S749
 183    1                   PARX,PMNT1,PMNT2 = 0  ;                                             D060S749
 184    1                   PYMT1,PYMT2,XPXY = 0 ;                                              D070S749
 185    1         PDX     : DO XX = XMIN TO XMAX BY .01  ;                                      D080S749
 186    1     1             L = L + 1  ;                                                        D090S749
 187    1     1             EX(L)  = XX  ;                                                      D100S749
 188    1     1             K,U =1  ;                                                           D120S749
 189    1     1   LOP1    : IF PX1(U) < EX(L) & PX1(U+1) > EX(L) THEN GO TO DCAL ;              D140S749
 191    1     1             U = U + 1  ;                                                        D160S749
 192    1     1             IF U >= 202 THEN GO TO PDXEND  ;                                    D180S749
 194    1     1             GO TO LOP1  ;                                                       D200S749
 195    1     1   DCAL    : IF (PX1(U)-PX1(U-1)) = 0 THEN GO TO PDXEND  ;                       D220S749
 197    1     1             EY1(L) = PY1(U)-((PX1(U)-EX(L))*(PY1(U)-PY1(U-1))/                  D240S749
```

```
STMT LEVEL NEST

                                  (PX1(U)-PX1(U-1)))  ;                                        D260S749
198     1     1     LOP2       : IF PX2(K) < EX(L) & PX2(K+1) > EX(L) THEN GO TO FCAL  ;       D280S749
200     1     1                  K = K+1  ;                                                    D300S749
201     1     1                  IF K >200 THEN GO TO PDXEND  ;                                D320S749
203     1     1                  GO TO LOP2  ;                                                 D340S749
204     1     1     FCAL       : IF (PX2(K) - PX2(K-1)) = 0 THEN GO TO PDXEND  ;               D360S749
206     1     1                  EY2(L) = PY2(K) - ((PX2(K)-EX(L))*(PY2(K)-PY2(K-1))/          D380S749
                                 (PX2(K)-PX2(K-1)))  ;                                         D400S749
207     1     1                  IF L = 2 THEN GO TO PDXEND ;                                  D420S749
209     1     1                  PXDEL = ((EY2(L)+EY2(L-1))-(EY1(L)+EY1(L-1)))*.005  ;         D440S749
210     1     1                  PARX = PARX + PXDEL  ;                                        D460S749
211     1     1                  PMNT1 = PMNT1 + (PXDEL*(EX(L)-.005)) ;                        D480S749
212     1     1                  PMNT2 = PMNT2 + (PXDEL*(EX(L)-.005)**2) ;                     D500S749
213     1     1                  XPXY = XPXY + (.5*PXDEL*(EX(L)-.005)*(EY2(L)+EY1(L))) ;       D505S749
214     1     1     PDXEND     : END PDX  ;                                                    D520S749
215     1                        XPBAR = PMNT1/PARX  ;                                         D540S749
216     1                        PRAD2 = PMNT2/PARX  ;                                         D560S749
217     1                        XRAD = SQRT(PRAD2)  ;                                         D580S749
218     1                        XPADG = SQRT(PRAD2-XPBAR**2)  ;                               D600S749
219     1                        XP = XPXY/PARX ;                                              D620S749
220     1                        PUT EDIT ('PRODUCTION SHAPE DX ELEMENTS ','AREA =',PARX,      D640S749
                                 'C OF G =',XPBAR,'RAD2 =',PRAD2,'R OG G =',XRAD,'XPADG =',    D660S749
                                 XPADG )(PAGE,SKIP(5),X(10),A,SKIP(2),X(10),A,F(9,5),X(20),    D680S749
                                 A,F(9,5),SKIP,X(10),A,F(9,5),X(10),A,F(9,5),X(10),A,F(9,5));D700S749
221     1                        PUT EDIT ('CROSSPRODUCT =',XP)(SKIP(2),X(10),A,F(9,5)) ;      D800S749
                                 /* PRODUCTION SURFACE  */                                     E020S749
                                 /* DY ELEMENTS  */                                            E040S749
222     1                        AMIN = 9  ;                                                   E060S749
223     1                        AMAX,BMAX = 0  ;                                              E065S749
224     1                        DO M = 1 TO 199 BY 3  ;                                       E070S749
225     1     1                  IF M >190 THEN GO TO Y1M  ;                                   E072S749
227     1     1                  YMIN = MIN(PY1(M),PY1(M+1),PY1(M+2),AMIN)  ;                  E075S749
228     1     1                  AMIN = YMIN  ;                                                E086S749
229     1     1     Y1M        : Y1MAX = MAX(PY1(M),PY1(M+1),PY1(M+2),AMAX )  ;                E080S749
```

```
STMT LEVEL NEST

 230     1    1                    YMAX = MAX(PY2(M),PY2(M+1),PY2(M+2),BMAX )  ;              E085S749
 231     1    1                    AMAX = Y1MAX  ;                                            E087S749
 232     1    1                    BMAX = YMAX  ;                                             E088S749
 233     1    1                    END  ;                                                     E089S749
 234     1                         J = 0 ;                                                    E100S749
 235     1                         PARY,PYMT1,PYMT2 =0  ;                                     E110S749
 236     1                         YPXY = 0  ;                                                E115S749
 237     1         YCAL          : DO PYE = YMIN TO (YMAX+.005) BY .005  ;                    E200S749
 238     1    1                    J = J+1  ;                                                 E220S749
 239     1    1                    PYA(J) = PYE + .0001  ;                                    E240S749
 240     1    1                    KA,KB = 1  ;                                               E260S749
 241     1    1                    ISHIFT,JSHIFT = 0  ;                                       E280S749
 242     1    1                    IF PYA(J) > Y1MAX THEN GO TO TLOP  ;                       E290S749
 244     1    1    SLOP          : IF PY1(KA) < PYA(J) & PY1(KA+1) >PYA(J) THEN GO TO MCAL  ;  E300S749
 246     1    1                    IF PY1(KA) > PYA(J) & PY1(KA+1) < PYA(J) THEN GO TO MCAL  ; E310S749
 248     1    1                    KA = KA + 1  ;                                             E320S749
 249     1    1                    IF KA > 200 & ISHIFT = 1 THEN GO TO PCAL  ;                E340S749
 251     1    1                    IF KA >200 THEN GO TO YCALE ;                              E360S749
 253     1    1                    GO TO SLOP  ;                                              E370S749
 254     1    1    MCAL          : IF ISHIFT = 1 THEN GO TO NCAL  ;                           E380S749
 256     1    1                    XA(J) =PX1(KA)-((PY1(KA)-PYA(J))*(PX1(KA)-PX1(KA-1))       E400S749
                                   /(PY1(KA)-PY1(KA-1))) ;                                    E420S749
 257     1    1                    IF J = 1 THEN DO  ;                                        E430S749
 259     1    2                    XB(J) = XA(J)  ;                                           E432S749
 260     1    2                    GO TO YCALE  ;                                             E433S749
 261     1    2                    END  ;                                                     E434S749
 262     1    1                    ISHIFT = 1  ;                                              E440S749
 263     1    1                    KA = KA + 2  ;                                             E450S749
 264     1    1                    GO TO SLOP  ;                                              E460S749
 265     1    1    NCAL          : XB(J) =PX1(KA)-((PY1(KA)-PYA(J))*(PX1(KA)-PX1(KA-1))       E480S749
                                   /(PY1(KA)-PY1(KA-1)));                                     E500S749
 266     1    1                    GO TO ARCALS  ;                                            E520S749
 267     1    1    PCAL          : XB(J) = XA(J)  ;                                           E540S749
 268     1    1    TLOP          : IF PY2(KB) < PYA(J) & PY2(KB+1) >PYA(J) THEN GO TO RCAL ;  E580S749
```

```
STMT LEVEL NEST

270     1    1                 IF PY2(KB) >PYA(J) & PY2(KB+1) < PYA(J) THEN GO TO RCAL  ;   E585S749
272     1    1                 KB = KB + 1  ;                                               E600S749
273     1    1                 IF KB > 200 & JSHIFT = 1 THEN DO  ;                          E622S749
275     1    2                 XB(J) = 2.095  ;                                             E624S749
276     1    2                 GO TO ARCALS  ;                                              E628S749
277     1    2                 END  ;                                                       E629S749
278     1    1                 IF KB >200 THEN GO TO YCALE  ;                               E630S749
280     1    1                 GO TO TLOP  ;                                                E640S749
281     1    1      RCAL     : IF JSHIFT = 1 THEN GO TO XCAL  ;                             E650S749
283     1    1                 XA(J) =PX2(KB)-((PY2(KB)-PYA(J))*(PX2(KB)-PX2(KB-1))         E660S749
                               /(PY2(KB)-PY2(KB-1)));                                       E680S749
284     1    1                 IF ISHIFT = 1 THEN GO TO ARCALS  ;                           E700S749
286     1    1                 JSHIFT = 1  ;                                                E710S749
287     1    1                 KB = KB + 2  ;                                               E712S749
288     1    1                 GO TO TLOP  ;                                                E720S749
289     1    1      XCAL     : XB(J) =PX2(KB)-((PY2(KB)-PYA(J))*(PX2(KB)-PX2(KB-1))         E740S749
                               /(PY2(KB)-PY2(KB-1))) ;                                      E760S749
290     1    1      ARCALS   : IF J = 1 THEN GO TO YCALE  ;                                 E780S749
292     1    1                 PYDEL =.0025*(XB(J)+XB(J-1)-XA(J)-XA(J-1)) ;                 E800S749
293     1    1                 PARY = PARY + PYDEL  ;                                       E820S749
294     1    1                 PYMT1 = PYMT1 + (PYDEL*(PYA(J)-.0025)) ;                     E840S749
295     1    1                 PYMT2 = PYMT2 + (PYDEL*(PYA(J)-.0025)**2)  ;                 E860S749
296     1    1                 YPXY = YPXY + (.5*PYDEL*(PYA(J)-.0025)*(XA(J)+XB(J))) ;      E860S749
297     1    1      YCALE    : END YCAL  ;                                                  E880S749
298     1                      YPBAR = PYMT1/PARY  ;                                        F020S749
299     1                      PRAD  =PYMT2/PARY  ;                                         F040S749
300     1                      YRAD = SQRT(PRAD)  ;                                         F060S749
301     1                      YPADG = SQRT(PRAD-YPBAR**2)  ;                               F080S749
302     1                      YP = YPXY/PARY  ;                                            F100S749
303     1                      PHB = (XP - XPBAR*YPBAR )  ;                                 F102S749
304     1                      PT2 = 2*PHB/(XPADG**2-YPADG**2)  ;                           F104S749
305     1                      PUT EDIT ('PRODUCTION DY ELEMENTS','AREA =',PARY,            F120S749
                               'C OF G =',YPBAR,'PRAD SQ =',PRAD,'R OF G =',YRAD,'YPADG =',F140S749
                               YPADG)(SKIP(10),X(10),A,SKIP,X(10),A,F(9,5),X(20),A,         F160S749
```

```
STMT LEVEL NEST

                                   F(9,5),SKIP,X(10),A,F(9,5),X(10),A,F(9,5),X(10),A,F(9,5)) ; F180S749
 306    1                          PUT EDIT ('CROSSPRODUCT =',YP) (SKIP(2),X(10),A,F(9,5)) ;   F190S749
                                   /* TO CALCULATE OVERALL DIFFERENCES  */                     F195S749
 307    1                          SS = XPBAR-XBAR  ;                                          F200S749
 308    1                          TT = YPBAR-YBAR  ;                                          F220S749
 309    1                          DFTAN = (PT2-RT2)/(1+PT2*RT2)  ;                            F290S749
 310    1                          DTAN = SQRT(1+1/(DFTAN**2))-1/DFTAN ;                       F292S749
 311    1                          ANGL = 57.3066*DTAN  ;                                      F294S749
 312    1                          PUT EDIT ('SHIFT PARAMETERS ','X DIRECTION =',SS,           F300S749
                                   'Y DIRECTION =',TT,'TAN OF ANGULAR DIFFERENCE =',DTAN)      F320S749
                                   (PAGE,SKIP(10),X(40),A,SKIP(2),X(30),A,F(9,5),SKIP,X(30),   F340S749
                                   A,F(9,5),SKIP,X(30),A,F(9,5)) ;                             F360S749
 313    1                          PUT EDIT ('ANGULAR DIFFERENCE IN DEGREES =',ANGL)(SKIP(5),  F400S749
                                   X(30),A,F(9,5)) ;                                           F420S749
 314    1                          GO TO DATA  ;                                               G100S749
 315    1             FINISH     : END SIMCAL  ;                                               G200S749
```

ATTRIBUTE AND CROSS-REFERENCE TABLE

DCL NO.	IDENTIFIER	ATTRIBUTES AND REFERENCES
	A	AUTOMATIC,ALIGNED,DECIMAL,FLOAT(SINGLE) 9,11,24,142
	AA	AUTOMATIC,ALIGNED,DECIMAL,FLOAT(SINGLE) 24,25,27
	AL	AUTOMATIC,ALIGNED,DECIMAL,FLOAT(SINGLE) 10,12,13,15,15,16,16,30,30,31,31,32,32,33,33,38,38,39,39
	AMAX	AUTOMATIC,ALIGNED,DECIMAL,FLOAT(SINGLE) 223,229,231
	AMIN	AUTOMATIC,ALIGNED,DECIMAL,FLOAT(SINGLE) 222,227,228
	ANG	AUTOMATIC,ALIGNED,DECIMAL,FLOAT(SINGLE) 40,41
	ANGL	AUTOMATIC,ALIGNED,DECIMAL,FLOAT(SINGLE) 311,313
290	ARCALS	STATEMENT LABEL CONSTANT 266,276,285
	B	AUTOMATIC,ALIGNED,DECIMAL,FLOAT(SINGLE) 9,11,27,135
	BL	AUTOMATIC,ALIGNED,DECIMAL,FLOAT(SINGLE) 13,14
	BMAX	AUTOMATIC,ALIGNED,DECIMAL,FLOAT(SINGLE)

DCL NO.	IDENTIFIER	ATTRIBUTES AND REFERENCES
		223,230,232
	CGX	AUTOMATIC,ALIGNED,DECIMAL,FLOAT(SINGLE) 38,41
	CGY	AUTOMATIC,ALIGNED,DECIMAL,FLOAT(SINGLE) 39,41
	CMAX	AUTOMATIC,ALIGNED,DECIMAL,FLOAT(SINGLE) 173,179,180
	CMIN	AUTOMATIC,ALIGNED,DECIMAL,FLOAT(SINGLE) 172,177,178
	COS	GENERIC,BUILT-IN FUNCTION 15,16,30,31,32,33,38,39
	COSD	GENERIC,BUILT-IN FUNCTION 105,106,107,108
	CXSH	AUTOMATIC,ALIGNED,DECIMAL,FLOAT(SINGLE) 109,111
	CYSH	AUTOMATIC,ALIGNED,DECIMAL,FLOAT(SINGLE) 110,111
	DA	AUTOMATIC,ALIGNED,DECIMAL,FLOAT(SINGLE) 135,136,140,141,141,142
	DANGL	AUTOMATIC,ALIGNED,DECIMAL,FLOAT(SINGLE) 101,104,105,105,106,106,107,107,108,108
9	DATA	STATEMENT LABEL CONSTANT 314

DCL NO.	IDENTIFIER	ATTRIBUTES AND REFERENCES
195	DCAL	STATEMENT LABEL CONSTANT 190
	DELR	AUTOMATIC,ALIGNED,DECIMAL,FLOAT(SINGLE) 117,118,119,120,121
	DFT	AUTOMATIC,ALIGNED,DECIMAL,FLOAT(SINGLE) 100,101
	DFTAN	AUTOMATIC,ALIGNED,DECIMAL,FLOAT(SINGLE) 309,310,310
	DFTN	AUTOMATIC,ALIGNED,DECIMAL,FLOAT(SINGLE) 99,100,100
	DROOT	AUTOMATIC,ALIGNED,DECIMAL,FLOAT(SINGLE) 142,143,144
	DS	AUTOMATIC,ALIGNED,DECIMAL,FLOAT(SINGLE) 47,50,51,52,53,54,55,65
	DSQ	AUTOMATIC,ALIGNED,DECIMAL,FLOAT(SINGLE) 46,47,48
	DTAN	AUTOMATIC,ALIGNED,DECIMAL,FLOAT(SINGLE) 310,311,312
132	DYCAL	STATEMENT LABEL CONSTANT
145	DYEND	STATEMENT LABEL CONSTANT 138
4	EX	(250)AUTOMATIC,ALIGNED,DECIMAL,FLOAT(SINGLE)

DCL NO.	IDENTIFIER	ATTRIBUTES AND REFERENCES
		187,189,189,197,198,198,206,211,212,213
4	EY1	(250)AUTOMATIC,ALIGNED,DECIMAL,FLOAT(SINGLE) 197,209,209,213
4	EY2	(250)AUTOMATIC,ALIGNED,DECIMAL,FLOAT(SINGLE) 206,209,209,213
204	FCAL	STATEMENT LABEL CONSTANT 199
315	FINISH	STATEMENT LABEL CONSTANT
*********	I	AUTOMATIC,ALIGNED,BINARY,FIXED(15,0) 20,22,22,23,24,28,29,30,30,30,31,31,31,32,32,32,33,33,33
*********	IA	AUTOMATIC,ALIGNED,BINARY,FIXED(15,0) 116,117,117,117,117,119,120,121,121,121
*********	IB	AUTOMATIC,ALIGNED,BINARY,FIXED(15,0) 131,133,133,134,135,143,144
*********	IC	AUTOMATIC,ALIGNED,BINARY,FIXED(15,0) 148,149,149,149,149,152,157,158,159,159,159
*********	ISHIFT	AUTOMATIC,ALIGNED,BINARY,FIXED(15,0) 241,249,254,262,284
*********	J	AUTOMATIC,ALIGNED,BINARY,FIXED(15,0) 234,238,238,239,242,244,244,246,246,256,256,257,259,259,265,265,267 267,268,268,270,270,275,283,283,289,289,290,292,292,292,292,294,295 296,296,296
*********	JSHIFT	AUTOMATIC,ALIGNED,BINARY,FIXED(15,0)

```
DCL NO.        IDENTIFIER                      ATTRIBUTES AND REFERENCES

                                               241,273,281,286

    ********* K                                AUTOMATIC,ALIGNED,BINARY,FIXED(15,0)
                                               188,198,198,200,200,201,204,204,206,206,206,206,206,206

    ********* KA                               AUTOMATIC,ALIGNED,BINARY,FIXED(15,0)
                                               240,244,244,246,246,248,248,249,251,256,256,256,256,256,256,263,263
                                               265,265,265,265,265,265

    ********* KB                               AUTOMATIC,ALIGNED,BINARY,FIXED(15,0)
                                               240,268,268,270,270,272,272,273,278,283,283,283,283,283,283,287,287
                                               289,289,289,289,289,289

    ********* KK                               AUTOMATIC,ALIGNED,BINARY,FIXED(15,0)
                                               8,112,171

    ********* L                                AUTOMATIC,ALIGNED,BINARY,FIXED(15,0)
                                               182,186,186,187,189,189,197,197,198,198,206,206,207,209,209,209,209
                                               211,212,213,213,213

45             LICAL                           STATEMENT LABEL CONSTANT

66             LICEND                          STATEMENT LABEL CONSTANT
                                               49,58

189            LOP1                            STATEMENT LABEL CONSTANT
                                               194

198            LOP2                            STATEMENT LABEL CONSTANT
                                               203

    ********* M                                AUTOMATIC,ALIGNED,BINARY,FIXED(15,0)
                                               224,225,227,227,227,229,229,229,230,230,230
```

DCL NO.	IDENTIFIER	ATTRIBUTES AND REFERENCES
	MAX	GENERIC,BUILT-IN FUNCTION 179,229,230
179	MAXI	STATEMENT LABEL CONSTANT 176
254	MCAL	STATEMENT LABEL CONSTANT 245,247
	MIN	GENERIC,BUILT-IN FUNCTION 177,227
*********	MM	AUTOMATIC,ALIGNED,BINARY,FIXED(15,0) 174,175,177,177,177,179,179,179
265	NCAL	STATEMENT LABEL CONSTANT 255
	P	AUTOMATIC,ALIGNED,DECIMAL,FLOAT(SINGLE) 9,11,15,16,17,24,38,39,107,108,109,143,144
	PARX	AUTOMATIC,ALIGNED,DECIMAL,FLOAT(SINGLE) 183,210,210,215,216,219,220
	PARY	AUTOMATIC,ALIGNED,DECIMAL,FLOAT(SINGLE) 235,293,293,298,299,302,305
267	PCAL	STATEMENT LABEL CONSTANT 250
	PDS	AUTOMATIC,ALIGNED,DECIMAL,FLOAT(SINGLE) 59,60,61,62,63,64
	PDSQ	AUTOMATIC,ALIGNED,DECIMAL,FLOAT(SINGLE)

DCL NO.	IDENTIFIER	ATTRIBUTES AND REFERENCES
		56,57,59
185	PDX	STATEMENT LABEL CONSTANT
214	PDXEND	STATEMENT LABEL CONSTANT 193,196,202,205,208
	PH1	AUTOMATIC,ALIGNED,DECIMAL,FLOAT(SINGLE) 44,65,65,90
	PHB	AUTOMATIC,ALIGNED,DECIMAL,FLOAT(SINGLE) 303,304
	PHBAR	AUTOMATIC,ALIGNED,DECIMAL,FLOAT(SINGLE) 91,92,96
	PHXY	AUTOMATIC,ALIGNED,DECIMAL,FLOAT(SINGLE) 90,91,96
	PLIN	AUTOMATIC,ALIGNED,DECIMAL,FLOAT(SINGLE) 43,60,60,82,83,84,85,90,93
	PLXB	AUTOMATIC,ALIGNED,DECIMAL,FLOAT(SINGLE) 82,87,91,93,97
	PLYB	AUTOMATIC,ALIGNED,DECIMAL,FLOAT(SINGLE) 84,89,91,93,98
	PMNT1	AUTOMATIC,ALIGNED,DECIMAL,FLOAT(SINGLE) 183,211,211,215
	PMNT2	AUTOMATIC,ALIGNED,DECIMAL,FLOAT(SINGLE) 183,212,212,216

DCL NO.	IDENTIFIER	ATTRIBUTES AND REFERENCES
	PP	AUTOMATIC,ALIGNED,DECIMAL,FLOAT(SINGLE) 105,107
	PRAD	AUTOMATIC,ALIGNED,DECIMAL,FLOAT(SINGLE) 299,300,301,305
	PRAD2	AUTOMATIC,ALIGNED,DECIMAL,FLOAT(SINGLE) 216,217,218,220
171	PROCAL	STATEMENT LABEL CONSTANT 113
	PT2	AUTOMATIC,ALIGNED,DECIMAL,FLOAT(SINGLE) 304,309,309
	PTAN2	AUTOMATIC,ALIGNED,DECIMAL,FLOAT(SINGLE) 92,96,99,99
3	PX1	(250)AUTOMATIC,ALIGNED,DECIMAL,FLOAT(SINGLE) 30,37,40,40,177,177,177,179,179,179,189,189,195,195,197,197,197,256 256,256,265,265,265
2	PX2	(250)AUTOMATIC,ALIGNED,DECIMAL,FLOAT(SINGLE) 32,37,56,56,61,61,62,62,65,65,198,198,204,204,206,206,206,283,283 283,289,289,289
	PXAD	AUTOMATIC,ALIGNED,DECIMAL,FLOAT(SINGLE) 83,86,87,94
	PXDEL	AUTOMATIC,ALIGNED,DECIMAL,FLOAT(SINGLE) 209,210,211,212,213
	PXM1	AUTOMATIC,ALIGNED,DECIMAL,FLOAT(SINGLE) 43,61,61,82

DCL NO.	IDENTIFIER	ATTRIBUTES AND REFERENCES
	PXM2	AUTOMATIC,ALIGNED,DECIMAL,FLOAT(SINGLE) 43,62,62,83
2	PY1	(250)AUTOMATIC,ALIGNED,DECIMAL,FLOAT(SINGLE) 31,37,40,40,197,197,197,227,227,227,229,229,229,244,244,246,246,256 256,256,265,265,265
3	PY2	(250)AUTOMATIC,ALIGNED,DECIMAL,FLOAT(SINGLE) 33,37,56,56,63,63,64,64,65,65,206,206,206,230,230,230,268,268,270 270,283,283,283,289,289,289
5	PYA	(250)AUTOMATIC,ALIGNED,DECIMAL,FLOAT(SINGLE) 239,242,244,244,246,246,256,265,268,268,270,270,283,289,294,295,296
	PYAD	AUTOMATIC,ALIGNED,DECIMAL,FLOAT(SINGLE) 85,88,89,95
	PYDEL	AUTOMATIC,ALIGNED,DECIMAL,FLOAT(SINGLE) 292,293,294,295,296
	PYE	AUTOMATIC,ALIGNED,DECIMAL,FLOAT(SINGLE) 237,239
	PYM1	AUTOMATIC,ALIGNED,DECIMAL,FLOAT(SINGLE) 43,63,63,84
	PYM2	AUTOMATIC,ALIGNED,DECIMAL,FLOAT(SINGLE) 43,64,64,85
	PYMT1	AUTOMATIC,ALIGNED,DECIMAL,FLOAT(SINGLE) 184,235,294,294,298
	PYMT2	AUTOMATIC,ALIGNED,DECIMAL,FLOAT(SINGLE)

DCL NO.	IDENTIFIER	ATTRIBUTES AND REFERENCES
		184,235,295,295,299
	Q	AUTOMATIC,ALIGNED,DECIMAL,FLOAT(SINGLE) 9,11,15,16,18,28,29,38,39,107,108,110,135
	QQ	AUTOMATIC,ALIGNED,DECIMAL,FLOAT(SINGLE) 106,108
7	********* R	AUTOMATIC,ALIGNED,BINARY,FIXED(15,0) 45,46,46,46,46,51,51,52,52,53,53,54,54,55,55,55,55,56,56,56,56,61,6 62,62,63,63,64,64,65,65,65,65
	RAD2	AUTOMATIC,ALIGNED,DECIMAL,FLOAT(SINGLE) 124,125,126,129
	RAREA	AUTOMATIC,ALIGNED,DECIMAL,FLOAT(SINGLE) 114,118,118,123,124,127,129
281	RCAL	STATEMENT LABEL CONSTANT 269,271
3	RDX1	(250)AUTOMATIC,ALIGNED,DECIMAL,FLOAT(SINGLE) 143,149,149,159
3	RDX2	(250)AUTOMATIC,ALIGNED,DECIMAL,FLOAT(SINGLE) 144,149,149,159
	RH1	AUTOMATIC,ALIGNED,DECIMAL,FLOAT(SINGLE) 44,55,55,75
	RHB	AUTOMATIC,ALIGNED,DECIMAL,FLOAT(SINGLE) 166,167
	RHBAR	AUTOMATIC,ALIGNED,DECIMAL,FLOAT(SINGLE)

DCL NO.	IDENTIFIER	ATTRIBUTES AND REFERENCES
		76,77,81
	RHXY	AUTOMATIC,ALIGNED,DECIMAL,FLOAT(SINGLE) 75,76,81
	RLIN	AUTOMATIC,ALIGNED,DECIMAL,FLOAT(SINGLE) 42,50,50,67,68,69,70,75,78
	RLXB	AUTOMATIC,ALIGNED,DECIMAL,FLOAT(SINGLE) 67,72,76,78,97,105,105,106
	RLYB	AUTOMATIC,ALIGNED,DECIMAL,FLOAT(SINGLE) 69,74,76,78,98,105,106,106
	RMNT1	AUTOMATIC,ALIGNED,DECIMAL,FLOAT(SINGLE) 114,119,119,123
	RMNT2	AUTOMATIC,ALIGNED,DECIMAL,FLOAT(SINGLE) 114,120,120,124
	RT2	AUTOMATIC,ALIGNED,DECIMAL,FLOAT(SINGLE) 167,169,309,309
	RTAN	AUTOMATIC,ALIGNED,DECIMAL,FLOAT(SINGLE) 81
	RTAN2	AUTOMATIC,ALIGNED,DECIMAL,FLOAT(SINGLE) 77,99,99
	RXAD	AUTOMATIC,ALIGNED,DECIMAL,FLOAT(SINGLE) 68,71,72,79
	RXM1	AUTOMATIC,ALIGNED,DECIMAL,FLOAT(SINGLE) 42,51,51,67

DCL NO.	IDENTIFIER	ATTRIBUTES AND REFERENCES
	RXM2	AUTOMATIC,ALIGNED,DECIMAL,FLOAT(SINGLE) 42,52,52,68
2	RY1	(250)AUTOMATIC,ALIGNED,DECIMAL,FLOAT(SINGLE) 28,30,31,37,117,117,121
2	RY2	(250)AUTOMATIC,ALIGNED,DECIMAL,FLOAT(SINGLE) 29,32,33,37,46,46,53,53,54,54,55,55,117,117,121
	RYAD	AUTOMATIC,ALIGNED,DECIMAL,FLOAT(SINGLE) 70,73,74,80
	RYD2	AUTOMATIC,ALIGNED,DECIMAL,FLOAT(SINGLE) 162,163,164,168
	RYM1	AUTOMATIC,ALIGNED,DECIMAL,FLOAT(SINGLE) 42,53,53,69
	RYM2	AUTOMATIC,ALIGNED,DECIMAL,FLOAT(SINGLE) 42,54,54,70
21	SCAL	STATEMENT LABEL CONSTANT
34	SCEND	STATEMENT LABEL CONSTANT 26
1	SIMCAL	ENTRY,DECIMAL,FLOAT(SINGLE)
	SIN	GENERIC,BUILT-IN FUNCTION 15,16,30,31,32,33,38,39
	SIND	GENERIC,BUILT-IN FUNCTION 105,106,107,108

DCL NO.	IDENTIFIER	ATTRIBUTES AND REFERENCES
244	SLOP	STATEMENT LABEL CONSTANT 253,264
	SQRT	GENERIC,BUILT-IN FUNCTION 27,47,59,71,72,73,74,86,87,88,89,100,125,126,142,163,164,217,218,30 301,310
	SR	AUTOMATIC,ALIGNED,DECIMAL,FLOAT(SINGLE) 10,11,17,17,19,30,32,38
	SS	AUTOMATIC,ALIGNED,DECIMAL,FLOAT(SINGLE) 307,312
	SYSIN	FILE,EXTERNAL 9,10
	SYSPRINT	FILE,EXTERNAL 11,12,14,19,35,36,37,41,78,79,80,81,93,94,95,96,102,103,104,111,128 129,130,152,168,169,170,220,221,305,306,312,313
6	********* T	AUTOMATIC,ALIGNED,BINARY,FIXED(15,0) 37,37,37,37,37,37,37,37,37
268	TLOP	STATEMENT LABEL CONSTANT 243,280,288
	TR	AUTOMATIC,ALIGNED,DECIMAL,FLOAT(SINGLE) 10,11,18,18,19,31,33,39
	TT	AUTOMATIC,ALIGNED,DECIMAL,FLOAT(SINGLE) 308,312
6	********* U	AUTOMATIC,ALIGNED,BINARY,FIXED(15,0)

DCL NO.	IDENTIFIER	ATTRIBUTES AND REFERENCES
		188,189,189,191,191,192,195,195,197,197,197,197,197,197
2	X	(250)AUTOMATIC,ALIGNED,DECIMAL,FLOAT(SINGLE) 23,24,30,31,32,33,37,46,46,51,51,52,52,55,55,119,120,121
5	XA	(250)AUTOMATIC,ALIGNED,DECIMAL,FLOAT(SINGLE) 256,259,267,283,292,292,296
5	XB	(250)AUTOMATIC,ALIGNED,DECIMAL,FLOAT(SINGLE) 259,265,267,275,289,292,292,296
	XBAR	AUTOMATIC,ALIGNED,DECIMAL,FLOAT(SINGLE) 123,126,129,166,307
289	XCAL	STATEMENT LABEL CONSTANT 282
	XIN	AUTOMATIC,ALIGNED,DECIMAL,FLOAT(SINGLE) 107,109
	XK	AUTOMATIC,ALIGNED,DECIMAL,FLOAT(SINGLE) 21,23
	XL	AUTOMATIC,ALIGNED,DECIMAL,FLOAT(SINGLE) 132,134
	XMAX	AUTOMATIC,ALIGNED,DECIMAL,FLOAT(SINGLE) 179,180,185
	XMIN	AUTOMATIC,ALIGNED,DECIMAL,FLOAT(SINGLE) 177,178,185
	XP	AUTOMATIC,ALIGNED,DECIMAL,FLOAT(SINGLE) 219,221,303

DCL NO.	IDENTIFIER	ATTRIBUTES AND REFERENCES
	XPADG	AUTOMATIC,ALIGNED,DECIMAL,FLOAT(SINGLE) 218,220,304
	XPADL	AUTOMATIC,ALIGNED,DECIMAL,FLOAT(SINGLE) 86,94
	XPBAR	AUTOMATIC,ALIGNED,DECIMAL,FLOAT(SINGLE) 215,218,220,303,307
	XPG	AUTOMATIC,ALIGNED,DECIMAL,FLOAT(SINGLE) 87,92,94
	XPXY	AUTOMATIC,ALIGNED,DECIMAL,FLOAT(SINGLE) 184,213,213,219
	XR	AUTOMATIC,ALIGNED,DECIMAL,FLOAT(SINGLE) 127,130,166
	XRAD	AUTOMATIC,ALIGNED,DECIMAL,FLOAT(SINGLE) 217,220
	XRAD2	AUTOMATIC,ALIGNED,DECIMAL,FLOAT(SINGLE) 125,129
	XRADG	AUTOMATIC,ALIGNED,DECIMAL,FLOAT(SINGLE) 126,129,167
	XRADL	AUTOMATIC,ALIGNED,DECIMAL,FLOAT(SINGLE) 71,79
	XRG	AUTOMATIC,ALIGNED,DECIMAL,FLOAT(SINGLE) 72,77,79

DCL NO.	IDENTIFIER	ATTRIBUTES AND REFERENCES
	XROOT	AUTOMATIC,ALIGNED,DECIMAL,FLOAT(SINGLE) 27,28,29
	XRXY	AUTOMATIC,ALIGNED,DECIMAL,FLOAT(SINGLE) 115,121,121,127
	XSHIFT	AUTOMATIC,ALIGNED,DECIMAL,FLOAT(SINGLE) 97,103,109
	XX	AUTOMATIC,ALIGNED,DECIMAL,FLOAT(SINGLE) 185,187
229	Y1M	STATEMENT LABEL CONSTANT 226
	Y1MAX	AUTOMATIC,ALIGNED,DECIMAL,FLOAT(SINGLE) 229,231,242
	YBAR	AUTOMATIC,ALIGNED,DECIMAL,FLOAT(SINGLE) 161,164,166,168,308
237	YCAL	STATEMENT LABEL CONSTANT
297	YCALE	STATEMENT LABEL CONSTANT 252,260,279,291
3	YD	(250)AUTOMATIC,ALIGNED,DECIMAL,FLOAT(SINGLE) 134,135,157,158,159
	YDELR	AUTOMATIC,ALIGNED,DECIMAL,FLOAT(SINGLE) 155,156,157,158,159
	YEL	AUTOMATIC,ALIGNED,DECIMAL,FLOAT(SINGLE) 149,150,155

DCL NO.	IDENTIFIER	ATTRIBUTES AND REFERENCES
148	YELA	STATEMENT LABEL CONSTANT
160	YELEND	STATEMENT LABEL CONSTANT 153
	YIN	AUTOMATIC,ALIGNED,DECIMAL,FLOAT(SINGLE) 108,110
	YMAX	AUTOMATIC,ALIGNED,DECIMAL,FLOAT(SINGLE) 230,232,237
	YMIN	AUTOMATIC,ALIGNED,DECIMAL,FLOAT(SINGLE) 227,228,237
	YP	AUTOMATIC,ALIGNED,DECIMAL,FLOAT(SINGLE) 302,306
	YPADG	AUTOMATIC,ALIGNED,DECIMAL,FLOAT(SINGLE) 301,304,305
	YPADL	AUTOMATIC,ALIGNED,DECIMAL,FLOAT(SINGLE) 88,95
	YPBAR	AUTOMATIC,ALIGNED,DECIMAL,FLOAT(SINGLE) 298,301,303,305,308
	YPG	AUTOMATIC,ALIGNED,DECIMAL,FLOAT(SINGLE) 89,92,95
	YPXY	AUTOMATIC,ALIGNED,DECIMAL,FLOAT(SINGLE) 236,296,296,302
	YR	AUTOMATIC,ALIGNED,DECIMAL,FLOAT(SINGLE)

DCL NO.	IDENTIFIER	ATTRIBUTES AND REFERENCES
		165,170
	YRAD	AUTOMATIC,ALIGNED,DECIMAL,FLOAT(SINGLE) 300,305
	YRAD2	AUTOMATIC,ALIGNED,DECIMAL,FLOAT(SINGLE) 163,168
	YRADG	AUTOMATIC,ALIGNED,DECIMAL,FLOAT(SINGLE) 164,167,168
	YRADL	AUTOMATIC,ALIGNED,DECIMAL,FLOAT(SINGLE) 73,80
	YRAR	AUTOMATIC,ALIGNED,DECIMAL,FLOAT(SINGLE) 146,156,156,161,162,165,168
	YRG	AUTOMATIC,ALIGNED,DECIMAL,FLOAT(SINGLE) 74,77,80
	YRMNT1	AUTOMATIC,ALIGNED,DECIMAL,FLOAT(SINGLE) 146,157,157,161
	YRMNT2	AUTOMATIC,ALIGNED,DECIMAL,FLOAT(SINGLE) 146,158,158,162
	YRXY	AUTOMATIC,ALIGNED,DECIMAL,FLOAT(SINGLE) 147,159,159,165
	YSHIFT	AUTOMATIC,ALIGNED,DECIMAL,FLOAT(SINGLE) 98,103,110
	ZX	AUTOMATIC,ALIGNED,DECIMAL,FLOAT(SINGLE) 15,17

DCL NO.	IDENTIFIER	ATTRIBUTES AND REFERENCES
	ZY	AUTOMATIC,ALIGNED,DECIMAL,FLOAT(SINGLE) 16,18

AGGREGATE LENGTH TABLE

STATEMENT NO.	IDENTIFIER	LENGTH IN BYTES
4	EX	1000
4	EY1	1000
4	EY2	1000
3	PX1	1000
2	PX2	1000
2	PY1	1000
3	PY2	1000
5	PYA	1000
3	RDX1	1000
3	RDX2	1000
2	RY1	1000
2	RY2	1000
2	X	1000
5	XA	1000
5	XB	1000
3	YD	1000

```
STORAGE REQUIREMENTS.
---------------------

THE STORAGE AREA FOR THE PROCEDURE LABELLED SIMCAL IS 16924 BYTES LONG.

THE PROGRAM CSECT IS NAMED SIMCAL   AND IS 17524 BYTES LONG.

THE STATIC  CSECT IS NAMED *SIMCALA AND IS 2283 BYTES LONG.

*STATISTICS*     SOURCE RECORDS =      358,PROG TEXT STMNTS =      315,OBJECT BYTES =    17524
```

```
   COMPILER DIAGNOSTICS.


WARNINGS.

   IEM0227I          NO FILE/STRING OPTION SPECIFIED IN ONE OR MORE GET/PUT STATEMENTS. SYSIN/SYSPRINT HAS BEEN
                     ASSUMED IN EACH CASE.

   IEM0764I          ONE OR MORE FIXED BINARY ITEMS OF PRECISION 15 OR LESS HAVE BEEN GIVEN HALFWORD STORAGE. THEY
                     ARE FLAGGED '*********' IN THE XREF/ATR LIST.

   IEM3898I        COMPILER CORE REQUIREMENT EXCEEDED SIZE GIVEN. AUXILIARY STORAGE USED.


END OF DIAGNOSTICS.

AUXILIARY STORAGE WILL NOT BE USED FOR DICTIONARY WHEN SIZE = 122K

COMPILE TIME          .31 MINS

ELAPSED TIME          .90 MINS
```

```
F128-LEVEL LINKAGE EDITOR OPTIONS SPECIFIED MAP,OVLY,SIZE=(172K,6K)
          VARIABLE OPTIONS USED -   SIZE=(176128,6144)
IEW0201
IEW0461   IHEUPAB
IEW0461   IHEUPBB
IEW0461   IHEDNCA
IEW0461   IHEDNBA
IEW0461   IHEVSAA
IEW0461   IHEVCAA
IEW0461   IHEDBNA
IEW0461   IHEVSBA
IEW0461   IHEVSFA
IEW0461   IHEDDDD
IEW0461   IHEVPCA
IEW0461   IHEVPDA
IEW0461   IHEVPFA
IEW0461   IHEVPGA
IEW0461   IHEVPHA
IEW0461   IHEVFBA
IEW0461   IHEVKBA
IEW0461   IHEVKCA
IEW0461   IHEVKFA
IEW0461   IHEVKGA
IEW0461   IHEUPAA
IEW0461   IHEUPBA
IEW0461   IHEM91A
IEW0461   IHEM91B
IEW0461   IHEM91C
IEW0461   IHETERA
```

MODULE MAP

CONTROL SECTION				ENTRY							
NAME	ORIGIN	LENGTH	SEG. NO.	NAME	LOCATION	NAME	LOCATION	NAME	LOCATION	NAME	LOCATION
SIMCAL	00	4474	1								
*SIMCALA	4478	8EB	1								

NAME		ORIGIN	LENGTH	SEG. NO.	NAME	LOCATION	NAME	LOCATION	NAME	LOCATION	NAME	LOCATION
IHEMAIN		4D68	4	1								
IHENTRY		4D70	C	1								
SYSIN		4D80	38	1								
IHESPRT		4DB8	38	1								
IHEDIA	*	4DF0	338	1								
					IHEDIAA	4DF0	IHEDIAB	4DF2				
IHEDOA	*	5128	23A	1								
					IHEDOAA	5128	IHEDOAB	512A				
IHEDOB	*	5368	144	1								
					IHEDOBA	5368	IHEDOBB	536A	IHEDOBC	536C		
IHEIOP	*	54B0	1EB	1								
					IHEIOPA	54B0	IHEIOPB	54B2	IHEIOPC	54B6		
IHEIOX	*	56A0	14C	1								
					IHEIOXA	56A0	IHEIOXB	56A2	IHEIOXC	56A6		
IHESAP	*	57F0	AB8	1								
					IHESADA	57F0	IHESAPC	580A	IHESAPD	5812	IHESAPA	581A
					IHESAPB	5822	IHESADF	582A	IHESADB	5832	IHESADE	583A
					IHESAFC	5842	IHESAFA	584A	IHESAFB	5852	IHESAFD	585A
					IHESARA	5862	IHESAFQ	586A	IHESARC	6026	IHESADD	6114
					IHESAFF	614E						
IHEIOA	*	62A8	16A	1								
					IHEIOAA	62A8	IHEIOAB	62AA	IHEIOAC	62AC	IHEIOAD	62AE
					IHEIOAT	6398						
IHEIOB	*	6418	1E4	1								
					IHEIOBA	6418	IHEIOBB	6420	IHEIOBC	6428	IHEIOBD	6430
					IHEIOBE	6438	IHEIOBT	6524				
IHEMXS	*	6600	5A	1								
					IHEMXSX	6600	IHEMXSN	660C				
IHESNS	*	6660	140	1								
					IHESNSK	6660	IHESNSC	666C	IHESNSZ	668E	IHESNSS	669A
IHESQS	*	67A0	A4	1								
					IHESQSO	67A0						
IHEDMA	*	6848	F8	1								
					IHEDMAA	6848						
IHEVFA	*	6940	16C	1								
					IHEVFAA	6940						
IHEVFC	*	6AB0	26	1								

NAME		ORIGIN	LENGTH	SEG. NO.	NAME	LOCATION	NAME	LOCATION	NAME	LOCATION	NAME	LOCATION
					IHEVFCA	6AB0						
IHEVFD	*	6AD8	66	1	IHEVFDA	6AD8						
IHEVFE	*	6B40	1C	1	IHEVFEA	6B40						
IHEVPA	*	6B60	1E0	1	IHEVPAA	6B60						
IHEVPB	*	6D40	1A2	1	IHEVPBA	6D40						
IHEVPE	*	6EE8	26C	1	IHEVPEA	6EE8						
IHEVQB	*	7158	494	1	IHEVQBA	7158						
IHEVSC	*	75F0	AC	1	IHEVSCA	75F0						
IHEDCN	*	76A0	21E	1	IHEDCNA	76A0	IHEDCNB	76A2				
IHEERR	*	78C0	729	1	IHEERRD	78C0	IHEERRC	78CA	IHEERRB	78D4	IHEERRA	78DE
					IHEERRE	7F56						
IHEIOD	*	7FF0	29A	1	IHEIODG	7FF0	IHEIODP	7FF2	IHEIODT	80EA		
IHEIOF	*	8290	2DC	1	IHEIOFB	8290	IHEIOFA	8292	IHEITAZ	852E	IHEITAX	853A
					IHEITAA	854E						
IHEOCL	*	8570	554	1	RROCLA	8570	IHEOCLB	8572	IHEOCLC	8574	IHEOCLD	8576
IHEVQC	*	8AC8	268	1	IHEVQCA	8AC8						
IHEBEG	*	8D30	80	1	IHEBEGN	8D30	IHEBEGA	8D70				
IHEPRT	*	8D80	2C8	1	IHEPRTA	8D80	IHEPRTB	8D82				
IHESIZ	*	9078	C	1	IHESIZE	9078						
IHETAB	*	9088	C	1	IHETABS	9088						

NAME	ORIGIN	LENGTH	SEG. NO.	NAME	LOCATION	NAME	LOCATION	NAME	LOCATION	NAME	LOCATION
IHEVQA *	9098	E6	1								
				IHEVQAA	9098						
IHEVSE *	9180	15D	1								
				IHEVSEA	9180	IHEVSEB	9182				
IHEOCLA *	92E0	4C	1								

PSEUDO REGISTERS

NAME	ORIGIN	LENGTH	NAME	ORIGIN	LENGTH	NAME	ORIGIN	LENGTH	NAME	ORIGIN	LENGTH
IHEQINV	00	4	IHEQERR	4	4	IHEQTIC	8	4	*SIMCALB	C	4
SYSIN	10	4	IHEQSPR	14	4	IHEQLSA	18	4	IHEQLW0	1C	4
IHEQLW1	20	4	IHEQLW2	24	4	IHEQLW3	28	4	IHEQLW4	2C	4
IHEQLWE	30	4	IHEQLCA	34	4	IHEQVDA	38	4	IHEQFVD	3C	4
IHEQFOP	40	4	IHEQCFL	44	8	IHEQADC	4C	4	IHEQLPR	50	4
IHEQSLA	54	4	IHEQSAR	58	4	IHEQLWF	5C	4	IHEQRTC	60	4
IHEQSFC	64	4	IHEQXLV	68	8	IHEQEVT	70	8			

TOTAL LENGTH OF PSEUDO REGISTERS 78
ENTRY ADDRESS 4D70
TOTAL LENGTH 9330

****PL#1FXEQ DOES NOT EXIST BUT HAS BEEN ADDED TO DATA SET

DIAGNOSTIC MESSAGE DIRECTORY

IEW0201 WARNING - OVERLAY STRUCTURE CONTAINS ONLY ONE SEGMENT -- OVERLAY OPTION CANCELED.
IEW0461 WARNING - SYMBOL PRINTED IS AN UNRESOLVED EXTERNAL REFERENCE; NCAL WAS SPECIFIED, OR THE REFERENCE WAS MARKED FOR RESTRICTED NO-CALL OR NEVERCALL.

INPUT PARAMETERS

A = 1.00000 B = 0.40000

P = 1.00000 Q = 0.60000

SHIFT PARAMETERS

X DIRECTION SR = 0.10000 Y DIRECTION TR = 0.10000

ANGLE OF ROTATION = 0.01745

ANGLE OF ROTATION IN DEGREES = 1.00000

SR = 0.11062 TR = 0.08264

SHAPE PARAMETERS

	REF X	Y1	Y2	PX1	PY1	PX2	PY2
1	0.00000	0.60000	0.60000	0.10015	0.68255	0.10015	0.68255
2	0.01000	0.54357	0.65643	0.11114	0.62631	0.10917	0.73914
3	0.02000	0.52040	0.67960	0.12154	0.60331	0.11876	0.76249
4	0.03000	0.50276	0.69724	0.13184	0.58585	0.12845	0.78030
5	0.04000	0.48800	0.71200	0.14210	0.57127	0.13819	0.79523
6	0.05000	0.47510	0.72490	0.15232	0.55854	0.14797	0.80830
7	0.06000	0.46353	0.73647	0.16252	0.54715	0.15776	0.82005
8	0.07000	0.45298	0.74702	0.17271	0.53677	0.16758	0.83077
9	0.08000	0.44323	0.75677	0.18288	0.52720	0.17740	0.84069
10	0.09000	0.43416	0.76584	0.19303	0.51830	0.18724	0.84994
11	0.10000	0.42564	0.77436	0.20318	0.50997	0.19709	0.85863
12	0.11000	0.41762	0.78238	0.21332	0.50211	0.20695	0.86683
13	0.12000	0.41001	0.78999	0.22345	0.49468	0.21682	0.87461
14	0.13000	0.40278	0.79722	0.23357	0.48763	0.22669	0.88201
15	0.14000	0.39588	0.80412	0.24369	0.48091	0.23657	0.88908
16	0.15000	0.38929	0.81071	0.25381	0.47449	0.24645	0.89585
17	0.16000	0.38297	0.81703	0.26391	0.46834	0.25634	0.90234
18	0.17000	0.37689	0.82311	0.27402	0.46245	0.26623	0.90859
19	0.18000	0.37105	0.82895	0.28412	0.45678	0.27613	0.91460
20	0.19000	0.36543	0.83457	0.29422	0.45133	0.28603	0.92040
21	0.20000	0.36000	0.84000	0.30431	0.44608	0.29593	0.92600
22	0.21000	0.35476	0.84524	0.31440	0.44101	0.30584	0.93142
23	0.22000	0.34969	0.85031	0.32449	0.43612	0.31575	0.93666
24	0.23000	0.34478	0.85522	0.33457	0.43139	0.32566	0.94174
25	0.24000	0.34003	0.85997	0.34465	0.42681	0.33558	0.94667
26	0.25000	0.33542	0.86457	0.35473	0.42238	0.34550	0.95145
27	0.26000	0.33096	0.86904	0.36481	0.41809	0.35542	0.95609
28	0.27000	0.32662	0.87338	0.37488	0.41392	0.36534	0.96060
29	0.28000	0.32241	0.87759	0.38495	0.40989	0.37527	0.96498

30	0.29000	0.31832	0.88168	0.39502	0.40597	0.38519	0.96925
31	0.30000	0.31434	0.88566	0.40509	0.40217	0.39512	0.97340
32	0.31000	0.31048	0.88952	0.41516	0.39848	0.40505	0.97744
33	0.32000	0.30672	0.89328	0.42522	0.39489	0.41499	0.98137
34	0.33000	0.30306	0.89694	0.43528	0.39141	0.42492	0.98521
35	0.34000	0.29949	0.90051	0.44534	0.38802	0.43486	0.98894
36	0.35000	0.29603	0.90397	0.45540	0.38473	0.44479	0.99259
37	0.36000	0.29265	0.90735	0.46546	0.38153	0.45473	0.99614
38	0.37000	0.28936	0.91064	0.47552	0.37842	0.46468	0.99960
39	0.38000	0.28616	0.91384	0.48557	0.37539	0.47462	1.00297
40	0.39000	0.28304	0.91696	0.49562	0.37244	0.48456	1.00627
41	0.40000	0.28000	0.92000	0.50567	0.36958	0.49451	1.00948
42	0.41000	0.27704	0.92296	0.51572	0.36679	0.50445	1.01262
43	0.42000	0.27415	0.92585	0.52577	0.36408	0.51440	1.01568
44	0.43000	0.27134	0.92866	0.53582	0.36145	0.52435	1.01866
45	0.44000	0.26860	0.93140	0.54587	0.35888	0.53430	1.02157
46	0.45000	0.26593	0.93407	0.55591	0.35639	0.54425	1.02442
47	0.46000	0.26333	0.93667	0.56596	0.35396	0.55421	1.02719
48	0.47000	0.26080	0.93920	0.57600	0.35160	0.56416	1.02990
49	0.48000	0.25833	0.94167	0.58604	0.34931	0.57412	1.03254
50	0.49000	0.25593	0.94407	0.59608	0.34708	0.58407	1.03512
51	0.50000	0.25359	0.94641	0.60612	0.34492	0.59403	1.03763
52	0.51000	0.25131	0.94869	0.61616	0.34281	0.60399	1.04008
53	0.52000	0.24909	0.95091	0.62620	0.34077	0.61395	1.04248
54	0.53000	0.24693	0.95307	0.63623	0.33879	0.62391	1.04481
55	0.54000	0.24483	0.95517	0.64627	0.33686	0.63387	1.04709
56	0.55000	0.24279	0.95721	0.65630	0.33499	0.64383	1.04930
57	0.56000	0.24080	0.95920	0.66633	0.33318	0.65380	1.05147
58	0.57000	0.23887	0.96113	0.67637	0.33142	0.66376	1.05357
59	0.58000	0.23699	0.96301	0.68640	0.32972	0.67373	1.05562
60	0.59000	0.23517	0.96483	0.69643	0.32807	0.68370	1.05762
61	0.60000	0.23339	0.96661	0.70646	0.32647	0.69366	1.05957
62	0.61000	0.23167	0.96833	0.71649	0.32493	0.70363	1.06146
63	0.62000	0.23001	0.96999	0.72651	0.32343	0.71360	1.06331
64	0.63000	0.22839	0.97161	0.73654	0.32199	0.72357	1.06510
65	0.64000	0.22682	0.97318	0.74657	0.32059	0.73354	1.06684
66	0.65000	0.22530	0.97470	0.75659	0.31925	0.74351	1.06853
67	0.66000	0.22383	0.97617	0.76661	0.31795	0.75349	1.07018
68	0.67000	0.22241	0.97759	0.77664	0.31671	0.76346	1.07178
69	0.68000	0.22103	0.97897	0.78666	0.31551	0.77344	1.07333

70	0.69000	0.21971	0.98029	0.79668	0.31435	0.78341	1.07483
71	0.70000	0.21842	0.98158	0.80670	0.31325	0.79339	1.07628
72	0.71000	0.21719	0.98281	0.81672	0.31219	0.80336	1.07769
73	0.72000	0.21600	0.98400	0.82674	0.31117	0.81334	1.07905
74	0.73000	0.21486	0.98514	0.83676	0.31020	0.82332	1.08037
75	0.74000	0.21376	0.98624	0.84678	0.30928	0.83330	1.08165
76	0.75000	0.21270	0.98730	0.85680	0.30840	0.84328	1.08288
77	0.76000	0.21169	0.98831	0.86681	0.30756	0.85326	1.08406
78	0.77000	0.21072	0.98928	0.87683	0.30677	0.86324	1.08520
79	0.78000	0.20980	0.99020	0.88684	0.30602	0.87322	1.08630
80	0.79000	0.20892	0.99108	0.89686	0.30531	0.88321	1.08736
81	0.80000	0.20808	0.99192	0.90687	0.30465	0.89319	1.08837
82	0.81000	0.20729	0.99271	0.91688	0.30403	0.90318	1.08934
83	0.82000	0.20653	0.99347	0.92689	0.30345	0.91316	1.09026
84	0.83000	0.20582	0.99418	0.93690	0.30292	0.92315	1.09115
85	0.84000	0.20515	0.99485	0.94691	0.30242	0.93313	1.09199
86	0.85000	0.20453	0.99547	0.95692	0.30197	0.94312	1.09280
87	0.86000	0.20394	0.99606	0.96693	0.30156	0.95311	1.09356
88	0.87000	0.20339	0.99661	0.97694	0.30119	0.96310	1.09428
89	0.88000	0.20289	0.99711	0.98695	0.30086	0.97309	1.09495
90	0.89000	0.20243	0.99757	0.99695	0.30057	0.98308	1.09559
91	0.90000	0.20201	0.99799	1.00696	0.30032	0.99307	1.09619
92	0.91000	0.20162	0.99838	1.01696	0.30011	1.00306	1.09674
93	0.92000	0.20128	0.99872	1.02697	0.29995	1.01305	1.09726
94	0.93000	0.20098	0.99902	1.03697	0.29982	1.02305	1.09774
95	0.94000	0.20072	0.99928	1.04698	0.29973	1.03304	1.09817
96	0.95000	0.20050	0.99950	1.05698	0.29969	1.04304	1.09857
97	0.96000	0.20032	0.99968	1.06698	0.29968	1.05303	1.09892
98	0.97000	0.20018	0.99982	1.07698	0.29972	1.06303	1.09923
99	0.98000	0.20008	0.99992	1.08698	0.29979	1.07302	1.09951
100	0.99000	0.20002	0.99998	1.09698	0.29991	1.08302	1.09974
101	1.00000	0.20000	1.00000	1.10698	0.30006	1.09302	1.09994
102	1.01000	0.20002	0.99998	1.11697	0.30026	1.10302	1.10009
103	1.02000	0.20008	0.99992	1.12697	0.30049	1.11302	1.10021
104	1.03000	0.20018	0.99982	1.13697	0.30076	1.12301	1.10028
105	1.04000	0.20032	0.99968	1.14696	0.30108	1.13301	1.10032
106	1.05000	0.20050	0.99950	1.15696	0.30143	1.14302	1.10031
107	1.05999	0.20072	0.99928	1.16695	0.30183	1.15302	1.10026
108	1.06999	0.20098	0.99902	1.17694	0.30226	1.16302	1.10018
109	1.07999	0.20128	0.99872	1.18694	0.30274	1.17302	1.10005

110	1.08999	0.20162	0.99838	1.19693	0.30325	1.18303	1.09988
111	1.09999	0.20200	0.99800	1.20692	0.30381	1.19303	1.09968
112	1.10999	0.20243	0.99757	1.21691	0.30441	1.20304	1.09943
113	1.11999	0.20289	0.99711	1.22690	0.30504	1.21304	1.09914
114	1.12999	0.20339	0.99661	1.23689	0.30572	1.22305	1.09881
115	1.13999	0.20394	0.99606	1.24688	0.30644	1.23306	1.09844
116	1.14999	0.20452	0.99548	1.25686	0.30720	1.24306	1.09803
117	1.15999	0.20515	0.99485	1.26685	0.30800	1.25307	1.09758
118	1.16999	0.20582	0.99418	1.27684	0.30885	1.26308	1.09708
119	1.17999	0.20653	0.99347	1.28682	0.30973	1.27309	1.09655
120	1.18999	0.20729	0.99271	1.29681	0.31066	1.28310	1.09597
121	1.19998	0.20808	0.99192	1.30679	0.31163	1.29311	1.09535
122	1.20998	0.20892	0.99108	1.31677	0.31264	1.30313	1.09469
123	1.21998	0.20980	0.99020	1.32676	0.31370	1.31314	1.09398
124	1.22998	0.21072	0.98928	1.33674	0.31479	1.32315	1.09323
125	1.23998	0.21169	0.98831	1.34672	0.31594	1.33317	1.09244
126	1.24998	0.21270	0.98730	1.35670	0.31712	1.34318	1.09160
127	1.25998	0.21375	0.98625	1.36668	0.31835	1.35320	1.09072
128	1.26998	0.21485	0.98515	1.37666	0.31962	1.36322	1.08980
129	1.27998	0.21600	0.98400	1.38664	0.32094	1.37323	1.08883
130	1.28998	0.21719	0.98281	1.39661	0.32230	1.38325	1.08781
131	1.29998	0.21842	0.98158	1.40659	0.32371	1.39327	1.08675
132	1.30998	0.21970	0.98030	1.41656	0.32517	1.40329	1.08565
133	1.31998	0.22103	0.97897	1.42654	0.32667	1.41331	1.08449
134	1.32998	0.22240	0.97760	1.43651	0.32822	1.42334	1.08329
135	1.33997	0.22383	0.97617	1.44649	0.32982	1.43336	1.08205
136	1.34997	0.22530	0.97470	1.45646	0.33146	1.44338	1.08075
137	1.35997	0.22681	0.97319	1.46643	0.33315	1.45340	1.07941
138	1.36997	0.22838	0.97162	1.47640	0.33490	1.46343	1.07802
139	1.37997	0.23000	0.97000	1.48637	0.33669	1.47346	1.07657
140	1.38997	0.23167	0.96833	1.49634	0.33853	1.48348	1.07508
141	1.39997	0.23339	0.96661	1.50630	0.34042	1.49351	1.07353
142	1.40997	0.23516	0.96484	1.51627	0.34237	1.50354	1.07194
143	1.41997	0.23698	0.96302	1.52624	0.34437	1.51357	1.07029
144	1.42997	0.23886	0.96114	1.53620	0.34642	1.52360	1.06858
145	1.43997	0.24079	0.95921	1.54617	0.34853	1.53363	1.06683
146	1.44997	0.24278	0.95722	1.55613	0.35069	1.54366	1.06501
147	1.45997	0.24483	0.95517	1.56609	0.35291	1.55370	1.06315
148	1.46996	0.24693	0.95307	1.57605	0.35518	1.56373	1.06122
149	1.47996	0.24908	0.95092	1.58601	0.35751	1.57377	1.05924

150	1.48996	0.25130	0.94870	1.59597	0.35991	1.58380	1.05719
151	1.49996	0.25358	0.94642	1.60593	0.36236	1.59384	1.05509
152	1.50996	0.25592	0.94408	1.61589	0.36487	1.60388	1.05292
153	1.51996	0.25832	0.94168	1.62584	0.36745	1.61392	1.05070
154	1.52996	0.26079	0.93921	1.63580	0.37009	1.62396	1.04840
155	1.53996	0.26332	0.93668	1.64575	0.37280	1.63400	1.04605
156	1.54996	0.26592	0.93408	1.65570	0.37557	1.64404	1.04362
157	1.55996	0.26859	0.93141	1.66565	0.37841	1.65409	1.04113
158	1.56996	0.27133	0.92867	1.67560	0.38133	1.66413	1.03856
159	1.57996	0.27414	0.92586	1.68555	0.38431	1.67418	1.03593
160	1.58996	0.27703	0.92297	1.69550	0.38737	1.68423	1.03322
161	1.59996	0.27999	0.92001	1.70545	0.39050	1.69428	1.03043
162	1.60995	0.28303	0.91697	1.71539	0.39372	1.70433	1.02757
163	1.61995	0.28614	0.91386	1.72534	0.39701	1.71438	1.02462
164	1.62995	0.28935	0.91065	1.73528	0.40039	1.72444	1.02160
165	1.63995	0.29263	0.90737	1.74522	0.40385	1.73449	1.01849
166	1.64995	0.29601	0.90399	1.75516	0.40740	1.74455	1.01528
167	1.65995	0.29948	0.90052	1.76509	0.41104	1.75461	1.01199
168	1.66995	0.30304	0.89696	1.77503	0.41477	1.76467	1.00861
169	1.67995	0.30670	0.89330	1.78496	0.41861	1.77473	1.00512
170	1.68995	0.31046	0.88954	1.79490	0.42254	1.78479	1.00154
171	1.69995	0.31432	0.88568	1.80482	0.42658	1.79486	0.99785
172	1.70995	0.31830	0.88170	1.81475	0.43073	1.80492	0.99405
173	1.71995	0.32239	0.87761	1.82468	0.43499	1.81499	0.99013
174	1.72995	0.32660	0.87340	1.83460	0.43938	1.82506	0.98610
175	1.73995	0.33093	0.86907	1.84453	0.44389	1.83514	0.98194
176	1.74994	0.33540	0.86460	1.85445	0.44853	1.84521	0.97765
177	1.75994	0.34000	0.86000	1.86436	0.45330	1.85529	0.97322
178	1.76994	0.34476	0.85524	1.87428	0.45823	1.86537	0.96864
179	1.77994	0.34966	0.85034	1.88419	0.46331	1.87545	0.96391
180	1.78994	0.35473	0.84527	1.89410	0.46855	1.88554	0.95902
181	1.79994	0.35997	0.84003	1.90401	0.47396	1.89563	0.95395
182	1.80994	0.36540	0.83460	1.91391	0.47956	1.90572	0.94870
183	1.81994	0.37102	0.82898	1.92381	0.48536	1.91582	0.94325
184	1.82994	0.37686	0.82314	1.93370	0.49137	1.92592	0.93759
185	1.83994	0.38293	0.81707	1.94360	0.49762	1.93602	0.93170
186	1.84994	0.38925	0.81075	1.95348	0.50411	1.94613	0.92555
187	1.85994	0.39584	0.80416	1.96337	0.51088	1.95624	0.91913
188	1.86994	0.40273	0.79727	1.97324	0.51794	1.96636	0.91242
189	1.87994	0.40996	0.79004	1.98312	0.52535	1.97648	0.90536

190	1.88993	0.41756	0.78244	1.99298	0.53312	1.98662	0.89794
191	1.89993	0.42559	0.77441	2.00284	0.54132	1.99675	0.89009
192	1.90993	0.43410	0.76590	2.01269	0.55000	2.00690	0.88175
193	1.91993	0.44317	0.75683	2.02253	0.55924	2.01705	0.87286
194	1.92993	0.45291	0.74709	2.03236	0.56916	2.02722	0.86330
195	1.93993	0.46345	0.73655	2.04217	0.57988	2.03740	0.85293
196	1.94993	0.47502	0.72498	2.05196	0.59161	2.04760	0.84154
197	1.95993	0.48790	0.71210	2.06174	0.60467	2.05783	0.82883
198	1.96993	0.50264	0.69736	2.07148	0.61958	2.06808	0.81427
199	1.97993	0.52026	0.67974	2.08117	0.63737	2.07839	0.79683
200	1.98993	0.54337	0.65663	2.09076	0.66065	2.08879	0.77390
201	1.99993	0.59515	0.60485	2.09986	0.71260	2.09969	0.72229
202	0.00000	0.00000	0.00000	0.00000	0.00000	0.00000	0.00000

```
ELLIPSE SHIFT PARAMETERS
CGX =  1.10000
CGY =  0.70000
ANG =  0.01503
```

LENGTH = REF LINE 2.29583	XBAR = 0.99794	YBAR = 0.89002
RAD OF G X SQ = 1.39430	XRADL = 1.18081	XRG = 0.63121
RAD OF G Y SQ = 0.80423	YRADL = 0.89679	YRG = 0.10995
CROSS PRODUCT RHXY = 0.88878	RHBAR = 0.00060	
TWICE ANGLE TAN-1 = 0.00000		

PROD LINE

LENGTH = 2.29583 PXBAR = 1.09288 PYBAR = 0.98994

RAD OF G Y SQ = 1.59267 XPADL = 1.26201 XPG = 0.63110
RAD OF G YSQ = 0.99221 YPADL = 0.99610 YPG = 0.11059

CROSS PRODUCT PHXY = 1.08922 PHBAR = 0.00734
TWICE ANGLE TAN-1 = 0.03803

LINE CENTROID

SHIFT PARAMETERS

XSHIFT = 0.09494 YSHIFT = 0.09992

ANGULAR DIFFERENCE IN DEGREES = 1.00122

EFFECTIVE SHIFT OF SECTIONAL CENTROID
XSHIFT = 0.10001 YSHIFT = 0.10000

ELLIPSE SECTIONS: SHIFT PARAMETER CALCULATIONS

SURFACE AREA = 1.25622

C OF G XBAR = 1.00006

RAD OF G SQ = 1.24988 XRAD2 = 1.11798 XRADG = 0.49977

CROSS PRODUCT = 0.60004

DY ELEMENTS AREA = 1.25597
C OF G YBAR 0.60001 RAD OF G SQ = 0.39995
YRAD2 = 0.63242 YRADG = 0.19985

TWICE ANGLE OF PRINCIPAL AXIS = -0.00004

CROSS PRODUCT = 0.59988

PRODUCTION SHAPE DX ELEMENTS

AREA = 1.25512
RAD2 = 1.45963 R OG G = 1.20815 C OF G = 1.10029 XPADG = 0.49899

CROSSPRODUCT = 0.77394

PRODUCTION DY ELEMENTS
AREA = 1.25741
PRAD SQ = 0.53005 R OF G = 0.72805 C OF G = 0.70005 YPADG = 0.19996

CROSSPRODUCT = 0.77391

SHIFT PARAMETERS

X DIRECTION = 0.10024
Y DIRECTION = 0.10004
TAN OF ANGULAR DIFFERENCE = 0.01761

ANGULAR DIFFERENCE IN DEGREES = 1.00909

INPUT PARAMETERS

A = 1.00000 B = 0.40000

P = 1.00000 Q = 0.60000

SHIFT PARAMETERS

X DIRECTION SR = 0.10000 Y DIRECTION TR = 0.10000

ANGLE OF ROTATION = 0.00873

ANGLE OF ROTATION IN DEGREES = 0.50029

SR = 0.10528 TR = 0.09129

SHAPE PARAMETERS

	REF X	Y1	Y2	PX1	PY1	PX2	PY2
1	0.00000	0.60000	0.60000	0.10004	0.69127	0.10004	0.69127
2	0.01000	0.54357	0.65643	0.11053	0.63493	0.10955	0.74778
3	0.02000	0.52040	0.67960	0.12073	0.61185	0.11934	0.77104
4	0.03000	0.50276	0.69724	0.13089	0.59429	0.12919	0.78877
5	0.04000	0.48800	0.71200	0.14101	0.57962	0.13906	0.80361
6	0.05000	0.47510	0.72490	0.15113	0.56681	0.14895	0.81660
7	0.06000	0.46353	0.73647	0.16123	0.55533	0.15884	0.82826
8	0.07000	0.45298	0.74702	0.17132	0.54486	0.16875	0.83890
9	0.08000	0.44323	0.75677	0.18140	0.53521	0.17867	0.84873
10	0.09000	0.43416	0.76584	0.19148	0.52622	0.18859	0.85789
11	0.10000	0.42564	0.77436	0.20156	0.51779	0.19851	0.86649
12	0.11000	0.41762	0.78238	0.21163	0.50985	0.20844	0.87461
13	0.12000	0.41001	0.78999	0.22169	0.50234	0.21837	0.88230
14	0.13000	0.40278	0.79722	0.23175	0.49519	0.22831	0.88962
15	0.14000	0.39588	0.80412	0.24181	0.48838	0.23825	0.89660
16	0.15000	0.38929	0.81071	0.25187	0.48187	0.24819	0.90328
17	0.16000	0.38297	0.81703	0.26193	0.47564	0.25814	0.90969
18	0.17000	0.37689	0.82311	0.27198	0.46966	0.26808	0.91585
19	0.18000	0.37105	0.82895	0.28203	0.46390	0.27803	0.92178
20	0.19000	0.36543	0.83457	0.29208	0.45837	0.28798	0.92749
21	0.20000	0.36000	0.84000	0.30213	0.45303	0.29794	0.93301
22	0.21000	0.35476	0.84524	0.31217	0.44787	0.30789	0.93834
23	0.22000	0.34969	0.85031	0.32221	0.44289	0.31784	0.94349
24	0.23000	0.34478	0.85522	0.33226	0.43807	0.32780	0.94849
25	0.24000	0.34003	0.85997	0.34230	0.43341	0.33776	0.95332
26	0.25000	0.33542	0.86457	0.35234	0.42889	0.34772	0.95802
27	0.26000	0.33096	0.86904	0.36238	0.42451	0.35768	0.96257
28	0.27000	0.32662	0.87338	0.37241	0.42026	0.36764	0.96700
29	0.28000	0.32241	0.87759	0.38245	0.41614	0.37760	0.97129

30	0.29000	0.31832	0.88168	0.39249	0.41213	0.38757	0.97547
31	0.30000	0.31434	0.88566	0.40252	0.40824	0.39753	0.97954
32	0.31000	0.31048	0.88952	0.41255	0.40446	0.40750	0.98349
33	0.32000	0.30672	0.89328	0.42259	0.40079	0.41747	0.98734
34	0.33000	0.30306	0.89694	0.43262	0.39722	0.42743	0.99108
35	0.34000	0.29949	0.90051	0.44265	0.39374	0.43740	0.99473
36	0.35000	0.29603	0.90397	0.45268	0.39036	0.44737	0.99829
37	0.36000	0.29265	0.90735	0.46271	0.38707	0.45734	1.00175
38	0.37000	0.28936	0.91064	0.47274	0.38387	0.46731	1.00513
39	0.38000	0.28616	0.91384	0.48276	0.38076	0.47728	1.00842
40	0.39000	0.28304	0.91696	0.49279	0.37773	0.48726	1.01162
41	0.40000	0.28000	0.92000	0.50282	0.37477	0.49723	1.01475
42	0.41000	0.27704	0.92296	0.51284	0.37190	0.50720	1.01780
43	0.42000	0.27415	0.92585	0.52287	0.36910	0.51718	1.02077
44	0.43000	0.27134	0.92866	0.53289	0.36638	0.52715	1.02367
45	0.44000	0.26860	0.93140	0.54291	0.36373	0.53713	1.02649
46	0.45000	0.26593	0.93407	0.55294	0.36115	0.54710	1.02925
47	0.46000	0.26333	0.93667	0.56296	0.35863	0.55708	1.03194
48	0.47000	0.26080	0.93920	0.57298	0.35619	0.56706	1.03456
49	0.48000	0.25833	0.94167	0.58300	0.35381	0.57704	1.03711
50	0.49000	0.25593	0.94407	0.59302	0.35149	0.58702	1.03960
51	0.50000	0.25359	0.94641	0.60304	0.34924	0.59699	1.04203
52	0.51000	0.25131	0.94869	0.61306	0.34705	0.60697	1.04440
53	0.52000	0.24909	0.95091	0.62308	0.34492	0.61695	1.04670
54	0.53000	0.24693	0.95307	0.63310	0.34284	0.62694	1.04895
55	0.54000	0.24483	0.95517	0.64312	0.34083	0.63692	1.05114
56	0.55000	0.24279	0.95721	0.65313	0.33887	0.64690	1.05327
57	0.56000	0.24080	0.95920	0.66315	0.33697	0.65688	1.05534
58	0.57000	0.23887	0.96113	0.67317	0.33513	0.66686	1.05736
59	0.58000	0.23699	0.96301	0.68318	0.33334	0.67685	1.05933
60	0.59000	0.23517	0.96483	0.69320	0.33160	0.68683	1.06124
61	0.60000	0.23339	0.96661	0.70322	0.32992	0.69681	1.06310
62	0.61000	0.23167	0.96833	0.71323	0.32828	0.70680	1.06491
63	0.62000	0.23001	0.96999	0.72324	0.32670	0.71678	1.06666
64	0.63000	0.22839	0.97161	0.73326	0.32517	0.72677	1.06837
65	0.64000	0.22682	0.97318	0.74327	0.32369	0.73676	1.07002
66	0.65000	0.22530	0.97470	0.75328	0.32226	0.74674	1.07163
67	0.66000	0.22383	0.97617	0.76330	0.32088	0.75673	1.07319
68	0.67000	0.22241	0.97759	0.77331	0.31954	0.76672	1.07470
69	0.68000	0.22103	0.97897	0.78332	0.31825	0.77670	1.07616

70	0.69000	0.21971	0.98029	0.79333	0.31701	0.78669	1.07757
71	0.70000	0.21842	0.98158	0.80334	0.31582	0.79668	1.07894
72	0.71000	0.21719	0.98281	0.81335	0.31467	0.80667	1.08026
73	0.72000	0.21600	0.98400	0.82336	0.31357	0.81666	1.08154
74	0.73000	0.21486	0.98514	0.83337	0.31251	0.82665	1.08277
75	0.74000	0.21376	0.98624	0.84338	0.31150	0.83664	1.08396
76	0.75000	0.21270	0.98730	0.85339	0.31053	0.84663	1.08510
77	0.76000	0.21169	0.98831	0.86340	0.30961	0.85662	1.08620
78	0.77000	0.21072	0.98928	0.87341	0.30873	0.86661	1.08725
79	0.78000	0.20980	0.99020	0.88341	0.30789	0.87660	1.08826
80	0.79000	0.20892	0.99108	0.89342	0.30710	0.88659	1.08923
81	0.80000	0.20808	0.99192	0.90343	0.30635	0.89659	1.09016
82	0.81000	0.20729	0.99271	0.91343	0.30564	0.90658	1.09104
83	0.82000	0.20653	0.99347	0.92344	0.30498	0.91657	1.09188
84	0.83000	0.20582	0.99418	0.93345	0.30435	0.92656	1.09268
85	0.84000	0.20515	0.99485	0.94345	0.30377	0.93656	1.09343
86	0.85000	0.20453	0.99547	0.95346	0.30323	0.94655	1.09415
87	0.86000	0.20394	0.99606	0.96346	0.30273	0.95655	1.09482
88	0.87000	0.20339	0.99661	0.97347	0.30227	0.96654	1.09545
89	0.88000	0.20289	0.99711	0.98347	0.30186	0.97654	1.09605
90	0.89000	0.20243	0.99757	0.99347	0.30148	0.98653	1.09660
91	0.90000	0.20201	0.99799	1.00348	0.30115	0.99653	1.09711
92	0.91000	0.20162	0.99838	1.01348	0.30085	1.00652	1.09757
93	0.92000	0.20128	0.99872	1.02348	0.30060	1.01652	1.09800
94	0.93000	0.20098	0.99902	1.03348	0.30039	1.02652	1.09839
95	0.94000	0.20072	0.99928	1.04349	0.30021	1.03652	1.09874
96	0.95000	0.20050	0.99950	1.05349	0.30008	1.04651	1.09905
97	0.96000	0.20032	0.99968	1.06349	0.29999	1.05651	1.09931
98	0.97000	0.20018	0.99982	1.07349	0.29993	1.06651	1.09954
99	0.98000	0.20008	0.99992	1.08349	0.29992	1.07651	1.09973
100	0.99000	0.20002	0.99998	1.09349	0.29995	1.08651	1.09988
101	1.00000	0.20000	1.00000	1.10349	0.30002	1.09651	1.09998
102	1.01000	0.20002	0.99998	1.11349	0.30012	1.10650	1.10005
103	1.02000	0.20008	0.99992	1.12349	0.30027	1.11650	1.10008
104	1.03000	0.20018	0.99982	1.13348	0.30046	1.12650	1.10007
105	1.04000	0.20032	0.99968	1.14348	0.30068	1.13650	1.10001
106	1.05000	0.20050	0.99950	1.15348	0.30095	1.14650	1.09992
107	1.05999	0.20072	0.99928	1.16348	0.30126	1.15650	1.09979
108	1.06999	0.20098	0.99902	1.17347	0.30161	1.16651	1.09961
109	1.07999	0.20128	0.99872	1.18347	0.30200	1.17651	1.09940

110	1.08999	0.20162	0.99838	1.19347	0.30242	1.18651	1.09915
111	1.09999	0.20200	0.99800	1.20346	0.30289	1.19651	1.09885
112	1.10999	0.20243	0.99757	1.21346	0.30340	1.20651	1.09852
113	1.11999	0.20289	0.99711	1.22345	0.30395	1.21652	1.09814
114	1.12999	0.20339	0.99661	1.23345	0.30454	1.22652	1.09772
115	1.13999	0.20394	0.99606	1.24344	0.30518	1.23652	1.09727
116	1.14999	0.20452	0.99548	1.25343	0.30585	1.24653	1.09677
117	1.15999	0.20515	0.99485	1.26343	0.30656	1.25653	1.09623
118	1.16999	0.20582	0.99418	1.27342	0.30732	1.26654	1.09565
119	1.17999	0.20653	0.99347	1.28341	0.30812	1.27654	1.09502
120	1.18999	0.20729	0.99271	1.29340	0.30896	1.28655	1.09436
121	1.19998	0.20808	0.99192	1.30340	0.30984	1.29655	1.09365
122	1.20998	0.20892	0.99108	1.31339	0.31077	1.30656	1.09290
123	1.21998	0.20980	0.99020	1.32338	0.31173	1.31657	1.09211
124	1.22998	0.21072	0.98928	1.33337	0.31274	1.32657	1.09127
125	1.23998	0.21169	0.98831	1.34336	0.31380	1.33658	1.09039
126	1.24998	0.21270	0.98730	1.35335	0.31490	1.34659	1.08947
127	1.25998	0.21375	0.98625	1.36334	0.31604	1.35660	1.08850
128	1.26998	0.21485	0.98515	1.37333	0.31723	1.36661	1.08749
129	1.27998	0.21600	0.98400	1.38332	0.31846	1.37661	1.08643
130	1.28998	0.21719	0.98281	1.39331	0.31973	1.38662	1.08533
131	1.29998	0.21842	0.98158	1.40330	0.32105	1.39663	1.08418
132	1.30998	0.21970	0.98030	1.41328	0.32242	1.40664	1.08299
133	1.31998	0.22103	0.97897	1.42327	0.32384	1.41665	1.08175
134	1.32998	0.22240	0.97760	1.43326	0.32530	1.42666	1.08046
135	1.33997	0.22383	0.97617	1.44324	0.32681	1.43668	1.07913
136	1.34997	0.22530	0.97470	1.45323	0.32837	1.44669	1.07774
137	1.35997	0.22681	0.97319	1.46321	0.32997	1.45670	1.07631
138	1.36997	0.22838	0.97162	1.47320	0.33163	1.46671	1.07483
139	1.37997	0.23000	0.97000	1.48318	0.33333	1.47672	1.07330
140	1.38997	0.23167	0.96833	1.49317	0.33509	1.48674	1.07172
141	1.39997	0.23339	0.96661	1.50315	0.33689	1.49675	1.07009
142	1.40997	0.23516	0.96484	1.51314	0.33875	1.50677	1.06840
143	1.41997	0.23698	0.96302	1.52312	0.34066	1.51678	1.06667
144	1.42997	0.23886	0.96114	1.53310	0.34263	1.52680	1.06488
145	1.43997	0.24079	0.95921	1.54308	0.34465	1.53681	1.06303
146	1.44997	0.24278	0.95722	1.55307	0.34672	1.54683	1.06113
147	1.45997	0.24483	0.95517	1.56305	0.34885	1.55685	1.05918
148	1.46996	0.24693	0.95307	1.57303	0.35104	1.56686	1.05716
149	1.47996	0.24908	0.95092	1.58301	0.35329	1.57688	1.05509

150	1.48996	0.25130	0.94870	1.59299	0.35559	1.58690	1.05296
151	1.49996	0.25358	0.94642	1.60297	0.35796	1.59692	1.05077
152	1.50996	0.25592	0.94408	1.61294	0.36039	1.60694	1.04852
153	1.51996	0.25832	0.94168	1.62292	0.36288	1.61696	1.04620
154	1.52996	0.26079	0.93921	1.63290	0.36543	1.62698	1.04382
155	1.53996	0.26332	0.93668	1.64288	0.36805	1.63700	1.04138
156	1.54996	0.26592	0.93408	1.65285	0.37074	1.64702	1.03886
157	1.55996	0.26859	0.93141	1.66283	0.37349	1.65704	1.03628
158	1.56996	0.27133	0.92867	1.67280	0.37632	1.66707	1.03363
159	1.57996	0.27414	0.92586	1.68278	0.37922	1.67709	1.03091
160	1.58996	0.27703	0.92297	1.69275	0.38219	1.68711	1.02811
161	1.59996	0.27999	0.92001	1.70273	0.38524	1.69714	1.02524
162	1.60995	0.28303	0.91697	1.71270	0.38836	1.70716	1.02229
163	1.61995	0.28614	0.91386	1.72267	0.39157	1.71719	1.01925
164	1.62995	0.28935	0.91065	1.73264	0.39486	1.72721	1.01614
165	1.63995	0.29263	0.90737	1.74261	0.39823	1.73724	1.01294
166	1.64995	0.29601	0.90399	1.75258	0.40170	1.74727	1.00965
167	1.65995	0.29948	0.90052	1.76255	0.40525	1.75730	1.00627
168	1.66995	0.30304	0.89696	1.77252	0.40890	1.76733	1.00280
169	1.67995	0.30670	0.89330	1.78248	0.41264	1.77736	0.99923
170	1.68995	0.31046	0.88954	1.79245	0.41649	1.78739	0.99556
171	1.69995	0.31432	0.88568	1.80241	0.42044	1.79743	0.99178
172	1.70995	0.31830	0.88170	1.81238	0.42451	1.80746	0.98789
173	1.71995	0.32239	0.87761	1.82234	0.42868	1.81749	0.98389
174	1.72995	0.32660	0.87340	1.83230	0.43298	1.82753	0.97976
175	1.73995	0.33093	0.86907	1.84226	0.43740	1.83757	0.97552
176	1.74994	0.33540	0.86460	1.85222	0.44196	1.84760	0.97114
177	1.75994	0.34000	0.86000	1.86218	0.44665	1.85764	0.96662
178	1.76994	0.34476	0.85524	1.87214	0.45149	1.86768	0.96196
179	1.77994	0.34966	0.85034	1.88210	0.45648	1.87773	0.95714
180	1.78994	0.35473	0.84527	1.89205	0.46163	1.88777	0.95216
181	1.79994	0.35997	0.84003	1.90200	0.46696	1.89781	0.94701
182	1.80994	0.36540	0.83460	1.91196	0.47247	1.90786	0.94167
183	1.81994	0.37102	0.82898	1.92191	0.47819	1.91791	0.93613
184	1.82994	0.37686	0.82314	1.93185	0.48411	1.92796	0.93038
185	1.83994	0.38293	0.81707	1.94180	0.49027	1.93801	0.92440
186	1.84994	0.38925	0.81075	1.95174	0.49667	1.94806	0.91817
187	1.85994	0.39584	0.80416	1.96168	0.50335	1.95812	0.91166
188	1.86994	0.40273	0.79727	1.97162	0.51034	1.96818	0.90485
189	1.87994	0.40996	0.79004	1.98156	0.51765	1.97824	0.89771

190	1.88993	0.41756	0.78244	1.99149	0.52534	1.98831	0.89020
191	1.89993	0.42559	0.77441	2.00142	0.53345	1.99838	0.88226
192	1.90993	0.43410	0.76590	2.01134	0.54205	2.00845	0.87384
193	1.91993	0.44317	0.75683	2.02127	0.55121	2.01853	0.86486
194	1.92993	0.45291	0.74709	2.03118	0.56103	2.02861	0.85521
195	1.93993	0.46345	0.73655	2.04109	0.57166	2.03870	0.84475
196	1.94993	0.47502	0.72498	2.05098	0.58331	2.04880	0.83327
197	1.95993	0.48790	0.71210	2.06087	0.59629	2.05891	0.82047
198	1.96993	0.50264	0.69736	2.07074	0.61112	2.06904	0.80582
199	1.97993	0.52026	0.67974	2.08058	0.62882	2.07919	0.78829
200	1.98993	0.54337	0.65663	2.09038	0.65201	2.08939	0.76527
201	1.99993	0.59515	0.60485	2.09993	0.70388	2.09984	0.71358
202	0.00000	0.00000	0.00000	0.00000	0.00000	0.00000	0.00000

ELLIPSE SHIFT PARAMETERS

```
CGX =  1.10000
CGY =  0.70000
ANG =  0.00631
```

```
         REF LINE
LENGTH =  2.29583              XBAR =  0.99794            YBAR =  0.89002

RAD OF G X SQ =  1.39430       XRADL =  1.18081           XRG =  0.63121

RAD OF G Y SQ =  0.80423       YRADL =  0.89679           YRG =  0.10995

CROSS PRODUCT RHXY =  0.88878  RHBAR =  0.00060
TWICE ANGLE TAN-1 =  0.00000
```

PROD LINE
LENGTH = 2.29583   PXBAR = 1.09541   PYBAR = 0.98999

RAD OF G Y SQ = 1.59830   XPADL = 1.26424   XPG = 0.63118
RAD OF G YSQ = 0.99221   YPADL = 0.99610   YPG = 0.11012

CROSS PRODUCT PHXY = 1.08841   PHBAR = 0.00397
TWICE ANGLE TAN-1 = 0.02054

LINE CENTROID

SHIFT PARAMETERS
XSHIFT = 0.09747   YSHIFT = 0.09997

ANGULAR DIFFERENCE IN DEGREES = 0.50017

EFFECTIVE SHIFT OF SECTIONAL CENTROID
XSHIFT = 0.10000   YSHIFT = 0.10000

PRODUCTION SHAPE DX ELEMENTS

AREA = 1.25512 C OF G = 1.10026
RAD2 = 1.45960 R OG G = 1.20814 XPADG = 0.49903

CROSSPRODUCT = 0.77202

PRODUCTION DY ELEMENTS
AREA = 1.25740 C OF G = 0.70003
PRAD SQ = 0.52997 R OF G = 0.72799 YPADG = 0.19982

CROSSPRODUCT = 0.77193

SHIFT PARAMETERS

```
X DIRECTION =  0.10020
Y DIRECTION =  0.10002
TAN OF ANGULAR DIFFERENCE =  0.00867


ANGULAR DIFFERENCE IN DEGREES =  0.49668
```

IHE140I FILE SYSIN - END OF FILE ENCOUNTERED IN STATEMENT 00009 AT OFFSET +00002 FROM ENTRY POINT SIMCAL

APPENDIX THREE

EXAMPLE OF CENTROID MANIPULATION

HOLOGRAPHIC CONTOURING PROGRAMME

INPUT CONSTANTS

POINTS =222.0 DELTA = 0.016

LIM1= 10900 LIM2 = 12300

NOISE LIMIT

DIFMIN = 100

START PARAMETER = 0.00

XMAX = 2150 XMIN = 14900

COMPONENT WIDTH 1.19000

DIRECTION INDICATOR= 1

X DIRECTION INVERSION REGION XLIM1 = 11000 XLIM2 = 12500

RUN TYPE 0 = REF 1 = SUBTRACT REF = 0

POINTS NUMBER	EX VALUE	Z VALUE
1	0.00000	0.00000
2	0.00000	0.00000
3	0.00000	0.00000
4	0.00000	0.00000
5	0.00000	0.00000
6	0.00000	0.00000
7	0.00000	0.00000
8	1.16667	0.00012
9	1.16247	0.00801
10	1.15789	0.01612
11	1.15323	0.02075
12	1.14893	0.02401
13	1.14445	0.03187
14	1.13960	0.02401
15	1.13447	0.03212
16	1.12961	0.04001
17	1.12457	0.04361
18	1.11963	0.04812
19	1.11496	0.05601
20	1.10936	0.05836
21	1.10525	0.06412
22	1.10021	0.06800
23	1.09573	0.07201
24	1.09013	0.07678
25	1.08491	0.08012
26	1.07912	0.08486
27	1.07305	0.08801
28	1.06745	0.09216
29	1.06195	0.09612
30	1.05551	0.09870
31	1.04953	0.10189
32	1.04421	0.10401
33	1.03787	0.10706
34	1.03264	0.10962
35	1.02741	0.11212
36	1.02247	0.11353
37	1.01724	0.11516
38	1.01201	0.11672
39	1.00707	0.11828

40	1.00193	0.12001
41	0.99773	0.12117
42	0.99288	0.12273
43	0.98831	0.12387
44	0.98392	0.12508
45	0.97963	0.12669
46	0.97505	0.12799
47	0.97029	0.12799
48	0.96525	0.12801
49	0.96040	0.12801
50	0.95517	0.12966
51	0.95013	0.13089
52	0.94481	0.13198
53	0.93949	0.13275
54	0.93427	0.13355
55	0.92876	0.13444
56	0.92307	0.13511
57	0.91765	0.13584
58	0.91159	0.13566
59	0.90655	0.13559
60	0.90020	0.13572
61	0.89404	0.13571
62	0.88863	0.13586
63	0.88312	0.13559
64	0.87687	0.13531
65	0.87127	0.13502
66	0.86604	0.13451
67	0.86007	0.13403
68	0.85540	0.13347
69	0.85027	0.13278
70	0.84513	0.13208
71	0.84019	0.13137
72	0.83477	0.13072
73	0.82945	0.12972
74	0.82497	0.12825
75	0.81975	0.12787
76	0.81433	0.12592
77	0.80976	0.12481
78	0.80425	0.12356
79	0.79903	0.12216

80	0.79389	0.12055
81	0.78885	0.11999
82	0.78353	0.11778
83	0.77812	0.11602
84	0.77168	0.11412
85	0.76627	0.11187
86	0.76011	0.10969
87	0.75460	0.10720
88	0.74900	0.10399
89	0.74284	0.10340
90	0.73677	0.10069
91	0.73052	0.09831
92	0.72445	0.09587
93	0.71867	0.09325
94	0.71307	0.09081
95	0.70635	0.08799
96	0.70093	0.08615
97	0.69552	0.08377
98	0.68945	0.08100
99	0.68479	0.07987
100	0.68049	0.07708
101	0.67527	0.07491
102	0.67153	0.07199
103	0.66621	0.07133
104	0.66099	0.06848
105	0.65641	0.06572
106	0.65156	0.06387
107	0.64680	0.06041
108	0.64195	0.05762
109	0.63700	0.05599
110	0.63215	0.05208
111	0.62683	0.04787
112	0.62095	0.04625
113	0.61647	0.04261
114	0.61105	0.03999
115	0.60415	0.03516
116	0.59836	0.03187
117	0.59276	0.02777
118	0.58669	0.02399
119	0.58053	0.02027

120	0.57465	0.01587
121	0.56905	0.01291
122	0.56336	0.00799
123	0.55720	0.00581
124	0.55160	0.00153
125	0.54600	-0.00012
126	0.54040	-0.00498
127	0.53527	-0.00801
128	0.53051	-0.01169
129	0.52547	-0.01612
130	0.52071	-0.01795
131	0.51632	-0.02094
132	0.51184	-0.02401
133	0.50680	-0.02747
134	0.50269	-0.03212
135	0.49793	-0.03397
136	0.49243	-0.03788
137	0.48804	-0.04001
138	0.48300	-0.04447
139	0.47824	-0.04812
140	0.47357	-0.05184
141	0.46853	-0.05601
142	0.46377	-0.05986
143	0.45799	-0.06412
144	0.45323	-0.06786
145	0.44744	-0.07201
146	0.44119	-0.08012
147	0.43484	-0.08181
148	0.42933	-0.08801
149	0.42317	-0.09255
150	0.41748	-0.09612
151	0.41179	-0.10266
152	0.40637	-0.10401
153	0.40021	-0.11212
154	0.39405	-0.11500
155	0.38873	-0.12001
156	0.38295	-0.12383
157	0.37735	-0.12812
158	0.37212	-0.13186
159	0.36699	-0.13601

160	0.36176	-0.13973
161	0.35663	-0.14412
162	0.35243	-0.14711
163	0.34757	-0.15201
164	0.34235	-0.15567
165	0.33768	-0.16012
166	0.33236	-0.16411
167	0.32732	-0.16801
168	0.32209	-0.17259
169	0.31715	-0.17612
170	0.31248	-0.18243
171	0.30660	-0.18401
172	0.30165	-0.19212
173	0.29605	-0.19545
174	0.29008	-0.20001
175	0.28439	-0.20812
176	0.27823	-0.21072
177	0.27272	-0.21601
178	0.26693	-0.22284
179	0.26059	-0.22412
180	0.25489	-0.23201
181	0.24855	-0.23759
182	0.24323	-0.24012
183	0.23679	-0.24801
184	0.23128	-0.25403
185	0.22596	-0.25612
186	0.22017	-0.26401
187	0.21429	-0.26680
188	0.20907	-0.27212
189	0.20496	-0.27673
190	0.19964	-0.28001
191	0.19423	-0.28653
192	0.18965	-0.28812
193	0.18424	-0.29601
194	0.17948	-0.30077
195	0.17435	-0.30412
196	0.16949	-0.31201
197	0.16427	-0.31540
198	0.15960	-0.32012
199	0.15447	-0.32801

200	0.14896	-0.33059
201	0.14411	-0.33612
202	0.13888	-0.34401
203	0.13393	-0.34632
204	0.12712	-0.35212
205	0.12171	-0.36001
206	0.11592	-0.36812
207	0.10976	-0.36991
208	0.10444	-0.37601
209	0.09847	-0.38412
210	0.09315	-0.38966
211	0.08596	-0.39201
212	0.08083	-0.40012
213	0.07513	-0.40801
214	0.06916	-0.41612
215	0.06319	-0.41855
216	0.05768	-0.42401
217	0.05292	-0.43187
218	0.00000	0.00000
219	0.00000	0.00000
220	0.00000	0.00000
221	0.00000	0.00000
222	0.00000	0.00000

```
CURVE LENGTH =  1.29902

XBAR =  0.59605                    ZBAR = -0.04392


RAD OF G X SQ =  0.45545           XRAD =  0.67487           XRG =  0.31649


RAD OF G Z SQ =  0.02830           ZRAD =  0.16822           ZRG =  0.16239


CROSS TERM =  0.02003          HBAR =  0.04621

TWICE ANGLE OF P AXES =  1.25221

REF DATA SET
```

IDENT =008720724 RUN =BACC-1-160

CORRECT CARD AND TAPE FOUND II = 10

RUNB_CEN_BACK_01DEFL

APPENDIX THREE

EXAMPLE OF CENTROID MANIPULATION

HOLOGRAPHIC CONTOURING PROGRAMME

INPUT CONSTANTS

POINTS =303.0   DELTA = 0.016

LIM1= 10900   LIM2 = 12300

NOISE LIMIT

DIFMIN = 100

START PARAMETER = 1.00

XMAX = 2150   XMIN = 14900

COMPONENT WIDTH 1.19000

DIRECTION INDICATOR= 1

X DIRECTION INVERSION REGION   XLIM1 = 11000   XLIM2 = 12500

RUN TYPE 0 = REF 1 = SUBTRACT REF = 1

POINTS NUMBER	EX VALUE	Z VALUE
1	0.00000	0.00000
2	0.00000	0.00000
3	0.00000	0.00000
4	0.00000	0.00000
5	0.00000	0.00000
6	0.00000	0.00000
7	0.00000	0.00000
8	0.00000	0.00000
9	1.17180	0.00812
10	1.16807	0.01601
11	1.16424	0.01766
12	1.16116	0.02412
13	1.15687	0.02927
14	1.15276	0.03199
15	1.14940	0.02412
16	1.14548	0.03201
17	1.14147	0.03695
18	1.13745	0.04012
19	1.13363	0.04801
20	1.12971	0.04945
21	1.12597	0.05612
22	1.12243	0.05728
23	1.11832	0.06401
24	1.11468	0.06634
25	1.11076	0.07081
26	1.10731	0.07212
27	1.10292	0.07769
28	1.09993	0.08001
29	1.09601	0.08378
30	1.09237	0.08812
31	1.08836	0.09019
32	1.08425	0.09284
33	1.08061	0.09601
34	1.07679	0.09830
35	1.07277	0.10073
36	1.06885	0.10412
37	1.06521	0.10425
38	1.06129	0.10716
39	1.05793	0.10931

40	1.05364	0.11201
41	1.04972	0.11327
42	1.04561	0.11504
43	1.04169	0.11664
44	1.03749	0.11828
45	1.03385	0.12012
46	1.02965	0.12162
47	1.02564	0.12333
48	1.02153	0.12485
49	1.01771	0.12603
50	1.01323	0.12711
51	1.00931	0.12801
52	1.00501	0.12946
53	1.00137	0.13052
54	0.99773	0.13158
55	0.99353	0.13252
56	0.98980	0.13341
57	0.98551	0.13437
58	0.98243	0.13612
59	0.97785	0.13644
60	0.97440	0.13728
61	0.97020	0.13805
62	0.96703	0.13881
63	0.96283	0.13952
64	0.95937	0.14023
65	0.95527	0.14083
66	0.95200	0.14154
67	0.94761	0.14209
68	0.94407	0.14262
69	0.94117	0.14312
70	0.93697	0.14372
71	0.93287	0.14330
72	0.92895	0.14491
73	0.92503	0.14462
74	0.92139	0.14448
75	0.91756	0.14426
76	0.91355	0.14481
77	0.90972	0.14505
78	0.90617	0.14501
79	0.90216	0.14500

80	0.89787	0.14505
81	0.89395	0.14504
82	0.88984	0.14479
83	0.88639	0.14454
84	0.88200	0.14440
85	0.87817	0.14420
86	0.87397	0.14330
87	0.87033	0.14328
88	0.86576	0.14387
89	0.86231	0.14322
90	0.85820	0.14266
91	0.85540	0.14208
92	0.85017	0.14144
93	0.84691	0.14083
94	0.84187	0.14031
95	0.83869	0.13962
96	0.83515	0.13884
97	0.83011	0.13819
98	0.82647	0.13775
99	0.82236	0.13703
100	0.81863	0.13587
101	0.81471	0.13431
102	0.81116	0.13353
103	0.80761	0.13264
104	0.80360	0.13153
105	0.79987	0.13044
106	0.79651	0.12920
107	0.79259	0.12799
108	0.78820	0.12677
109	0.78465	0.12570
110	0.78045	0.12441
111	0.77691	0.12303
112	0.77271	0.12153
113	0.76925	0.11987
114	0.76543	0.11853
115	0.76123	0.11711
116	0.75871	0.11584
117	0.75404	0.11431
118	0.75003	0.11199
119	0.74629	0.11152

120	0.74191	0.10966
121	0.73920	0.10791
122	0.73528	0.10634
123	0.73136	0.10387
124	0.72707	0.10375
125	0.72315	0.10166
126	0.71857	0.09962
127	0.71521	0.09791
128	0.71101	0.09599
129	0.70719	0.09452
130	0.70261	0.09316
131	0.69907	0.09147
132	0.69487	0.08966
133	0.69104	0.08787
134	0.68731	0.08536
135	0.68320	0.08353
136	0.67919	0.08178
137	0.67508	0.07999
138	0.67116	0.07876
139	0.66733	0.07680
140	0.66360	0.07487
141	0.65987	0.07187
142	0.65604	0.07016
143	0.65156	0.06807
144	0.64895	0.06639
145	0.64475	0.06399
146	0.64064	0.06255
147	0.63756	0.06031
148	0.63373	0.05787
149	0.62944	0.05587
150	0.62571	0.05278
151	0.62225	0.05051
152	0.61889	0.04799
153	0.61497	0.04594
154	0.61105	0.04350
155	0.60695	0.03987
156	0.60349	0.03853
157	0.59911	0.03555
158	0.59603	0.03250
159	0.59211	0.03199

160	0.58753	0.02806
161	0.58427	0.02531
162	0.58035	0.02387
163	0.57587	0.02059
164	0.57195	0.01823
165	0.56840	0.01599
166	0.56485	0.01341
167	0.56009	0.01108
168	0.55571	0.00787
169	0.55197	0.00519
170	0.54843	0.00234
171	0.54376	-0.00001
172	0.54031	-0.00305
173	0.53564	-0.00606
174	0.53125	-0.00812
175	0.52743	-0.01123
176	0.52360	-0.01399
177	0.51977	-0.01601
178	0.51576	-0.01912
179	0.51137	-0.02156
180	0.50811	-0.02412
181	0.50400	-0.02712
182	0.50036	-0.02975
183	0.49765	-0.03201
184	0.49439	-0.03475
185	0.49187	-0.03719
186	0.48767	-0.04012
187	0.48440	-0.04237
188	0.48048	-0.04542
189	0.47665	-0.04801
190	0.47283	-0.05152
191	0.46909	-0.05612
192	0.46601	-0.05848
193	0.46209	-0.06145
194	0.45771	-0.06401
195	0.45472	-0.06673
196	0.45043	-0.07028
197	0.44604	-0.07212
198	0.44305	-0.07637
199	0.43913	-0.08001

200	0.43437	-0.08316
201	0.43055	-0.08641
202	0.42635	-0.08812
203	0.42280	-0.09262
204	0.41860	-0.09601
205	0.41533	-0.09914
206	0.41123	-0.10281
207	0.40731	-0.10412
208	0.40329	-0.10805
209	0.39965	-0.11201
210	0.39564	-0.11481
211	0.39125	-0.11786
212	0.38789	-0.12012
213	0.38388	-0.12436
214	0.37865	-0.12801
215	0.37501	-0.13123
216	0.37156	-0.13612
217	0.36699	-0.13681
218	0.36260	-0.14062
219	0.35971	-0.14401
220	0.35495	-0.14661
221	0.35149	-0.15009
222	0.34757	-0.15212
223	0.34328	-0.15606
224	0.34011	-0.16001
225	0.33609	-0.16259
226	0.33245	-0.16591
227	0.32872	-0.16812
228	0.32433	-0.17278
229	0.31995	-0.17601
230	0.31743	-0.17930
231	0.31267	-0.18412
232	0.30968	-0.18647
233	0.30473	-0.19024
234	0.30137	-0.19201
235	0.29708	-0.19697
236	0.29381	-0.20012
237	0.28989	-0.20375
238	0.28588	-0.20801
239	0.28065	-0.21145

240	0.27739	-0.21612
241	0.27309	-0.21923
242	0.26973	-0.22401
243	0.26507	-0.22473
244	0.26133	-0.22969
245	0.25723	-0.23212
246	0.25275	-0.23732
247	0.24892	-0.24001
248	0.24519	-0.24430
249	0.24164	-0.24812
250	0.23753	-0.25137
251	0.23343	-0.25601
252	0.22913	-0.25881
253	0.22456	-0.26412
254	0.22092	-0.26616
255	0.21681	-0.27201
256	0.21271	-0.27354
257	0.20860	-0.27834
258	0.20412	-0.28012
259	0.20029	-0.28566
260	0.19637	-0.28801
261	0.19329	-0.29267
262	0.18909	-0.29612
263	0.18461	-0.30052
264	0.18163	-0.30401
265	0.17789	-0.30786
266	0.17425	-0.31212
267	0.17024	-0.31531
268	0.16697	-0.32001
269	0.16296	-0.32255
270	0.15820	-0.32812
271	0.15493	-0.33056
272	0.15167	-0.33601
273	0.14728	-0.33916
274	0.14336	-0.34412
275	0.14065	-0.34741
276	0.13701	-0.35201
277	0.13253	-0.35562
278	0.12824	-0.36012
279	0.12516	-0.36319

280	0.12115	-0.36801
281	0.11657	-0.37223
282	0.11265	-0.37612
283	0.10883	-0.38028
284	0.10556	-0.38401
285	0.10108	-0.38934
286	0.09725	-0.39212
287	0.09315	-0.39641
288	0.08904	-0.40001
289	0.08540	-0.40562
290	0.08111	-0.40812
291	0.07672	-0.41256
292	0.07355	-0.41601
293	0.06953	-0.42387
294	0.00000	0.00000
295	0.00000	0.00000
296	0.00000	0.00000
297	0.00000	0.00000
298	0.00000	0.00000
299	0.00000	0.00000
300	0.00000	0.00000
301	0.00000	0.00000
302	0.00000	0.00000
303	0.00000	0.00000

CURVE LENGTH = 1.34285

XBAR = 0.59603 ZBAR = -0.04531

RAD OF G X SQ = 0.46053 XRAD = 0.67862 XRG = 0.32446

RAD OF G Z SQ = 0.03151 ZRAD = 0.17750 ZRG = 0.17162

CROSS TERM = 0.02292 HBAR = 0.04992

TWICE ANGLE OF P AXES = 1.31686

DIFFERENCE PARAMETERS

XSHIFT = 0.00002 ZSHIFT = 0.00139

DIFTAN = 0.02440

ANGULAR DIFFERENCE = 0.69954

IDENT =009720724 RUN =BACC-1-160

CORRECT CARD AND TAPE FOUND II = 9

RUN9_CEN_BACK_02DEFL

APPENDIX THREE

EXAMPLE OF CENTROID MANIPULATION

HOLOGRAPHIC CONTOURING PROGRAMME

INPUT CONSTANTS

POINTS =234.0 DELTA = 0.016

LIM1= 10900 LIM2 = 12300

NOISE LIMIT

DIFMIN = 100

START PARAMETER = 3.00

XMAX = 2150 XMIN = 14900

COMPONENT WIDTH 1.19000

DIRECTION INDICATOR= 1

X DIRECTION INVERSION REGION XLIM1 = 11000 XLIM2 = 12500

RUN TYPE 0 = REF 1 = SUBTRACT REF = 1

POINTS NUMBER	EX VALUE	Z VALUE
1	0.00000	0.00000
2	0.00000	0.00000
3	0.00000	0.00000
4	0.00000	0.00000
5	0.00000	0.00000
6	0.00000	0.00000
7	0.00000	0.00000
8	0.00000	0.00000
9	0.00000	0.00000
10	0.00000	0.00000
11	1.18085	0.02412
12	1.17563	0.02798
13	1.17152	0.02880
14	1.16657	0.03201
15	1.16135	0.04012
16	1.15640	0.04801
17	1.15145	0.04879
18	1.14669	0.05612
19	1.14165	0.06401
20	1.13671	0.06645
21	1.13157	0.07212
22	1.12635	0.07702
23	1.12159	0.08001
24	1.11655	0.08612
25	1.11104	0.08812
26	1.10637	0.09341
27	1.10096	0.09601
28	1.09611	0.10037
29	1.09069	0.10412
30	1.08565	0.10675
31	1.08033	0.10959
32	1.07520	0.11201
33	1.06979	0.11470
34	1.06409	0.11700
35	1.05887	0.11975
36	1.05355	0.12012
37	1.04823	0.12291
38	1.04291	0.12508
39	1.03796	0.12688

40	1.03283	0.12801
41	1.02760	0.12984
42	1.02228	0.13120
43	1.01724	0.13258
44	1.01220	0.13403
45	1.00744	0.13612
46	1.00296	0.13650
47	0.99764	0.13728
48	0.99391	0.13803
49	0.98887	0.13911
50	0.98420	0.14002
51	0.97944	0.14086
52	0.97449	0.14166
53	0.96992	0.14242
54	0.96432	0.14322
55	0.95928	0.14552
56	0.95396	0.14527
57	0.94864	0.14497
58	0.94313	0.14457
59	0.93809	0.14483
60	0.93287	0.14546
61	0.92745	0.14572
62	0.92195	0.14569
63	0.91616	0.14575
64	0.91065	0.14566
65	0.90477	0.14523
66	0.89945	0.14479
67	0.89329	0.14429
68	0.88769	0.14317
69	0.88237	0.14291
70	0.87677	0.14311
71	0.87089	0.14313
72	0.86567	0.14211
73	0.86007	0.14124
74	0.85456	0.14030
75	0.84915	0.13923
76	0.84383	0.13819
77	0.83879	0.13703
78	0.83393	0.13587
79	0.82871	0.13500

80	0.82376	0.13308
81	0.81891	0.13156
82	0.81368	0.13002
83	0.80827	0.12799
84	0.80313	0.12683
85	0.79763	0.12502
86	0.79203	0.12300
87	0.78680	0.11987
88	0.78111	0.11900
89	0.77551	0.11678
90	0.77037	0.11461
91	0.76459	0.11199
92	0.75880	0.11027
93	0.75292	0.10798
94	0.74760	0.10528
95	0.74144	0.10387
96	0.73565	0.10056
97	0.72996	0.09812
98	0.72408	0.09599
99	0.71857	0.09344
100	0.71325	0.09114
101	0.70775	0.08787
102	0.70243	0.08616
103	0.69608	0.08355
104	0.69160	0.08073
105	0.68665	0.07999
106	0.68133	0.07712
107	0.67676	0.07483
108	0.67237	0.07187
109	0.66836	0.06956
110	0.66379	0.06681
111	0.65875	0.06399
112	0.65417	0.06128
113	0.64951	0.05842
114	0.64456	0.05587
115	0.63933	0.05209
116	0.63429	0.04799
117	0.62897	0.04564
118	0.62421	0.04106
119	0.61880	0.03987

120	0.61357	0.03506
121	0.60825	0.03199
122	0.60293	0.02803
123	0.59733	0.02387
124	0.59136	0.02072
125	0.58585	0.01599
126	0.58063	0.01453
127	0.57521	0.01019
128	0.56952	0.00787
129	0.56401	0.00314
130	0.55860	-0.00001
131	0.55309	-0.00375
132	0.54787	-0.00812
133	0.54283	-0.01087
134	0.53788	-0.01442
135	0.53265	-0.01601
136	0.52799	-0.02045
137	0.52295	-0.02412
138	0.51921	-0.02733
139	0.51427	-0.03117
140	0.50979	-0.03201
141	0.50652	-0.03581
142	0.50223	-0.04012
143	0.49821	-0.04259
144	0.49476	-0.04587
145	0.49103	-0.04801
146	0.48683	-0.05233
147	0.48272	-0.05612
148	0.47768	-0.05939
149	0.47311	-0.06401
150	0.46769	-0.06795
151	0.46284	-0.07212
152	0.45771	-0.07645
153	0.45276	-0.08001
154	0.44595	-0.08548
155	0.44184	-0.08812
156	0.43605	-0.09601
157	0.43055	-0.09789
158	0.42495	-0.10412
159	0.41981	-0.10752

160	0.41412	-0.11201
161	0.40899	-0.11639
162	0.40292	-0.12012
163	0.39732	-0.12521
164	0.39172	-0.12801
165	0.38621	-0.13431
166	0.38089	-0.13612
167	0.37557	-0.14264
168	0.37035	-0.14401
169	0.36605	-0.15062
170	0.36083	-0.15212
171	0.35579	-0.15911
172	0.35112	-0.16001
173	0.34627	-0.16812
174	0.34169	-0.16928
175	0.33703	-0.17601
176	0.33199	-0.17869
177	0.32732	-0.18412
178	0.32247	-0.18792
179	0.31752	-0.19201
180	0.31201	-0.19894
181	0.30707	-0.20012
182	0.30175	-0.20801
183	0.29596	-0.21266
184	0.29157	-0.21612
185	0.28607	-0.22401
186	0.28037	-0.22806
187	0.27449	-0.23212
188	0.26843	-0.24001
189	0.26283	-0.24251
190	0.25751	-0.24812
191	0.25181	-0.25601
192	0.24584	-0.25641
193	0.24024	-0.26412
194	0.23483	-0.26898
195	0.22895	-0.27201
196	0.22353	-0.28012
197	0.21849	-0.28353
198	0.21289	-0.28801
199	0.20739	-0.29612

200	0.20291	-0.29825
201	0.19740	-0.30401
202	0.19264	-0.31012
203	0.18788	-0.31212
204	0.18321	-0.32001
205	0.17808	-0.32348
206	0.17379	-0.32812
207	0.16893	-0.33601
208	0.16361	-0.33916
209	0.15913	-0.34412
210	0.15372	-0.35201
211	0.14877	-0.35486
212	0.14401	-0.36012
213	0.13916	-0.36801
214	0.13356	-0.37042
215	0.12843	-0.37612
216	0.12292	-0.38401
217	0.11779	-0.39212
218	0.11237	-0.39306
219	0.10649	-0.40001
220	0.10071	-0.40812
221	0.09501	-0.41291
222	0.08932	-0.41601
223	0.08335	-0.42412
224	0.07793	-0.43201
225	0.07261	-0.43987
226	0.00000	0.00000
227	0.00000	0.00000
228	0.00000	0.00000
229	0.00000	0.00000
230	0.00000	0.00000
231	0.00000	0.00000
232	0.00000	0.00000
233	0.00000	0.00000
234	0.00000	0.00000

CURVE LENGTH = 1.34818

XBAR = 0.60059 ZBAR = -0.04916

RAD OF G X SQ = 0.46543 XRAD = 0.68223 XRG = 0.32361

RAD OF G Z SQ = 0.03328 ZRAD = 0.18243 ZRG = 0.17569

CROSS TERM = 0.02204 HBAR = 0.05156

TWICE ANGLE OF P AXES = 1.39632

DIFFERENCE PARAMETERS

XSHIFT = -0.00454

ZSHIFT = 0.00524

DIFTAN = 0.05243

ANGULAR DIFFERENCE = 1.50227

****
****
****

			LINE NUMBER =		1	8	10	8	5	2	11	10	11	8	2	2	3	5	11	6	7
15	44	74	110	170	253	282	228	162	151	232	358	488	612	674	674	639	575	499	441	378	319
289	280	282	295	328	382	455	528	593	652	708	751	748	715	672	609	538	460	375	314	249	208
170	168	182	208	257	322	388	462	522	581	640	692	746	777	798	811	819	822	798	759	719	69[illegible]
659	628	575	551	515	475	451	415	388	358	334	305	275	268	253	244	231	217	211	202	188	185
186	184	185	177	186	195	200	202	210	210	208	217	228	228	245	251	255	259	288	300	322	332
348	380	400	415	455	477	515	528	557	577	622	658	688	722	751	768	775	788	791	777	759	73[illegible]
715	695	668	638	608	563	528	475	408	343	299	252	228	195	180	152	140	138	148	173	222	268
307	352	415	478	528	594	639	694	728	735	740	708	659	611	541	477	401	333	271	222	182	152
148	162	195	237	294	359	445	515	589	655	705	709	699	668	608	535	471	397	328	251	208	17[illegible]
180	205	248	309	393	480	568	628	669	695	682	638	580	502	417	345	274	222	188	188	211	267
339	428	515	588	650	668	655	606	535	451	348	268	212	200	217	280	358	451	529	593	630	620
571	499	428	348	282	228	208	222	262	330	418	500	562	602	593	555	479	410	335	268	222	21[illegible]
250	308	382	455	522	571	571	528	455	368	283	238	227	251	305	368	445	508	548	538	505	439
368	310	253	238	255	311	380	438	488	518	504	455	388	319	259	242	255	301	368	428	477	498
469	417	351	298	268	275	305	368	422	475	482	468	415	358	305	268	271	311	358	412	448	45[illegible]
440	388	338	295	272	288	331	375	422	432	428	388	341	295	275	282	317	362	402	408	388	358
320	279	273	292	331	375	408	410	388	345	315	284	285	311	345	381	395	382	355	315	288	295
328	358	388	388	378	348	315	295	298	319	355	375	368	342	309	288	288	304	328	355	362	35[illegible]
322	298	277	288	310	330	350	335	315	291	277	288	308	340	350	338	319	298	268	242	209	188
160	145	132	138	158	191	208	215	213	208	205	189	182	148	115	75	38	28	20	8	14	11
8	10	5	8	8	4	3	8	11	2	5	8	5	5	5	8	4	10	11	4	11	[illegible]
5	8	3	5	11	8	5	11	8	10	5	11	8	4	11	8	2	5	5	8	3	4

LINE READ & STORED

COMPLETE FRAME READ & STORED

APPENDIX 4

80	4	753.00000
82	5	690.42847
84	6	620.28564
86	7	550.57129
88	8	481.42847
90	9	419.42847
92	10	360.85693
94	11	311.57129
96	12	272.85693
98	13	242.71428
100	14	220.85713
102	15	202.85713
104	16	191.57143
106	17	184.42856
108	18	187.57143
110	19	193.57143
112	20	201.57143
114	21	210.71428
116	22	220.85713
118	23	233.14285
120	24	250.57143
122	25	274.28564
124	26	300.57129
126	27	338.57129
128	28	378.85693
130	29	427.14282
132	30	478.14282
134	31	533.00000
136	32	592.14282
138	33	653.57129
140	34	712.00000
142	35	754.71411
144	36	772.71411
146	37	763.28564
148	38	734.71411
150	39	688.71411
152	40	630.71411
154	41	555.42847
156	42	460.57129
158	43	361.85693

```
     160          44          272.14282
     162          45          206.57143
     164          46          168.71428
     166          47          164.71428
     168          48          199.42856
     170          49          269.28564
     172          50          367.14282
     VMIN =    184          I =106.0               COUNT = 6.0
R =  1.04276           BL =  26Z =  0.06718
R =  0.87430           BL =  27Z =  0.06844
R =  0.72547           BL =  28Z =  0.06956
R =  0.54065           BL =  29Z =  C.07095
R =  0.37710           BL =  30Z =  0.07217
R =  0.24463           BL =  31Z =  0.07317
R =  0.13668           BL =  32Z =  0.07397
R =  0.07617           BL =  33Z =  0.07443
R =  0.02874           BL =  34Z =  C.07478
R =  0.00257           BL =  35Z =  C.07498


          INVERSION ON POINT EX =  C.13593
     VMAX =    773          I =144.0          COUNT =  7.0


          INVERSION POINT AT MIN  START =  10
R = -0.01263           BL =  36Z =  0.07509
R =  0.02647           BL =  37Z =  0.07480
R =  0.04347           BL =  38Z =  0.07467
R =  0.07407           BL =  39Z =  0.07444
R =  0.11316           BL =  40Z =  0.07415
R =  0.17606           BL =  41Z =  C.07368
R =  0.25085           BL =  42Z =  0.07312
R =  0.36644           BL =  43Z =  C.07225
R =  0.49733           BL =  44Z =  0.07127
R =  0.63332           BL =  45Z =  C.07025
R =  0.80500           BL =  46Z =  C.06896
```

```
R =   0.96309           BL =   47Z =   0.06778
R =   1.02598           BL =   48Z =   0.06731
      VMIN =    165          I =166.0            COUNT = 1.0
R =   1.02514           BL =   48Z =   0.06769
R =   0.97744           BL =   49Z =   0.06733
R =   0.87218           BL =   50Z =   0.06654
R =   0.72909           BL =   51Z =   0.06547
R =   0.51034           BL =   52Z =   0.06383
R =   0.22086           BL =   53Z =   0.06166
R =   0.04981           BL =   54Z =   0.06037
R =  -0.04065           BL =   55Z =   0.05970
      VMAX =    740          I =181.0        COUNT =  2.0
R =   0.01440           BL =   56Z =   0.05989
R =   0.24733           BL =   57Z =   0.05815
R =   0.54457           BL =   58Z =   0.05592
R =   0.82443           BL =   59Z =   0.05382
R =   0.99131           BL =   60Z =   0.05257
      VMIN =    148          I =193.0            COUNT = 3.0
R =   0.86318           BL =   61Z =   0.05147
R =   0.55574           BL =   62Z =   0.04917
R =   0.20777           BL =   63Z =   0.04656
R =   0.00676           BL =   64Z =   0.04505
      VMAX =    709          I =204.0        COUNT =  4.0
R =   0.08378           BL =   65Z =   0.04437
R =   0.37611           BL =   66Z =   0.04218
R =   0.78610           BL =   67Z =   0.03910
R =   1.00000           BL =   68Z =   0.03750
      VMIN =    172          I =214.0            COUNT = 5.0
R =   1.00000           BL =   68Z =   0.03750
R =   0.81192           BL =   69Z =   0.03609
R =   0.41899           BL =   70Z =   0.03314
R =   0.06704           BL =   71Z =   0.03050
      VMAX =    695          I =224.0        COUNT =  6.0
R =   0.06310           BL =   72Z =   0.02953
R =   0.42256           BL =   73Z =   0.02683
R =   0.87189           BL =   74Z =   0.02346
      VMIN =    188          I =233.0            COUNT = 7.0
R =   0.97436           BL =   75Z =   0.02231
R =   0.61933           BL =   76Z =   0.01964
R =   0.16963           BL =   77Z =   0.01627
```

```
         VMAX =    668              I =242.0            COUNT =  8.0
R =      0.00000           BL =    78Z =   0.01500
R =      0.31458           BL =    79Z =   0.01264
R =      0.83333           BL =    80Z =   0.00875
         VMIN =    200              I =250.0                    COUNT = 9.0
R =      0.97222           BL =    81Z =   0.00729
R =      0.53632           BL =    82Z =   0.00402
R =      0.02564           BL =    83Z =   0.00019
         VMAX =    630              I =257.0            COUNT = 10.0
R =      0.18605           BL =    84Z = -0.00140
R =      0.76512           BL =    85Z = -0.00574
         VMIN =    208              I =265.0                    COUNT =11.0
R =      0.97630           BL =    86Z = -0.00768
R =      0.52133           BL =    87Z = -0.01109
R =      0.04739           BL =    88Z = -0.01464
         VMAX =    602              I =272.0            COUNT = 12.0
R =      0.13706           BL =    89Z = -0.01603
R =      0.74112           BL =    90Z = -0.02056
         VMIN =    215              I =280.0                    COUNT =13.0
R =      0.97674           BL =    91Z = -0.02267
R =      0.50388           BL =    92Z = -0.02622
R =      0.01809           BL =    93Z = -0.02986
         VMAX =    571              I =286.0            COUNT = 14.0
R =      0.26124           BL =    94Z = -0.03196
R =      0.86236           BL =    95Z = -0.03647
         VMIN =    227              I =293.0                    COUNT =15.0
R =      0.87500           BL =    96Z = -0.03844
R =      0.16279           BL =    97Z = -0.04378
         VMAX =    548              I =299.0            COUNT = 16.0
R =      0.07477           BL =    98Z = -0.04556
R =      0.67913           BL =    99Z = -0.05009
         VMIN =    238              I =306.0                    COUNT =17.0
R =      0.96774           BL =   100Z = -0.05274
R =      0.41935           BL =   101Z = -0.05685
R =      0.00000           BL =   102Z = -0.06000
         VMAX =    518              I =312.0            COUNT = 18.0
R =      0.00000           BL =   102Z = -0.06000
R =      0.50714           BL =   103Z = -0.06380
R =      1.00000           BL =   104Z = -0.06750
         VMIN =    242              I =318.0                    COUNT =19.0
```

```
R =  1.00000          BL = 104Z = -0.06750
R =  0.52899          BL = 105Z = -0.07103
R =  0.00000          BL = 106Z = -0.07500
     VMAX =   498          I =324.0          COUNT = 20.0
R =  0.00000          BL = 106Z = -0.07500
R =  0.49219          BL = 107Z = -0.07869
R =  1.00000          BL = 108Z = -0.08250
     VMIN =   268          I =329.0               COUNT =21.0
R =  1.00000          BL = 108Z = -0.08250
R =  0.36087          BL = 109Z = -0.08729
     VMAX =   482          I =335.0          COUNT = 22.0
R =  0.03271          BL = 110Z = -0.09025
R =  0.71963          BL = 111Z = -0.09540
     VMIN =   268          I =340.0               COUNT =23.0
R =  0.93458          BL = 112Z = -0.09799
R =  0.17290          BL = 113Z = -0.10370
     VMAX =   457          I =346.0          COUNT = 24.0
R =  0.22751          BL = 114Z = -0.10671
R =  0.95238          BL = 115Z = -0.11214
     VMIN =   272          I =351.0               COUNT =25.0
R =  0.62703          BL = 116Z = -0.11530
R =  0.00000          BL = 117Z = -0.12000
     VMAX =   432          I =356.0          COUNT = 26.0
R =  0.00000          BL = 117Z = -0.12000
R =  0.64375          BL = 118Z = -0.12483
     VMIN =   275          I =361.0               COUNT =27.0
R =  0.97452          BL = 119Z = -0.12769
R =  0.12739          BL = 120Z = -0.13404
     VMAX =   408          I =366.0          COUNT = 28.0
R =  0.31579          BL = 121Z = -0.13737
R =  1.00000          BL = 122Z = -0.14250
     VMIN =   273          I =371.0               COUNT =29.0
R =  1.00000          BL = 122Z = -0.14250
R =  0.34815          BL = 123Z = -0.14739
     VMAX =   410          I =376.0          COUNT = 30.0
R =  0.13869          BL = 124Z = -0.15104
R =  0.98540          BL = 125Z = -0.15739
     VMIN =   284          I =380.0               COUNT =31.0
R =  0.48413          BL = 126Z = -0.16137
     VMAX =   395          I =385.0          COUNT = 32.0
```

```
R =   0.00901           BL = 127Z = -0.16507
R =   0.87387           BL = 128Z = -0.17155
      VMIN =    288          I =389.0                 COUNT =33.0
R =   0.62617           BL = 129Z = -0.17530
      VMAX =    388          I =393.0         COUNT = 34.0
R =   0.07000           BL = 130Z = -0.18052
R =   1.00000           BL = 131Z = -0.18750
      VMIN =    295          I =398.0                 COUNT =35.0
R =   1.00000           BL = 131Z = -0.18750
R =   0.56989           BL = 132Z = -0.19073
      VMAX =    375          I =402.0         COUNT = 36.0
R =   0.03750           BL = 133Z = -0.19528
R =   1.00000           BL = 134Z = -0.20250
      VMIN =    288          I =406.0                 COUNT =37.0
R =   1.00000           BL = 134Z = -0.20250
R =   0.24138           BL = 135Z = -0.20819
      VMAX =    362          I =411.0         COUNT = 38.0
R =   0.21622           BL = 136Z = -0.21162
R =   1.00000           BL = 137Z = -0.21750
      VMIN =    277          I =415.0                 COUNT =39.0
R =   1.00000           BL = 137Z = -0.21750
R =   0.24706           BL = 138Z = -0.22315
      VMAX =    350          I =419.0         COUNT = 40.0
R =   0.45205           BL = 139Z = -0.22839
      VMIN =    277          I =423.0                 COUNT =41.0
R =   0.79452           BL = 140Z = -0.23404
R =   0.00000           BL = 141Z = -0.24000
      VMAX =    350          I =427.0         COUNT = 42.0
R =   0.00000           BL = 141Z = -0.24000
R =   0.86301           BL = 142Z = -0.24647
      VMIN =    132          I =437.0                 COUNT =43.0
R =   0.85780           BL = 143Z = -0.24857
R =   0.50459           BL = 144Z = -0.25122
R =   0.12844           BL = 145Z = -0.25404
      VMAX =    215          I =442.0         COUNT = 44.0
R =   0.07229           BL = 146Z = -0.25554
R =   0.91566           BL = 147Z = -0.26187
```

120	0.63828	-0.13404
121	0.64419	-0.13737
122	0.65010	-0.14250
123	0.65601	-0.14739
124	0.66192	-0.15104
125	0.66783	-0.15739
126	0.67374	-0.16137
127	0.67965	-0.16507
128	0.68556	-0.17155
129	0.69147	-0.17530
130	0.69738	-0.18052
131	0.70329	-0.18750
132	0.70920	-0.19073
133	0.71511	-0.19528
134	0.72102	-0.20250
135	0.72693	-0.20819
136	0.73284	-0.21162
137	0.73875	-0.21750
138	0.74466	-0.22315
139	0.75057	-0.22839
140	0.75648	-0.23404
141	0.76239	-0.24000
142	0.76830	-0.24647
143	0.77421	-0.24857
144	0.78012	-0.25122
145	0.78603	-0.25404
146	0.79194	-0.25554
147	0.79785	-0.26187
148	0.80376	-0.26496
149	0.80967	-0.26805
150	0.81558	-0.27115
151	0.82149	0.00000
152	0.82740	0.00000
153	0.83331	0.00000
154	0.83922	0.00000
155	0.84513	0.00000
156	0.85104	0.00000
157	0.85695	0.00000
158	0.86286	0.00000
159	0.86877	0.00000

160	0.87468	0.00000
161	0.88059	0.00000
162	0.88650	0.00000
163	0.89241	0.00000
164	0.89832	0.00000
165	0.90423	0.00000

KA = 6 KB =149

40	0.16548	0.07415
41	0.17139	0.07368
42	0.17730	0.07312
43	0.18321	0.07225
44	0.18912	0.07127
45	0.19503	0.07025
46	0.20094	0.06896
47	0.20685	0.06778
48	0.21276	0.06769
49	0.21867	0.06733
50	0.22458	0.06654
51	0.23049	0.06547
52	0.23640	0.06383
53	0.24231	0.06166
54	0.24822	0.06037
55	0.25413	0.05970
56	0.26004	0.05989
57	0.26595	0.05815
58	0.27186	0.05592
59	0.27777	0.05382
60	0.28368	0.05257
61	0.28959	0.05147
62	0.29550	0.04917
63	0.30141	0.04656
64	0.30732	0.04505
65	0.31323	0.04437
66	0.31914	0.04218
67	0.32505	0.03910
68	0.33096	0.03750
69	0.33687	0.03609
70	0.34278	0.03314
71	0.34869	0.03050
72	0.35460	0.02953
73	0.36051	0.02683
74	0.36642	0.02346
75	0.37233	0.02231
76	0.37824	0.01964
77	0.38415	0.01627
78	0.39006	0.01500
79	0.39597	0.01264

80	0.40188	0.00875
81	0.40779	0.00729
82	0.41370	0.00402
83	0.41961	0.00019
84	0.42552	-0.00140
85	0.43143	-0.00574
86	0.43734	-0.00768
87	0.44325	-0.01109
88	0.44916	-0.01464
89	0.45507	-0.01603
90	0.46098	-0.02056
91	0.46689	-0.02267
92	0.47280	-0.02622
93	0.47871	-0.02986
94	0.48462	-0.03196
95	0.49053	-0.03647
96	0.49644	-0.03844
97	0.50235	-0.04378
98	0.50826	-0.04556
99	0.51417	-0.05009
100	0.52008	-0.05274
101	0.52599	-0.05685
102	0.53190	-0.06000
103	0.53781	-0.06380
104	0.54372	-0.06750
105	0.54963	-0.07103
106	0.55554	-0.07500
107	0.56145	-0.07869
108	0.56736	-0.08250
109	0.57327	-0.08729
110	0.57918	-0.09025
111	0.58509	-0.09540
112	0.59100	-0.09799
113	0.59691	-0.10370
114	0.60282	-0.10671
115	0.60873	-0.11214
116	0.61464	-0.11530
117	0.62055	-0.12000
118	0.62646	-0.12483
119	0.63237	-0.12769

FIN = 150

POINTS NUMBER	EX VALUE	Z VALUE
1	-0.06501	0.00000
2	-0.05910	0.00000
3	-0.05319	0.00000
4	-0.04728	0.00000
5	-0.04137	0.00000
6	-0.03546	0.01765
7	-0.02955	0.02162
8	-0.02364	0.02559
9	-0.01773	0.03116
10	-0.01182	0.03661
11	-0.00591	0.03817
12	0.00000	0.04194
13	0.00591	0.04483
14	0.01182	0.04524
15	0.01773	0.04779
16	0.02364	0.05092
17	0.02955	0.05254
18	0.03546	0.05433
19	0.04137	0.05734
20	0.04728	0.05949
21	0.05319	0.06016
22	0.05910	0.06177
23	0.06501	0.06406
24	0.07092	0.06601
25	0.07683	0.06722
26	0.08274	0.06718
27	0.08865	0.06844
28	0.09456	0.06956
29	0.10047	0.07095
30	0.10638	0.07217
31	0.11229	0.07317
32	0.11820	0.07397
33	0.12411	0.07443
34	0.13002	0.07478
35	0.13593	0.07498
36	0.14184	0.07509
37	0.14775	0.07480
38	0.15366	0.07467
39	0.15957	0.07444

MOIRE CONTOURING PROGRAM USING T V SCAN

INPUT CONSTANTS

NUMBER OF LINES IN FRAME = 1

DELTA = 0.01500
POINT X DIRECTION INTERVAL = 0.00197

NOISE COMPENSATION REGION XLIM1 = 0.55600 XLIM2 = 0.72500 XLIM3 = 0.12500 XLI

,NOISE LIMIT DIFMIN = 10.0000

INVERSION GRADIENT GRAD = 0.0900

PRODUCTION BLADE DATA ON THIS FRAME

MAIN PROG

```
      TS =     6
      VMAX =    282              I = 23.0            COUNT = -1.0
      VMIN =    151              I = 26.0                  COUNT = 0.0
R =   0.58779          BL =   8Z =   0.02559
      VMAX =    674              I = 31.0            COUNT =  1.0
R =   0.15488          BL =   9Z =   0.03116
R =   0.88145          BL =  10Z =   0.03661
      VMIN =    280              I = 40.0                  COUNT = 2.0
R =   0.91117          BL =  11Z =   0.03817
R =   0.40863          BL =  12Z =   0.04194
R =   0.02284          BL =  13Z =   0.04483
      VMAX =    751              I = 50.0            COUNT =  3.0
R =   0.03185          BL =  14Z =   0.04524
R =   0.37155          BL =  15Z =   0.04779
R =   0.78981          BL =  16Z =   0.05092
      VMIN =    168              I = 62.0                  COUNT = 4.0
R =   0.99485          BL =  17Z =   0.05254
R =   0.75643          BL =  18Z =   0.05433
R =   0.35506          BL =  19Z =   0.05734
R =   0.06861          BL =  20Z =   0.05949
      VMAX =    822              I = 78.0            COUNT =  5.0
R =   0.02141          BL =  21Z =   0.06016
R =   0.23547          BL =  22Z =   0.06177
R =   0.54128          BL =  23Z =   0.06406
R =   0.80122          BL =  24Z =   0.06601
R =   0.96330          BL =  25Z =   0.06722
R =   1.00000          BL =  26Z =   0.06750
       74             1             754.71411
       76             2             795.85693
       78             3             789.42847
```